A COMPREHENSIVE STUDY OF

THE ELECTROCHEMISTRY AND FLOATABILITY OF PYRITE

IN COAL FLOTATION

by

Dongping Tao

Dissertation submitted to the Faculty of the
Virginia Polytechnic Institute and State University
in partial fulfillment of the requirement for the degree of

Doctor of Philosophy

in

Mining and Minerals Engineering

APPROVED:

G.H. Luttrell, Chairman

R.-H. Yoon, Co-Chairman

P.E. Richardson

G.T. Adel

R.B. Read

August, 1994

Blacksburg, Virginia

A COMPREHENSIVE STUDY OF THE ELECTROCHEMISTRY AND FLOATABILITY OF PYRITE IN COAL FLOTATION

by

Dongping Tao

Committee Chairman: G. H. Luttrell

Mining and Minerals Engineering

(ABSTRACT)

Pyrite (FeS_2) is the major source of sulfur in various coals, and its efficient removal has proven to be a more difficult task than expected. Flotation is generally considered to be the most practicable process for the preparation of coal fines. However, even this technique is usually unable to remove more than 50% of pyrite from a -65 mesh coal sample, which is the typical feed to flotation. There are three major reasons for the low separation efficiency of liberated pyrite from coal by flotation. They include self-induced hydrophobicity of pyrite caused by superficial oxidation, nonselective hydraulic entrainment of pyrite particles into froth product, and incomplete liberation of pyrite from coal that results in composite coal-pyrite particles, i.e., middlings. The present study was undertaken to address problems associated with these recovery mechanisms of pyrite and develop techniques to enhance pyrite rejection in coal flotation.

To better understand self-induced hydrophobicity of pyrite, chronoamperometry and voltammetry on freshly fractured electrodes were used to explore incipient oxidation and reduction of the mineral. Voltammetry on rotating ring-disc electrodes (RRDE) was

carried out to provide information on soluble species and kinetics of oxidation and reduction processes. X-ray photoelectron spectroscopy (XPS) was used for chemical identification of oxidation products. Galvanic coupling with sacrificial anodes was investigated as a practical method to cathodically protect pyrite and prevent its oxidation. Microflotation tests were conducted under controlled potentials at different solution pH's, and the results were correlated with electrochemical studies. The feasibility of improving pyrite rejection by controlling its surface chemistry was tested in flotation experiments conducted with a 2"-diameter microbubble flotation column and a conventional 5-liter Denver flotation cell.

Effects of froth stability on the microbubble flotation of coal were studied with an objective of minimizing hydraulic entrainment of pyrite. The operating parameters were systematically varied to study their effects on water recovery which was used as a measure of froth stability. It has been demonstrated that the upgrading of coal in a flotation column can be significantly improved when froth stability is properly controlled.

In an attempt to enhance the rejection of pyrite in middlings, various column circuits were experimentally examined and theoretically analyzed. The effect of circuit configuration on the overall circuit performance was evaluated by separation efficiency and separation curves. It has been shown that the overall separation efficiency of column flotation is rather insensitive to circuitry due to the unique characteristics of the unit flotation column, i.e., the addition of the wash water into the froth.

ACKNOWLEDGEMENTS

The author would like to express the utmost appreciation to his adviser, Dr. Gerald H. Luttrell, for his guidance, inspiration, confidence and support in the course of this investigation. Deepest appreciation also goes to Dr. Paul E. Richardson for his invaluable expertise on electrochemistry. Special thanks are delivered to Dr. Roe-Hoan Yoon and Dr. Gregory T. Adel for their invaluable advice, continued assistance and informative discussion. Sincere gratitude is expressed to Dr. Richard B. Read for his valuable time and constructive comments.

The author is also grateful for the financial support from the United States Department of Energy under grants No. DE-AC22-88PC88881, DE-AC22-86PC91221 and DE-AC22-92PC92246.

Special thanks are given to Eric Yan for his invaluable aid in computer graphics, to Dr. Zeshen Ou, Dr. Maixi Lu, and Dr. Cesar Basilio, for their precious suggestions and experimental assistance, to Dr. Zhenghe Xu, Dr. Mike Mankosa, Dr. Ricky Honaker, Dr. Damin Wang, Dr. Dong-su Kim, Asa Weber, Richard Forrest, John Looney, Suha Aksoy, and Yanqing Li for their friendship, assistance and support. Thanks are extended to Wayne Slusser, Jerry Rose, Lisa Jones, Roy Hill, and Jim Overfelt for their technical assistance.

Finally, the most cordial appreciation is expressed to my beloved parents for their continued encouragement, to my wife, Li Zheng, and my son, Ye Tao, for their constant support, understanding, and love.

TABLE OF CONTENTS

LIST OF FIGURES

LIST OF TABLES

CHAPTER 1 INTRODUCTION

1.1 General

Sulfur in coal exists in three major forms: pyritic sulfur, organic sulfur and sulfate sulfur. Sulfate sulfur usually makes up no more than 1% of the total sulfur while pyritic sulfur often accounts for 70~95%. Organic sulfur is intimately associated with the coal matrix and can only be removed by chemical methods. Physical coal cleaning techniques, such as gravity separation, flotation and agglomeration, have the potential to remove pyrite from coal and are generally more cost-effective than alternative post-combustion processes such as flue gas scrubbing.

Effective application of physical coal cleaning methods requires sufficient liberation of the gangue material which can be achieved by pulverizing coal, in many cases, to micron size. Most of available conventional coal cleaning technologies are not effective in this fine size range. New physical techniques for fine particle separation have emerged as a result of considerable efforts during the past decade, and the microbubble column flotation process developed at Virginia Tech is one of the most successful.

The principle of column flotation is illustrated in Figure 1.1. Although the fundamentals are the same as in mechanically-agitated cells, column flotation is

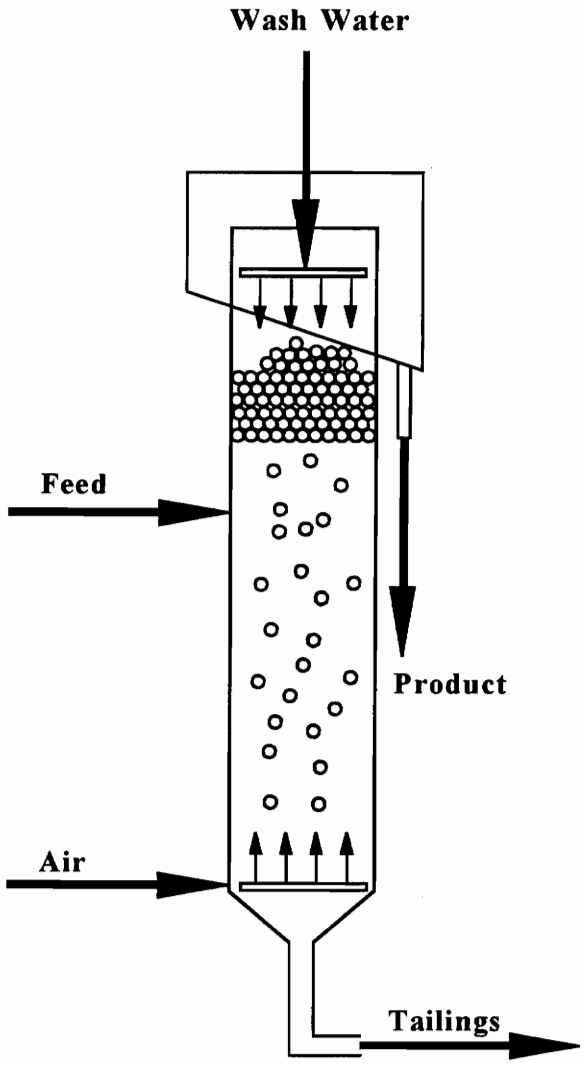

Figure 1.1 Schematic illustration of column flotation.

remarkably different in many aspects. The flow inside the column is countercurrent, with rising air bubbles encountering the particles in the countercurrent feed stream. The hydrophobic particles attach to air bubbles following collisions and are carried to the froth phase, while the hydrophilic particles remain in suspensions and discharge from the bottom as tailings. The unique feature of flotation columns is the addition of wash water in the froth zone to return hydraulically entrained gangue particles to the pulp zone. This cleaning action improves the separation efficiency considerably.

Column flotation usually suffers from low throughput and, therefore, is not considered favorable for rougher flotation. This is particularly the case when the bubbles generated in columns are comparable to, or larger than, those used in conventional flotation machines. The Microcel™ flotation column developed at Virginia Tech exhibits superior performance over other columns in terms of collection capacity and throughput due to the finer bubble sizes (200-600 μm) employed [1-4].

However, it has been demonstrated that even the most advanced coal cleaning processes often fail to reject 90-95% pyrite. The major reasons are [5]:

(1) superficial oxidation of pyrite *via* corrosion-type electrochemical processes that occurs during mining, transportation and preparation. Oxidation processes produce hydrophobic species on pyrite surfaces which induce its collectorless flotation.

(2) incomplete liberation of pyrite from coal, i.e., coexistence of pyrite and coal in middling particles. This naturally leads to lower recovery when

middling particles report to tailings or reduced grade when they go to the froth product.

(3) hydraulic entrainment within the liquid films between air bubbles in the froth. This particle recovery mechanism is nonselective and controlled by the hydraulic transfer of flotation pulp into the froth product. Hydraulic entrainment is particularly prominent with feeds containing large quantities of ultrafine particles.

(4) nonselective entrapment of particles trapped between hydrophobic particles attached to air bubbles. This mechanism can be an important recovery mechanism when the froth is highly mineralized, very dry at the top of froth and contains relatively large entrained particles.

It has been concluded [5] that pyrite rejection problems associated with the entrapment mechanism are relatively minor for most coal flotation systems. The solution to the second problem appears to be obvious: comminution of coal to a size at which the pyrite is fully liberated. Unfortunately, this approach is too costly for the coal industry to adopt because of the high energy required for comminution. It is believed that more realistic and cost-effective methods of enhancing pyrite rejection would be to control the hydrophobicity of pyrite and middlings, and to minimize hydraulic entrainment. For this to be possible, problems related to pyrite oxidation, hydraulic entrainment and middlings have to be addressed. Previous studies on these topics are summarized as follows.

1.2 Literature Review

1.2.1 Electrochemistry of pyrite oxidation and collectorless flotation

1.2.1.1 *Oxygen reduction on pyrite*

It is widely recognized [6] that pyrite oxidation occurs by mixed potential, corrosion-type electrochemical reactions where pyrite undergoes anodic oxidation and oxygen is simultaneously reduced to maintain overall charge neutrality. In contrast to the vast volume of literature on the anodic process of pyrite oxidation, the cathodic process, i.e., the reduction of oxygen, has received only limited attention.

Peters and Majima [7] reported polarization curves for oxygen reduction on pyrite, which exhibited a mass-transport limited current. However, there was not sufficient data to obtain kinetic parameters for oxygen reduction. Biegler, Rand and Woods [8] studied oxygen reduction on rotating mineral-pyrite electrodes in 1 *M* $HClO_4$ acid solutions in an effort to obtain detailed information on the characteristics of oxygen reduction on sulfide minerals, including pyrite. Their results indicated that in acidic solutions the first electron transfer step to form O_2^- is rate-determining, while in alkaline solutions the rates of subsequent steps, such as the formation of H_2O_2, become important.

Biegler [9] conducted a similar study of oxygen reduction in acid solutions with eight different synthetic and mineral pyrite specimens, which reportedly included n-type, n-type metallic and p-type samples. The shape of voltammograms, Tafel slopes and

electrocatalytic activities for oxygen reduction varied from sample to sample to some extent. The variations are attributed to trace impurities in pyrite samples. However, no correlation was observed between kinetic parameters for oxygen reduction and the semiconducting properties of pyrite.

Rand [10] extended the study of oxygen reduction to other sulfides including arsenopyrite (FeAsS), bornite (Cu_5FeS_4), chalcocite (Cu_2S), chalcopyrite ($CuFeS_2$), covellite (CuS), galena (PbS), pentlandite ($(Fe,Ni)_9S_8$), pyrite (FeS_2) and pyrrhotite ($Fe_{1-x}S$). He found that pyrite is the most active of the sulfides as a catalyst for oxygen reduction and the ranking of activity of iron-containing sulfides for oxygen reduction is consistent with their requirement for oxygen in flotation with xanthate collectors, which suggests that the rate of flotation of a given sulfide is determined by its ability to reduce oxygen.

Doo and Sohn [11] provided additional information for oxygen reduction on pyrite in acidic solutions by using d-c polarization and a-c impedance techniques. They reported that in the Tafel region above 0 V versus Standard Hydrogen Electrode (SHE, hereinafter), a single electron transfer process to form the superoxide (O_2^-) was the rate determining step and that the reaction was relatively independent of pH. Below 0 V, the diffusion of dissolved oxygen to form hydrogen peroxide was rate-determining. No comparative study has been done on this subject on mineral- and coal-pyrites.

1.2.1.2 *Anodic oxidation of pyrite*

The anodic half-cell reaction of pyrite oxidation has been extensively investigated. Figure 1.2 shows the E_h-pH diagram of the FeS_2-H_2O system obtained by Kocabag et al. [12]. The sulfur-containing products are H_2S and HS^-, S^o and SO_4^{2-} for regions below and above the domain of stability of pyrite, respectively. The iron component of pyrite exists in the form of ferric or ferrous hydroxide above the domain, and elemental iron below the domain. The E_h-pH diagram provides thermodynamic information on stable species under equilibrium conditions, but it does not suggest reaction mechanisms or kinetics.

Pyrite oxidation involves both iron component and sulfur component. While it is widely accepted [7, 13-16] that pyrite oxidation produces Fe^{2+} and Fe^{3+} in acidic solutions, $Fe(OH)_2$ and $Fe(OH)_3$ in alkaline solutions, the nature of the sulfur oxidation product is controversial. Significantly, it is believed that the sulfur oxidation product(s) generated under mildly oxidizing conditions is hydrophobic and can impart floatability to pyrite in the absence of conventional sulfide collectors [17-23], as has been observed with many other sulfide minerals [20-28].

Hamilton and Woods [13] conducted voltammetry on pyrite electrodes in a nitrogen atmosphere in a glove bag to study the surface oxidation. They reported that a monolayer of elemental sulfur was formed at pH 9.2 and 13 and multilayers at pH 4.6. Peters [15] concluded that oxidation of pyrite to sulphate requires high overpotentials and occurs at significant rates only at potentials at which elemental sulfur is also a product.

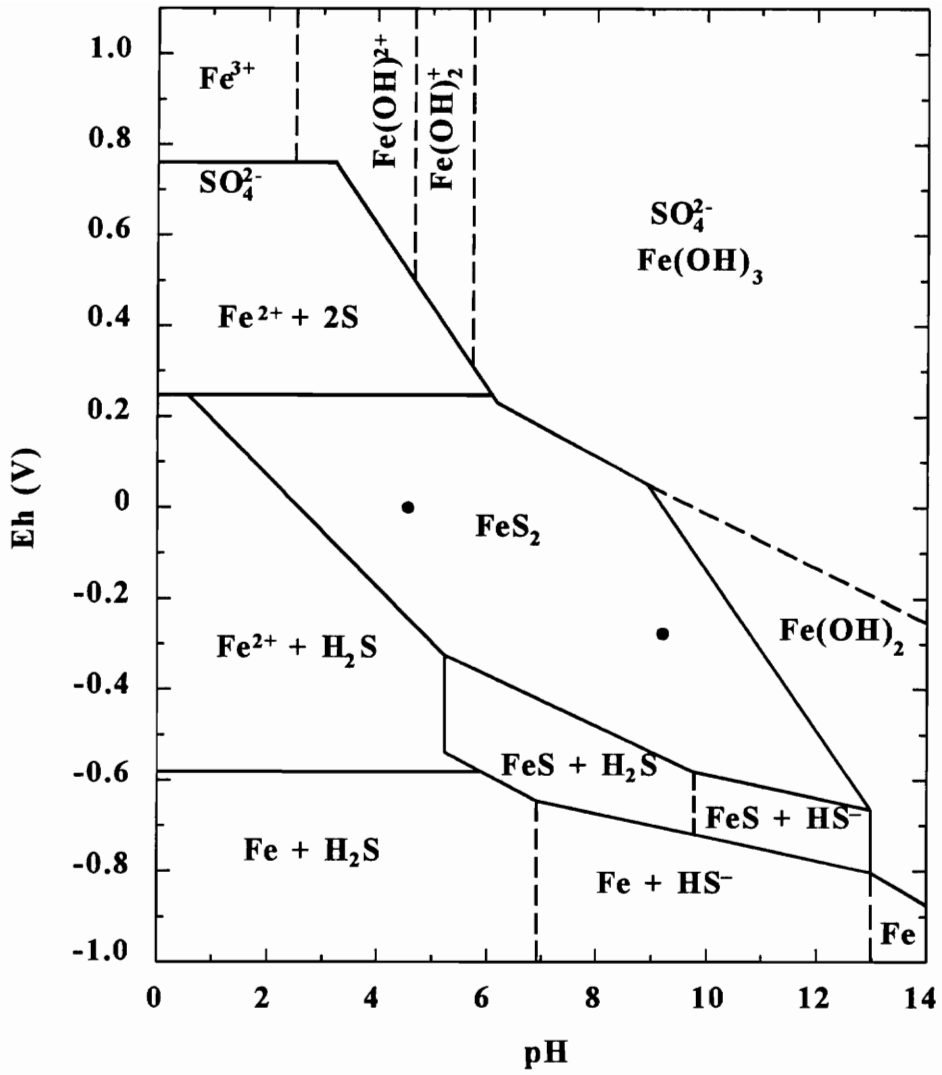

Figure 1.2 E_h-pH diagram for Fe-S-H_2O system at 298 K and 10^{-5} M [12]. Two points in the middle of stability domain were obtained in this study and will be discussed in Chapter 2.

Peters [14] later observed the formation of elemental sulfur from pyrite oxidation at low overpotentials in acidic solutions. Heyes and Trahar [23] also suggested that elemental sulfur is the likely product of pyrite oxidation.

However, there is ample evidence that pyrite oxidation does not produce elemental sulfur. Yoon et al. [17], Zhu et al. [29], and Mycroft et al. [30] suggested that polysulfides (FeS_n, $n>2$) are the more likely oxidation products. Woods et al. [31, 32] studied the oxidation of high concentrations of HS^- ions on gold and sulfide minerals, and identified polysulfide ions as intermediates in the formation of elemental sulfur. On the other hand, Buckley and Woods [33, 34] and Buckley et al. [35] concluded, from studies by voltammetry and XPS spectroscopy, that a metal-deficient sulfide($Fe_{1-x}S_2$, $x<1$) results from pyrite oxidation. It is believed that the metal atoms removed from pyrite lattice during oxidation lead to the formation of an overlayer of iron hydroxy-oxide in alkaline solutions, and the formation of soluble cations in acidic solutions [23]. The removal of metal component leaves sulfur in its normal lattice sites, thereby producing a metal-deficient layer underneath the iron hydroxy-oxide.

At higher potentials, pyrite is oxidized directly to sulfate [16, 36]. While elemental sulfur can be further oxidized to sulfate, this process is extremely slow at room temperature [16].

Mishra and Osseo-Asare [37] provided more details of pyrite oxidation by considering its semiconducting properties. They proposed that the initial step in pyrite oxidation is the electrocatalytic electroadsorption of OH^- on pyrite due to the presence

of Fe 3d electrons in the upper portion of the valence band. The adsorbed OH^- ions are then oxidized to OH by holes on Fe 3d states. This process is followed by the transfer of OH to S_2^{2-} sites. Preferential release of Fe^{2+} from the pyrite lattice takes place subsequently, resulting in the formation of thiosulfate ($S_2O_3^{2-}$). Thiosulfate either rapidly decomposes to elemental sulfur and bisulfite (HSO_3^-) or further oxidizes to sulfate (SO_4^{2-}) at higher potentials. This mechanism is unique in that it explains why acidic and high temperature conditions are favorable for the formation of elemental sulfur and the maximum theoretical yield of elemental sulfur is 50%.

There is also a great deal of inconsistency on the dissolution preference of sulfur and iron components in pyrite during oxidation. The literature on this aspect can be grouped into two distinct categories:

1. Preferential removal of iron. In this mechanism, it is believed that the oxidation of pyrite takes place preferentially on the iron sites. As a result, iron is released into the solution. The sulfur left behind in the reacted layer forms elemental sulfur, polysulfides or metal-deficient sulfides, as mentioned above. Released iron either exists as soluble ions in solution or precipitates on the mineral surface as hydroxide, depending on the solution pH.

2. Preferential dissolution of sulfur. In this reaction mechanism, it is assumed that the sulfur component in pyrite oxidizes first and leaves the surface as a sulfoxy anion [38]. Hydroxide ions then react with iron sites to form a reacted layer of iron hydroxide.

Chander and Briceno [39] and Chander [40] studied the kinetics of pyrite

oxidation and growth characteristics of the surface oxidation film using cyclic voltammetry and a-c impedance measurements. They proposed that the unreacted pyrite is adjacent to a sulfur-rich layer which is covered by precipitated iron hydroxide/oxide. The metal hydroxide/oxide film grows either perpendicular to the interface, giving rise to multilayers, or parallel to the surface, leading to a patchwise distribution [39, 40]. When the iron hydroxide is removed by complexation and dissolution, strong collectorless flotation of pyrite can be observed [18, 19].

For most practical purposes, a good understanding of the conditions under which the hydrophobic entity is produced is more important than a knowledge of the precise nature of this species. Voltammetry is the method most commonly used to identify the oxidation/reduction reactions on pyrite [13, 18, 30, 41-44]. The voltammetry curve or voltammogram shows the correlation between current and potential obtained by sweeping the potential from one limit to the other. The process in which potential varies from higher to lower values is called the cathodic sweep and the opposite process is referred to as the anodic sweep. The anodic and cathodic peaks on the voltammogram are generated by oxidation and reduction reactions occurring during the anodic and cathodic sweeps. Valuable information on the specific reaction can be derived from the peak position and other properties related to the peak. Numerous reactions have been postulated for oxidation and reduction processes on pyrite in aqueous solutions, unfortunately, without convincing verification in most cases.

Janetski et al. [44] observed an anodic peak at -0.05 V and a cathodic peak at -0.3

V on the voltammogram of pyrite obtained at pH 9.2. These peaks were attributed to the oxidation and reduction between $Fe(OH)_2$ and $Fe(OH)_3$. This interpretation was based on the observation that the shape of voltammograms on pyrite in pure borate solutions and the potentials at which the peaks appear are similar to those on gold in borate solutions saturated with ferrous iron. It was determined by integration of the charge passed on a potential cycle that the oxide layer on a pyrite surface freshly ground in open air was 2.5 nm thick, under the assumption that the structure of the layer approximates that of Fe_2O_3. Zhu et al. [29, 43] attributed the anodic peak at 0.10 V and the cathodic peak at -0.4 V to oxidation/reduction processes involving the $Fe(OH)_2/Fe(OH)_3$ couple. They reported that charges associated with the anodic and cathodic peaks were about the same and independent of scan rate. The shift in peak positions may have been caused by the different potential ranges used.

Mitchell and Woods [45] analyzed oxidation layers on pyrite surfaces by means of X-ray emission spectroscopy and voltammetry. They found that the ferric hydroxide coverage on pyrite surface determined from the charge passed during the anodic oxidation is "in good agreement with the value obtained from the X-ray emission spectroscopy." They thus supported the conclusion of Janetski et al. [44]. They believed that this result rules out the possibility that the anodic oxidation peak at -0.05 V involves oxidation of the mineral itself. However, careful examination of their data reveals that the quantities of oxides on three pyrite electrodes calculated from the integrated charges are 38, 32, and 18% larger than those determined from X-ray

emission measurements. This may, in fact, indicate that the anodic oxidation involves species other than iron hydroxide, probably pyrite itself whose oxidation contributes additional current.

Hamilton and Woods [13] and Buckley et al. [35] observed an anodic peak at 0 V and a cathodic peak at -0.3 V at pH 9.2 on the first voltammogram. These peaks were present even when the surface was prepared under a nitrogen atmosphere and, therefore, should be free of iron oxide at the commencement of the potential sweep. They assigned the anodic peak to the oxidation of pyrite itself to elemental sulfur and ferric hydroxide. The cathodic peak was believed to correspond to the reduction of ferric to ferrous hydroxide and the combination of ferric hydroxide with elemental sulfur to form FeS. Pang and Chander and his co-workers [46, 47] observed that the oxidation peak at -0.09 V on pyrite voltammogram was quite broad. They resolved it into two distinct peaks in carbonate solutions and EDTA (ethylene diamine tetraacetic acid, disodium salt) solutions. The oxidation of both ferrous and sulfur species was believed to contribute to the anodic current. However, the sulfur species was not identified in these studies.

It is noticed that the potential range used in a number of previous studies extended as far as -1.0 V to 1.0 V (SHE) [18, 29, 43]. Under such a condition, it is very doubtful that the results can be used to explain or predict the flotation behavior of pyrite since oxidation and reduction reactions at extremely high potentials (positive or negative) could completely and irreversibly alter the pyrite surface. In this case, the voltammetric response observed no longer represents that of pyrite. For example, it was observed in

these studies that the formation of hydrophobic species occurred at potentials above 0.7 V [29], which apparently is not in agreement with the collectorless flotation results of pyrite showing the onset potential of -0.1 V [17].

Different electrode preparation techniques have been used in different studies, contributing to the inconsistence reported in literature. XPS and voltammetry studies [34, 35] have shown that the electrochemical behavior of a freshly fractured pyrite surface differed significantly from that of a surface prepared by polishing in air. The open circuit potential for the fractured surface is close to that for the surface prepared by grinding in the absence of oxygen, indicating that little surface oxidation of the fracture surface has taken place. However, the open circuit potential for the surface ground in air is 0.2 V more positive, and the resulting cathodic potential sweep shows a cathodic peak due to the reduction of the surface oxidation products. It is believed that grinding in air produces iron oxide and sulfur oxidation species. Chmielewski and Wheelock [42] obtained a similar conclusion. Richardson and Yoon [48] compared the semiconducting behavior of abraded and fractured sulfide electrodes. They reported a substantial decrease in the photocurrent of pyrite electrodes caused by abrasion. It was believed that abrasion generated lattice defects. Thus, *in-situ* fractured pyrite electrodes appear to be more appropriate to the investigation of superficial oxidation.

1.2.1.3 *Comparison of electrochemistry of coal- and mineral-pyrite*

Coal-pyrite has been shown to significantly differ from mineral-pyrite in many

aspects, such as morphology, surface properties and reaction rates [49]. Ogunsola and Osseo-Asare [50] first reported that the electrochemical behavior of coal-pyrite is affected by heterogeneity and morphological variations. They observed only one peak at about 0.25 V on the anodic polarization curves in the range of 0.1 to 0.75 V, which is in contrast with two peaks observed at 0.06 and 0.25 V for mineral-pyrites. The rest potentials of coal-pyrites containing more impurities such as quartz and iron sulphate are more positive than that of relatively pure pyrite. They also suggested that organic acids formed by the oxidation of coal could render coal-pyrite more noble by the formation of strong non-porous film such as β-$FeC_2O_4 \cdot 2H_2O$ on the pyrite surface.

Briceno and Chander [51] noticed large difference in charge transfer resistance between coal- and mineral-pyrites determined by a-c impedance measurements. They proposed that an oxide layer is initially formed only on mineral-pyrite surface during sample preparation which acts as a passivating film. The corrosion potential is 0.15 V for mineral-pyrite at pH 9.3, whereas it is -0.3 V for the coal-pyrite from a Lower Kittanning coal seam. This finding indicates that coal-pyrite is more reactive than mineral-pyrite.

Wang et al. [52] concluded that high carbon content ($>3\%$) coal-pyrite behaves more like a coal/carbon material than pyrite itself and the surface oxidation rate of this type of pyrite is considerably lower than pure pyrite. Lai et al. [53] observed drastic differences in the flotation response and in voltammograms obtained with coal- and mineral-pyrite samples. They also established that coal-pyrite is not electroactive towards

oxygen reduction. Zhu et al. [43, 54] demonstrated that coal-pyrite exhibited fewer anodic and cathodic peaks on voltammograms than mineral-pyrite and that current densities on coal-pyrite could be 10 to 100 times higher than mineral-pyrite.

All these results suggest that coal-pyrites possess unique characteristics, and further study on this subject is warranted. A comprehensive understanding of coal-pyrite electrochemistry is particularly important for the development of new techniques to improve coal-pyrite rejection in flotation.

1.2.2 Galvanic coupling and floatability of pyrite

1.2.2.1 *Galvanic coupling*

When two different electrodes are in electronic and electrolytic contact, electron transfer from one to the other may occur. This behavior is referred to as galvanic coupling (or galvanic interaction). The electron movement between electrodes gives rise to the galvanic current. Galvanic coupling arises from the different electrochemical reactivities of the electrodes represented by their rest potential. The electrode with more positive (noble) rest potential will act as a cathode, drawing electrons from the other electrode that possesses a more negative (active) potential, which is called the anode. The anode accelerates the dissolution by releasing electrons and is thus sacrificed. In contrast, the cathode is protected from oxidation or dissolution due to decreased potential by excess electrons. The electrons at the cathode is consumed by a reduction process,

usually oxygen reduction. Galvanic coupling has been widely used in materials engineering to prevent metal corrosion by connecting an object to be protected with a more active metal such as magnesium, zinc, aluminum or their alloys. The same technique can be applied to semiconductor sulfide minerals.

Rest potentials of sulfide minerals in aqueous solutions have been determined by a number of investigators [39, 55-57]. Pyrite is found to be electrochemically most noble in the thermodynamic sense. Its rest potential is 0.66 V at pH 4 [55], 0.43 V at pH 6, and 0.34 V at pH 9.2 [56]. When pyrite is in electrochemical contact with another sulfide mineral or metal, it becomes a cathode to which electrons flow from the anode. This lowers the potential at pyrite, making it more reducing. Previous studies have shown that galvanic coupling between sulfide minerals themselves and between sulfide minerals and grinding media has a pronounced effect on their flotation response.

Majima [55] reported that galvanic coupling between pyrite and galena, chalcopyrite and sphalerite in a sulfuric acid solution of pH 2 led to the increased production of elemental sulfur on galena, chalcopyrite and sphalerite and promoted their flotation. Nakazawa and Iwasaki [58] used Auger electron spectroscopy, XPS, and scanning electron microscopy to study the effect of pyrite-pyrrhotite contact on their floatabilities, and concluded that the formation of hydroxide and sulfate species of iron on pyrrhotite decreased, whereas that on pyrite increased when these minerals were held in contact. Similar behavior was observed with nickel arsenide and pyrrhotite in contact, in which case the former acted as the anode and the latter as the cathode [59].

Rao and Finch [56] investigated the effect of N_2 and O_2 on galvanic interactions between pyrite, chalcopyrite, galena and sphalerite. They showed that galvanic coupling is stronger in the presence of dissolved O_2. The adsorption of xanthate on pyrite is reduced upon its contact with other sulfides in oxygenated solution and this effect is less significant by the introduction of N_2 at the adsorption stage which weakens galvanic coupling.

Galvanic coupling between sulfide minerals (pyrite, pyrrhotite, galena, chalcopyrite and sphalerite) and grinding media has also been investigated [60-64]. It was revealed that floatability of these minerals were adversely affected due to the formation of iron hydroxide on the surface of minerals that are all more noble than grinding media and, therefore, act as the cathode. Pozzo et al. [64] extended the study of galvanic coupling to a two-sulfide/grinding media system. They proposed that the noblest electrode will act as the cathode, whereas the grinding media will always function as the anode. The other sulfide is expected to exhibit an intermediate cathodic or anodic behavior depending on its rest potential, relative position with respect to the main cathode and the main anode, and the polarization characteristics of the electrodes.

In an interesting study on the effect of galvanic interaction on the behavior of the froth phase, Van Deventer et al. [65] observed that the galvanic interaction between a complex sulfide ore and added metallic iron powder generated a stable, well drained froth which gave rise to improved copper recovery and copper-lead selectivity in flotation by xanthates. It is believed that galvanic interaction preferentially reduced floatabilities of

iron-bearing minerals which would otherwise destabilize the froth phase due to bubble-overloading.

1.2.2.2 *Collectorless flotation of pyrite*

Chernosky [66] studied the flotation characteristics of mineral- and coal-pyrites in the absence of conventional collectors for sulfides. No collectorless flotation of mineral-pyrite was observed while coal-pyrite showed a recovery of 20% when pH > 6.5. Rao et al. [20] reported similar results. They also demonstrated that collectorless flotation of pyrite increased with aeration time at pH 9.2 and decreased with aeration time at pH 6.6. In contrast, Kawatra et al. [67] showed that mineral pyrite was very floatable at pH < 2.5 but lost its natural floatability almost completely at pH > 5.0. Coal-pyrite maintained essentially constant flotation recovery (31-43%) over the pH range of 2.2 to 8.8.

Fuersteau et al. [68] attributed the differences in sulfide floatabilities obtained by various investigators to the oxygen contents of the system. They developed an apparatus in which an atmosphere containing less than 10^{-6} mole fraction oxygen and water containing less than 5 ppb oxygen could be maintained. They reported that chalcocite, chalcopyrite, galena, sphalerite and pyrite exhibited natural flotation.

Oblad [69] performed flotation tests on various size fractions of mineral- and coal-pyrite. By examining flotation products and tailings under a microscope, he found that nearly all the particles that floated had small amounts of coal attached to the surface.

Kocabag et al. [12] suggested that pyrite may be hydrophobic enough to float in a mineral/oil (isooctane)/water system but not in a mineral/vapor/water system. Yoon et al. [17] concluded that the collectorless flotation of pyrites is determined by the relative abundance of hydrophobic sulfur species and hydrophilic iron hydroxides on the surface, which is dependent on pH, E_h, and oxidation time. They also reported that the hydrophobicity of pyrite is considerably enhanced by the presence of oily collectors of coal, which is confirmed in the most recent study performed by Jiang et al. [70].

As mentioned previously, the collectorless flotation of pyrite arises from superficial oxidation which produces hydrophobic species on the surface. Fe^{2+} and Fe^{3+} are preferentially released into the solution and then precipitated as hydroxides [33, 34, 37, 46, 47], forming outer layers on pyrite. Pang [19] and Chander and Briceno [39] indicated that mild abrasion between particles due to stirring in flotation cells may be sufficient in removing these layers. In fact, pronounced flotation of pyrite has been observed by various investigators in the presence of an iron chelating agent, EDTA [18, 19, 71, 72]. It is believed that EDTA dissolves hydrophilic iron hydroxide on the surface and thereby exposes the underlying sulfur-rich layer. Chander [40] reported flotation response of pyrite and chalcopyrite with the addition of quartz to the solution. The collectorless flotation recovery of these minerals increased significantly when they were conditioned with quartz, presumably due to the precipitation of some iron hydroxide on quartz rather than on pyrite or chalcopyrite.

1.2.3 Froth phase and hydraulic entrainment in flotation

1.2.3.1 *Flotation froth*

Froth in flotation cells is thermodynamically unstable and bubbles tend to contract and combine with each other to reduce the total interfacial area in the system. This process proceeds through liquid drainage from lamellar regions into Plateau borders. When the lamellar layer reaches a critical thickness of 5 to 15 nm, bubble coalescence occurs since the liquid film can no longer support the pressure of the gas in the bubble.

The processes occurring in the froth give rise to the "secondary cleaning" of flotation. Froth drainage removes particles not strongly attached to the bubble surface; froth coalescence introduces shocks and reduces bubble surface area, both of which cause weakly attached particles to detach from the bubble films. Froth can be made to last minutes, days, or even months by manipulating viscosity of the liquid phase and surface viscosity of bubbles that retard liquid drainage from between bubble interfaces and electrostatic and steric repulsions between adjacent interfaces that prevent bubbles from approaching each other.

The froth phase was described mathematically by Arbiter and Harris [73] who assumed it to be a perfectly mixed phase. This perfectly mixed concept is generally recognized to be applicable to mechanically agitated flotation cells. Cooper [74] first used the plug flow concept to describe the variation of froth grade with height. Moys [75] developed a detailed model for the froth phase based on this concept and correlate

it with data obtained in a cell in which plug-flow conditions existed. The plug flow concept has proven most useful in the modelling of the behavior of the froth phase in flotation columns in which uniaxial transport is dominant [76] and has gained considerable attention due to increased interest in column flotation. Yianatos et al. [77] identified that the column froth zone consists of three regions, i.e., (1) an expanded bubble bed (next to the froth-pulp interface), (2) a packed bubble bed above that, and (3) a conventional draining froth above the wash water inlet.

1.2.3.2 *Froth stability*

A froth phase in flotation cells that possesses appropriate stability is essential to achieve satisfactory separation performance. Too stable a froth is difficult to handle and results in unwanted hydraulic entrainment of particles while an unstable froth can not successfully carry attached hydrophobic particles to the froth product.

Effects of flotation operating parameters on froth stability have been investigated by a number of authors. Szatkowski [78] concluded that the coalescence of bubbles at the pulp-froth interface and in the lowest part of the froth enhances gangue rejection. In coal flotation, the rate of ash rejection was fairly high and most of the froth upgrading action occurred within the initial 1-3 cm of the froth height. He also showed that higher froth residence time yields higher concentrations of ash at all levels of the froth by reducing ash drainage.

Finch et al. [79] studied the influence of wash water on the stability of two-phase

column froth and showed that wash water can stabilize the froth providing bias rate $J_b > 0.1$ cm/s. Moys [80] showed that the increase in gas rate would result in more stable froth and higher water recovery based on the work with several minerals. Feteris et al. [81] and Engelbrecht and Woodburn [82] demonstrated that froth stability is also dependent on the height (depth) of froth zone. Froth would eventually collapse with increasing height due to liquid film thinning by drainage. Smaller bubble size is very helpful in improving flotation rate constant but Moys [80] concluded that it could deteriorate the separation efficiency by entraining more water.

1.2.3.3 *Effects of mineral particles on froth stability*

The presence of solid particles, incorporated within the froth structure, has a profound effect on the characteristics of the froth and its stability. This effect depends on many factors associated with particles. They include particle size, hydrophobicity, shape, concentration in solution, etc.

Szatkowski and Freyberger [83] observed that quartz particles in three size fractions, i.e., +20 μm, -20+10 μm and -10 μm, rendered fine bubbles (10-100μm) to be more resistant to coalescence and promoted the production of the stable froth. Klassen and Mokrousov [84] reported that more hydrophobic particles had greater effects on stabilizing the froth. Only coarse particles were considered to be able to act as buffers between bubbles and prevent bubble coalescence, consequently strengthening the

stability of the froth [85]. Studies carried out by Lovell [86] on apatite and calcite showed that the froth produced in the presence of tall oil fatty acid could be destabilized by both minerals of lower concentrations in the pulp and stabilized at higher solids concentrations.

Johansson and Pugh [87] investigated the effects of particle size and hydrophobicity on the stability of froths with methylated quartz samples. They concluded that particles of intermediate hydrophobicity (corresponding contact angle $\theta \approx 65°$) would enhance froth stability but more hydrophobic particles ($\theta > 90°$) would destabilize the froth. More hydrophilic particles ($\theta < 40°$) would not influence the froth properties. By recording artificial thinning process of water film with high-speed cinematography, Dippenaar [88] performed a detailed study of the role in determining froth stability played by hydrophobicity of solid particles, the shape of the particles, particle roughness and size, the type of frother, etc. He found that highly hydrophobic particles (contact angles greater than 90°) have froth breaking ability due to facilitated thinning of interbubble liquid bridged by the particle. This result is in agreement with the study of Johansson and Pugh [87]. He concluded that the liquid lamellae separating bubbles has to be thinned to half the diameter of a particle or less before it can be ruptured by the particle. This suggests that smaller particles are more powerful than larger particles in destabilizing froths, which was confirmed in his experiments. With moderately hydrophobic particles (e.g., cubic galena particles with a contact angle of about 74°), stabilization or destabilization of froth could occur depending on the orientation of the

cleavage plane. Stable films were formed when the cleavage plane formed a smooth regular arrangement along the interface and allowed easy movement of the three-phase contact. However, film rupture occurred as soon as the bubble bridged both surfaces of the film regardless of the value of contact angle. Dippenaar [89] also demonstrated that although the froth stability can be drastically reduced by the presence of a relatively small number of hydrophobic particles, a large number of small particles could stabilize froth by forming a closely packed monolayer which prevents the particles from being forced out of the film and prevents the interfaces from touching.

Engel and Smitham [90] investigated the stability of froths produced in a coal flotation process and has revealed that increased froth stability occurs as the size distribution of the feed material is made finer. Coals of higher rank generate froths with exceptional stability and the volume and stability of the product froths decreases as coal rank decreases. In the presence of collector, froth stability is determined solely by particle size.

1.2.3.4 *Froth profile*

Particles that are collected by bubbles in the pulp and carried into the froth phase may drop back into the pulp because of the continuous drainage of liquid and bubble coalescence. Hydrophilic or relatively less hydrophobic particles are more likely to detach from the surface of bubbles, leading to the cleaning action in the froth. Consequently, the grade of particles in the froth is a function of froth height.

Moys [91] observed a steady increase in the grades of valuable minerals and a decrease in the gangue grade with increasing froth height. Cutting [92] made the similar observation of the rougher cell floating sulfide minerals in a pilot plant. Using a specially designed column-like flotation machine, Szatkowski [78] examined changes in ash content of the froth along the froth zone during coal flotation. He demonstrated that although the overall effect of froth formation on ash content profiles is similar to that observed with minerals [75, 93-95], the rate of froth upgrading differs. The coal flotation froth showed faster upgrading action.

Moys [91] reported that in the flotation of sulfide minerals, gangue rejection occurs in the region of 10-20 cm from the bottom of the froth phase. Also with sulfide minerals, Cutting et al. [94] observed a region of gangue rejection that extends from the pulp-froth interface to 10 cm up. In contrast, Szatkowski [78] found that the major cleaning action of froth in coal flotation takes place at lower region in the froth (1-3 cm above the interface). Yianatos et al. [96] conducted the study of the hydraulic entrainment of fine particles with the impulse and response tracer technique in a flotation column and showed that this action occurs close to the interface (< 10 cm) at moderate superficial gas velocity (< 1 cm/s).

1.2.3.5 *Hydraulic entrainment*

Particle collection takes place in fine particle flotation either by true flotation or entrainment. True flotation is accomplished by attaching particles to bubble surfaces.

Entrainment is the process by which particles, including pyrite particles, enter the base of a flotation froth and are transferred up and out of the flotation cell suspended in the water between bubbles. The true flotation rate of particles is principally determined by their hydrophobicity and is chemically selective in nature while entrainment is nonselective and plays an adverse role in separation of particles. Entrainment was found to be closely related to the froth stability. The higher the water recovery, i.e., the wetter the froth, the higher the proportion of gangue and the lower the concentrate [97]. To achieve maximum separation of particles of differing hydrophobicity, hydraulic entrainment should be minimized.

Jowett [98] carried out small-scale continuous flotation tests on an artificial mixture of fluorite and quartz. His results showed that the free quartz concentration in the concentrate was linearly related to that in the flotation cell, but that the straight line did not pass through the origin. Englebrecht and Woodburn [82] studied flotation of a finely ground mixture of pyrite and silica. A linear relationship was shown to exist between gangue recovery and water recovery, above a minimum water recovery.

Johnson et al. [99] reported data from plants floating chalcopyrite from a siliceous gangue which indicates a direct correlation between the rates of recovery for gangue and water. Since they defined "recovery" as the rate of recovery into the concentrate rather than percentage recovery relative to the feed, the relationship appeared to be parabolic (convex). Bisshop and White [93] made similar observations with a number of gangue minerals. Trahar [100] performed careful batch flotation tests on quartz and quartz-

chalcopyrite mixtures and concluded that the recovery of ultrafines is directly proportional to the water recovery and the ratio is not affected by the presence of hydrophobic particles on the bubble surfaces in the froth.

Yianatos [96] reported that in a flotation column feed water is completely rejected at superficial gas rates of less than 1.5 cm/s with froth depths greater than 1 m. The effects of gas rate and froth depth on the entrainment are more significant than those of the bias rate. Yianatos et al. [76] studied and modelled selectivity in the froth zone of two industrial flotation columns (both are 12 m in height, one is 0.45 m square and the other 0.91 m square), in a molybdenite-cleaning circuit. Their results demonstrated that froths deeper than 1 m gave selective recovery of molybdenite which upgraded molybdenite by 10% to 15% absolute. Froths shallower than 0.5 m exhibited no cleaning action due to mixing caused by the addition of wash water.

1.2.4 Column flotation circuit configuration

Flotation circuits for mineral processing are generally composed of a combination of rougher, cleaner(s) and scavenger(s) and could be further complicated by flow splits and recycle flows back to the previous stage [101-105]. Although coal flotation circuits commonly use a single stage, i.e., rougher, there are a number of alternative circuits in practice using more than a single cell bank, especially in the treatment of metallurgical coking coal [106, 107]. Moreover, as the requirement for the production of super-clean

coal increases [108, 109], it appears worthwhile to consider alternative coal flotation circuits so that both high ash rejection and high sulfur rejection can be achieved while high combustible recovery can be maintained. In fact, multi-stage coal flotation circuits have been shown to be favored in treating poorly floatable coals [110]. Complicated coal flotation circuits have been proposed to produce ultra-clean coal containing less than 0.7% ash and to reduce the sulfur content of the coal concentrate [111-113].

The configuration of the flotation circuit is one of the most important factors affecting the performance of a flotation circuit for a given feed material. Optimization of a conventional flotation circuit includes two different aspects [105]. One is to demonstrate how many cells are required in a bank to produce a satisfactory residence time distribution of pulp within the bank, which has been addressed by Nesset [114] and others [105, 115-117]. The other is to decide how to interconnect banks to obtain the overall optimum performance of the circuit. Numerous approaches and mathematical models have been developed to optimize flotation circuits of conventional mechanic cells by means of modelling, simulation, synthesis, mathematical analysis, graphics, etc [101, 103-105, 110, 118-126].

Meloy [127] proposed that separation circuit optimization is governed by four independent functions: the criterion, feed, selectivity and the composition functions. Of all criterion functions used for circuit optimization, separation efficiency is the most common because the amount of misplaced material is a minimum at maximum technical efficiency. Jowett [128] suggested a graphic method to illustrate this concept.

Agar et al. [104] reached the same conclusion *via* a mathematical route and came up with three alternative criteria for the optimum flotation circuit:

- Add no material to the concentrate that is lower in grade than the feed to that stage.
- Maximize the difference in recovery between the valuable mineral and the gangue.
- Maximize the separation efficiency

They experimentally demonstrated that application of any of these three criteria generated similar results.

Numerical methods have been widely used to determine the best circuit configuration and optimal residence time distribution of particles in individual cells. Mehrotra and Kapur [124] optimized the mean residence time of mineral species in each flotation cell and obtained an optimal structure of flotation cells by direct search methods which, however, did not correspond to circuit configurations generally encountered in the industrial plant. King [121] developed the NIM simulator consisting of mass balance equations for mineral classes which were solved interactively to produce mineral class flow rates and flotation bank retention time. Similar work was done by Green et al. [129] using parametric programming and by Reuter et al. [130] using linear programming. Sutherland [105] simulated the flotation circuit at fixed overall circuit capacity and a given feed rate by varying the relative numbers of cells in the rougher, scavenger and cleaner stages as well as the amount of recycle from stage to stage. He

concluded that the separation efficiency of the flotation system is rather insensitive to circuit arrangement. Circuit performance is dependent on the flotation conditions and selectivity in the banks to a much greater extent.

Under linearity assumption that in a separation operation there is no particle-particle interaction effecting the probability of a particle to be selected for the product or waste stream, Meloy [131] introduced circuit analysis technique involving mathematically closed functions rather than matrices or numerical methods used by others to analytically study and optimize mineral processing circuits independent of feed. Using this technique, one can also readily reduce complex circuits to simple equivalent circuits that behave identically. Williams and Meloy [122] applied circuit analysis to the study of dynamic behavior of flotation cell banks. They concluded that the countercurrent circuits were better than the cocurrent ones because cocurrent circuits were oscillatory and required larger first cell; it also took longer time to reach steady-state. Williams and Meloy [126] presented a graphical technique for achieving feasible designs of simple separation circuits for the mineral, chemical, powder and process industries. They found that the number of stages the recycle stream is fed back may be greater than one.

Firth et al. [110] investigated a number of flotation circuits for the recovery of a poorly floatable coal by laboratory batch testing. They concluded that the best circuits were those which would allow a balanced distribution of collector between the coarse and fine size fractions were superior. They particularly recommended the reflotation of classified tailings circuit because it not only produced the optimum metallurgical

performance, it also was relatively stable to variations of pulp density and size distribution.

It is rapidly becoming a common practice to incorporate flotation columns into existing mechanical cell flotation circuits. However, few studies have been directed toward understanding the behavior of column flotation circuits. Castillo and Dobby [132] examined column circuit configuration for zinc sulfide flotation using data from a portable 2 t/day pilot plant. It was concluded that a three column cleaning circuit gave at least equivalent performance to a circuit with two columns and one bank of mechanical cells of similar capacity to one column. Their results indicated that wash water was not generally required when the column was used as zinc or copper cleaner scavenger. Subramanian et al. [102] demonstrated that columns can be used in rougher, scavenger and cleaner flotation stages based on pilot plant tests with a 11 cm diameter column cell.

1.2.5 Flotation processes for improving pyrite rejection

There are four general methods to achieve relatively high rejection of pyritic sulfur during coal flotation: (1) multiple flotation, (2) pyrite depression, (3) reverse flotation of pyrite, and (4) "grab and run."

The use of multiple stages of cleaner flotation can minimize pyrite recovery caused by nonselective hydraulic entrainment. In this technique, the coal froth product is diluted with fresh water and refloated several times. The dilution water reduces the

concentration of pyrite and other mineral matter in the flotation pulp and, therefore, lower the ratio of particles attached to bubbles to those entrained in liquids in froth phase. For most coals, approximately three stages of cleaner flotation are required to essentially eliminate the entrainment problem. However, multiple flotation is high in cost, complex in operation, and often not particularly effective [133].

Pyrite depression in coal flotation is a reasonable approach to removing pyrite. A number of pyrite depressants (mainly pH modifiers, oxidants, and reductants) have been examined for its pyrite depression effects [134]. However, these depressants are found to either have only marginal effect on pyrite depression or depress coal as well.

The process of reverse flotation of pyrite for coal desulfurization involves two stages. The first stage flotation is identical to conventional coal flotation with the purpose of removing the bulk of ash-forming minerals. The froth product is the feed to the second stage flotation where a coal depressant is added and pyrite is floated with a xanthate collector. The major problems associated with this process include high reagent (coal depressant) dosage, high cost, and low coal recovery [135].

The "grab and run" scheme is essentially a process that sacrifices coal recovery to obtain an acceptable sulfur content in product. In this method, a fraction of coal low in pyrite is floated under gentle operating conditions, i.e., starvation quantities of reagents, low air rate, low impeller speed, short flotation residence time, etc. This approach has been specially promoted by Aplan [136]. Apparently, this process may not be an ideal alternative due to a substantial loss of combustible material.

1.3 Research Objectives

The overall objective of the present study is to enhance pyrite rejection from coal in flotation. This will be achieved by developing a novel electrochemical technique to eliminate surface hydrophobicity of pyrite and minimizing entrainment in column flotation by properly manipulating the froth phase and circuit configuration.

In spite of the abundance of literature on pyrite oxidation, there is much controversy on the mechanisms and products of the surface oxidation of the mineral. More work is needed to understand the surface chemistry of pyrite, especially coal-pyrites, in aqueous solutions. Fundamental mechanisms of pyrite oxidation and conditions under which hydrophobic species are produced during oxidation have to be well identified if new schemes are to be devised for enhanced pyrite rejection from coal by flotation or other surface-related techniques. To address these deficiencies, electrochemical and spectroscopic techniques were employed to study mechanisms and kinetics of surface reactions of pyrite. Galvanic coupling was explored as a practical method to control the potential of pyrite and prevent its oxidation. The effectiveness of this technique to enhance pyrite rejection from coal was examined in various flotation tests.

The characteristic of the froth phase in column flotation of coal plays an important role in flotation performance. The stability of froth is closely related to the entrainment mechanism of particle recovery. Pyrite rejection can be improved by minimizing the

hydraulic entrainment in the froth in coal flotation. Studies were, therefore, carried out to establish effects of the key operating parameters of column flotation on three-phase froth stability and resultant flotation response. The data can be used for the design and operation of column flotation cells for fine particle processing to achieve maximum separation efficiency.

A number of column flotation circuits were experimentally examined with several coal samples and theoretically analyzed. The effect of circuit configuration was established on the overall circuit performance evaluated by separation efficiency and separation curves. The flotation circuits examined are composed of single stage, two stages, and three stages that are relatively common in the flotation industry.

1.4 Report Organization

Research conducted in the present study is reported in four separate, stand-alone chapters. Each chapter consists of an introduction, research objectives, experimental, results and discussion, and conclusions. The organization of this report is based on three major recovery mechanisms of pyrite in flotation: hydrophobicity (Chapters 2 and 3), hydraulic entrainment (Chapter 4), and middlings (Chapter 5).

Chapter 2 deals with surface reactions on pyrite in aqueous solutions at different pH's. The mechanisms and kinetics of oxygen reduction on pyrites were investigated as the cathodic half-cell reaction occurring during pyrite oxidation. This was performed on

rotating ring-disc electrodes in oxygen saturated solutions. Formation of possible soluble intermediate species of oxygen reduction can be directly detected by this technique. Incipient oxidation of pyrite itself was explored on fresh surfaces of pyrite created by *in-situ* fracturing electrodes under electrolytes. Rotating ring-disc electrodes were also used in an extensive study of various surface reactions on pyrite in moderate potential ranges. Mineral- and coal-pyrites were used in the study and their electrochemical behaviors were compared.

Self-induced hydrophobicity of pyrite and the electrochemical technique developed for pyrite depression are described in Chapter 3. Collectorless flotation of the mineral pyrite was investigated in an electrochemical-microflotation cell where potential is directly controlled by a potentiostat and a Patridge and Smith-type microflotation cell [137] in which pyrite potential was adjusted by the addition of oxidizing or reducing agents into the solution. Galvanic coupling process was explored as a practical method for the control of the potential of pyrite to prevent the formation of, and/or to remove, if already present, hydrophobic species on pyrite surface. Active metals such as manganese, zinc, iron, aluminum, and their alloys were tested as possible sacrificial anodes for cathodic protection of pyrite. The mechanism and effectiveness of this process was studied in a specially designed galvanic cell. The surface of pyrite altered by galvanic coupling was examined by cyclic voltammetry to reveal the influence of galvanic coupling on surface products. This technique was then applied to coal flotation in a microbubble column and a mechanic flotation cell to show its effect on pyrite

rejection.

Chapter 4 is dedicated to the study of froth behavior in column flotation to minimize the recovery of pyrite by nonselective entrainment. Column operating parameters were systematically examined for their effects on froth stability measured by water recovery. Dependence of ash recovery and combustible recovery on water recovery in the froth product was established to demonstrate the importance of entrainment in flotation. Particular efforts were made to identify the effects of solid particles on the stability of froth and understand factors determining their behavior. Froth cleaning action by liquid drainage and bubble coalescence was investigated by developing froth profiles under different conditions.

Chapter 5 focuses on column circuit configuration and its effect on separation efficiency. Six different column flotation circuits that are most likely to be adopted in the mineral processing industry are experimentally examined in an endeavor to improve the separation efficiency of middlings. They include single-stage, rougher-scavenger, rougher-cleaner, rougher-scavenger-scavenger cleaner, rougher-scavenger-cleaner, and rougher-cleaner-recleaner. Numerical circuit analysis techniques developed by Meloy [122] were employed to provide theoretical explanation for experimental results.

Finally, the summary and conclusions are provided in Chapter 6, and recommendations for future work in Chapter 7.

1.5 References

1. Luttrell, G.H., Adel, G.T., and Yoon, R.-H., 1988. "Hydrodynamics and mathematical modeling of fine coal flotation," *Proceedings of XVI International Mineral Processing Congress*, Ed. by E. Forssberg, Elsevier, Amsterdam, pp. 1791-1802.
2. Yoon, R.-H., 1993. "Microbubble flotation," *Minerals Engineering*, **6**(6), pp 619-629.
3. Levenspiel, O., 1972. "Chemical Reaction Engineering," John Wiley & Sons, Inc., New York, N.Y.
4. Yoon, R.-H., 1993. "Microbubble flotation," *Minerals Engineering*, **6**(6), pp. 619-630.
5. Luttrell, G.H. and Yoon, R.-H., 1992. "Methods for improving sulfur rejection in fine coal flotation circuits," in *Proceedings of the Coal Preparation '92 conference*, May 3-7, Cincinnati, Ohio.
6. Rand, D.A.J. and Woods, R., 1984. "E_h measurements in sulphide mineral slurries," *International Journal of Mineral Processing*, **13**, pp. 29-42.
7. Peters, E. and Majima, H., 1968. "Electrochemical reactions of pyrite in acid perchlorate solution," *Canadian Metallurgical Quarterly*, **7**, No.3, pp. 111-117.
8. Biegler, T., Rand, D.A.J., and Woods, R., 1975. "Oxygen reduction on sulfide minerals, part I, Kinetics and mechanism at rotated pyrite electrode,"

Electroanalytical Chemistry and Interfacial Electrochemistry, **60**, pp. 151-162.

9. Biegler, T., 1976. "Oxygen reduction on sulfide minerals, Part II, relation between activity and semiconducting properties of pyrite electrodes," *Journal of Electroanalytical Chemistry*, **70**, pp. 265-275.

10. Rand, D.A.J., 1977. "Oxygen reduction on sulfide minerals, part III. Comparison of activities of various copper, iron, lead and nickel mineral electrodes," *Journal of Electroanalytical Chemistry*, **83**, pp. 19-32.

11. Doo, S.G. and Sohn, H.-J., 1989. "Electrochemical reduction of oxygen on a pyrite surface," *Minerals and Metallurgical Processing*, November, 1989, pp. 201-205.

12. Kocabag, D., Shergold, H.L., and Kelsall, G.H., 1990. "Natural oleophilicity /hydrophobicity of sulfide minerals, II. pyrite," *International Journal of Mineral Processing*, **29**, pp. 211-219.

13. Hamilton, I.C. and Woods, R., 1981. "An investigation of surface oxidation of pyrite and pyrrhotite by linear potential sweep voltammetry," *Journal of Electroanalytical Chemistry*, **118**, pp. 327-343.

14. Peters, E., 1986. "Leaching of sulfides," in: *Advances in Mineral Processing*, Ed. by P. Somasundaran, SME-AIME, Littleton, CO, pp. 445-462.

15. Peters, E., 1977. "The electrochemistry of sulfide minerals," in: *Trends in Electrochemistry*, Ed. by J.O.M. Bockris, D.A.J. Rand and B.J. Welch, Plenum, N.Y., pp. 267-290.

16. Biegler, T. and Swift, D.A., 1979. "Anodic behavior of pyrite in acid solutions," *Electrochimica Acta*, **24**, pp. 415-420.

17. Yoon, R.-H., Lagno, M.L., Luttrell, G.H., and Mielczarski, J.A., 1991. "On the hydrophobicity of coal pyrite," In: *Processing and Utilization of high sulfur coals IV*, Ed. by P.R. Dugan, D.R. Quigley, and Y.A. Attia, Elsevier Science Publishers, Amsterdam.

18. Ahlberg, E., Forssberg, K.S.E., and Wang, X., 1990. "The surface oxidation of pyrite in alkaline solution," *Journal of Applied Electrochemistry*, **20**, pp. 1033-1039.

19. Pang, J. and Chander, S., 1992. "The effect of EDTA on collectorless flotation of pyrite," in: *Proceedings of the Third International Symposium on Electrochemistry in Mineral and Metal Processing*, Ed. by R. Woods, P.E. Richardson, The Electrochemical Society, Inc., Pennington, N.J., pp. 221-234.

20. Rao, S.R. and Finch, J.A., 1987. "Electrochemical studies on the flotation of sulfide minerals with special reference to pyrite-sphalerite II flotation studies," *Canadian Metallurgical Quarterly*, **26**(3), pp. 173-175.

21. Richardson, P.E. and Walker, G.W., 1985. "The flotation of chalcocite, bornite, chalcopyrite, and pyrite in an electrochemical-flotation cell," In: *Proceedings of the XVth International Mineral Processing Congress*, Cannes, **2**, pp. 198-210.

22. Walker, G.W., Walters, C.P., and Richardson, P.E., 1986. "Hydrophobic effects of sulfur and xanthate on metal and mineral surfaces," *International*

Journal of Mineral Processing, **18**, pp. 119-137.

23. Heyes, G.W. and Trahar, W.J., 1984. "The flotation of pyrite and pyrrhotite in the absence of conventional collectors," in: *Proceedings of International Symposium on Electrochemistry in Mineral and Metal Processing*, Ed. by P.E. Richardson, S. Srinivasan and R. Woods, The Electrochemical Society, Inc., Pennington, N.J., pp. 219-232.

24. Luttrell, G.H. and Yoon, R.-H., 1984. "Surface studies of the collectorless flotation of chalcopyrite," *Colloids and surfaces*, **12**, pp. 239-254.

25. Gardner, J.R. and Woods, R., 1979. "An electrochemical investigation of the natural floatability of chalcopyrite," *International Journal of Mineral Processing*, **6**, pp. 1-16.

26. Heyes, G.W., and Trahar, W.J., 1977. "The natural floatability of chalcopyrite," *International Journal of Mineral Processing*, **4**, pp. 317-344.

27. Kelebek, S. and Smith, G.W., 1989. "Collectorless flotation of galena and chalcopyrite: correlation between flotation rate and the amount of extracted sulfur," *Minerals and Metallurgy Processing*, **6**, pp. 123-129.

28. Buckley, A.N. and Riley, K.W., 1991. "Self-induced floatability of sulfide minerals: examination of recent evidence for elemental sulfur as the hydrophobic entity," *Surface and Interface Analysis*, **17**, pp. 655-659.

29. Zhu, X., Li, J., Bodily, D.M., and Wadsworth, M.E., 1992. "Transpassive oxidation of pyrite," in: *Proceedings of the Third International Symposium on*

Electrochemistry in Mineral and Metal Processing, Ed. by R. Woods, P.E. Richardson, The Electrochemical Society, Inc., Pennington, N.J., pp. 391-409.

30. Mycroft, J.R., Bancroft, G.M., McIntyre, N.S., Lorimer, J.W., and Hill, I.R., 1990. "Detection of sulfur and polysulphides on electrochemically oxidized pyrite surfaces by X-ray photoelectron spectroscopy and Raman spectroscopy," *Journal of Electroanalytical Chemistry*, **292**, pp. 139-152.

31. Hamilton, I.C. and Woods, R., 1984. "A voltammetric study of the surface oxidation of sulfide minerals," in: *Proceedings of International Symposium on Electrochemistry in Mineral and Metal Processing*, Ed. by P.E. Richardson, S. Srinivasan and R. Woods, The Electrochemical Society, Inc., Pennington, N.J., pp. 259-285.

32. Woods, R., Constable, D.C., and Hamilton, I.C., 1988. "A rotating ring disc electrode study of the oxidation of sulfur (-II) species on gold and sulfide minerals," in: *Proceedings of International Symposium on Electrochemistry in Mineral and Metal Processing*, Ed. by P.E. Richardson, and R. Woods, The Electrochemical Society, Inc., Pennington, N.J., pp. 113-130.

33. Buckley, A.N and Woods, R., 1984. "An X-Ray photoelectron spectroscopic investigation of the surface oxidation of sulfide minerals," in: *Proceedings of International Symposium on Electrochemistry in Mineral and Metal Processing*, Ed. by P.E. Richardson, S. Srinivasan and R. Woods, The Electrochemical Society, Inc., Pennington, N.J., pp. 286-302.

34. Buckley, A.N. and Woods, R., 1987. "The surface oxidation of pyrite," *Applied Surface Science*, **27**, pp. 437-452.

35. Buckley, A.N., Hamilton, I.C., and Woods, R., 1988. "Studies of the surface oxidation of pyrite and pyrrhotite using X-ray photoelectron spectroscopy and linear potential sweep voltammetry," in: *Proceedings of International Symposium on Electrochemistry in Mineral and Metal Processing*, Ed. by P.E. Richardson, and R. Woods, The Electrochemical Society, Inc., Pennington, N.J., pp. 234-246.

36. Bailey, L.K. and Peters, E, 1976. "Decomposition of pyrite in acids by pressure leaching and anodization: the case for an electrochemical mechanism," *Canadian Metallurgical Quarterly*, **15**(4), pp. 333-344.

37. Mishra, K.K. and Osseo-Asare, K., 1988. "Aspects of the interfacial electrochemistry of semiconductor pyrite (FeS_2)," *Journal of Electrochemical Society: Electrochemical Science and Technology*, **135**, pp. 2502-2509.

38. Goldhaber, M.B., 1983. "Experimental study of metastable sulfur oxyanion formation during pyrite oxidation at pH 6-9 and 30 °C," *American Journal of Science"*, **283**(3), pp. 193-217.

39. Chander, S. and Briceno, A., 1987. "Kinetics of pyrite oxidation," *Minerals and Metallurgical Processing*, **4, pp.** 171-176.

40. Chander, S., 1991. "Electrochemistry of sulfide flotation: growth characteristics of surface coatings and their properties, with special reference to chalcopyrite and

pyrite," *International Journal of Mineral Processing*, **33**, pp. 121-134.

41. Rao, S.R. and Finch, J.A., 1987. "Electrochemical studies on the flotation of sulfide minerals with special reference to pyrite-sphalerite I. cyclovoltammetry and pulp potential measurements," *Canadian Metallurgical Quarterly*, **26**(3), pp. 167-172.

42. Chmielewski, T. and Wheelock, T.D., 1990. "Some electrochemical aspect of pyrite hydrophobicity-Investigations on cleaved electrodes," *Journal of Mining and Metallurgy*, **26**(2), pp. 133-144.

43. Zhu, X., Wadsworth, M.E., Bodily, D.M., and Riley, A.M., 1991. "Surface properties of mineral and coal pyrite after electrochemical alteration," In: *Processing and Utilization of high sulfur coals IV*, Ed. by P.R. Dugan, D.R. Quigley, and Y.A. Attia, Elsevier Science Publishers, Amsterdam, pp. 205-222.

44. Janetski, N.D., Woodburn, D.A.J., and Woods, R., 1977. "An electrochemical investigation of pyrite flotation and depression," *International Journal of Mineral Processing*, **4**, pp. 227-239.

45. Michell, D. and Woods, R., 1978. "Analysis of oxidized layers on pyrite surfaces by X-ray emission spectroscopy and cyclic voltammetry," *Australian Journal of Chemistry*, **31**, pp. 27-34.

46. Pang, J. and Chander S., 1993. "Properties of surface films on chalcopyrite and pyrite and their influence in flotation," in *Proceedings of XVIII International Mineral Processing Congress*, Sydney, May 23-28, pp. 669-677.

47. Chander, S., Briceno, A., and Pang, J., 1992. "On the mechanism of sulfur oxidation in pyrite," *SME/AIME Annual Meeting*, Phoenix, Arizona, February 24-27, Preprint No. 92-240.

48. Richardson, P.E. and Yoon, R.-H., 1993. "A comparison of the semiconducting properties of abraded and fractured sulfide electrodes: pyrite and galena," in *Hydrometallurgy, Fundamentals, Technology and Innovation, Proceedings of the Milton E. Wardsworth (IV) International Symposium on hydrometallurgy*, pp. 101-117.

49. Esposito, M.C., Chander, S., and Aplan,F.F., 1987. "Characterization of pyrite from coal sources," in: *Process Mineralogy VII*, Ed. by A.H. Vassiliou, TMS/AIME, pp. 475-493.

50. Ogunsola, O.M. and Osseo-Asare, Kwadwo, 1986. "The electrochemical behavior of coal pyrite 1. Effects of mineral source and composition," *Fuel*, **65**, pp. 811-815.

51. Briceno, A. and Chander, S., 1988. "An electrochemical characterization of pyrites from coal and ore sources," *International Journal of Mineral Processing*, **24**, pp. 73-80.

52. Wang, X.-H., Jiang, C.L., Raichur, A.M., Parekh, B.K., and Leonard, J.W., 1992. "Comparative studies of surface properties of pyrite from coal and ore sources," in: *Proceedings of the Third International Symposium on Electrochemistry in Mineral and Metal Processing*, Ed. by R. Woods, P.E.

Richardson, The Electrochemical Society, Inc., Pennington, N.J., pp. 410-432.

53. Lai, R.W., Diehl, J.R., Hammack, R.W., and Khan, S.U.M., 1990. "Comparative studies of the surface properties and the reactivity of coal pyrite and mineral pyrite," *Minerals and Metallurgical Processing*, February, pp. 43-48.

54. Zhu, X., Wadsworth, M.E., Bodily, D.M., and Hu, W.B., 1991. "A comparative study of the electrochemical properties of mineral and coal pyrite," *EPD Congress 91*, Ed. by D.R. Gaskell, pp. 179-195.

55. Majima, H., 1969. "How oxidation affects selective flotation of complex sulfide ores," *Canadian Metallurgical Quarterly*, **8**(3), pp. 269-273.

56. Rao, S.R. and Finch, J.A., 1988. "Galvanic interaction studies on sulfide minerals," *Canadian Metallurgical Quarterly*, **2**(4), pp. 253-259.

57. Cheng, X. and Iwasaki, I., 1992. "Effect of chalcopyrite and pyrrhotite interaction on flotation separation," *Minerals and Metallurgical Processing*, pp. 73-79.

58. Nakazawa, H. and Iwasaki, I., 1985. "Effect of pyrite-pyrrhotite contact on their floatabilities," *Minerals and Metallurgical Processing*, November, pp. 206-211.

59. Nakazawa, H. and Iwasaki, I., 1986. "Galvanic contact between nickel arsenide and pyrrhotite and its effect on flotation," *International Journal of Mineral Processing*, **18**, pp. 203-215.

60. Pavlica, J.J. and Iwasaki, I., 1982. "Electrochemical and magnetic interactions in pyrrhotite flotation," *Trans of SME-AIME*, **272**, pp. 1885-1889.

61. Adam, K., Natarajan, K.A., and Iwasaki, I., 1984. "Grinding media wear and its effect on the flotation of sulfide minerals," *International Journal of Mineral Processing*, **12**, pp. 39-54.

62. Learmont, M.E. and Iwasaki, I., 1984. "Effect of grinding media on galena flotation," *Minerals and Metallurgical Processing*, **1**, pp. 136-142.

63. Yelloji, M.K. and Natarajan, K.A., 1989. "Effect of electrochemical interactions among sulfide minerals and grinding medium on chalcopyrite flotation," *Minerals and Metallurgical Processing*, August, pp. 146-151.

64. Pozzo, P.L., Malicsi, A.S., and Iwasaki, I., 1990. "Pyrite-pyrrhotite-grinding media contact and its effect on flotation," *Minerals and Metallurgical Processing*, February, pp. 16-21.

65. Van Deventer, J.S.J., Ross, V.E., and Dunne, R.C., 1993. "The effect of galvanic interaction on the behavior of the froth phase during the flotation of a complex sulfide ore," *Minerals Engineering*, **6**(12), pp. 1217-1229.

66. Chernosky, T.J. and Lyon, F.M., 1972. "Comparison of the flotation and adsorption characteristics of ore and coal-pyrite with ethyl xanthate," *Transactions of AIME*, March, pp. 11-14.

67. Kawatra, S.K. and Eisele, T.C., 1991. "Recovery of pyrite in coal flotation, entrainment or hydrophobicity," *Proceedings, SME/AIME Annual Meeting*, Denver, Colorado, February 25-28, Preprint 91-89.

68. Fuerstenau, M.C. and Sabacky, B.J., 1981. "On the natural floatability of

sulfide," *International Journal of Mineral Processing*, **8**, pp. 79-84.

69. Oblad, H.B., 1985. "The rate of pyrite recovery during coal flotation," *SME/AIME Fall Meeting*, Albuquerque, New Mexico, October 16-18, Preprint No. 85-427.

70. Jiang, C., Wang, X.H., Leonard, J.W. and Parekh, B.K., 1993. "On the natural and induced floatability of coal and pyrite," *Processing and Utilization of High Sulfur Coals V*, Ed. by B.K. Parekh and J.G. Groppo, Elsevier Science Publishers, Amsterdam, pp. 171-188.

71. Guy, P.J., and Trahar, W.J., 1985. "The effects of oxidation and mineral interaction on sulfide flotation," in: *Flotation of Sulfide Minerals*, Ed. by K.S.E. Forssberg, New York, Elsevier, pp. 91-110.

72. Shannon, L.K. and Trahar, W.J., 1986. "The role of collector in sulfide ore flotation," In: *Advances in Mineral Processing*, Ed. by P. Somasundaran, pp. 408-425.

73. Arbiter, N. and Harris, C.C., 1962. "Flotation kinetics," In: *Froth Flotation, 50th Anniversary Volume, AIME*, Ed. by D.W. Fuerstenau, pp. 215-246.

74. Cooper, H.R., 1966. "Feedback process model of mineral flotation. Part I. development of a model for froth flotation," *Trans. SME AIME*, **235**, pp. 439-446.

75. Moys, M.H., 1978. "A study of a plug-flow model for flotation froth behavior," *International Journal of Mineral Processing*, **5**, pp. 21-38.

76. Yianatos, J.B., Finch, J.A., and Laplante, A.R., 1988. "Selectivity in column flotation froths," *International Journal of Mineral Processing*, **23**, pp. 279-292.

77. Yianatos, J.B., Finch, J,A., and Laplante, A.R., 1986. "Holdup profile and bubble size distribution of flotation column froths," *Canadian Metallurgical Quarterly*, **25**(1), pp. 23-29.

78. Szatkowski, M., 1987. "Factors influencing behavior of flotation froth," *Trans. Instn. Min. Metall., Sec. C, Mineral Process. Extr. Metall.*, **96**, C115-122.

79. Finch, J.A., Yianatos, J., and Dobby, G., 1989. "Column froths," *Mineral processing and Extractive Metallurgy Review*, **5**, pp. 281-305.

80. Moys, M.H., 1989. "Mass transport in column froths," *Mineral Processing and Extractive Metallurgy Review*, **5**, pp. 203-228.

81. Feteris, S.M., Frew, J.A., and Jowett, A., 1987. "Modelling the effect of Froth depth in flotation," *International Journal of Mineral Processing*, **20**, pp. 121-135.

82. Engelbrecht, J.A. and Woodburn, E.T., 1975. "The effect of froth height, aeration rate and gas precipitation on flotation," *Journal of S. African Institute of Mining and Metallurgy*, **76**, pp. 125-132.

83. Szatkowski, M. and Freyburger, W.L., 1985. "Kinetics of flotation with fine bubbles," *Trans. Instn. Min. Metall., Sec. C*, **94**, C61-70.

84. Klassen, V.I. and Mokrousov, V.A., 1963. "An introduction to the theory of flotation," London, Butterworth.

85. Livshits, A.K. and Dudenkov, S.V., 1965. "Some factors in flotation froth

stability," in *Proceedings, VIIth Int. Proc. Longr Gordon and Breach*, New York, N. Y., pp. 597-621.

86. Lovell, V.M., 1976. "Froth characteristics in phosphate flotation," in *Flotation A. M. Gaudin Memorial Volume, I*, Ed. by M. C. Fuersteau, AIME, New York, N. Y., pp. 597-621.

87. Johansson, G., and Pugh, R.J., 1992. "The influence of particle size and hydrophobicity on the stability of mineralized froths," *International Journal of Mineral Processing*, **34**, pp. 1-21.

88. Dippenaar, A., 1982. "The destabilization of froth by solids, I. The mechanism of film rupture," *International Journal of Mineral Processing*, **9**, pp. 1-14.

89. Dippenaar, A., 1982. "The destabilization of froth by solids, II. The rate determining step," *International Journal of Mineral Processing*, **9**, pp. 15-27.

90. Engel, M.D. and Smitham J.B., 1988. "The relationship between coal particle size and hydrophobicity in the formation of particle-stabilised froths," *Australian IMM Bulletin and Processing*, **293**, pp. 63-66.

91. Moys, M.H., 1978. "A study of a plug-flow model for flotation froth behaviour," *International Journal of Mineral Processing*, **5**, pp. 21-38.

92. Cutting, G.W., 1989. "Effect of froth structure and mobility on plant performance," *Mineral Processing and Extractive Metallurgy Review*, **5**, pp. 169-201.

93. Bisshop, J.P. and White, M.E., 1976. "Study of particle entrainment in flotation

froths," *Trans. Instn. Min. Metall., (Sec. C, Mineral Process. Extr. Metall.)*, C191-194.

94. Cutting, G.W., Watson, D., Whitehead, A. and Barber, S.P., 1981. "Froth structure in continuous flotation cells: relation to the prediction of plant performance from laboratory data using process models," *International Journal of Mineral Processing*, **7**, pp 347-369.

95. Cutting, G.W., Barber, S.P. and Newton, S., 1986. "Effects of froth structure and mobility on the performance and simulation of continuously operated flotation cells," *International Journal of Mineral Processing*, **16**, pp. 43-61.

96. Yianatos, J.B., Finch, J.A., and Laplante, A.R., 1987. "Cleaning action in column flotation froths," *Trans. Instn Min. Metall. (Sect C: Mineral Process. Extr. Metall.)*, **96**, December, pp. C199-205.

97. Smith, P.G. and Warren, L.J., 1989. "Entrainment of particles into flotation froths," *Mineral Processing and Extractive Metallurgy Review*, **5**, pp. 123-145.

98. Jowett, A., 1966. "Gangue mineral contamination of froth," *British Chemical Engineering*, **2**, pp. 330-333.

99. Johnson, N.W., McKee, D.J., and Lynch, A.J., 1974. "Flotation rates of non-sulfide minerals in chalcopyrite flotation processes," *Trans. Am. Inst. Min. Pet. Eng.*, **256**, pp. 204-226.

100. Trahar, W.J., 1981. "A rational interpretation of the role of particle size in flotation," *International Journal of Mineral Processing*, **8**, pp. 289-327.

101. Green, J.C.A., 1984. "The Optimization of Flotation networks," *International Journal of Mineral Processing*, **13**, pp. 83-103.

102. Subramanian, K.N., Lonnelly, D.E.G., and Wong, K.Y., 1988. "Commercialization of a column flotation circuit for gold sulphide ore," *Column Flotation'88*, Ed. by K. V. S. Sastry, Society of Mining Engineers, Inc., Littleton, Colorado, pp. 13-18.

103. Reuter, M.A. and Van Deventer, J.S.J., 1990. "The use of linear programming in the optimal design of flotation circuits incorporating regrind mills," *International Journal of Mineral Processing*, **28**, pp. 15-43.

104. Agar, G.E., Startton-Crawley, R. and Bruce, T.J., 1980. "Optimizing the design of flotation circuits," *CIM Bulletin*, December, pp. 173-181.

105. Sutherland, D.N., 1981. "A study on the optimization of the arrangement of flotation circuits," *International Journal of Mineral Processing*, **7**, pp. 319-346.

106. Osborne, D.G., 1988. "Coal preparation technology," Graham & Trotman Limited.

107. Leonard, J.W., 1979. "Coal preparation," The American Institute of Mining, Metallurgical and Petroleum Engineers, Inc., pp. 10-75.

108. U. S. Department of Energy, 1987. "Energy information administration, international energy outlook 1987 projections to 2000," *DOE Report No. DOE/EIA-0484.*

109. U. S. Department of Energy, 1988. "Electric utility coal conversion market

analysis," *DOE Report No. DOE/DETC/TR-89/1(DE98003459)*.

110. Firth, B.A., Swanson, A.R., and Nicol, S.K., 1979. "Flotation circuits for poorly floating coals," *International Journal of Mineral Processing*, **11**, pp. 321-334.

111. Lynch, A.J., Johnson, N.W., Manlapig, E.V., and Thorne, C.G., 1981. "Mineral and coal flotation circuits: their simulation and control," Elsevier, Amsterdam, p. 13.

112. Miller, F.G., 1964. "Reduction of sulfur in minus 28 mesh bituminous coal," *Trans. SME/AIME*, **229**, pp. 7-15.

113. Miller, K.J., 1975. "Coal-Pyrite Flotation", *Trans. SME/AIME*, **258**, pp. 30-33.

114. Nesset, J.E., 1988. "The application of residence time distributions to flotation and mixing circuits," *CIM Bulletin*, November, pp. 75-83.

115. Mehrotra, S.P., 1988. "Design of optimal flotation circuits - a review," *Minerals and Metallurgical Processing*, August, pp. 142-151.

116. Jowett, A., 1961. "Investigation of residence time of fluid in froth flotation cells," *British Chemical Engineering*, **6**, pp. 254-258.

117. Kapur, P.C. and Mehrotra, S.P., 1974. "Estimation of the flotation rate distribution by numerical inversion of the Laplace transform," *Chemical Engineering Science*, **29**, pp. 411-415.

118. Davis, W.J.N., 1964. "The development of a mathematical model of the lead flotation circuit at the Zinc Corp. Ltd," *Proceedings of Australasian Institute of*

Mining and Metallurgy, **212**, pp. 61-89.

119. Agar, G.E. and Stratton-Crawley, R., 1982. "Bench scale simulation of flotation plant performance," *Bulletin of Canadian Institute of Mining and Metallurgy*, **75**, pp. 93-98.

120. King, R.P., 1975. "Simulation of flotation plants," *Trans. SME-AIME*, **258**, pp. 286-293.

121. King, R.P., 1976. "The use of simulation in the design and modification of flotation plants," *Flotation, Vol. 2*, Ed. by M.C. Fuerstenau, AIME, New York, pp. 937-961.

122. William, M.C. and Meloy, T.P., 1983. "Dynamic model of flotation cell banks-circuit analysis," *International Journal of Mineral processing*, **10**, pp. 141-160.

123. William, M.C., Fuersteau, D.W., and Meloy, T.P., 1986. "Circuit analysis-general product equations for multifeed, multistage circuits containing variable selectivity function," *International Journal of Mineral Processing*, **17**, pp. 99-111.

124. Mehrotra, S.P. and Kapur, P.C., 1974. "Optimal-suboptimal synthesis and design of flotation circuits," *Separation Science*, **9**, pp. 167-184.

125. Umeda, T., Hirai, A., and Ichikawa, A., 1972. "Synthesis of optimal processing system by an integrated approach," *Chemical Engineering Science*, **27**(IV), pp. 795-804.

126. Williams, M.C. and Meloy, T.P., 1991. "Feasible designs for separation

networks: a selection technique," *International Journal of Mineral Processing*, **32**, pp. 161-174.

127. Meloy, T.P., 1983. "Optimizing for grade or profit in mineral processing circuits-circuit analysis," *International Journal of Mineral Processing*, **1**, pp. 89-99.

128. Jowett, A., 1975. "Formulae for the technical efficiency of mineral separations," *International Journal of Mineral processing*, **2**, pp. 287-301.

129. Green, J.C.A., Meij, J.T., Du Plooy, A., and Van Heerden, P., 1985. "The use of inequalities in the design and optimization of complex chemical and metallurgical plants," *Computers and Chemical Engineering*, **9**, pp. 183-193.

130. Reuter, M.A., Van Deventer, J.S.J., Green, J.C.A., and Sinclair, M., 1988. "Optimal design of mineral separation circuits by use of linear programming," *Chemical Engineering Science*, **43**, pp. 1039-1049.

131. Meloy, T.P., 1983. "Analysis and optimization of mineral processing and coal cleaning circuits-circuit analysis," *International Journal of Mineral Processing*, **10**, pp. 61-80.

132. Castillo, D., Dobby, G.S., and Kosick, G.A., 1990. "Column flotation circuit design," *Preprint No. 90-101*, SME Annual Meeting, Salt Lake City, Utah.

133. Miller, F.G., Podgursky, J.M., and Aikman, R.P., 1967. "Study of the mechanism of coal flotation and its role in a system for processing fine coal," *Trans. AIME*, **238**, p. 276.

134. Aplan, F.F., 1976. "Coal flotation," in: *A.M. Gaudin Memorial International Flotation Symposium*, Ed. by M.C. Fuerstenau, AIME, New York, pp. 1235-1264.

135. Miller, J.D., Lin, C.L., and Chang, S.S., 1984. "Coadsorption phenomena in the separation of pyrite from coal by reverse flotation," *Coal Preparation*, **1**, pp. 21-38.

136. Aplan, F.F., 1977. "Use of the flotation process for desulfurization of coal," In *Coal Desulfurization - Chemical and Physical Methods*, Ed. by T.D. Wheelock, ACS Symposium Series 64, Washington, D.C., pp. 70-81.

137. Partridge, A.C. and Smith, G.W., 1971. "Small-sample Flotation Testing," *Trans. Inst. Min. Metall., Sec C*, **80**, pp. C199-205.

CHAPTER 2 SURFACE REACTIONS ON PYRITE

2.1 Introduction

In recent years, numerous studies have been directed at developing a low-cost froth flotation process to remove pyritic sulfur from coal. These studies have been stimulated by increasingly stringent restrictions on sulfur dioxide emissions from coal fired power plants and the recognition that pyrite (FeS_2) is one of the major sources of sulfur in coal. However, development of a practical flotation process for pyrite rejection has proven to be more difficult than expected. Yoon et al. [1] and Luttrell and Yoon [2] established that a major factor complicating pyrite rejection is the considerable hydrophobicity it acquires due to superficial oxidation. Thus, in most flotation processes, a significant fraction of the pyrite floats with the coal.

Superficial oxidation of pyrite produces both hydrophilic and hydrophobic species on the surface. The relative abundance of hydrophobic and hydrophilic oxidation species on the surface is believed to determine the floatability of pyrite [1]. The hydrophilic species is generally recognized as ferrous or ferric hydroxide. The identity of hydrophobic sulfur oxidation product is a topic of debate, with possible species including polysulfide (FeS_n, $n>2$), metal-deficient sulfide ($Fe_{1-x}S_2$, $x<1$) and elemental sulfur (S^o) [1, 3, 4]. The uncertainty on the nature of sulfur oxidation products and, more

importantly, the conditions under which they form stems from two major reasons.

The first relates to the different methods of preparing pyrite surfaces for study. Most electrochemical studies have been conducted on abraded and/or polished pyrite electrodes; however, these sample preparation techniques may oxidize the surface [5, 6], making it difficult to study the oxidation of pyrite itself. Buckley and Woods [5] and Richardson et al. [7] have shown that electrochemical and photoelectrochemical properties of fractured surfaces of sulfides are considerably different from those of ground surfaces.

The second reason is associated with the complexity of the oxidation mechanism associated with pyrite. Depending on the kinetics of oxidation, a variety of different sulfur oxidation products can be formed and affect the hydrophobicity of pyrite. This is illustrated in Figure 2.1, which shows cyclic voltammograms of pyrite obtained by different investigators at pH 9.2. Table 2.1 lists reactants/products suggested by different authors [8, 9, 10].

The bottom two voltammograms, (A) and (B), are results of Yoon et al. [10] and Zhu et al. [8], respectively, in which relatively high negative and positive overpotentials (-1.05 ~ 1.05 V) were employed. Ahlberg et al. [9] performed similar studies at pH 11 and the overall behavior of their voltammograms were the same. There are five or six distinct anodic reactions on the positive going sweep, forming $Fe(OH)_2$, $Fe(OH)_3$, FeS, FeS_n, S°, SO_4^{2-}, etc., as oxidation products. On the negative going sweep, various reduction products including $Fe(OH)_2$, Fe°, FeS and HS^- are formed.

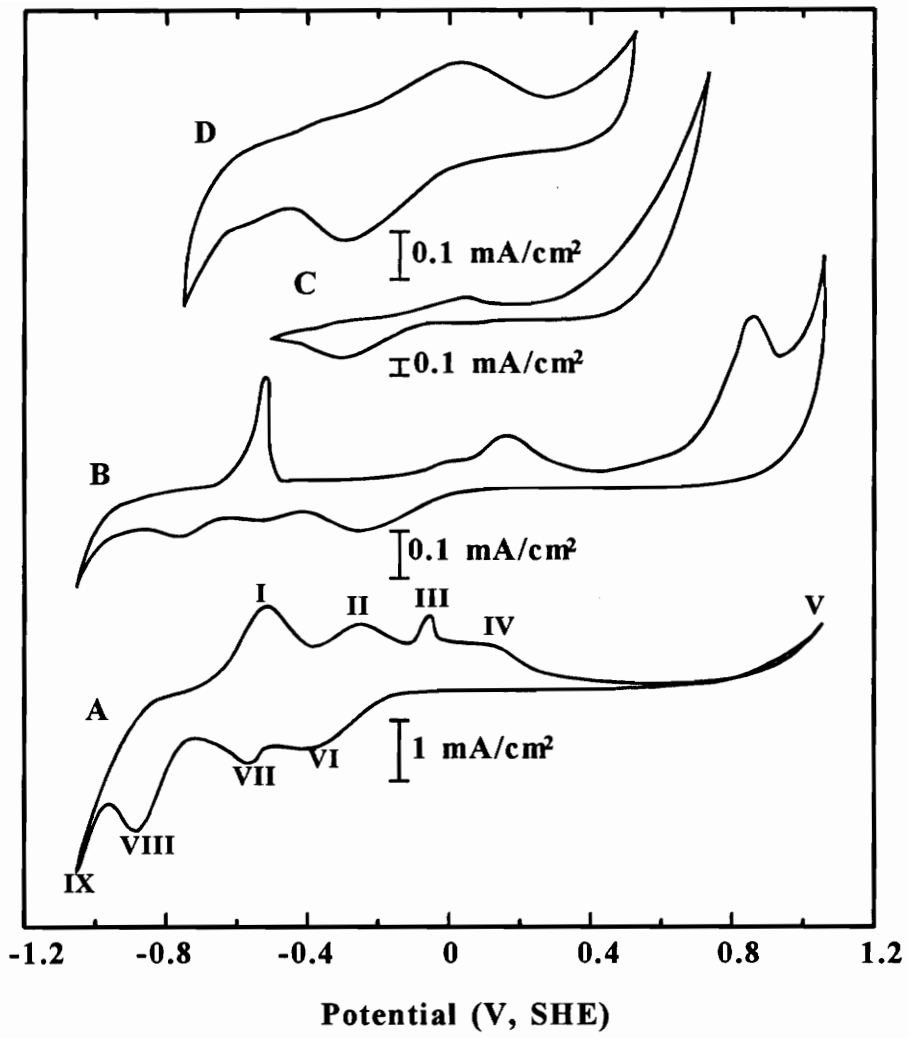

Figure 2.1 Voltammetry curves on pyrite at pH 9.2. A: from Yoon et al.[10]; B: from Zhu et al. [8]; C: from Hamilton and Woods [3]; D: from Tao et al. [11].

Table 2.1 Identification of reactions peaks on pyrite voltammograms at pH 9.2.

Peak	Reactants/Products Zhu et al. [8]	Reactants/Products Ahlberg et al. [9]	Reactants/Products Yoon et al. [10]
I	$Fe/Fe(OH)_2$	$Fe/Fe(OH)_2$, Fe/FeS	$Fe/Fe(OH)_2$
II		$Fe(OH)_2/Fe(OH)_3$	$Fe(OH)_2$, HS^-/FeS_n
III	HS^-/S^o	$Fe(OH)_2/Fe(OH)_3$	HS^-/S^o
IV	$Fe(OH)_2/Fe(OH)_3$	FeS/S^o, HS^-/S^o	FeS/S^o, $Fe(OH)_3$
V	$FeS_2/Fe(OH)_3$, SO_4^{2-}	Same	Same
VI	$Fe(OH)_3/Fe(OH)_2$	Same	Same
VII			S^o/HS^-
VIII	$Fe(OH)_2/Fe$	Same	Same
IX	FeS_2/Fe, HS^-	Same	Same

The top two voltammograms (C) and (D) were obtained by Hamilton and Woods [3] and Tao et al. [11] at moderate overpotentials. The voltammograms are much less complex when moderate oxidation and reduction potentials were employed. The anodic peak at approximately 0 V and the cathodic peak at about -0.3 V are generally assigned to the redox couple $Fe(OH)_2/Fe(OH)_3$ [8, 9]. It will be shown in this section that the reactions resulting from iron and sulfur oxidation species are so overwhelming that they mask the superficial oxidation of pyrite itself, which is believed to be responsible for its self-induced hydrophobicity and, hence, collectorless flotation. It is established that electrode polishing and aggressive oxidation of pyrite at high overpotentials produce thick layers of iron hydroxide and S^o-like species on pyrite surface [4]. Thus, using polished electrodes and conducting multisweep studies do not allow details of the superficial oxidation of pyrite to be determined, due to the dominance of the $Fe(OH)_2/Fe(OH)_3$ couple.

2.2 Research Objectives

The present study was undertaken to better understand surface oxidation/reduction reactions on pyrites from mineral and coal sources by electrochemical and spectroscopic techniques. This fundamental study will provide guidelines for the development of effective electrochemical techniques to enhance pyrite rejection from coal by flotation.

To study the initial oxidation/reduction processes of pyrite itself, which is the

most relevant to flotation, fresh surfaces were produced by *in-situ* fracturing electrodes potentiostated at a predetermined potential. Chronoamperometry immediately after fracture and subsequent cyclic voltammetry were used to elucidate the initial oxidation/reduction reactions. Rotating ring-disc electrodes (RRDE) were used to identify soluble oxidation and reduction species on pyrite surface in oxygen-free solutions. RRDE was also employed to investigate the mechanisms and kinetics of oxygen reduction on pyrite. With the RRDE technique, soluble products are transported away from a disc electrode and can be detected by an outer ring electrode held at different potentials. These studies employed moderate overpotentials, which are believed to be relevant to conditions encountered in most flotation processes. Pyrite surfaces that were fresh and that underwent oxidation were analyzed by X-ray photoelectron spectroscopy (XPS) to identify hydrophobic and hydrophilic species formed under different conditions.

It is believed that these studies are essential to delineate the role of surface oxidation and reduction in pyrite flotation and depression and to determine appropriate conditions for efficient coal desulfurization.

2.3 Experimental

2.3.1 Materials

Large specimens of mineral pyrite, originating from Huanzala, Peru, were obtained through Ward's Scientific Co. The Pittsburgh No. 8 coal-pyrite was originally a chunk of 2.5"×2.3"×2" pyrite found in a run-of-mine coal sample. This pyrite sample contained approximately 3% coal on the surface. The coal pyrite specimen from Sichuan, China contained no visible specks of coal and had the appearance of mineral pyrite.

2.3.2 Ring-disc electrodes

The rotating ring-disc electrode is schematically illustrated in Figure 2.2. It was constructed using core drilled discs of pyrite (0.7 cm diameter) and pure gold rings. The disc was separated from the ring by a small gap of nonconductive epoxy resin. The discs were contacted with a copper electrical lead. After mounting the ring-disc assembly, the surfaces were abraded and polished with successively finer grades of silicon carbide paper from 240 to 600 grit. The samples were then cleaned with acetone and hydrochloric acid followed by a thorough rinse with distilled water. Solutions were purged with N_2 for at least one hour prior to each experiment. A pine RDE-4 double potentiostat was used to control the potential and a pine rotating ring-disc assembly was used to rotate the electrode. The electrode rotation speed was generally set at 2000 rpm and voltammograms were recorded on the second cycle, unless otherwise specified. Voltammetry curves and ring currents were recorded on a Linseis LY 18100 recorder.

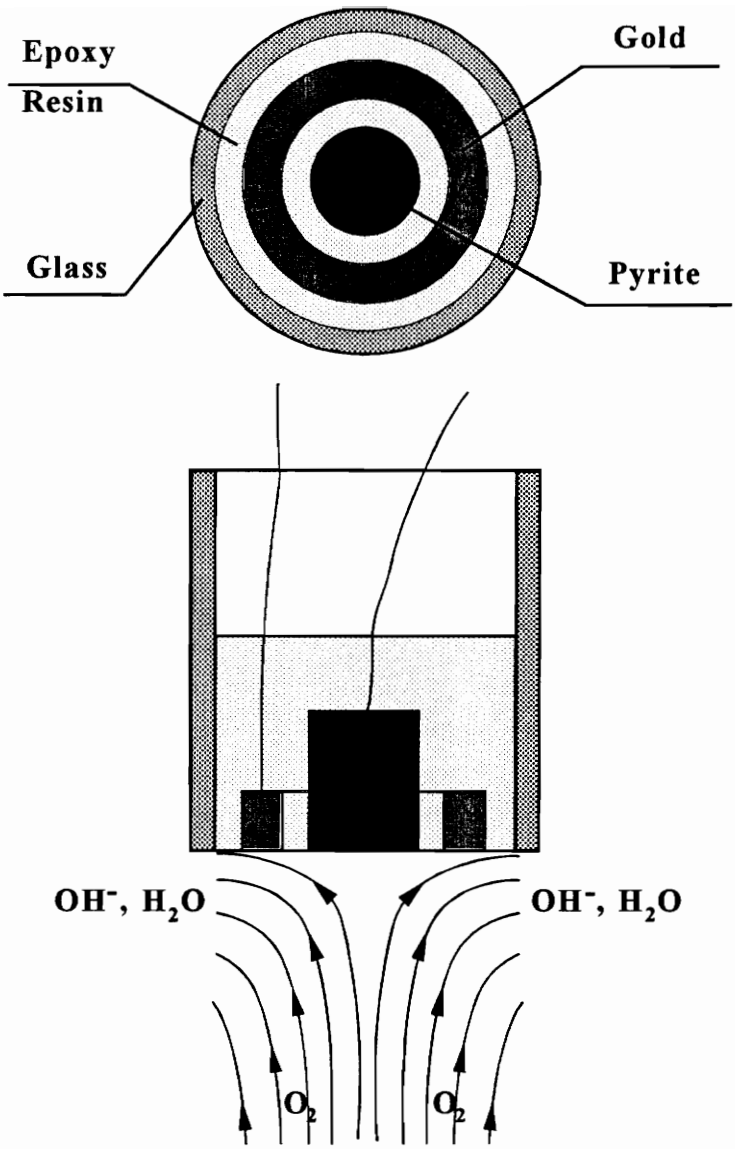

Figure 2.2 Schematic illustration of the rotating ring-disc electrode.

The collection efficiencies (N) of the three ring-disc electrodes made of different pyrite specimens were determined using freshly prepared 1.0×10^{-3} *M* $CuCl_2$ in 0.5 *M* KCl solution [12]. The pyrite electrodes were held at 0.1 V (SHE) at which no significant current arises from reactions of pyrite itself and Cu^{2+} reduction is under diffusion control. The values of N for the mineral-, Pittsburgh No. 8 coal-, and Chinese coal-pyrite were found to be 0.38, 0.28 and 0.36, respectively.

A saturated Calomel electrode (SCE) was used as the reference electrode and a platinum wire as the counter electrode. Potentials are expressed on the standard hydrogen electrode (SHE) scale by adding 0.245 V.

2.3.3 In-situ fractured electrodes

The mineral pyrite samples for *in-situ* fractured electrodes had dimensions of approximately $3\times2\times10$ mm. A copper lead-wire was connected to one of the 3×2 mm faces using a conducting silver epoxy. The assembly was then mounted at the end of a 7 mm diameter glass tube with non-conducting epoxy (Torr Seal, Varian), encapsulating about one-half of the electrode. The other half of the electrode was exposed, with the desired fracture plane carefully delineated with epoxy. After the electrode was inserted into the electrochemical cell through an O-ring seal, the projecting portion was subjected to a sharp blow through a glass rod that was inserted through another cell port, resulting in a freshly fractured surface which was usually flush with the epoxy. Each electrode

was carefully inspected after experiments to ensure that only fresh surface was exposed to the electrolyte before the results were accepted.

2.3.4 XPS study of the surface oxidation of pyrite

The XPS studies were conducted on slabs (10×10×2 mm) cut from Pittsburgh No. 8 coal-pyrite samples. The measurements were made using a Perkin Elmer Phi 5400 XPS spectrometer equipped with a monochromatized Al Kα X-ray source and a specially-designed drying and cooling chamber. The analyzing chamber of the spectrometer was modified to maintain sample temperature near 130 K. Maintaining the temperatures at this value prevented the loss of volatile elemental sulfur (if present) from the sample surface.

2.3.5 Reagents

Buffer solutions used in all tests were prepared in double-distilled water using reagent grade chemicals with the following compositions:

pH 4.6; 0.5 *M* CH_3COOH and 0.5 *M* CH_3COONa

pH 6.8; 0.05 *M* KH_2PO_4 and 0.0224 *M* NaOH

pH 8.0; 0.05 *M* KH_2PO_4 and 0.0461 *M* NaOH

pH 9.2; 0.05 *M* $Na_2B_4O_7$

Fresh iron (II) solutions were prepared by dissolving $FeCl_2$ in deoxygenated distilled water and HS^- solutions by dissolving Na_2S. Both $FeCl_2$ and Na_2S were of reagent grade.

2.4 Results and discussion

2.4.1 Oxygen reduction on pyrite

The oxidation of sulfide minerals, including that of pyrite, is controlled by mixed potential, corrosion-type electrochemical reactions, in which the mineral undergoes anodic oxidation while oxygen is cathodically reduced. Oxygen serves as an electron scavenger, so the kinetics of its reduction is important in determining the rate of pyrite oxidation and the mixed potential at which it occurs.

Studies of oxygen reduction on pyrite electrodes were conducted with the RRDE. Figure 2.3 (top) shows the current resulting from linear potential sweeps from 0.25 to -0.75 V on the Chinese coal-pyrite disc electrode at pH 9.2 for various rotation speeds in a solution saturated with oxygen. The current was negligible in the absence of oxygen in this potential range. At the beginning of the sweeps, the current is controlled by electron transfer (activation control) and is only slightly dependent on rotation rate, ω. As the potential becomes more negative, the diffusion of oxygen to the disc surface gradually predominates over charge transfer in determining the reaction rate and, hence, the current is increasingly dependent on rotation speed. At more negative potentials, the

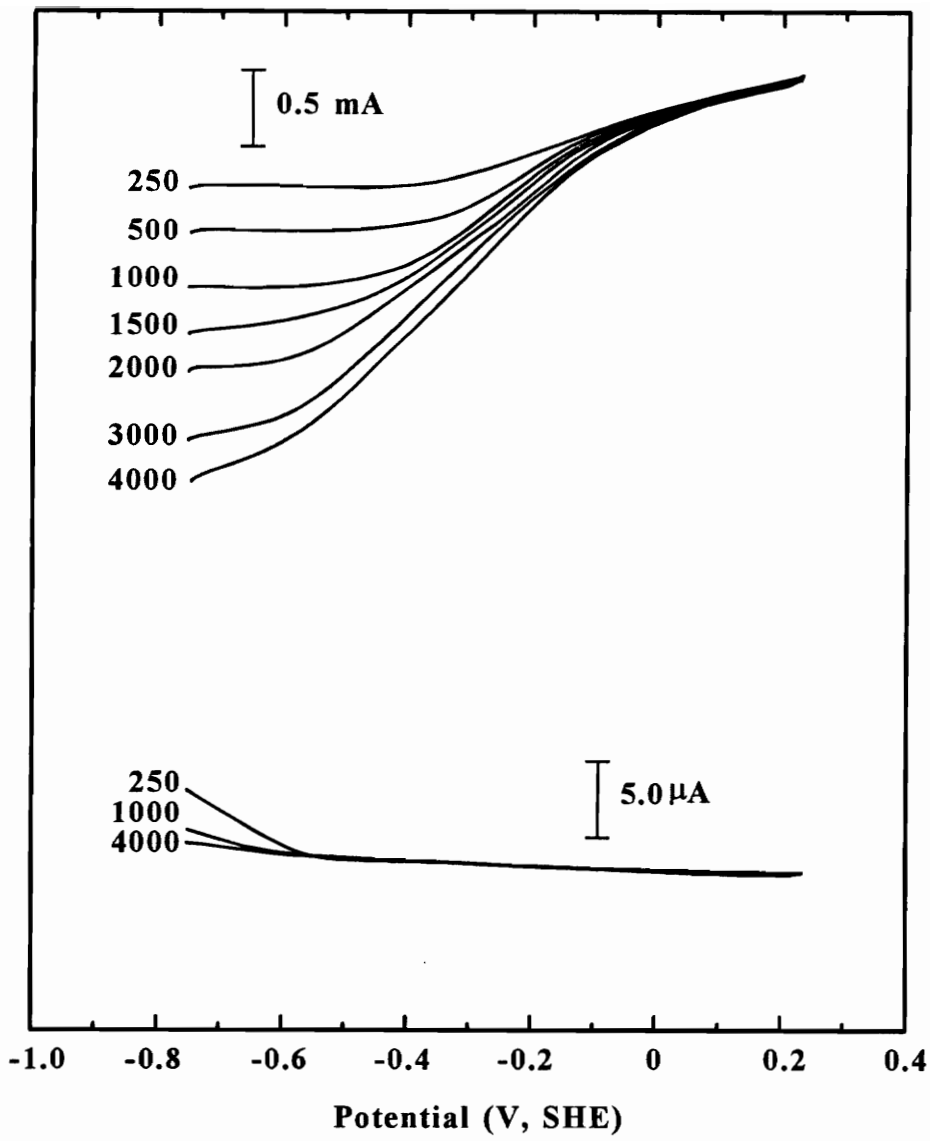

Figure 2.3 Ring-disc linear sweep current for oxygen reduction on Chinese coal-pyrite at pH 9.2 (ring at 0.25 V).

current is diffusion-limited. The onset of the diffusion-limited current shifts to more negative potentials with increasing rotation speed. The limiting current, i_L (mA/cm^2), is given by the Levich Equation (2.1) [13],

$$i_L = 0.62nFD^{2/3}\nu^{-1/6}C_b\omega^{1/2}, \quad (2.1)$$

where n is the number of electrons in the overall reaction, F the Faraday's constant, D the diffusion coefficient for the relevant species undergoing oxidation or reduction, ν the kinematic viscosity, C_b the concentration of the electroactive species in the bulk solution, and ω is the angular velocity of the electrode. According to Biegler et al. [14], D = 1.93×10^{-5} cm^2/sec, ν = 0.941×10^{-3} cm^2/sec and C_b = 1.21×10^{-6} mole/cm^3 for oxygen. Substituting these values and other relevant constants into Equation (2.1), one obtains,

$$I_L = 0.0457n\omega^{1/2}, \quad (2.2)$$

where I_L is in units of mA. A plot of I_L vs. $\omega^{1/2}$, as shown in Figure 2.4, is linear, in agreement with Equation (2.2). The value of n calculated from Equation (2.2) is 3.5, suggesting that the reduction of oxygen proceeds to OH^- primarily by the 4-electron process,

$$O_2 + 2H_2O + 4e^- = 4OH^- \quad (E = 1.229 - 0.059pH). \quad (2.3)$$

The presence of a single wave on the disc during linear sweeps indicates that no intermediate soluble species is generated during oxygen reduction at pH 9.2. This is substantiated by the absence of a ring current from 0.25 to -0.55 V when the ring was held at 0.25 V, which is positive enough to oxidize any hydrogen peroxide (H_2O_2) produced on the disc. The small ring current observed at potentials $<$-0.55 V is due to

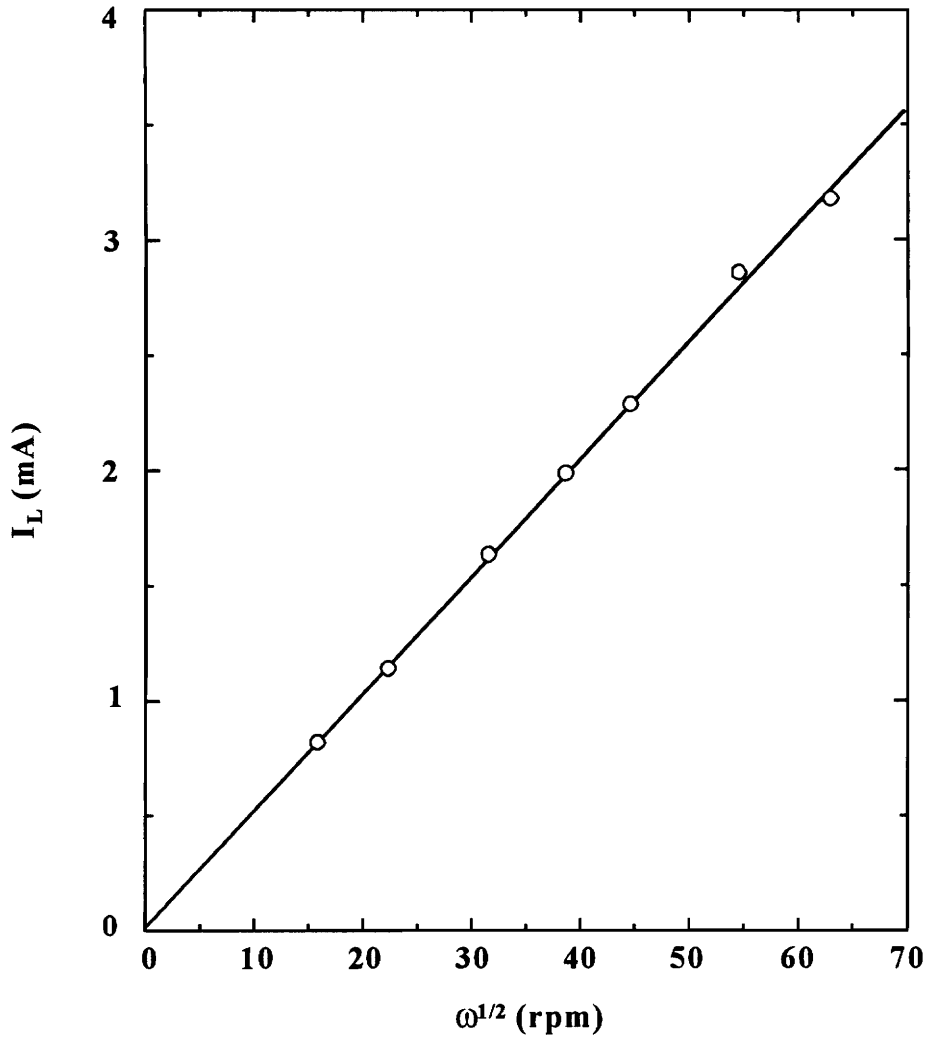

Figure 2.4 **Limiting current of oxygen reduction as a function of electrode rotation speed on Chinese coal-pyrite at pH 9.2.**

the cathodic decomposition of pyrite and will be discussed later.

The reaction order with respect to O_2 can be determined from the slope of the plot of log I vs. log $(1 - I/I_L)$, as shown in Equation (2.4) [15]:

$$\log I = \log I_k + m \log (1 - I/I_L) \tag{2.4}$$

where I_k is the kinetic current density and m is the reaction order with respect to dissolved oxygen molecules. The values of current I at all rotation rates were chosen at -0.2 V and -0.25 V for the plot of log I against log $(1 - I/I_L)$. The results are shown in Figure 2.5. The slopes are found to be 0.9372 and 0.9515, respectively, indicating that oxygen reduction on pyrite at pH 9.2 is a first order reaction. This is in agreement with Biegler et al.'s conclusion [14] that the formation of O_2^- is the rate determining step.

The results shown in Figure 2.3 can be expressed in Equation (2.5) [15]:

$$\log\frac{II_L}{I_L - I} = Constant + logC_b - \frac{\alpha nF}{2.3RT}E \tag{2.5}$$

Therefore, Tafel slopes at different electrode rotation speeds can be determined from the plot of E against log $[II_L/(I_L - I)]$. In all cases, a straight line was observed over one or two decades of current with an average slope of 0.224 V/dec, as shown in Figure 2.6.

The results of oxygen reduction on Pittsburgh No.8 coal- and mineral-pyrite were similar with regard to the shape of the disc current during linear sweeps and the ring response. Mineral- and Chinese coal-pyrite electrodes showed nearly identical disc currents for oxygen reduction that were higher than those exhibited by Pittsburgh No.

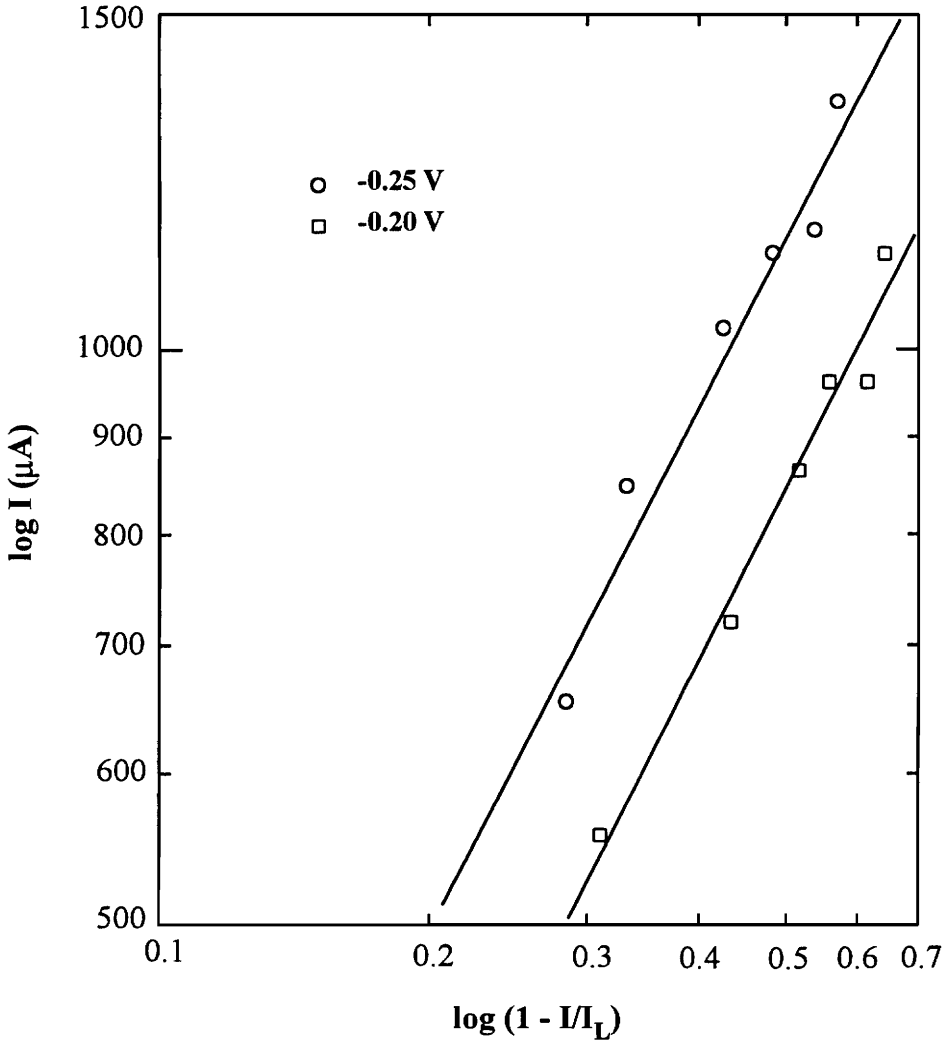

Figure 2.5 **Dependence log I on log (1 - I/I_L) for oxygen reduction on Chinese coal-pyrite at -0.2 V and -0.25 V at pH 9.2.**

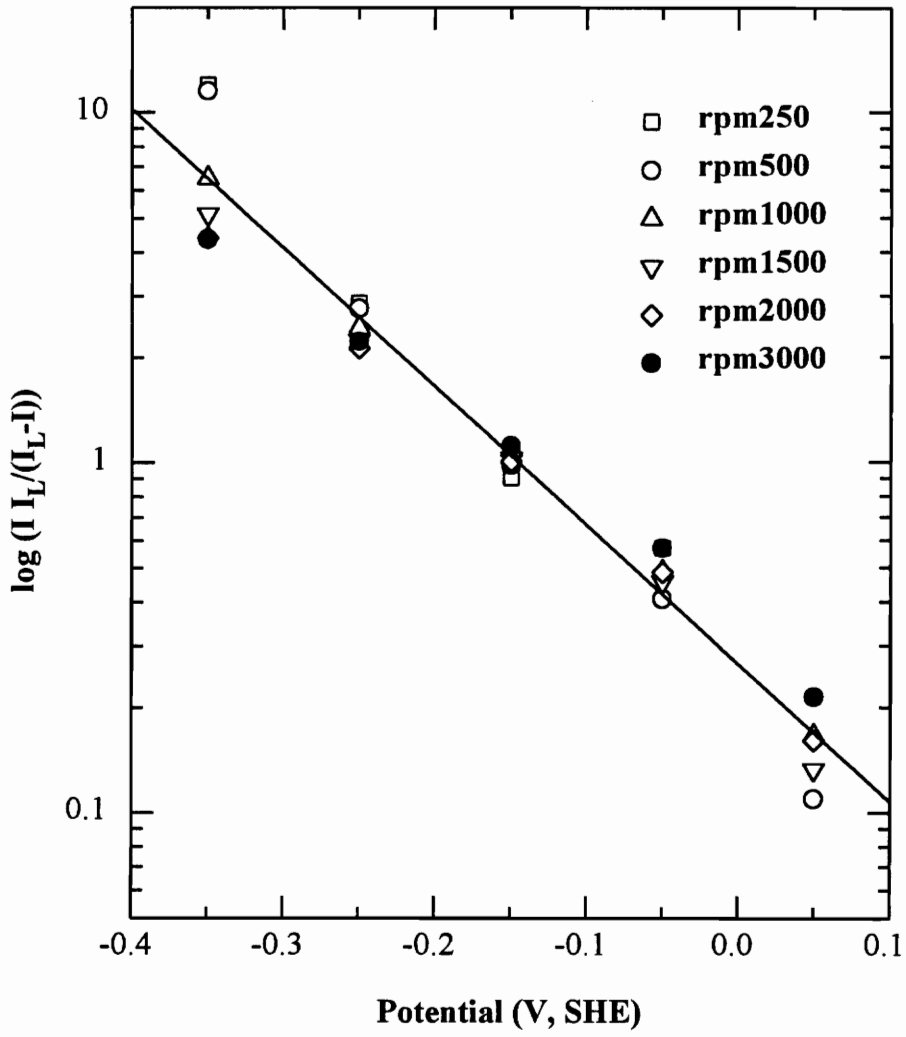

Figure 2.6 **Tafel plots for oxygen reduction on Chinese coal-pyrite at pH 9.2 at specified rotation speed in rpm.**

8 coal-pyrite.

The disc currents during linear potential sweeps in the negative direction for oxygen reduction on Pittsburgh No. 8 coal-pyrite, Chinese coal-pyrite and mineral pyrite at pH 6.8 are shown in Figure 2.7. The overall features of these currents are similar to those at pH 9.2 for all three pyrite samples, with no evidence of the formation of hydrogen peroxide. The magnitude of the disc currents at identical overvoltages at pH 6.8 is in the order of Pittsburgh No. 8 coal-pyrite > Chinese coal-pyrite ≈ mineral-pyrite.

However, there are some remarkable differences on sweeps obtained at pH 9.2 and 6.8 and these differences are sample-dependent. Oxygen reduction at pH 6.8 consistently showed a higher current than at pH 9.2 for all three pyrites. For mineral-pyrite, the diffusion-limited current was observed at lower potentials at pH 6.8 than at pH 9.2. For Chinese coal-pyrite, although the current was higher at pH 6.8 than at pH 9.2, the potential at which the diffusion-limited current was reached did not change remarkably as the solution pH decreases from 9.2 to 6.8. For Pittsburgh No. 8 coal-pyrite, the oxygen reduction current increased considerably with decreasing pH from 9.2 to 6.8 and the potential where the diffusion-limited current was reached shifted significantly, especially at the higher electrode rotation speed.

In acidic solution, oxygen reduction on pyrite proceeded *via* a different route. Figure 2.8 shows the linear sweep voltammograms for oxygen reduction on Chinese coal-pyrite at pH 4.6. In the activation-controlled region, there are two distinct cathodic

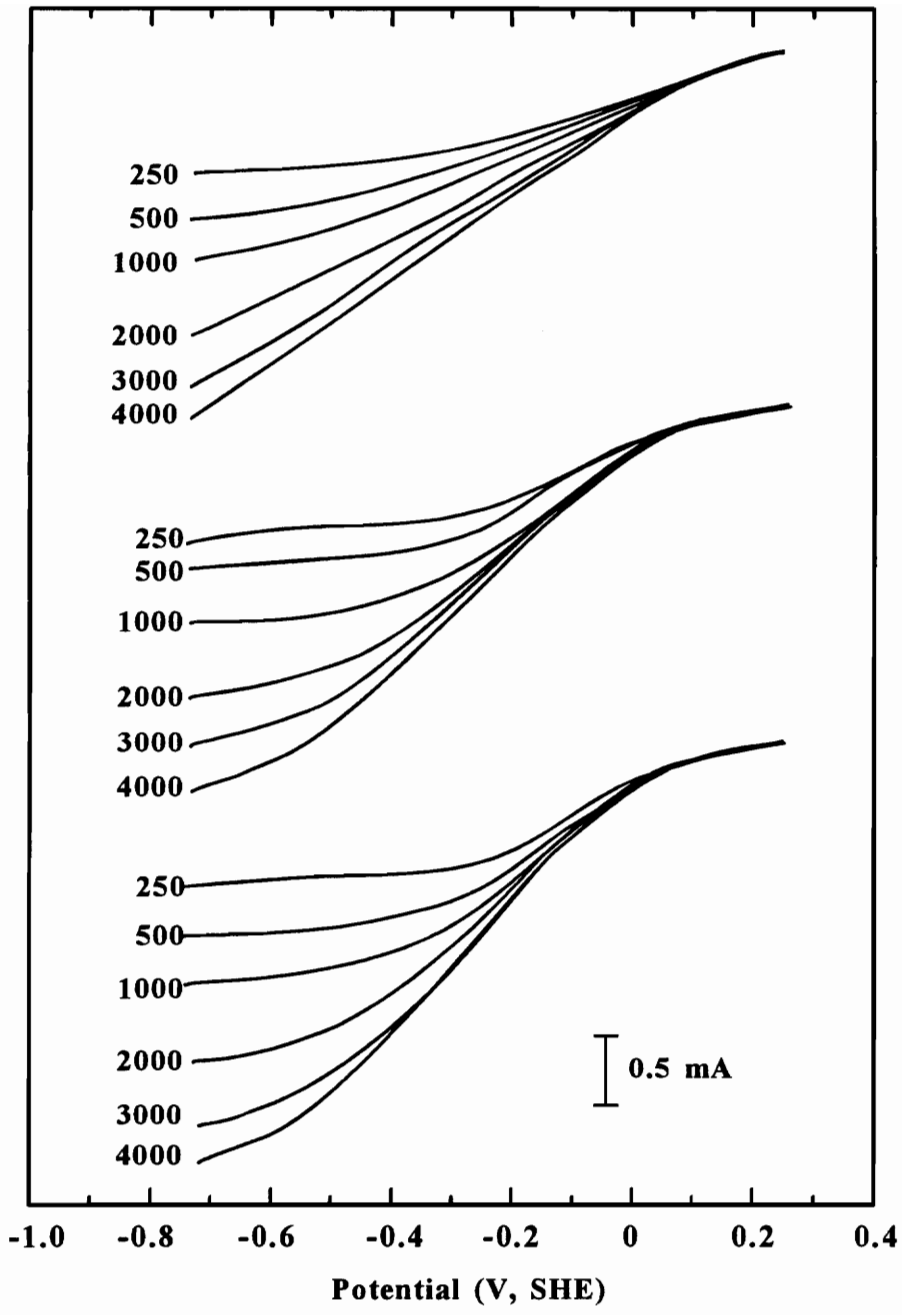

Figure 2.7 Disc current during potential sweep, for O_2 reduction at pH 6.8 on Pittsburgh No. 8 coal-pyrite (top); Chinese coal-pyrite (middle); mineral-pyrite (bottom) at specified rpm.

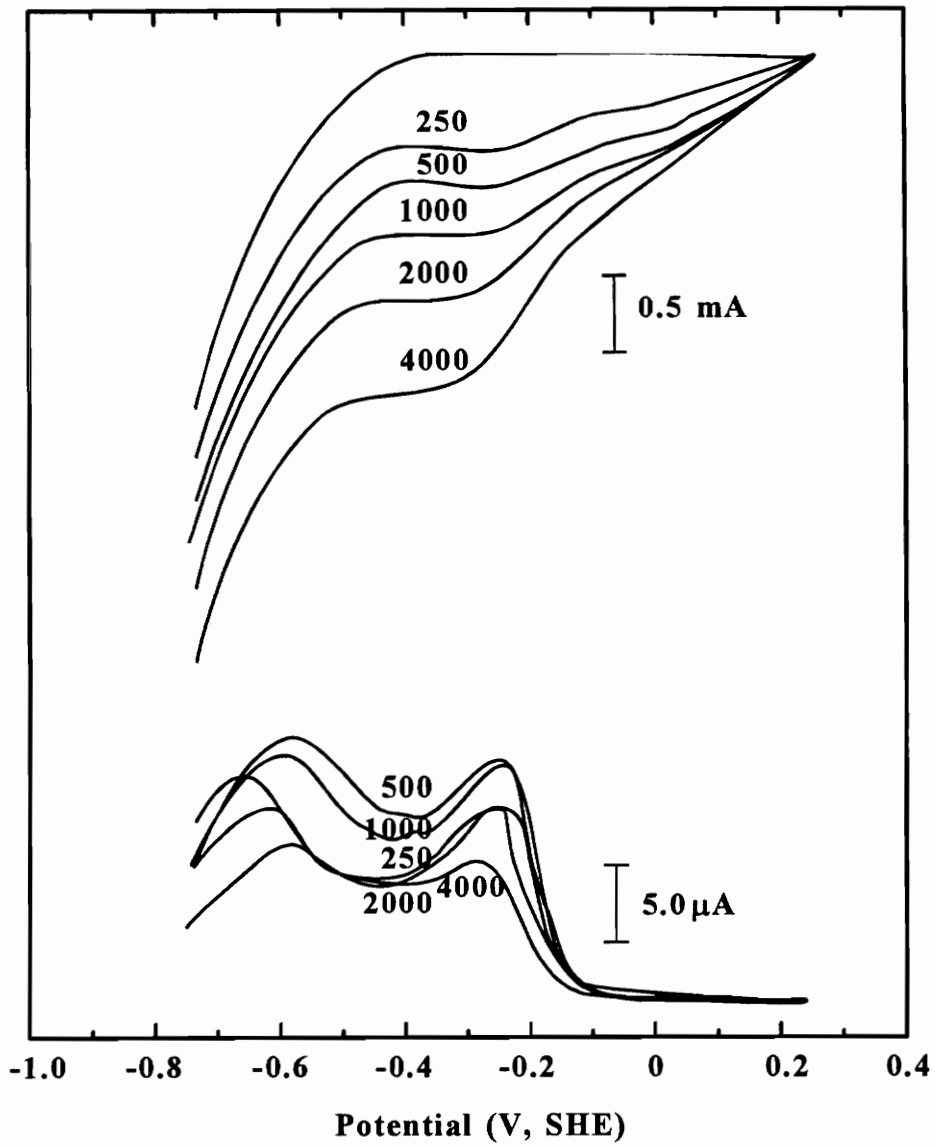

Figure 2.8 **Ring-disc currents during linear potential sweeps for oxygen reduction on Chinese coal-pyrite at pH 4.6 (ring at 0.55 V, dashed line is the current in N_2 bubbled solution).**

reduction processes occurring, as evidenced by the change in slope of the curves at about 0 V. The current on the ring, which was held at 0.55 V during the potential sweep, shows that a soluble intermediate species was produced at disc potentials $\leq$-0.15 V. This can be attributed to hydrogen peroxide produced on the disc by the reaction,

$$O_2 + 2H^+ + 2e^- = H_2O_2 \quad (E = 0.695 - 0.059pH) \tag{2.6}$$

followed by its re-oxidation on the ring. The ring current reached a maximum at a disc potential of -0.25 V. When the limiting current on the disc was reached ($<$-0.3 V), the overpotential was large enough that hydrogen peroxide was reduced at the disc to OH^-, with less diffusing to the ring. Consequently, the ring current decreased. At more negative potentials ($<$-0.5 V), significant cathodic decomposition of pyrite occurred, producing decomposition products which were oxidized at the ring.

Mineral-pyrite showed a behavior similar to that shown in Figure 2.8. However, on Pittsburgh No. 8 coal-pyrite, most of the oxygen was reduced to water, with only a small amount of hydrogen peroxide escaping the disc surface. The electroactivity towards oxygen reduction at pH 4.6 for the three pyrite samples is in the same order as at pH 6.8.

All three pyrite samples examined in this study possessed a consistent characteristic, i.e., the magnitude of the diffusion-limited current for oxygen reduction followed the order: pH 6.8 > pH 9.2 > pH 4.6. The lowest oxygen reduction rate at pH 4.6 may be attributed to the cathodic decomposition of pyrite to elemental iron. The

formation of passivating layers of iron hydroxide on the surface at pH 9.2 may explain the observation that the rate at pH 9.2 was lower than at pH 6.8.

Biegler et al. [14] studied oxygen reduction on mineral-pyrite using the rotating disc electrode. They suggested the formation of hydrogen peroxide during oxygen reduction in acid solutions from the change in the slope on the voltammetry curves. Under neutral or alkaline conditions iron-hydroxides or oxides on the surface may catalyze the decomposition of peroxide [16]. The present study clearly demonstrated that coal-pyrites are electroactive with respect to oxygen reduction, contrary to the conclusion of Lai et al. [17]. The difference in electroactivity for oxygen reduction among three pyrite samples may be attributed to differences in crystalline defects and the morphology of the surface. While Chinese coal-pyrite exhibits a morphological appearance similar to that of mineral pyrite, Pittsburgh No. 8 coal-pyrite appears very different in that it is much more porous and poorly crystallized (evidence will be provided later). It is believed that in neutral and acidic solutions, the more porous nature of Pittsburgh No. 8 coal-pyrite may hinder the diffusion of hydrogen peroxide away from the disc, fostering its further reduction to OH^- before it can be convected to the ring. At pH 9.2, the electroactivity of Pittsburgh No. 8 coal-pyrite to reduce oxygen is lower than that of the other two pyrites. This is possibly because in alkaline solutions, the pores of Pittsburgh No. 8 coal-pyrite become blocked with reaction precipitates.

2.4.2 Pyrite oxidation/reduction reactions on in-situ fractured electrodes

It has been known that polishing or grinding causes significant oxidation of pyrite, generating iron hydroxide on the surface [5-7]. Therefore, it is necessary to either remove the oxidation products by surface etching or to use fractured pyrite surface for the study of the incipient oxidation of pyrite. The present study used *in-situ* fractured electrodes.

Figure 2.9 illustrates chronoamperometry curves (current as a function of time) of Chinese coal-pyrite electrodes after fracture at pH 9.2. Before discussing these curves, it is worthwhile pointing out the similarity between chronoamperometry on a fractured surface to the better known technique of controlled potential step chronoamperometry for studying electroactive species in solution. In the latter, the potential is stepped from an electrochemically inactive region to a value where an electroactive species is rapidly reduced or oxidized. This requires, initially, a large current to reduce or oxidize those species within the reaction layer at the surface. Charging of the double layer and redox processes involving any adsorbed species are fast processes that contribute to the initial current. The current then decays as a concentration gradient that controls the diffusion of the electroactive species to the surface develops. The present experiments differ from the usual controlled potential step method in several aspects. First, the electroactive species is the pyrite electrode itself. Second, the potential step experienced at fracture represents the difference between the

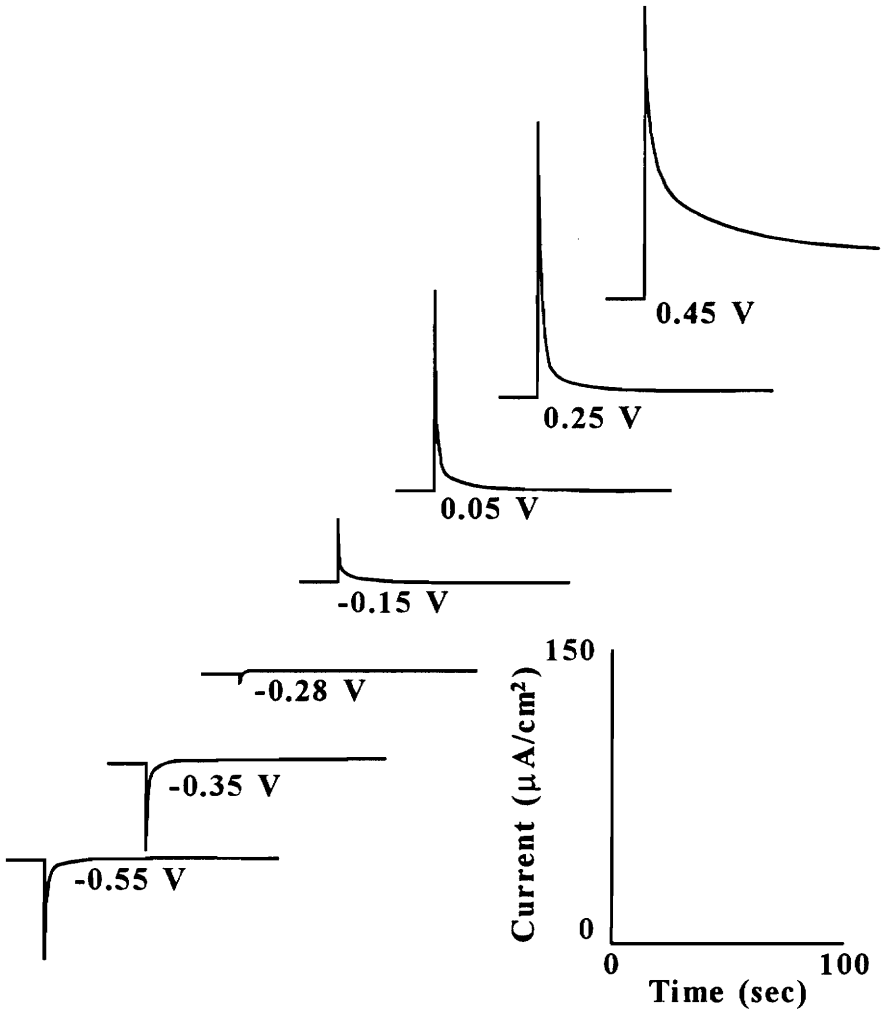

Figure 2.9 **Chronoamperometry curves of Chinese coal-pyrite fractured at different potentials at pH 9.2.**

applied potential and the potential a newly created surface assumes at the instant of fracture. Third, fracture momentarily destroys the preexisting double layer, and a double layer must be formed on the new surface. Based on these comparisons, it is believed that the initial spike observed on the current-time curves at the moment of fracture represents a combination of double layer charging and faradaic oxidation (or reduction) of the fresh pyrite surfaces. Double layer charging is fast compared to the time scale used in Figure 2.9, and thus the decay in the current after the initial spike is believed to represent primarily faradaic reactions involving pyrite.

In chronoamperometry experiments, electrodes were potentiostated at different potentials in the range -0.55 V to 0.45 V. Before fracture the electrodes were held for 5 to 20 minutes at the indicated potentials until a steady state current (usually very close to zero) was reached. Anodic (positive) currents obtained after fracture indicate pyrite undergoes oxidation following fracture and cathodic (negative) currents suggest pyrite undergoes reduction. A zero current at fracture indicates pyrite is neither oxidized nor reduced. Figure 2.9 establishes that pyrite undergoes spontaneous oxidation when fractured at potentials of -0.15 V or higher, and spontaneous reduction when fractured at -0.35 V or lower. The fresh surface created at -0.28 V exhibited nearly zero current. Precisely, a negligible cathodic current was observed on some electrodes and a negligible anodic current on other electrodes when they were fractured at -0.28 V. It appears that the "zero-reaction" potential of pyrite is at about -0.28 V at pH 9.2. This represents the potential at which neither oxidation nor reduction of pyrite takes place to a significant

extent. It can be assumed that a fresh pyrite surface remains stable at this potential. When pyrite is placed in air-saturated solutions or exposed to the open air, it will inevitably undergo significant oxidation since the potential is always higher than -0.28 V. The fact that the mixed potential of pyrite is determined to be 0.18 V at pH 9.2 [18] establishes that pyrite is oxidized in normal aqueous solutions.

Electrodes fractured in aqueous solutions at pH 4.6 exhibited chronoamperometry curves similar to these shown in Figure 2.9 with the "zero-reaction" potential shifted to ~0 V. The "zero-reaction" potentials of -0.28 V and 0 V obtained at pH 9.2 and pH 4.6 lie within the thermodynamic stability domain on E_h-pH diagram for pyrite, as shown in Figure 1.2. The chronoamperometry technique developed in the present work is significant because it specifies not only a method of *obtaining* an unreacted pyrite surface, but also a way of *maintaining* an unreacted surface, i.e., fracture pyrite while holding its potential in the region where pyrite is thermodynamically stable. This procedure overcomes one of the usual difficulties of interpreting electrochemical measurements on sulfide electrodes due to the presence of oxidized products arising from the preparation of the electrodes, e.g., products introduced by polishing. For pyrite, pre-oxidation leads to voltammograms that appear to be dominated by Fe^{o}/Fe^{2+} and Fe^{2+}/Fe^{3+} redox couples. The presence of these species makes it difficult to determine when pyrite itself begins to oxidize to form incipient oxidation products. The identification of the sulfur oxidation products, e.g., polysulfides, metal-deficient sulfide, or elemental sulfur, is of particular interest in flotation and the reactions leading to these

products may be masked by iron containing species.

The first three voltammograms obtained on a fresh pyrite surface generated by fracture at -0.28 V is shown in Figure 2.10. The potential sweep was started at -0.28 V in the anodic direction and reversed at 0.25 V on the first cycle. The lower potential limit was chosen to be -0.55 V to avoid possible complications that may arise from the aggressive reductive decomposition of pyrite to elemental iron that was found to occur near -0.7 V at pH 9.2. On the second potential sweep, the upper potential limit was set at 0.55 V to show the effect of aggressive oxidation of pyrite on the subsequent voltammogram.

An oxidation current appears at about -0.20 V on the first voltammogram with an anodic peak at about 0 V. Since pyrite has not been subjected to oxidation or reduction while it was held at -0.28 V during fracture, and therefore no elemental iron or ferrous hydroxide should be present on the surface, this current can only arise from the oxidation of pyrite itself. The possible reactions are [1, 3, 4]:

$$FeS_2 + 3OH^- = 2S^o + Fe(OH)_3 + 3e^- \quad (E = 0.628 - 0.059pH), \tag{2.7}$$

$$nFeS_2 + 3(n-2)OH^- = 2FeS_n + (n-2)Fe(OH)_3 + 3(n-2)e^-, \tag{2.8}$$

$$FeS_2 + 3xOH^- = Fe_{1-x}S_2 + xFe(OH)_3 + 3xe^-. \tag{2.9}$$

Hamilton and Woods [3] studied pyrite abraded under nitrogen to prevent oxidation and found an oxidation peak at approximately 0 V at pH 9.2. They attributed

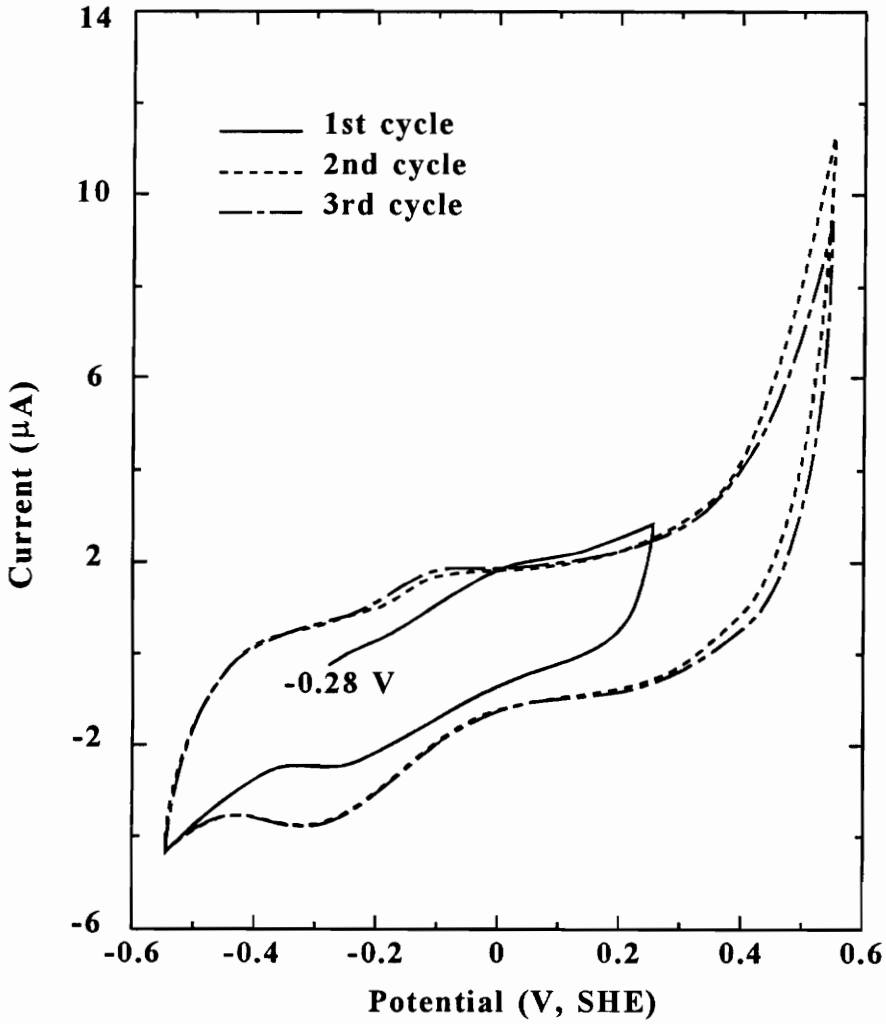

Figure 2.10 Voltammograms on Chinese coal-pyrite freshly fractured at -0.28 V at pH 9.2. The potential sweep started anodically.

this peak to pyrite oxidation to $Fe(OH)_3$ and elemental sulfur. From XPS studies, Buckley and Woods [4] established that moderate oxidation of pyrite leaves sulfur in normal lattice sites, creating a metal-deficient surface ($Fe_{1-x}S_2$). Yoon et al. [1] observed significant flotation of pyrite at potentials slightly above -0.1 V and suggested from XPS and electrochemical studies that polysulfides (FeS_n) are more likely oxidation products. XPS and Laser Raman spectroscopic studies conducted by Zhu et al. [19] and Mycroft et al. [20] supported this conclusion. Since the equilibrium potential for reaction (2.7) is 0.09 V, i.e., significantly above -0.15 V, Figure 2.10 suggests polysulfides or a metal-deficient sulfide is formed rather than elemental sulfur. It is believed that this sulfur-rich sulfide or S^o-like species could render pyrite floatable at -0.1 V as observed by Yoon et al. [1].

Oxidation behavior near 0 V is considerably different with second and third sweeps than on the first sweep. No peak is observed at 0 V on the second and third sweeps, but a new peak occurs at -0.1 V. This peak is known to represent the oxidation of $Fe(OH)_2$ to $Fe(OH)_3$ [8],

$$Fe(OH)_2 + OH^- = Fe(OH)_3 + e^- \quad (E = 0.271 - 0.059pH). \qquad (2.10)$$

The presence of passivating layers of $Fe(OH)_3$ on the surface may retard or even inhibit the oxidation of the mineral, making it difficult to observe the initial oxidation of pyrite on the second and third sweeps. The same problem arises when polished electrodes are used. It can thus be concluded that multiple potential sweeps and/or polished electrodes

can not be used to study early stages of pyrite oxidation.

The cathodic peak at -0.25 V arises from the reduction of oxidation products formed during the prior anodic sweep. One of the possible reduction processes can be represented by the reverse of reaction (2.10). In addition, if sulfur is present on the surface in the form of polysulfides or excess lattice sulfur, it may also be reduced over the same potential range as for reaction (2.11) to reform iron sulfide,

$$(n-1)Fe(OH)_3 + FeS_n + 3(n-1)e^- = nFeS + 3(n-1)OH^- \qquad (2.11)$$

The peak at -0.25 V on the second and third reduction cycles is larger than that on the first cycle. The difference between the first and the other two voltammograms can be attributed to the presence of more ferric hydroxide on the second and third voltammograms.

Figure 2.11 shows the first voltammetry curve obtained on a fresh surface of pyrite that was fractured at 0.25 V. The inset illustrates the current passed as a function of time after fracture. The charge generated during the first two minutes is approximately 550 $\mu C/cm^2$, based on the geometric surface area of the electrode. This charge density corresponds to the oxidation of approximately two or three monolayers of pyrite for a three electron oxidation process such as reaction (2.7). After holding the electrode at 0.25 V for approximately four minutes after fracture, voltammograms were obtained with the potential sweep starting in the negative direction to reduce the oxidation products formed at 0.25 V. There is a reduction process beginning at about -0.05 V with a

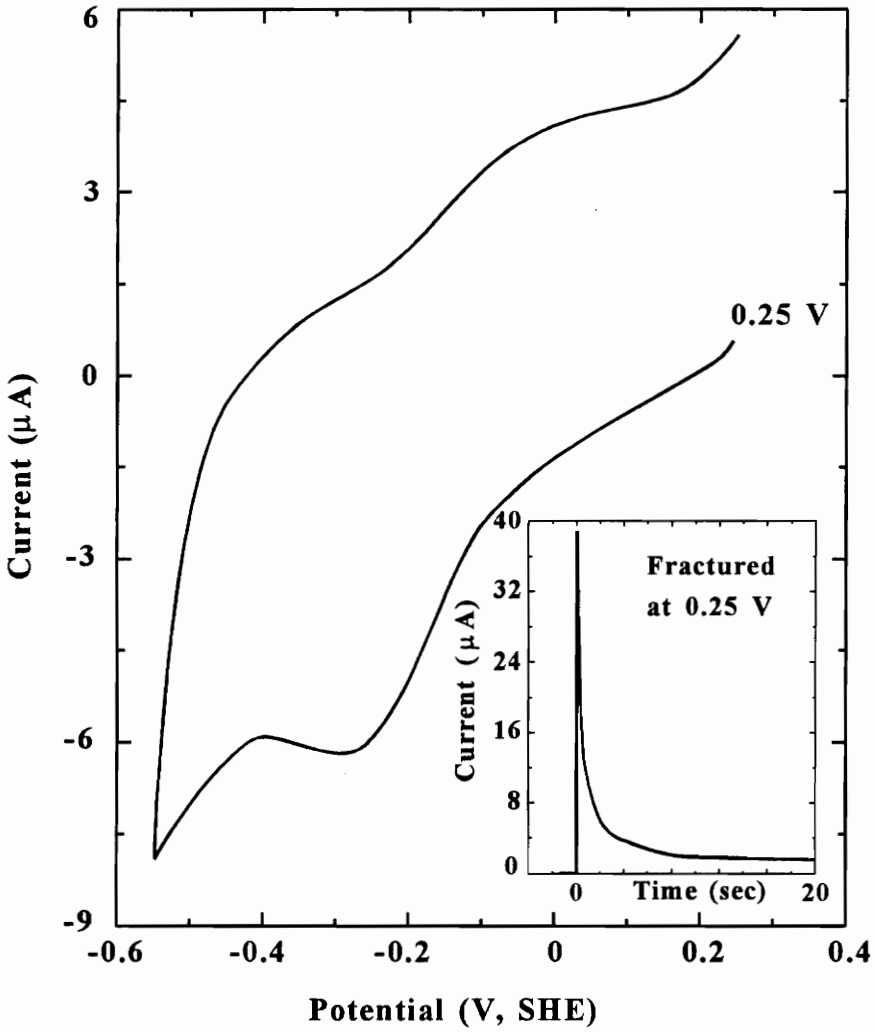

Figure 2.11 The first voltammogram on Chinese coal-pyrite freshly fractured at 0.25 V at pH 9.2. The inset is the chronoamperometry curve upon fracture.

cathodic peak at -0.27 V. The integrated charge is about 510 $\mu C/cm^2$ between -0.05 and -0.55 V. This reduction current confirms that solid oxidation products formed on pyrite during oxidation at 0.25 V can be reduced at -0.05 V. Since approximately the same charge was consumed at fracture as on the subsequent negative going potential scan, reduction of sulfur oxidation products (polysulfide or metal-deficient sulfide) must also be involved in this process, in addition to reduction of ferric to ferrous hydroxide.

Experiments were also carried out to investigate the reduction of pyrite, as shown in Figure 2.12. The electrode was freshly fractured at -0.28 V to minimize surface alteration of pyrite. The potential sweep began cathodically from -0.28 V. Since the fresh surface has not undergone oxidation, the first cathodic current must arise from the reduction of pyrite. The initial cathodic current observed from -0.28 V to -0.7 V is believed to be the reduction of pyrite to iron sulfide. The greater current below -0.7 V represents the aggressive reduction of pyrite to elemental iron. The possible reactions are [8, 9, 21],

$$\begin{aligned} FeS_2 + H_2O + 2e^- &= FeS + HS^- + OH^- \\ (E &= -0.403 - 0.03pH - 0.03\log[HS^-]) \end{aligned} \tag{2.12}$$

and

$$\begin{aligned} FeS_2 + 2H_2O + 4e^- &= Fe + 2HS^- + 2OH^- \\ (E &= -0.491 - 0.03pH - 0.03\log[HS^-]) \end{aligned} \tag{2.13}$$

Interestingly, the cathodic process between -0.3 and -0.6 V observed on the first sweep (finite slope) is absent on the second and third voltammograms. This shows that

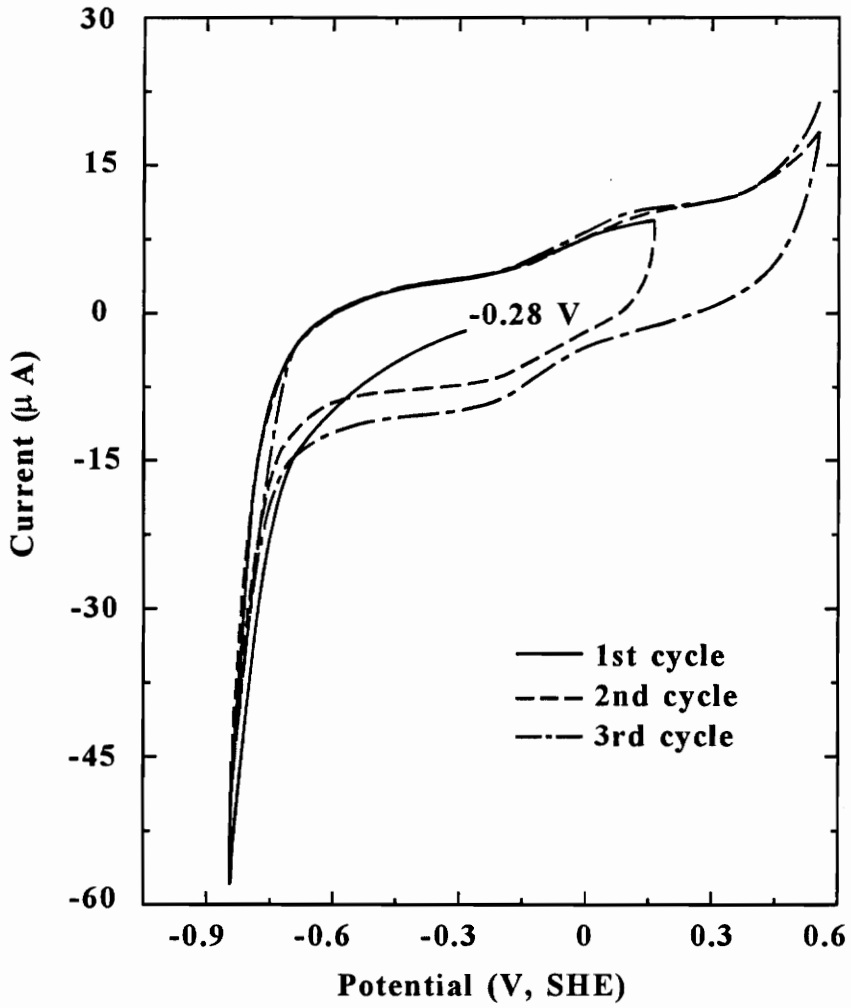

Figure 2.12 Voltammograms on Chinese coal-pyrite freshly fractured at -0.28 V at pH 9.2. The potential sweep started cathodically.

the initial reduction of pyrite observed on the first reduction cycle is different than that on subsequent sweeps. Continued sweeps shifted the pyrite reduction potential toward more negative values and eventually resolved a small cathodic peak at -0.7 V. The potential of this peak became more negative when the upper potential limit was increased. This indicates that the process requires higher overpotential for reductive dissolution, possibly due to the increased thickness of the passivating layer formed by pyrite oxidation at higher positive potentials.

When the pyrite electrode was fractured at -0.45 V, a significant cathodic current was observed, as shown by the inset in Figure 2.13. This current gave rise to a charge density of 106 $\mu C/cm^2$ after fracture for two minutes, which corresponds to a reduction reaction involving less than a monolayer of pyrite. The first two voltammograms after fracture at -0.45 V are shown in Figure 2.13. The potential sweep was initiated in the positive direction to oxidize reduction products formed following fracture. An anodic current appears at -0.25 V which reaches a peak at about 0 V. The position of this peak is consistent with Figures 2.9 and 2.10. The integrated charge density from -0.25 V to 0.25 V on the voltammogram is 240 $\mu C/cm^2$, considerably larger than 110 $\mu C/cm^2$ produced when the electrode was fractured and held at -0.45 V. This difference provides further evidence that the oxidation of pyrite itself contributes to the anodic current in this range.

Similar studies were performed on mineral- and Pittsburgh No. 8 coal-pyrite. Mineral-pyrite exhibited electrochemical characteristics close to those observed with

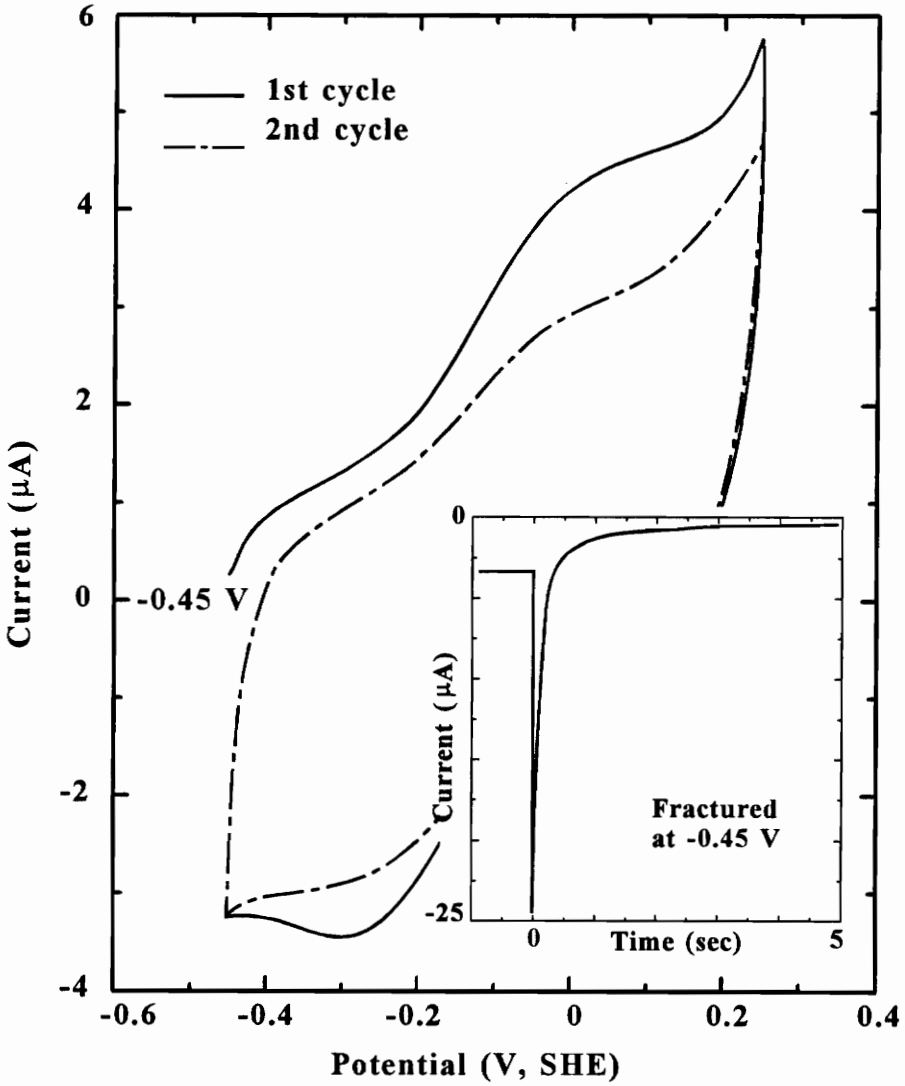

Figure 2.13 Voltammograms on Chinese coal-pyrite freshly fractured at -0.45 V at pH 9.2. The inset is the chronoamperometry curve upon fracture.

Chinese coal-pyrite, and its *stable* potential was at -0.28 V. An anodic peak at 0 V was also observed on the first sweep voltammogram at pH 9.2. Pittsburgh No. 8 coal-pyrite, however, demonstrated significant difference from the other two pyrite samples. It had nearly zero current at fracture at about -0.15 V, rather than -0.28 V as observed with mineral- and Chinese coal-pyrite. This may suggest that Pittsburgh No. 8 coal-pyrite is already oxidized or that its stoichiometry is not identical to the other pyrites. In addition, voltammograms obtained on Pittsburgh No. 8 coal-pyrite after fracture differed remarkably in terms of the position of the peaks and their height, indicating surface reactions on Pittsburgh No. 8 coal-pyrite may be different.

2.4.3 Pyrite surface reactions on rotating ring-disc electrodes

Figure 2.14 (top) shows the first and fifth voltammograms on a RRDE of Chinese coal-pyrite at pH 9.2. Previous studies with mineral pyrite at pH 11 [9] and at pH 9.2 [3, 8] concluded that the anodic peak I at -0.4 V represents the oxidation of elemental iron to $Fe(OH)_2$ by the reaction,

$$Fe + 2OH^- = Fe(OH)_2 + 2e^- \quad (E = -0.047 - 0.059pH). \qquad (2.14)$$

Elemental iron is produced by the cathodic reduction of pyrite or of iron oxidation products during the negative going sweep. Anodic currents in this potential region may also be associated with the reaction,

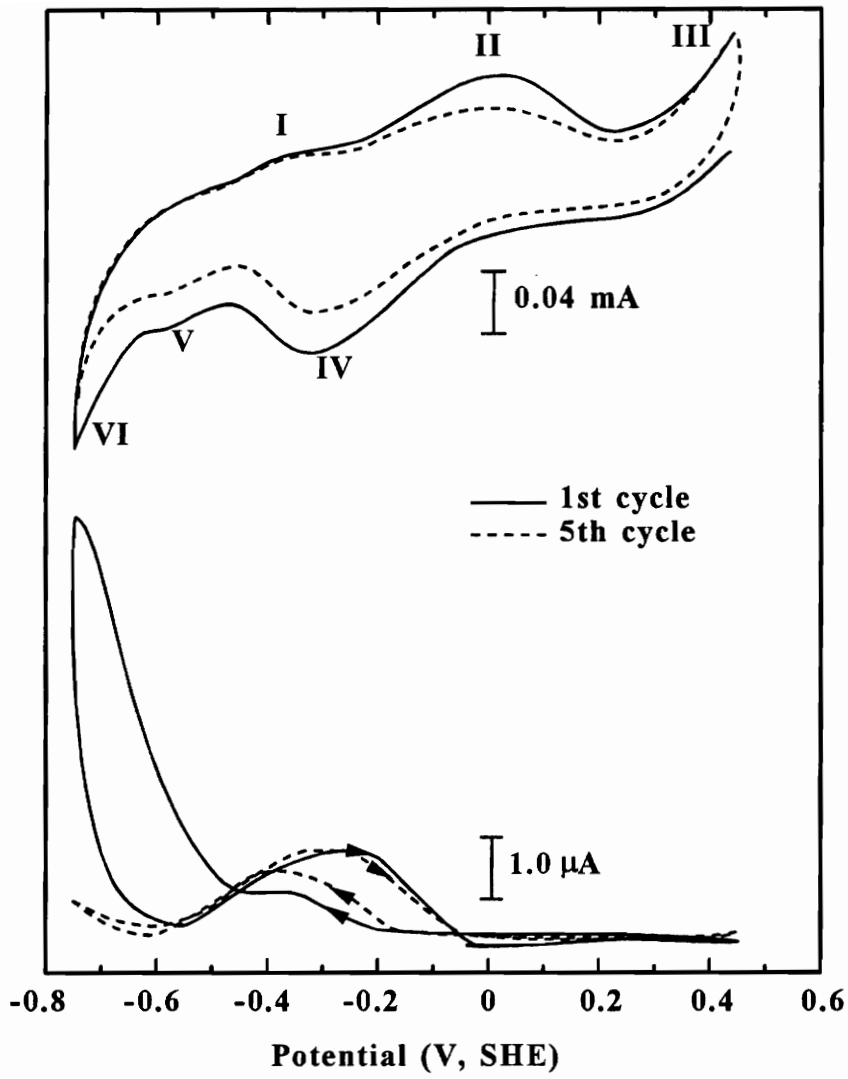

Figure 2.14 The first and fifth voltammograms on RRDE of Chinese coal-pyrite at pH 9.2 with ring held at 0.25 V.

$$Fe + HS^- + OH^- = FeS + H_2O + 2e^- \quad (E = -0.578 - 0.03pH - 0.03log[HS^-]), \tag{2.15}$$

where HS^- is also produced on the surface of pyrite by cathodic decomposition.

The current (III) on the anodic sweep at potentials above 0.25 V increases with increase in the upper potential limit up to 0.65 V, and has been attributed to the oxidation of pyrite itself to form sulfate and ferric hydroxide by the reaction [3, 9, 22],

$$FeS_2 + 11H_2O = Fe(OH)_3 + 2SO_4^{2-} + 19H^+ + 15e^- \quad (E = 0.412 - 0.0749pH + 0.0078\log[SO_4^{2-}]). \tag{2.16}$$

Reductive decomposition of pyrite takes place at potentials more negative than -0.65 V, which is indicated by a consistent increase in cathodic current (VI) at potentials $<$-0.7 V. The reactions can be represented by reactions (2.12) and (2.13).

The above reactions do not involve the production and conversion of hydrophobic species that render pyrite floatable in the absence of collectors and can not explain the origin of collectorless flotation. For studying the self-induced flotation and depression of pyrite, the most important reactions are represented by peaks II and IV in Figure 2.14. Peak II, which occurs at 0 V on the anodic sweep, is generally attributed to the oxidation of $Fe(OH)_2$ to $Fe(OH)_3$ [8, 9]. This reaction presupposes that pyrite has been oxidized and a layer of $Fe(OH)_2$ has been formed on the surface which can be further oxidized to $Fe(OH)_3$. However, if only reaction (2.10) is responsible for peak II, the charge associated with this peak can not exceed that of peak I which represents the formation of ferrous hydroxide. However, peak II obviously contains more charge than peak I in

Figure 2.14.

Hamilton and Woods [3] and Buckley et al. [6] reported that peak II was observed on sweeps commencing at potentials positive of peak I, even when a fresh surface free of iron hydroxide was generated by polishing under a nitrogen atmosphere. Our experiments confirmed their results. Chander et al. [23] resolved the anodic peak at -0.09 V into two current peaks by conducting voltammetry experiments in carbonate and EDTA (ethylenediaminetetraacetic acid) solutions. They suggested that oxidation of ferrous hydroxide and sulfur species both contribute to the anodic current. Michell and Woods [22] determined the ferric hydroxide coverage on pyrite from the anodic peak at about -0.05 V on voltammograms and the X-ray emission spectroscopy. Careful examination of their data reveals that the amount of oxides on three different pyrite electrodes calculated from the integrated charge are considerably larger than that determined from X-ray emission measurements although they claimed that there is a "good agreement" between them. The results suggest that the anodic oxidation may involve species other than iron hydroxide. Work on freshly fractured electrodes discussed in the previous section provides convincing evidences that peak II arises from both the oxidation of ferrous to ferric hydroxide and the oxidation of pyrite to a S^o-like species. When a surface has been previously oxidized to a significant extent, the current due to pyrite oxidation on voltammetry curves may be essentially masked by the oxidation of $Fe(OH)_2$ to $Fe(OH)_3$.

The cathodic peak IV occurring at about -0.32 V in Figure 2.14 arises from

reaction (2.11) and the reverse of reaction (2.10). The fact that this peak is at -0.32 V on the first sweep voltammogram rather than at -0.25 V as observed in Figure 2.10 with the fresh electrode indicates that the pyrite disc electrode may be slightly oxidized by electrode polishing. It was reported [3, 8] that in basic solutions, peaks II and IV are independent of solution convection (rotation speeds) and contain the same charge. This indicates that the species are insoluble surface products. It is not surprising, therefore, that standard voltammetry techniques do not separate reaction (2.11) and the reverse of reaction (2.10). When electrodes are prepared by routine polishing techniques in air, the reduction of ferric hydroxide predominates, masking reaction (2.11) which is more relevant to flotation.

Figure 2.14 (bottom) shows the current observed at the gold ring held at 0.25 V. During the cathodic sweep, a ring current commences at -0.1 V which is clearly associated with oxidation of the species reduced over peak IV. The reduction product for this peak is believed to be a soluble ferrous hydroxide species such as $Fe(OH)_2$, $Fe(OH)^+$, Fe^{2+}, etc. [24]. From the measured collection efficiency, it is determined that approximately 10% to 20% of the species reduced over peak IV is reoxidized on the ring. This value appears to be unreasonable if one only considers thermodynamics of the hydrolysis of ferrous ions ($K_{sp} = 4.79\times10^{-17}$ for $Fe(OH)_2$). However, thermodynamic data are true only at equilibrium. It is believed that pyrite oxidation may generate a number of intermediates. For example, Chander and Briceno [18] and Chander et al. [23] suggested that intermediate sulfur oxidation products may include $S_2O_3^{2-}$, $S_xO_y^{2-}$, etc.

Zhu et al. [8] proposed the reaction,

$$FeS_2 + (y+1)H_2O = Fe(OH)^{2+} + S_2O_y^{2-} + (2y+1)H^+ + (2y+1)e^- \qquad (2.17)$$

to explain the loss of passivation of pyrite during oxidation in stirred solution. In addition, hydrogen ions produced in reaction (2.16) can significantly reduce the local pH of the solution in the vicinity of the electrode, enhancing the dissolution of ferric hydroxide. It has been reported that the pH near an electrode can be different from its bulk value in a solution layer of a thickness of up to 1 mm [25]. Finally, the intense centrifugal force and solution turbulence created by electrode rotation may facilitate the diffusion of ferrous species before they can be nucleated and precipitated on the surface of pyrite.

It is of particular interest that on the subsequent anodic sweep, an additional oxidation current is observed on the ring (Figure 2.14). This indicates that a double oxidation process occurs, i.e., a soluble oxidation species is generated at the disc on the initial portion of the positive going sweep, and this oxidation product is further oxidized at the ring. This double oxidation process is also consistent with the known electrochemistry of pyrite and the existence, as shown above, of a soluble ferrous hydroxide reaction product. When pyrite, or previously existing iron oxides or hydroxides on pyrite are reduced at potentials near -0.7 V, elemental iron is formed. On the return anodic sweep, iron is oxidized to yield $Fe(OH)_2$ and possibly $Fe(OH)^+$. The ring current on the initial portion of the anodic sweep thus results from the oxidation of

a soluble ferrous hydroxide species. Essentially, the same species (soluble ferrous hydroxide) is responsible for the ring current on the cathodic sweep, where it is produced by reduction of $Fe(OH)_3$, and for the ring current on the anodic sweep, where it is produced by the oxidation of elemental iron.

Figure 2.14 also shows that the ring current below -0.6 V during the cathodic sweep is associated with the reduction process labeled VI and perhaps also with peak V, particularly on the first sweep. Peak V has been attributed to the reduction of sulfur to HS^- [8], with the sulfur produced on the positive going sweep. The height of this peak increases considerably with the addition of 1 mM Na_2S (not shown). The current increase at VI arises from the decomposition of pyrite by reactions (2.12) and (2.13), both of which produce HS^-. The ring current on the cathodic sweep at disc potentials $<$ -0.6 V is due to the oxidation of HS^- to S°.

It is noticed in Figure 2.14 that there is a substantial difference in ring current between the first and the subsequent cycles. This can be explained by assuming that at least two reduction processes are associated with peak IV, one being the reverse of reaction (2.10) which produces a soluble ferrous hydroxide and the other producing an insoluble iron sulfide *via* a process such as reaction (2.11) [3]. As a result, peak IV would depend on the total amount of $Fe(OH)_3$ and sulfur-rich species (as excess sulfur in the lattice, polysulfide, or elemental sulfur) produced on the prior anodic sweep, and the ring current only on the amount of $Fe(OH)_3$ that is reduced to a soluble ferrous species. On the first cathodic sweep, there was less iron hydroxide to react with sulfur-

rich species by reaction (2.11), and hence more HS^- was released from the disc as the reduction product. On subsequent sweeps, the abundance of sulfur-rich species relative to iron hydroxide diminishes since most of the iron hydroxide produced on anodic sweeps remains on the surface while the major portion of HS^- diffuses into the bulk solution.

Further support for assigning at least two reduction processes to peak IV is provided in Figure 2.15, where the anodic limit has been increased. It is mentioned previously that pyrite oxidation can occur *via* two paths, reactions (2.16) and one or more of reactions (2.7)-(2.9), where the relative yield of S^o-like species and SO_4^{2-} depends on the anodic limit. Higher potentials favor sulfate formation and thus lead to a reduction in the quantity of insoluble, reducible sulfur species on the electrode relative to the quantity of $Fe(OH)_3$. On the reverse cathodic sweep, a lower surface concentration of reducible sulfur species should decrease the contribution of reaction (2.11) to peak IV and increase the amount of soluble ferrous hydroxide that is reoxidized on the ring. This is consistent with Figure 2.15 which shows that the ring current increases with increase in the anodic limit, while the charge associated with peak IV changes only slightly with the anodic limit.

Figure 2.16 illustrates the effect of the addition of ferrous chloride on the disc voltammograms and the ring response. It can be seen that with 5×10^{-5} M Fe^{2+} in solution, the cathodic peak IV on the disc voltammograms increased considerably and the peak potential shifted to about -0.4 V, confirming the suggestion that part of the peak results from the reduction of ferric compounds. A second cathodic peak is also resolved

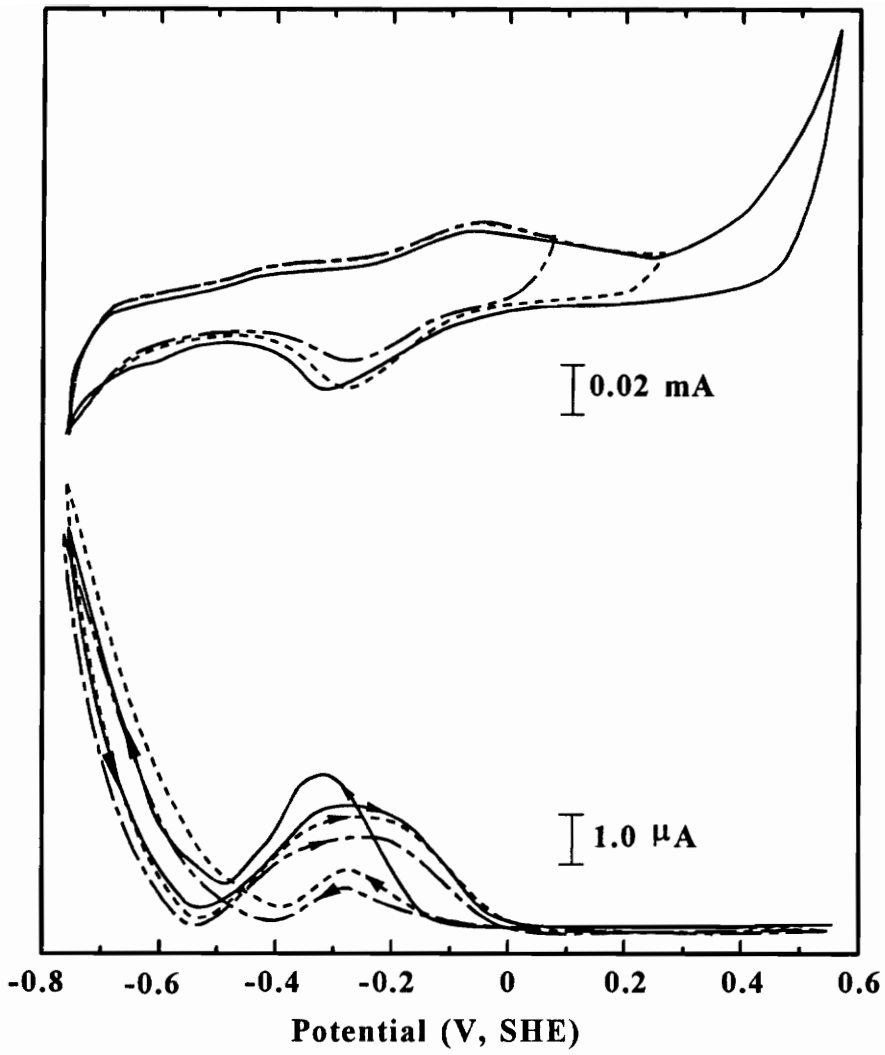

Figure 2.15 Voltammograms on RRDE of Chinese coal-pyrite at pH 9.2 with upper potential limit at 0.05 V, 0.25 V and 0.55 V. Ring was held at 0.25 V.

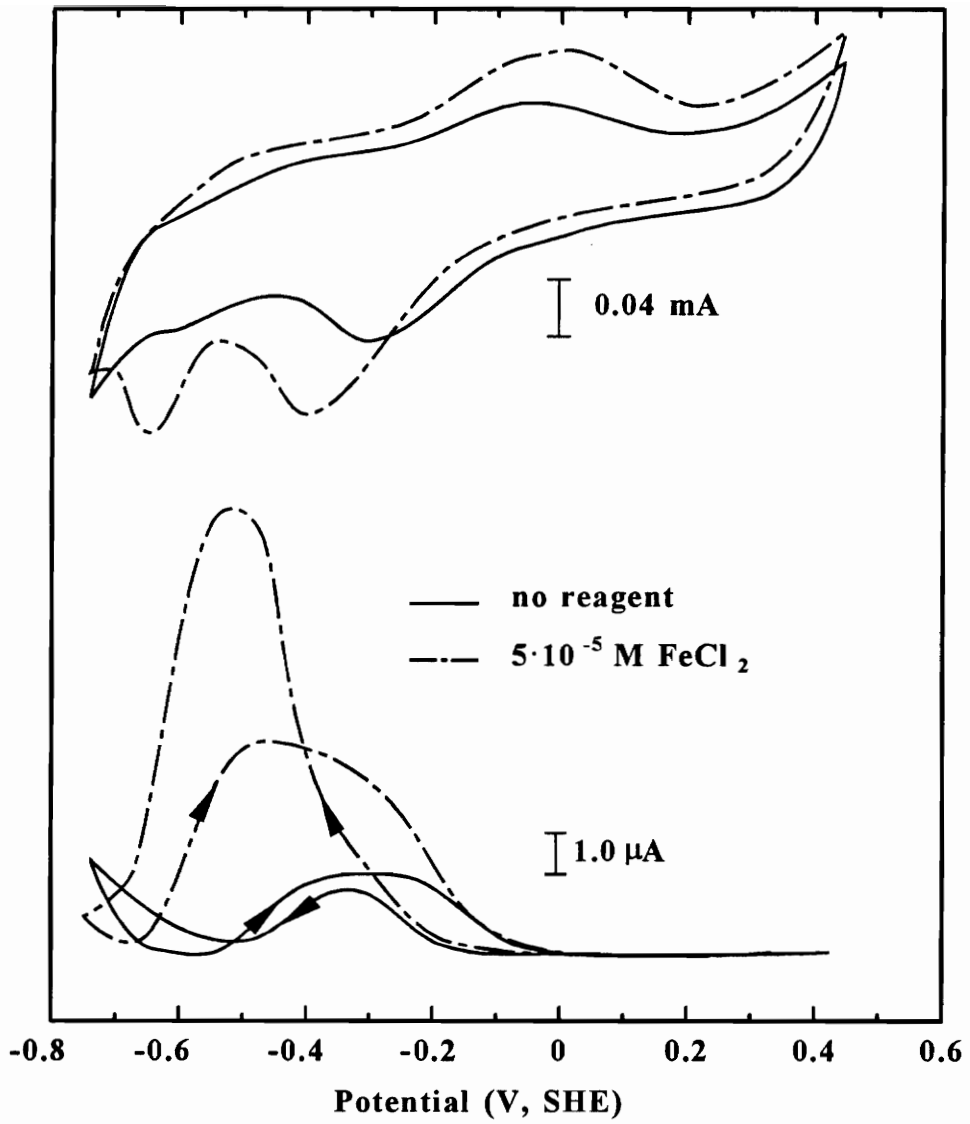

Figure 2.16 Voltammograms on RRDE of Chinese coal-pyrite at pH 9.2 in the absence/presence of ferrous chloride with ring held at 0.25 V.

at -0.65 V and can be attributed to the reduction of ferrous hydroxide to elemental iron. The additional ring current observed during both the cathodic and anodic sweeps indicates that the addition of Fe^{2+} leads to an increase in $Fe(OH)_3$ formation during the anodic sweep at potentials near 0 V (apparent on the voltammogram), and a subsequent increase in the concentration of soluble ferrous hydroxide produced during the cathodic sweep (also evident on the voltammogram). The addition of Fe^{2+} also increased the ring current during the subsequent anodic scan, indicating a larger amount of elemental iron was produced at the negative potential limit which was then oxidized to form the soluble ferrous hydroxide species. However, it appears that the addition of ferrous ions hinders the reduction of pyrite at potentials $<$-0.7 V, possibly due to the existence of a thick passivating layer on the surface. This effect is similar to that observed when a high upper potential limit is used [4,8], where the potential for pyrite reduction shifts to values more negative than -0.9 V.

Mineral- and Pittsburgh No. 8 coal-pyrite exhibit voltammograms similar to those for the Chinese coal-pyrite at pH 9.2. Figure 2.17 shows the second voltammograms and ring currents of the three pyrites for comparison. Both of the coal-pyrites are significantly more reactive than mineral-pyrite. It is very interesting to notice that the oxidation of Pittsburgh No. 8 coal-pyrite produces less soluble species than the other two pyrites, while it forms more insoluble products than mineral-pyrite; on the other hand, mineral-pyrite generates the least amount of insoluble products. The difference in the relative amount of soluble to insoluble oxidation products may partially explain the

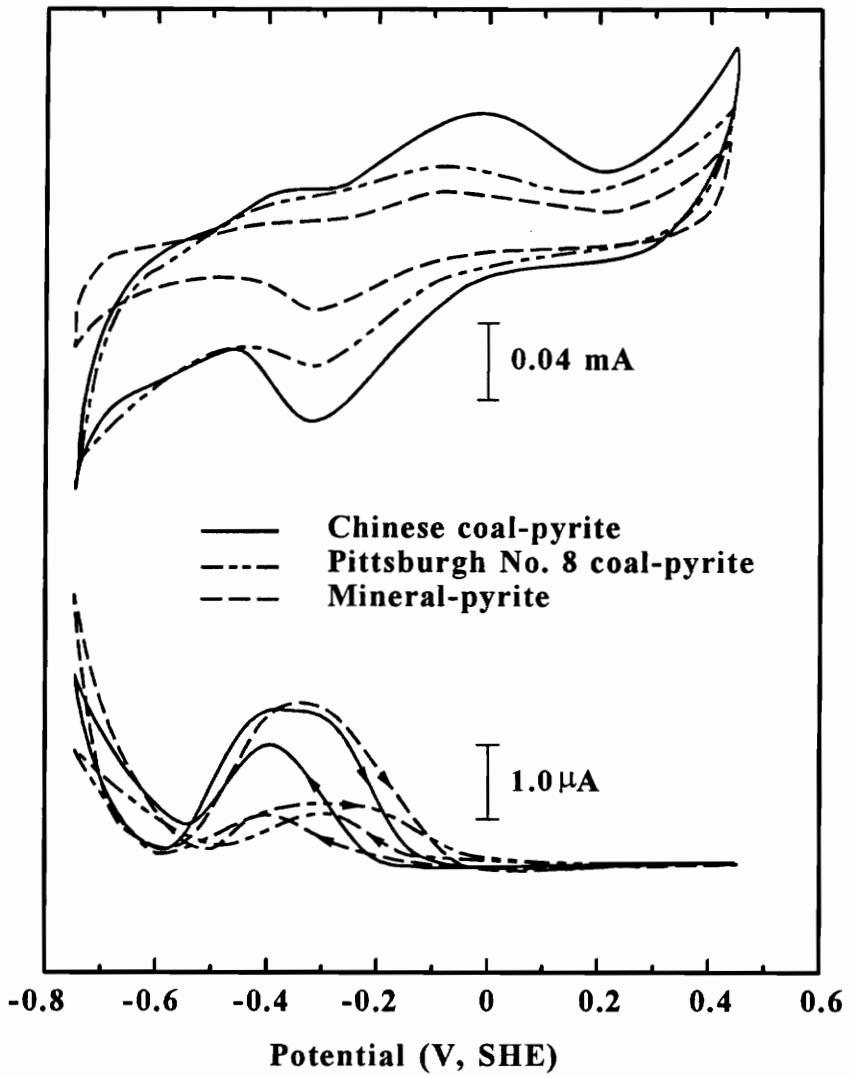

Figure 2.17 Ring-disc voltammograms of different pyrite samples at pH 9.2 (ring at 0.25 V).

difference of flotation behavior of various pyrites. It will be shown in the next chapter that mineral-pyrite is more floatable than coal pyrites, which can be expected from the above study.

Figure 2.18 shows the disc voltammograms and ring responses for three pyrite specimens at pH 6.8. Chinese coal-pyrite behaves similarly to mineral-pyrite but Pittsburgh No. 8 coal-pyrite exhibits considerably different characteristics. For mineral- and Chinese coal-pyrite, the cathodic peak on the disc voltammogram is observed at -0.1 V and results in a ring current. This behavior is similar to that exhibited at pH 9.2, with the peak shift due to the pH dependence of the reaction. Two small anodic peaks at -0.25 V and 0.1 V are more clearly discernable using a more sensitive current scale (not shown). The ring current is significant at the beginning of the anodic sweep and seems to be relatively constant up to 0.15 V, but no peak is present, in contrast with the observation at pH 9.2. In contrast, Pittsburgh No. 8 coal-pyrite exhibits a cathodic peak at -0.28 V which does not yield a corresponding ring current, implying that no soluble species is formed during cathodic reduction. The voltammetry curves and ring currents on the three pyrites clearly establish that the oxidation and reduction processes on Pittsburgh No. 8 coal-pyrite are considerably different than those on mineral-pyrite and those on well-crystallized Chinese coal-pyrite. Pittsburgh No. 8 coal-pyrite is much more reactive than the other pyrites and the products of the reaction appear to be different since no soluble reaction products are detected at the ring during the voltammetry sweeps.

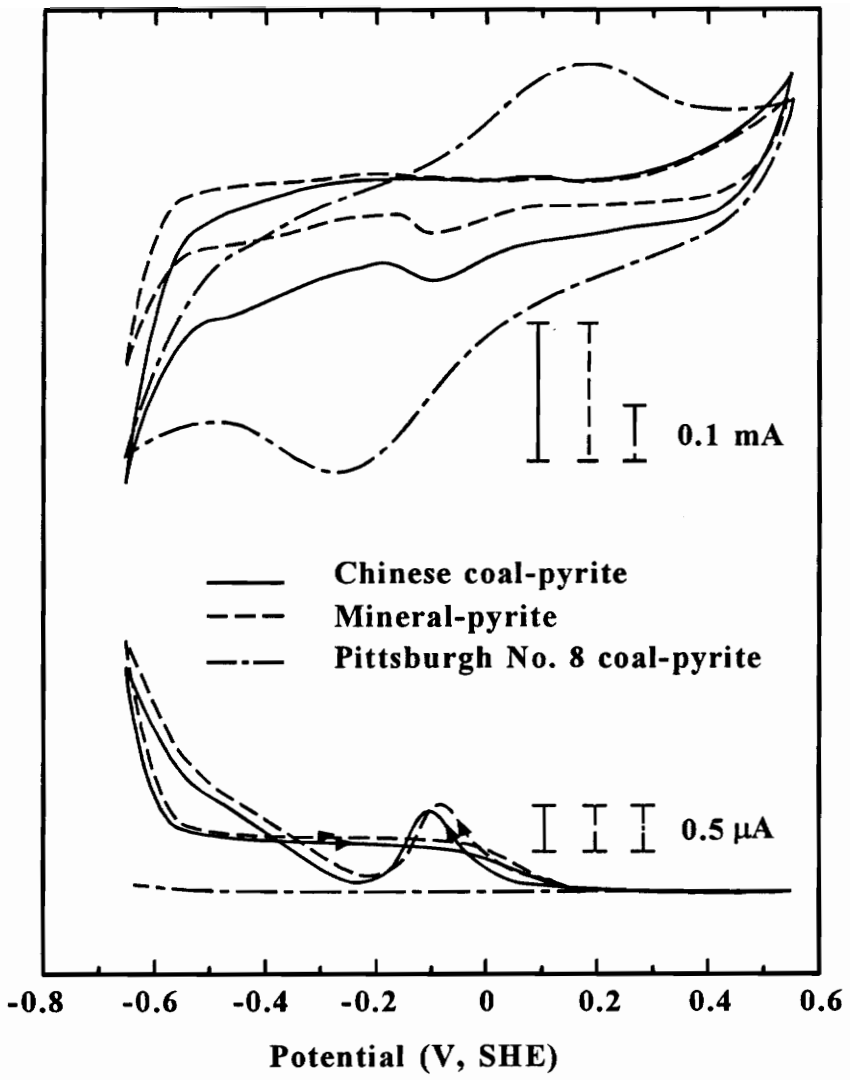

Figure 2.18 Ring-disc voltammograms of different pyrite samples at pH 6.8 (ring at 0.25 V).

The increased reactivity and the absence of soluble reaction products on Pittsburgh No. 8 coal-pyrite may arise from its porous nature, with the reactions taking place internally in pores. The large surface area associated with numerous pores would increase the apparent reactivity, whereas the reactions in pores would hinder diffusion of soluble products to the surface of electrode where they could be convected to the ring to undergo further reaction.

At acidic pH's, pyrite exhibited a considerably different electrochemical behavior than at pH 9.2 and at pH 6.8. Figure 2.19 illustrates the disc voltammograms and ring currents between -0.4 V and 0.55 V at pH 4.6, when the potential of the ring electrode was held 0.25 V. Hamilton and Woods [3] showed that a step is present on voltammograms of mineral pyrite at 0.4 V in pH 4.6 solutions during anodic sweeps on stationary electrodes but not on rotating electrodes. The step was attributed to the reaction,

$$Fe^{2+} + 3H_2O = Fe(OH)_3 + 3H^+ + e^- \quad (E = 0.971 - 0.177pH - 0.059\log[Fe^{2+}]) \tag{2.18}$$

and its absence on rotating electrodes was explained by the convection of the reactant away from the surface. In agreement with their results, there is no step at 0.4 V on rotating electrodes of mineral- and Chinese coal-pyrite in Figure 19. However, a distinct oxidation peak is observed at this potential on the Pittsburgh No. 8 pyrite. There is a corresponding reduction process on the subsequent negative going sweep that begins at 0.3 V and is believed to represent the reverse of reaction (2.18). This provides further

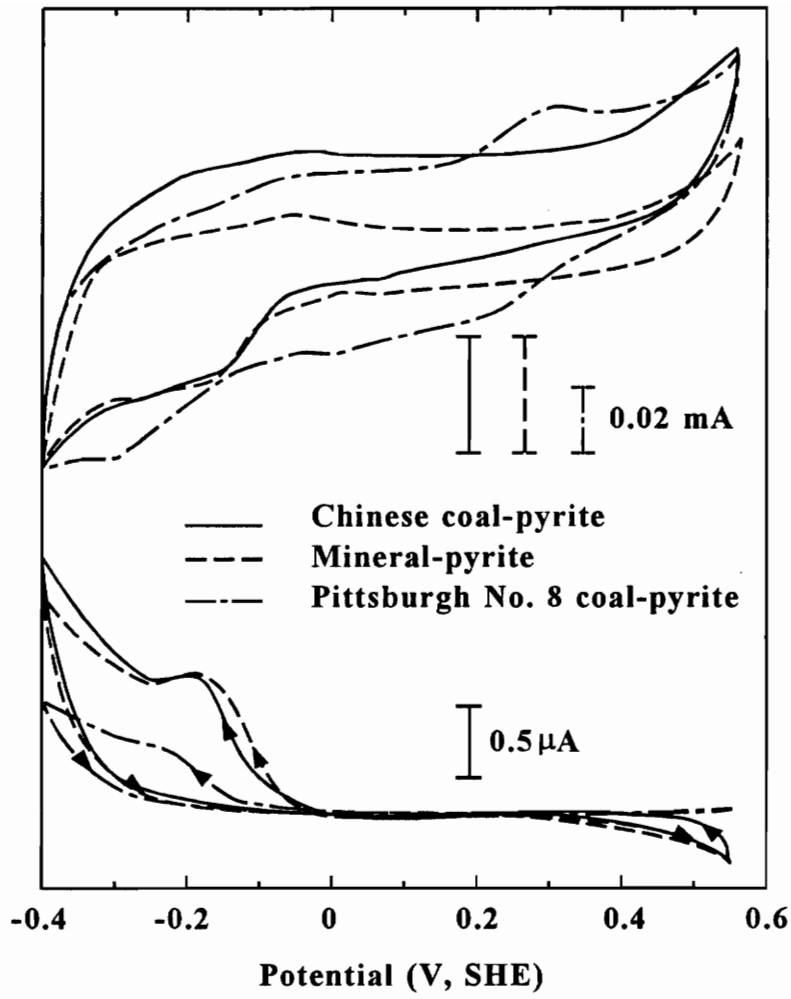

Figure 2.19 Ring-disc voltammograms of different pyrite samples at pH 4.6 (ring at 0.25 V).

evidence that Pittsburgh No. 8 coal-pyrite is different from mineral-pyrite and Chinese coal-pyrite. Again, this difference can be accounted for by assuming that the surface area of the Pittsburgh No. 8 coal-pyrite is much larger than that of the other pyrites due to the presence of numerous pores and that the diffusion and convection of soluble reactants and products in the pores are hindered.

Distinct reduction processes are observed at potentials $<$-0.05 V on the voltammetry curves for the mineral- and coal-pyrite electrodes. The reduction currents in this range of potentials are believed to primarily arise from the reduction of excess sulfur produced by anodic reaction at potentials $>$0.4 V. Since the formation of $Fe(OH)_3$ is suppressed by dispersion of Fe^{2+} on the rotating electrode, the major insoluble reaction product formed at anodic potentials is excess sulfur, i.e., there is little $Fe(OH)_3$ to be reduced on the mineral- and Chinese coal-pyrite. On these two pyrites, the reduction of excess sulfur and oxidation of the reduction product give rise to a finite ring current. On the Pittsburgh No. 8 coal-pyrite, a broad reduction process begins at about 0.3 V on the cathodic sweep and continues until the cathodic limit is reached. Both $Fe(OH)_3$ and excess sulfur are present on the surface at the beginning of the cathodic sweep and the broad reduction process initially represents the reformation of an iron sulfide (FeS) when these products are reduced. It is believed that the $Fe(OH)_3$ is depleted before the excess surface sulfur. Thus, at more negative potentials, a sulfur species is reduced to H_2S and its reoxidation produces a small ring current. The H_2S does not appear to be trapped in the pores. This may be because the production of

gaseous H_2S builds up sufficient pressure to force the product out of the pores.

Previous studies have also shown that coal-pyrite possesses significantly different electrochemical behavior than mineral-pyrite because of differences in morphology, carbon inclusions, heterogeneity and so on [26-29]. Wang et al. [28] concluded that the rate of oxidation of Pittsburgh No. 8 and Upper Freeport coal-pyrites decreases when it contains carbon inclusions. Zhu et al. [30] showed that voltammograms of Pittsburgh No. 8 and Upper Freeport coal-pyrites have fewer anodic and cathodic waves than those of mineral-pyrite but the current density on coal-pyrites were 10-100 times larger than that of mineral-pyrite.

The remarkable differences between the three pyrite samples observed in the present study led to the study of their microstructure. Figures 2.20 and 2.21 show SEM (scanning electron microscope) microphotographs of Pittsburgh No. 8 coal- and mineral-pyrite electrodes respectively (SEM microphotograph of Chinese coal-pyrite electrode is not shown because of its close similarity to that of mineral-pyrite). The microphotograph clearly demonstrate that Pittsburgh No. 8 coal-pyrite is truly much more porous, therefore of larger surface area, which verifies earlier conclusions.

The above experiments with freshly fractured electrodes and rotating ring-disc electrodes establish that mineral- and Chinese coal-pyrite oxidizes at potentials above about -0.28 V and 0 V at pH 4.6. Oxidation of Pittsburgh No. 8 coal-pyrite takes place above -0.15 V at pH 9.2. Based on the first sweep voltammetry curves on pyrite surfaces produced by *in-situ* fracture, $Fe(OH)_3$ is one of the oxidation products. From

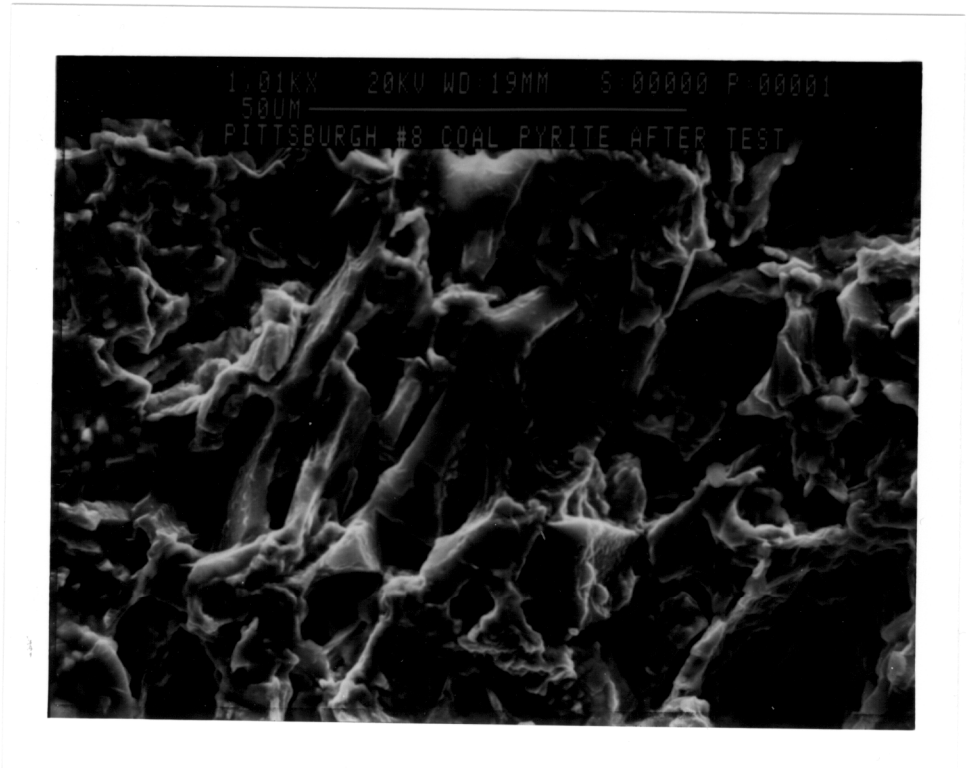

Figure 2.20 SEM microphotograph of Pittsburgh No. 8 coal-pyrite electrode.

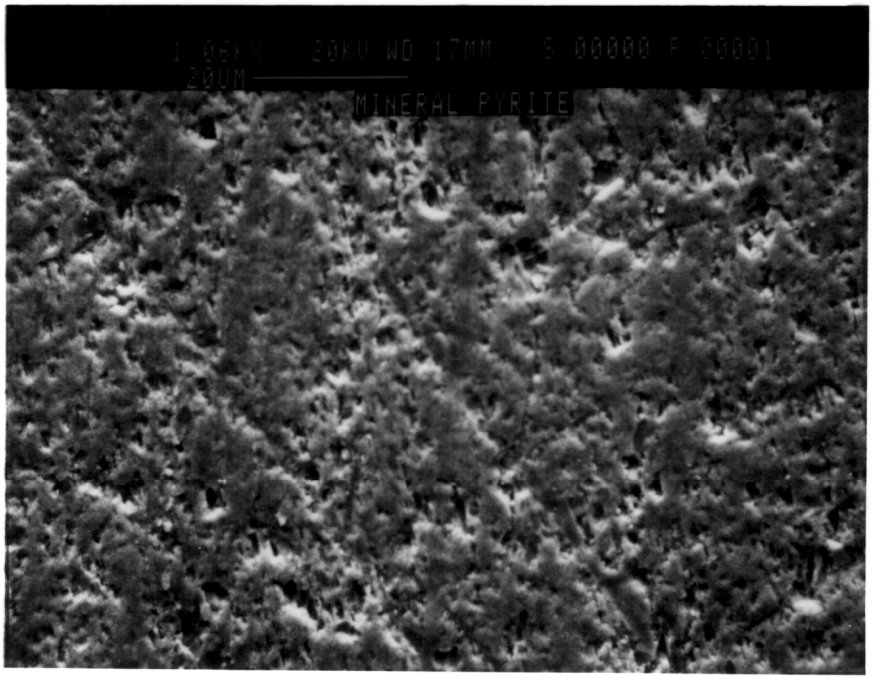

Figure 2.21 SEM microphotograph of mineral-pyrite electrode.

the standpoint of flotation, $Fe(OH)_3$ is hydrophilic and should depress pyrite. However, the oxidation state of sulfur at the surface should also change when pyrite is oxidized to $Fe(OH)_3$. The most likely sulfur product resulting from initial pyrite oxidation is iron polysulfides or iron-deficient sulfides. Based on cyclic voltammetry and A-C impedance spectroscopy, Chander and his co-workers [18, 31] proposed that hydrophilic iron oxide/hydroxide overlays a hydrophobic sulfur-rich layer after oxidation. Mild abrasion due to stirring is sufficient to remove iron oxides and hydroxides, thereby exposing the sulfur-rich layer underneath and giving rise to self-induced (or collectorless) flotation [1, 9]. It is also important to notice that a soluble ferrous hydroxide is produced on pyrite in alkaline solutions. It is known that sulfides are neither strongly hydrophobic nor strongly hydrophilic [32] and that slight changes in the surface can have a profound effect on their floatability. The formation of soluble iron compounds may provide a mechanism which explains why pyrite can exhibit self-induced flotation in alkaline solutions. Essentially, the loss of soluble iron species coupled with the retention of sulfur at the surface may increase the net hydrophobicity of pyrite after oxidation.

2.4.4 XPS study of the surface oxidation of Pittsburgh No. 8 coal-pyrite

The foregoing study of surface reactions on pyrite by cyclic voltammetry yielded detailed kinetic and mechanistic information on processes taking place on the mineral. However, electrochemical techniques lack the molecular specificity required to give

unequivocal identification of the nature of species on the surface of electrodes. To complement electrochemical studies, X-ray photoelectron spectroscopy (XPS) was employed to provide information on the elemental and molecular composition of surface oxidation products of Pittsburgh No. 8 coal-pyrite.

XPS is one of the most widely used surface analysis techniques. It subjects the sample to monochromatized X-ray radiation and detects the photoemitted electrons. The observed photoelectrons come from the outermost 2-6 atomic layers, i.e., 5-40 Å, and carry information on the surface electronic structures and bonding. The value of the binding energy determines the type of atoms present in the solid and the chemical shifts give information on the chemical bonds of the elements, i.e., difference in the oxidation state, difference in molecular environment, and difference in lattice site. Quantitative information on atomic ratios can be obtained by the analysis of the photoelectron emission intensities.

It has been well established [1, 5, 20] that the binding energy of the $S2p_{3/2}$ component of unoxidized pyrite is in the range of 162.2-162.4 eV while the corresponding value for bulk elemental sulfur is 163.5-164.0 eV; the binding energy of $Fe2p_{3/2}$ component of unoxidized pyrite is 707-707.5 eV. The peak at 168 or 169 eV in the S2p spectrum is characteristic of iron sulfate [4, 5]. Yoon et al. [1] also found a broad shoulder in the 710-715 eV in the Fe2p spectrum which is believed to represent the oxidized iron in the form of $Fe(OH)_3$, FeO(OH), Fe_2O_3, Fe_3O_4, etc. Buckley and Woods [4] reported three distinct binding energy regions in the O1s spectrum at about

530, 531 to 532 and near 533 eV are associated with oxide, hydroxide and chemisorbed oxygen species, and physically adsorbed water, respectively.

Recently, more XPS work has been carried out by Basilio et al. [33] on Pittsburgh No. 8 coal-pyrite to better understand surface oxidation of the mineral. The surface of the coal-pyrite sample was wet polished with a 600 grit silicon carbide paper before being subjected to oxidation treatment. The oxidation was accomplished under different conditions, including (i) exposure to air for one hour, (ii) conditioning in aqueous solution at pH 9.2 at open circuit potential for 10 minutes, and (iii) conditioning in aqueous solutions at pH 9.2 at 0.7 V for 10 minutes. For comparison, fresh coal-pyrite surfaces were also characterized. Those were prepared by scraping the sample surface under ultra high vacuum (UHV) in a special scraping chamber of the XPS spectrometer.

Figure 2.22 shows the S2p spectrum of that coal-pyrite scraped under UHV. Unoxidized pyrite surfaces generally exhibit a well resolved doublet composed of $S2p_{3/2}$ and $S2p_{1/2}$, which are split by 1.2 eV with an intensity ratio of 2:1 [5]. In the S2p spectrum of this coal-pyrite sample, additional signals were observed on both sides of the main S2p doublet. The spectrum can be fitted reasonably well with three different components. The main component shown by the most intense peaks at 162.5 eV and 163.7 eV is attributed to the $S2p_{3/2}$ and $S2p_{1/2}$ doublet from bulk FeS_2. The additional S2p doublet component at the lower binding energy side is apparent in Figure 2.22 with the $S2p_{3/2}$ peak at 161.5 eV. This peak was also observed by Mycroft et al. [20] at 161.8 eV on fresh mineral-pyrite surface. Buckley and Woods [34] reported that unoxidized

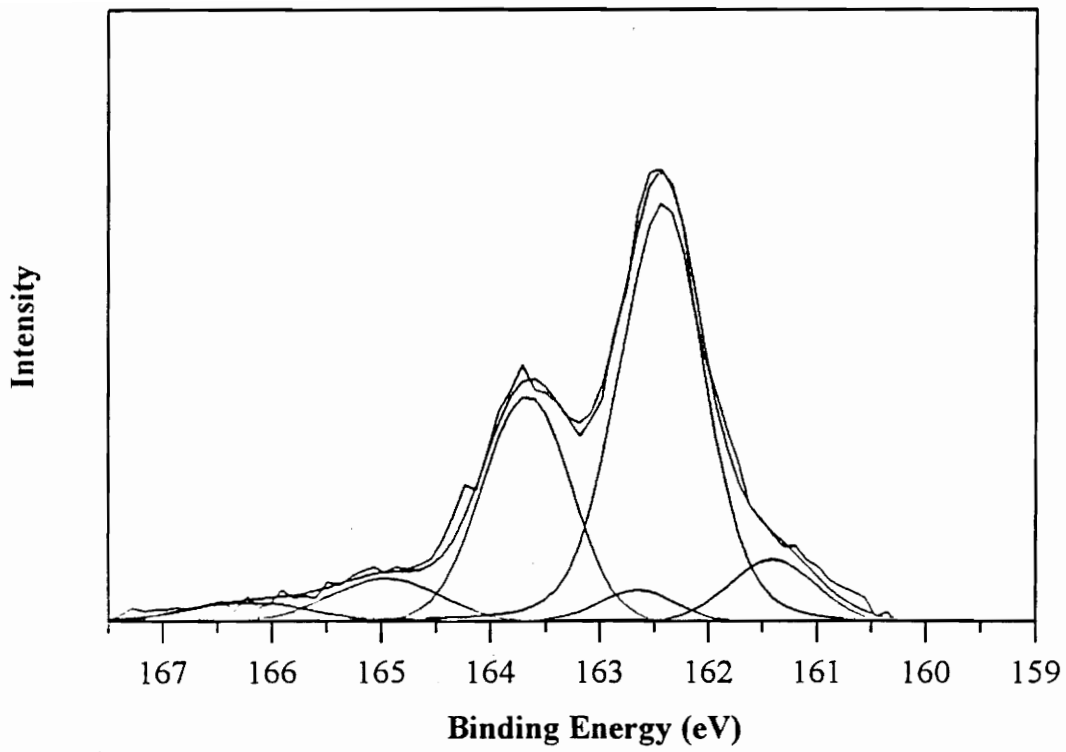

Figure 2.22 S2p spectrum of Pittsburgh No. 8 coal-pyrite scraped under UHV.

pyrrhotite exhibits a doublet with the $S2p_{3/2}$ component at near 161.1 eV. Therefore, it is likely that the doublet with the $S2p_{3/2}$ component at 161.5 eV arises from the FeS-like species in the FeS_2 substrate, which accounts for about 10% of the total S2p intensity. This FeS-like surface component on Pittsburgh No. 8 coal-pyrite may explain why freshly fractured electrodes of Pittsburgh No. 8 coal-pyrite exhibited zero-current upon fracture at -0.15 V while mineral- and Chinese coal-pyrites had zero-current at -0.28 V. The broad S2p doublet component in the 164-166 eV region may be attributed to energy loss of S2p electrons escaping from an unaltered pyrite surface [5] and a possible residual effect due to inelastic scattering [20].

The Fe2p spectrum of the sample scraped under UHV (Figure 2.23a) [33] showed a single doublet with the ($Fe2p_{3/2}$) component at 707.3 eV, indicative of FeS_2 based on previous studies [1, 5, 20]. No discernible signals from iron oxidation products are present in the Fe2p spectrum, which is in good agreement with results obtained by Buckley and Woods [5] with fresh surfaces of mineral-pyrite. There is a small signal near 708 eV, which may be caused by FeS-like species.

The fresh surface showed small amounts of oxygen and carbon contaminants indicated by relatively small quantities of O1s and C1s photoemissions (not shown). These contaminants were not observed on mineral-pyrite scraped under UHV. Oxygen and carbon contamination of the coal-pyrite sample may be associated with small amounts of coal inclusions in the sample. An appreciable amount of oxygen-containing species was reported on the fresh fracture surface of mineral-pyrite exposed to air for no more

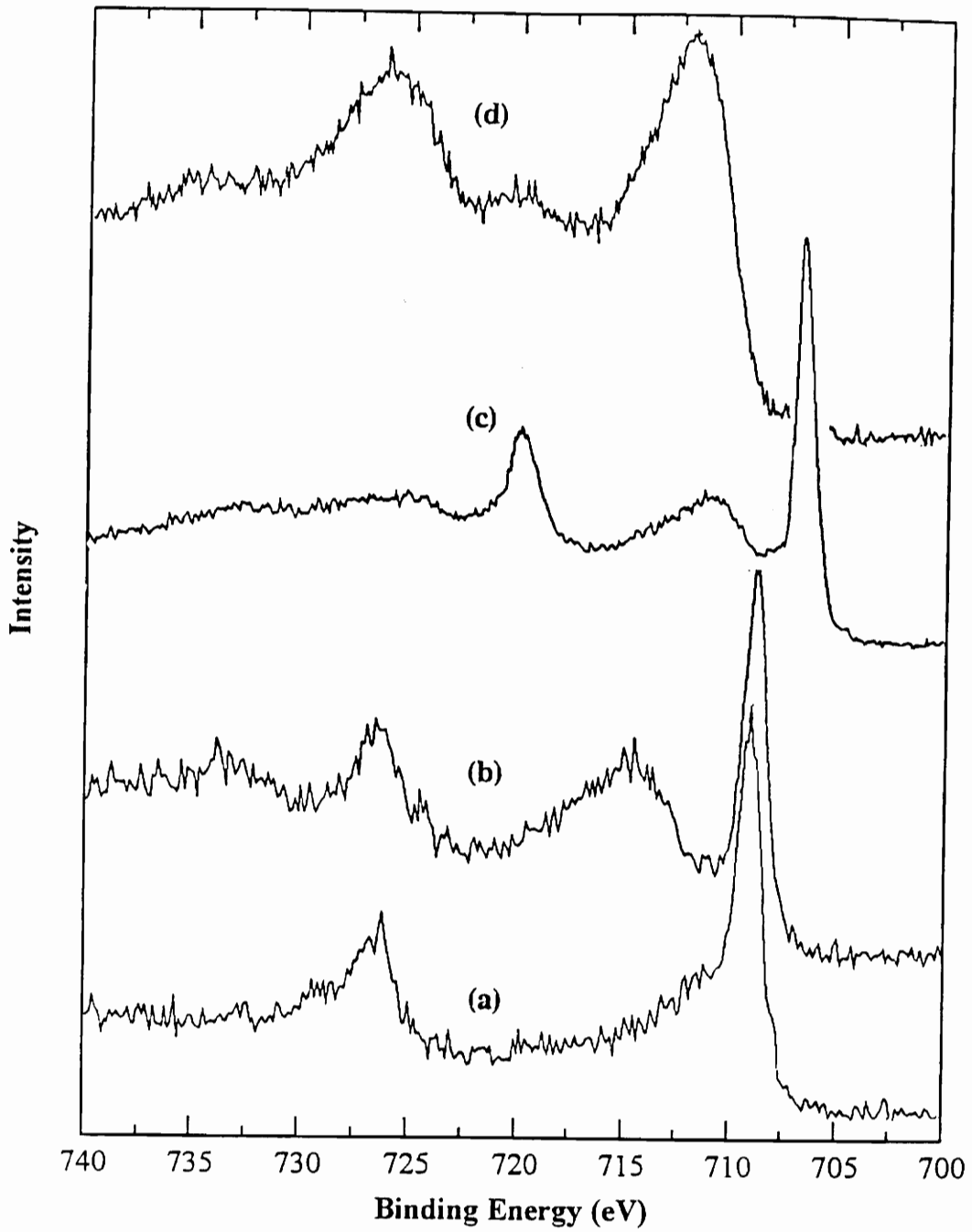

Figure 2.23 **Fe2p spectrum of Pittsburgh No. 8 coal pyrite (a) scraped under UHV; (b) exposed to air for one hour; (c) oxidized at pH 9.2 at open circuit potential for 10 min; (d) same as (c) but at 0.7 V.**

than a few seconds, and this species was identified to be chemisorbed water or hydroxide by Brundle et al. [35].

Figure 2.24a shows the S2p spectrum for the Pittsburgh No. 8 coal-pyrite sample oxidized in air for one hour [33]. Oxidation of the sample in air results in a decrease of the $S2p_{3/2}$ component at 161.5 eV, possibly due to the oxidation of the FeS-like surface species to FeS_2 . The signal of the S2p doublet of the FeS-like product decreased to about 1 % of the total S2p intensity. However, there is no indication of the formation of elemental sulfur or sulfate.

The Fe2p spectrum shows a new component at around 711.5 eV (Figure 2.23b) which indicates the presence of iron oxide and/or iron hydroxy-oxide [36, 37, 38]. This is confirmed by the shift of the O1s peak to a lower binding energy. The same behavior was exhibited by mineral-pyrite surfaces that were abraded under oxygen-free water, dried, and then exposed to air [5]. Theoretically, the oxidation of the iron component of pyrite must be accompanied with the oxidation of sulfur component. The absence of sulfur oxidation products under these particular conditions suggests that iron oxides or hydroxides are formed during wet-polishing or abrading in solutions while sulfate produced is dissolved. The presence of iron oxides and hydroxides passivates the surface and prevents the oxidation of pyrite on exposure to air.

Freshly fractured mineral-pyrite surfaces oxidized under similar conditions were reported to have spectra that are considerably different from those shown above. Buckley and Woods [5] found that exposure of a fresh fracture surface to ambient air at

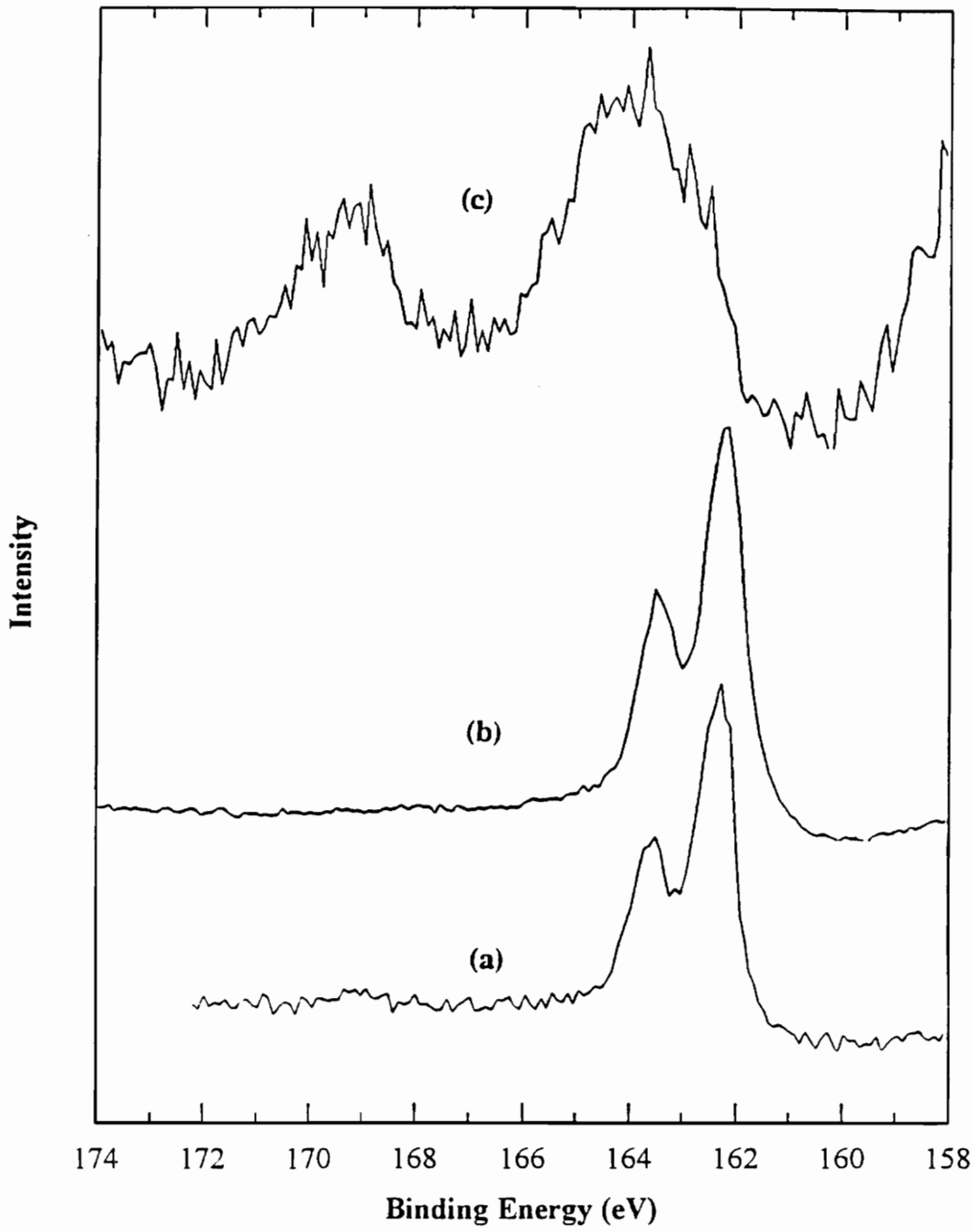

Figure 2.24 **S2p spectrum of Pittsburgh No. 8 coal-pyrite oxidized (a) in open air for one hour; (b) in pH 9.2 solution at open circuit for 10 minutes; (c) in pH 9.2 solution at 0.7 V for 10 minutes.**

65% relative humidity and 295 K for a few days produced a peak near 168.5 eV in the S2p spectrum, which they attributed to sulfate, and new intensity at 711 eV in the Fe2p spectrum, which they identified as ferrous sulfate rather than hydrated iron oxide. The onset of sulfate formation was apparent in spectra from fracture surfaces exposed to air for a few minutes. The formation of iron oxide, most probably hydrated, was just evident on the surface of pyrite exposed to air for 14 days.

Pittsburgh No. 8 coal-pyrite treated in pH 9.2 aqueous solutions at open circuit showed an S2p spectrum (Figure 2.24b) similar to that observed with the sample oxidized in air for one hour (Figure 2.24a). No sulfur oxidation products other than FeS-like species are evident in Figure 2.24b. On the other hand, the corresponding Fe2p spectrum shown in Figure 2.23c also exhibits a component near 711.5 eV, indicating the existence of iron oxides or hydroxides. The O1s and C1s spectra are almost identical to those for the sample oxidized in air for one hour. It is very likely that the sulfur component in pyrite was oxidized to sulfate that dissolved in solutions. These results suggest that the degree of oxidation obtained in air for one hour is similar to that achieved in pH 9.2 aqueous solutions at the open circuit potential for 10 minutes, which appears to confirm the preceding postulation that iron oxides or hydroxides produced during polishing hinders further oxidation of pyrite due to the formation of a passivating layer.

Figure 2.23c shows the S2p spectrum of Pittsburgh No. 8 coal-pyrite oxidized at 0.7 V in aqueous solutions of pH 9.2 for 10 minutes. The spectrum is significantly

different from that of the fresh surface. The difference arises from aggressive oxidation of the mineral at 0.7 V which is shown in Figure 2.17. The S2p line is shifted to higher binding energy due to surface charging caused by the formation of an insulating oxidation product overlayer. The spectrum can be curve-fitted with at least three doublets which are different from those obtained for the fresh surface shown in Figure 2.22. Pyritic sulfur is shown by the doublet on the low binding energy side with a corrected binding energy for $S2p_{3/2}$ of 162.4 eV. The presence of elemental sulfur is indicated by the doublet whose corrected $S2p_{3/2}$ component is observed at 164.1 eV. The third doublet is between those for pyritic and elemental sulfur, which can be attributed to the formation of polysulfides. There is also another component observed at 168.5 eV that indicates the presence of iron sulfate.

It is interesting to note that after warming the sample overnight to about 300 K, the intensity associated with the $S2p_{3/2}$ component at 164.1 eV decreased from 23% to about 17% of the total sulfur intensity, which confirms that this doublet arises from elemental sulfur. There are no changes in the spectrum for the other sulfur components except for the loss of surface charging.

The corresponding Fe2p spectrum obtained after oxidation at 0.7 V for 10 minutes, as given in Figure 2.24d, shows a substantial decrease in the FeS_2 component represented by $Fe2p_{3/2}$ at 707.4 eV, while the iron oxide, iron hydroxide and iron sulfate species indicated by $Fe2p_{3/2}$ component in the 711 to 713 eV region increased sharply. The presence of iron sulfate is confirmed by the S2p and O1s spectra and the presence

of the iron oxide and/or iron hydroxide is substantiated by the O1s spectrum.

The above data indicates that Pittsburgh No. 8 coal pyrite is aggressively oxidized at 0.7 V to iron oxides or hydroxides, iron sulfate, elemental sulfur and polysulfides. While the formation of polysulfides or a metal-deficient region on mineral-pyrite under alkaline conditions has been reported previously [1, 4, 5, 20], elemental sulfur has not been observed before on other pyrites by XPS. Both elemental sulfur and polysulfides are hydrophobic species that are able to induce surface hydrophobicity of pyrite. The presence of iron oxides and sulfates, on the other hand, would tend to render the mineral hydrophilic. The observed floatability of pyrite is determined by the balance between the hydrophobic and hydrophilic species on the surface. The decrease in the floatability of pyrite at high positive potentials in alkaline solutions is attributed to the high abundance of iron oxides or hydroxides rather than the lack of hydrophobic products. These XPS results are in good agreement with those derived from electrochemical studies.

2.5 Conclusions

1. The voltammetry behavior of conventional polished pyrite electrodes is dominated by oxidation/reduction reactions involving ferrous and ferric hydroxides, not by the oxidation and reduction of pyrite itself.
2. Incipient oxidation of mineral and Chinese coal-pyrites takes place above -0.28

V at pH 9.2, which gives rise to a sulfur-rich surface and renders pyrite floatable at potentials as low as -0.1 V; Incipient oxidation of Pittsburgh No. 8 coal-pyrite occurs above -0.15 V.

3. The most likely product of initial sulfur oxidation of pyrite is polysulfides or metal-deficient sulfides since the thermodynamic potential for the formation of elemental sulfur is 0.09 V, significantly higher than -0.28 V or -0.15 V. The iron component is preferentially released from pyrite lattice during oxidation.

4. At pH 9.2, initial reductive decomposition of fresh pyrite surfaces occurs at potentials more negative than -0.28 V. Gross reductive decomposition was observed at potentials $<$-0.7 V for relatively clean surfaces. Passivating layers on the surface may shift these potentials considerably.

5. The rates of oxidation and reduction of Pittsburgh No. 8 coal-pyrite are higher than those of Chinese coal-pyrite and mineral-pyrite, which may be attributed to its higher porosity and larger surface area.

6. Soluble ferrous hydroxide species are produced by oxidation and reduction processes on pyrite. A soluble sulfur species, HS^-, is the product formed during cathodic reduction processes.

7. XPS studies of the oxidation of Pittsburgh No. 8 coal-pyrite show that wet-polishing of electrodes produces iron oxides/hydroxides on the surface which hinder the oxidation of pyrite at open circuit potential in open air or aqueous solutions.

8. XPS studies show that the oxidation of Pittsburgh No. 8 coal-pyrite at 0.7 V in alkaline solution produces elemental sulfur and polysulfides, which are hydrophobic and iron oxides/hydroxides and sulfate which are hydrophilic.

9. Oxygen is directly reduced to hydroxyl ion on pyrite in alkaline and neutral solutions. The reaction order with respect to O_2 is one and the Tafel slope is 0.224 V.

10. Oxygen reduction takes place on mineral- and Chinese coal-pyrites *via* hydrogen peroxide as intermediate in acidic solutions. Hydrogen peroxide is trapped in the pores of Pittsburgh No. 8 coal-pyrite and can not be detected using rotating ring-disc electrodes.

2.6 References

1. Yoon, R.-H., Lagno, M.L., Luttrell, G.H., and Mielczarski, J.A., 1991. "On the hydrophobicity of coal pyrite," In: *Processing and Utilization of high sulfur coals IV*, Ed. by P.R. Dugan, D.R. Quigley, and Y.A. Attia, Elsevier Science Publishers, Amsterdam, pp. 241-253.

2. Luttrell, G.H., and Yoon, R.-H., 1992. "Methods for improving sulfur rejection in fine coal flotation circuits," in: *Proceedings of the Coal Prep'92 Conference*, May 3-7, Cincinnatic, Ohio.

3. Hamilton, I.C., and Woods, R., 1981. "An investigation of surface oxidation of

pyrite and pyrrhotite by linear potential sweep voltammetry," *Journal of Electroanalytical Chemistry*, **118**, pp. 327-343.

4. Buckley, A.N, and Woods, R., 1984. "An X-Ray photoelectron spectroscopic investigation of the surface oxidation of sulfide minerals," in: *Proceedings of International Symposium on Electrochemistry in Mineral and Metal Processing*, Ed. by P.E. Richardson, S. Srinivasan and R. Woods, The Electrochemical Society, Inc., Pennington, N.J., pp. 286-302.

5. Buckley, A.N., and Woods, R., 1987. "The surface oxidation of pyrite," *Applied Surface Science*, **27**, pp. 437-452.

6. Buckley, A.N., Hamilton, .C., and Woods, R., 1988. "Studies of the surface oxidation of pyrite and pyrrhotite using X-ray photoelectron spectroscopy and linear potential sweep voltammetry," in: *Proceedings of International Symposium on Electrochemistry in Mineral and Metal Processing*, Ed. by P.E. Richardson, and R. Woods, The Electrochemical Society, Inc., Pennington, N.J., pp. 234-246.

7. Richardson, P.E., Li, Y.-Q., and Yoon, R.-H., 1992. "The photoelectrochemistry of in-situ fractured pyrite electrodes," in: *Proceedings of the Third International Symposium on Electrochemistry in Mineral and Metal Processing*, Ed. by R. Woods, P.E. Richardson, The Electrochemical Society, Inc., Pennington, N.J., pp. 342-353.

8. Zhu, X., Wadsworth, M.E., Bodily, D.M., and Riley, A.M., 1991. "Surface

properties of mineral and coal pyrite after electrochemical alteration," In: *Processing and Utilization of high sulfur coals IV*, Ed. by P.R. Dugan, D.R. Quigley, and Y.A. Attia, Elsevier Science Publishers, Amsterdam, pp. 205-222.

9. Ahlberg, E., Forssberg, K.S.E., and Wang, X., 1990. "The surface oxidation of pyrite in alkaline solution," *Journal of Applied Electrochemistry*, **20**, pp. 1033-1039.

10. Yoon, R.-H., Luttrell, G.H., Adel, G.T., and Richardson, P.E., 1993. "Fourth quarterly report of DOE project, Development of enhanced sulfur rejection processes," Contract No.: DE-AC22-92PC92246.

11. Tao, D.P., Richardson, P.E., Luttrell, G.H., and Yoon, R.-H., 1993. "An electrochemical investigation of surface reactions of coal- and Mineral-pyrite in aqueous solutions," *Processing and Utilization of High Sulfur Coals V*, Ed. by B.K. Parekh and J.G. Groppo, Elsevier Science Publishers, Amsterdam, pp. 219-235.

12. Albery, W.J., and Hitchman, M.L., 1971. "Ring-disc electrodes," Clarendon Press Oxford.

13. Greef, R., Peat, R., Peter, L.M., Pletcher, D., and Robinson, J., 1985. "Instrumental methods in electrochemistry," Ellis Horwood Limited, Chichester, p. 124.

14. Biegler, T., Rand, D.A.J., and Woods, R., 1975. "Oxygen reduction on sulfide minerals, part I, Kinetics and mechanism at rotated pyrite electrode,"

Electroanalytical Chemistry and Interfacial Electrochemistry, **60**, pp. 151-162.

15. Babic, R. and Metikos-Hukovic, M., 1993. "Oxygen reduction on stainless steel," *Journal of Applied Electrochemistry*, **23**, pp. 352-357.

16. McIntyre, J.D.E. and Peck, W.F., Jr., 1979. "Electrochemical catalysis by foreign metal adatoms," in: *Proceedings of the Third Symposium on Electrode Processes*, Ed. by S. Bruckenstein, S. Miller, J.D.E. McIntyre, and E. Yeager, pp. 322-349.

17. Lai, R.W., Diehl, J.R., Hammack, R.W., and Khan, S.U.M., 1990. "Comparative studies of the surface properties and the reactivity of coal pyrite and mineral pyrite," *Minerals and Metallurgical Processing*, February, pp. 43-48.

18. Chander, S. and Briceno, A., 1987. "Kinetics of pyrite oxidation," *Minerals and Metallurgical Processing*, **4**, pp. 171-176.

19. Zhu, X., Li, J., Bodily, D.M., and Wadsworth, M.E., 1992. "Transpassive oxidation of pyrite," in: *Proceedings of the Third International Symposium on Electrochemistry in Mineral and Metal Processing*, Ed. by R. Woods, P.E. Richardson, The Electrochemical Society, Inc., Pennington, N.J., pp. 391-409.

20. Mycroft, J.R., Bancroft, G.M., McIntyre, N.S., Lorimer, J.W., and Hill, I.R., 1990. "Detection of sulfur and polysulphides on electrochemically oxidized pyrite surfaces by X-ray photoelectron spectroscopy and Raman spectroscopy," *Journal of Electroanalytical Chemistry*, **292**, pp. 139-152.

21. Peters, E. and Majima, H., 1968. "Electrochemical reactions of pyrite in acid

perchlorate solution,", *Canadian Metallurgical Quarterly*, **7**, No.3, pp. 111-117.

22. Michell, D. and Woods, R., 1978. "Analysis of oxidized layers on pyrite surfaces by X-ray emission spectroscopy and cyclic voltammetry," *Australian Journal of Chemistry*, **31**, pp. 27-34.

23. Chander, S., Briceno, A., and Pang, J., 1992. "On the mechanism of sulfur oxidation in pyrite," *SME/AIME Annual Meeting*, Phoenix, Arizona, February 24-27, Preprint No. 92-240.

24. Fornasiero, D. and Ralston, J., 1992. "Iron hydroxide complexes and their influence on the interaction between ethyl xanthate and pyrite," *Journal of Colloids and Interface Science*, **151**, No.1, pp. 225-235.

25. Kuhn, A.T. and Chan, C.Y., 1983. "pH changes at near-electrode surfaces," *Journal of Applied Electrochemistry*, **13**, pp. 189-207.

26. Ogunsola, O.M. and Osseo-Asare, Kwadwo, 1986. "The electrochemical behavior of coal pyrite 1. Effects of mineral source and composition," *Fuel*, **65**, pp. 811-815.

27. Briceno, A. and Chander, S., 1988. "An electrochemical characterization of pyrites from coal and ore sources," *International Journal of Mineral Processing*, **24**, pp. 73-80.

28. Wang, X.-H., Jiang, C.L., Raichur, A.M., Parekh, B.K., and Leonard, J.W., 1992. "Comparative studies of surface properties of pyrite from coal and ore sources," in: *Proceedings of the Third International Symposium on*

Electrochemistry in Mineral and Metal Processing, Ed. by R. Woods, P.E. Richardson, The Electrochemical Society, Inc., Pennington, N.J., pp. 410-432.

29. Esposito, M.C., Chander, S., and Aplan, F.F., 1987. "Characterization of pyrite from coal sources," in: *Process Mineralogy VII*, Ed. by A.H. Vassiliou, TMS/AIME, pp. 475-493.

30. Zhu, X., Wadsworth, M.E., Bodily, D.M., and Hu, W.B., 1991. "A comparative study of the electrochemical properties of mineral and coal pyrite," *EPD Congress 91*, Ed. by D.R. Gaskell, pp. 179-195.

31. Chander, S., 1991. "Electrochemistry of sulfide flotation: growth characteristics of surface coatings and their properties, with special reference to chalcopyrite and pyrite," *International Journal of Mineral Processing*, **33**, pp. 121-134.

32. Finkelstein, N.P., Allison, S.A., Lovell, V.M., and Stewart, B.V., 1975. "Natural and induced hydrophobicity in sulfide mineral systems," In *Advances in Interfacial Phenomena of Particulate/Solution/Gas System, Applications to Flotation Research*, AIChE, Symp. Ser. No. 150, **71**, pp. 165-175.

33. Basilio, C.I., Kartio, I.J., Suoninen, E., Tao, D.P., Richardson, P.E., and Yoon, R.-H., 1994. "XPS study of the oxidation of coal pyrite surfaces," To be submitted for publication.

34. Buckley, A.N. and Woods, R., 1985. "X-ray photoelectron spectroscopy of oxidized pyrrhotite surfaces," *Applications of Surface Science*, **22/23**, pp. 280-287.

35. Brundle, C.R., Chuang, T.J., and Wandelt, K., 1977. "Core and valence level photoemission studies of iron oxide surfaces and the oxidation of iron," *Surface Science*, **68**, pp. 459-468.

36. Brion, D., 1980. "Etude par spectroscopie de photoelectrons de la degradation superficielle de FeS_2, $CuFeS_2$, ZnS, et PbS a L'air et Dans L'eau," Applied Surface Science, **5**, pp. 133-152.

37. Baltrus, J.P. and Proctor, A.,, 1990. "Composition of overlayers on oxidized pyrite surfaces," Applied Surface Science, **44**, pp. 147-150.

38. Harvey, D.T. and Linton, R.W., 1981. "Chemical characterization of hydrous ferric oxides by X-ray photoelectron spectroscopy," Analytical Chemistry, **53**, pp. 1684-1688.

CHAPTER 3 COLLECTORLESS FLOTATION AND ELECTROCHEMICAL DEPRESSION OF PYRITE

3.1 Introduction

The flotation behavior of pyrite is important not only in coal desulfurization by surface-based techniques such as flotation, but also in the extraction of valuable components from sulfide ore deposits. It is well established that flotation is not very efficient in removing pyrite from coal [1]. One of the major reasons is associated with the hydrophobicity of pyrite due to surface oxidation, which leads to collectorless flotation (i.e., self-induced flotation) in the absence of conventional sulfide collectors, a behavior that has also been observed with other sulfide minerals such as galena, chalcopyrite, pyrrhotite, and sphalerite. The flotation recovery of pyrite is particularly high when sodium sulfide or EDTA is used to remove metal hydroxides from the surface [2, 3]. However, in the absence of sodium sulfide or EDTA, the collectorless flotation of pyrite is relatively low and is not well characterized [4-6].

It is recognized [7] that the surfaces of sulfide minerals are generally neither strongly hydrophobic nor strongly hydrophilic. The hydrophobicity of unoxidized sulfides is caused by the lack of hydrogen bonding with sulfur. This can be understood

by considering the nature of hydrophobicity. Thermodynamically, for a surface to be hydrophobic, the work of adhesion of water to the surface W_a must be less than the work of cohesion of water W_c, i.e.,

$$W_a < W_c \tag{3.1}$$

It is well known that $W_c = 146$ erg/cm^2 at 25° C for pure water. W_a can be expressed as:

$$W_a = W^d + W^{nd} \tag{3.2}$$

where W^d is the dispersion component of W_a and W^{nd} the nondispersion component of W_a, including contributions from hydrogen bonding, hydration force, etc.

Since $W^d < 146$ erg/cm^2 for all solids, they are naturally hydrophobic when only dispersion forces are present. Sulfide minerals are much less hydrophilic than oxide minerals because W^{nd} is much smaller for metal sulfides due to the absence of hydrogen bonding.

As a result, whether sulfide minerals float or not can be determined by relatively minor changes on their surfaces. Superficial oxidation of sulfides provides a way of altering their surface hydrophobicity and is widely considered to be the origin of collectorless flotation. The oxidation of pyrite has been investigated in Chapter 2. Chapter 3 is devoted to studies of collectorless flotation of pyrite and development of an electrochemical technique for its depression.

3.2 Research Objectives

Collectorless flotation of pyrite was studied under conditions of controlled E_h and pH. The potential of pyrite was adjusted either directly by a potentiostat or indirectly by the addition of chemical reagents. The results were used to direct the development of practical electrochemical methods for pyrite depression. A galvanic coupling technique was explored to control the potential of pyrite and prevent its oxidation. Various sacrificial anodes were examined and their influences on pyrite surfaces after galvanic interaction studied by means of cyclic voltammetry. Mechanisms of enhancing pyrite rejection by galvanic coupling were investigated from electrochemical aspects of pyrite oxidation and flotation. Flotation conditioning stages were used to achieve optimum effect of galvanic coupling on pyrite rejection.

3.3 Experimental

3.3.1 Materials

Mineral-pyrite specimens, originally from Huanzala, Peru, were supplied by Ward's Scientific Co. The Chinese coal-pyrite was received from Chongqing, Sichuan Province, China. It contained no visible specks of coal and had the appearance of

mineral-pyrite. The Illinois No. 6 coal-pyrite and the Pittsburgh No. 8 coal-pyrite were in the form of chunks obtained from run-of-mine coals. They did not appear as shiny as mineral-pyrite. The Pittsburgh No. 8 coal-pyrite looks poorly crystallized.

Lumps of high-sulfur, high-ash Lower Kittanning coal (containing approximately 9% total sulfur, 8% pyritic sulfur and 30% ash) was obtained from the Bradford Coal Company's Manor Mine in Clearfield County, Pennsylvania. The Chinese high-sulfur coal was obtained from Chongqing, Sichuan Province, China. It contained about 5% pyritic sulfur and negligible organic sulfur and coal. The ash content of that coal was around 24%.

3.3.2 Flotation

3.3.2.1 *Pure Pyrite*

Flotation tests of nearly pure pyrite were conducted both in a Partridge and Smith-type microflotation cell [8] with a volume of 150 ml and in a specially designed electrochemical-microflotation cell. Pyrite samples were hand selected and freshly ground to the required size fraction prior to each experiment in order to minimize oxidation.

In the Partridge and Smith cell, the potential of pyrite was adjusted by the addition of oxidizing agents (potassium permanganate) and reducing agents (hydrazine

or sodium sulfide). Each flotation test was done with a 0.8 g sample of -100+200 mesh particles. The sample was conditioned for 3 minutes at designated potentials before flotation was initiated. Methylisobutylcarbinol (MIBC) was used as frother at a concentration of 30 ppm, unless otherwise specified.

Figure 3.1 illustrates the electrochemical-microflotation cell in which a compacted pyrite bed is used as the working electrode. A coiled platinum wire lead, entering at (F) and resting on the ground glass frit (E), served as the electrical connection to the mineral bed. A platinum wire, housed in a fine porosity fritted tube (H), served as the counter electrode, and the tube itself served as a plunger to compact the particles to ensure physical and electrical contact throughout the bed. The fine porosity frit prevented diffusion of solutions between the counter and working electrode compartments. Potentials were measured against a saturated Calomel electrode using a Luggin capillary connection through port B. Ports A and C served as the inlet and the outlet for electrolyte circulation respectively. For flotation tests, the counter electrode plunger was raised until the fritted tube was above the center tube but still making electrical contact with the electrolyte. Nitrogen, entering through port D, was bubbled through the frit and mineral bed. Particles levitated by bubbles were deflected by the counter electrode compartment and deposited around the outside of the center tube.

In order to remove possible surface products on pyrite formed during dry grinding, samples were subjected to electrochemical cleaning at -0.5 V in acidic solutions

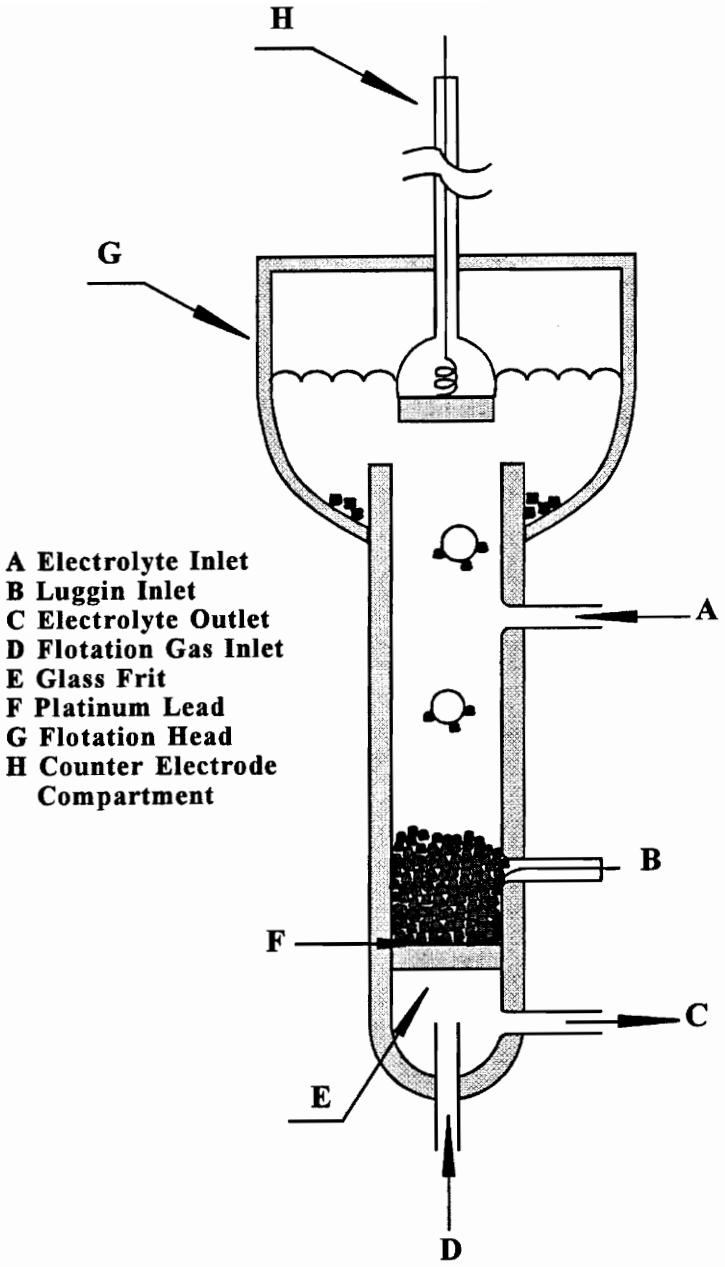

Figure 3.1 Schematic illustration of the electrochemical-microflotation cell.

for 5 minutes. The solution was then pumped out and replaced by freshly deoxygenated solution at required pH.

The main advantage of using the particulate mineral bed instead of a single specimen as the working electrode is that electrochemical studies and flotation tests can be done in the same system under conditions close to the actual flotation environment. In addition, the solution can be continuously circulated between the cell and UV spectrophotometer so that the solution phase can be monitored. The bed used in the present study consisted of a 1.5 g sample of pyrite particles. The bed potential was controlled with a PAR 273 potentiostat and voltammograms were recorded on a Linseis LY 18100 recorder.

3.3.2.2 *Coal*

The as-received coal samples were immediately crushed to -6 mm using a laboratory jaw crusher and split into representative lots of approximately 1.5 kg each. The samples were stored in a freezer at -20° C to minimize oxidation. Prior to flotation, they were dry pulverized in a laboratory hammermill to -100 mesh.

Coal flotation tests were done both in a 2" diameter microbubble flotation column and a conventional flotation cell to examine the effect on pyrite rejection under various conditions. The microbubble flotation column has been described in detail elsewhere [9]. The operating conditions were set as follows: aeration rate of 1.2 l/min, wash water flow

rate 0.4 l/min, frother dosage of 0.45 kg/ton, froth height of 30 cm, and feed solids content of 5%. Conventional flotation tests were performed in a 5-liter laboratory Denver cell. The basic operating conditions were: impeller speed of 1700 rpm, air inlet fully open, frother dosage of 0.23 kg/ton, automatic froth scraping, sampling times of 0.25, 0.5, 1.0, 2.0, and 4.0 min; and feed sample weight of 200 g.

3.3.3 Electrodes

Pyrite electrodes for galvanic coupling studies were prepared from specimens cut into rectangular prisms with dimensions of approximately $10\times10\times5$ mm, unless otherwise specified. A copper wire was attached to one of the 10×10 mm faces using a conducting silver epoxy cement. A thick layer of non-conducting epoxy resin was then applied to the other faces to prevent their contact with solution. Metal electrodes were fabricated in a similar way. Electrodes for the measurement of potential in flotation were of smaller dimensions and mounted at the end of a 7 mm diameter glass tube.

3.3.4 Reagents

Buffer solutions employed in the present study possessed the following compositions:

pH 4.6; 0.5 *M* CH_3COOH and 0.5 *M* CH_3COONa

pH 6.8; 0.05 *M* KH_2PO_4 and 0.0224 *M* NaOH

pH 8.0; 0.05 *M* KH_2PO_4 and 0.0461 *M* NaOH

pH 9.2; 0.05 *M* $Na_2B_4O_7$

All chemicals were of reagent grade except methylisobutylcarbinol (MIBC) and kerosene, which were used as frother and collector, respectively, in flotation experiments and of industrial grade. Recovery, as reported herein, is based on weight %.

3.3.5 Electrochemical Measurements

Electrochemical experiments were carried out at ambient temperature using a conventional three-electrode system. The working electrode (pyrite) was polished with 600 grit silicon carbide paper prior to each test and cleaned with acetone, hydrochloric acid and double distilled water. Solutions were bubbled with N_2 for at least half an hour before experiments were started and N_2 was kept flowing over the solution surface during experiments to prevent the diffusion of air into the cell. Electrochemical examinations of pyrite after conditioning under various conditions were done using a Pine RDE-4 potentiostat. Voltammograms and Chronoamperometry curves were recorded on a Linseis LY 18100 recorder. Potentials were measured against a saturated calomel reference electrode (SCE) and transformed to the standard hydrogen electrode (SHE)

scale by adding 0.245 V.

3.3.6 Galvanic Coupling

Galvanic interaction between pyrite and active metals as sacrificial anodes was studied in a electrochemical system illustrated in Figure 3.2. The system essentially consists of two independent electrochemical cells connected by a salt bridge. Galvanic coupling between pyrite and metal electrodes was accomplished by connecting them with a copper wire. The effect of galvanic coupling on pyrite was investigated by carrying out voltammetry on pyrite after galvanic coupling and after disconnecting two electrodes.

3.4. Results and Discussion

3.4.1 Collectorless flotation of pyrite

Figure 3.3 shows the flotation results obtained with -100+65 mesh mineral-pyrite particles in the electrochemical-microflotation cell at pH 4.6 and 9.2. It is clearly demonstrated that flotation recovery was strongly dependent on the potential of pyrite. The lower and higher flotation edges are, respectively, -0.3 V and 0.4 V at pH 9.2, 0.1 V and 0.8 V at pH 4.6. Maximum flotation recovery occurred between 0.25 and 0.7 V

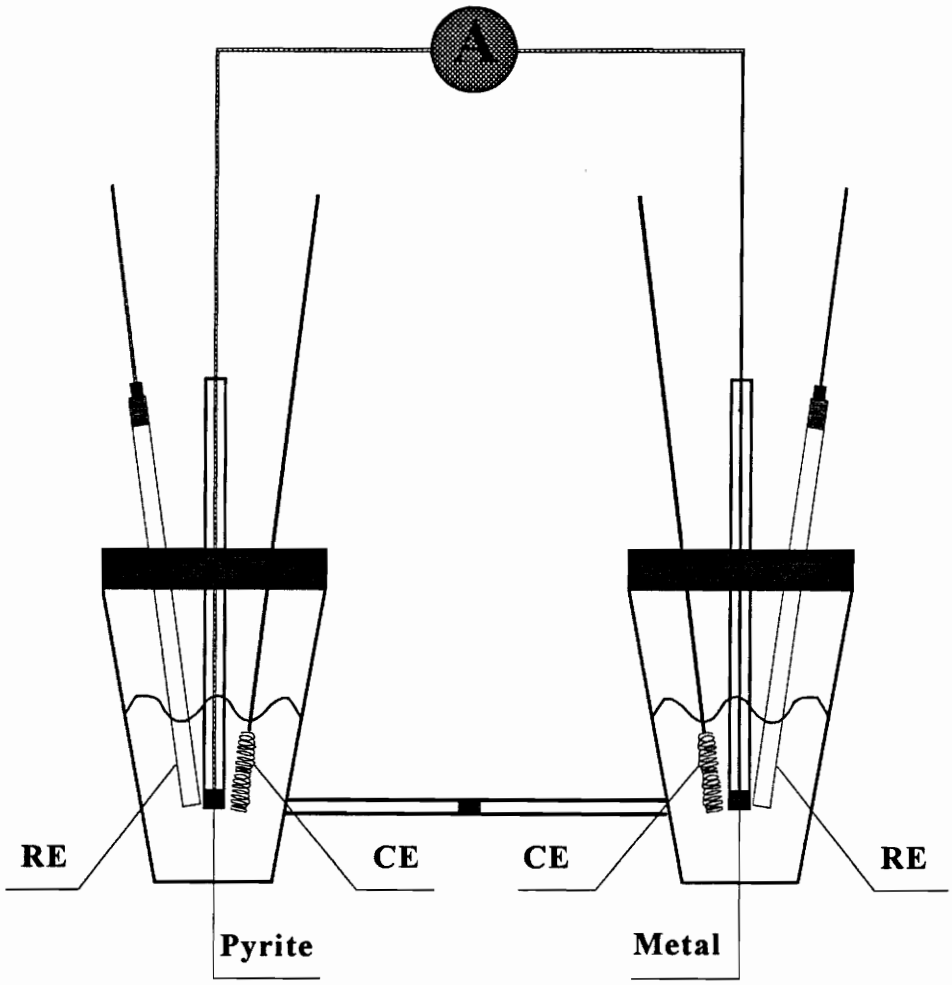

Figure 3.2 **Schematic illustration of the electrochemical cell for galvanic coupling experiments.**

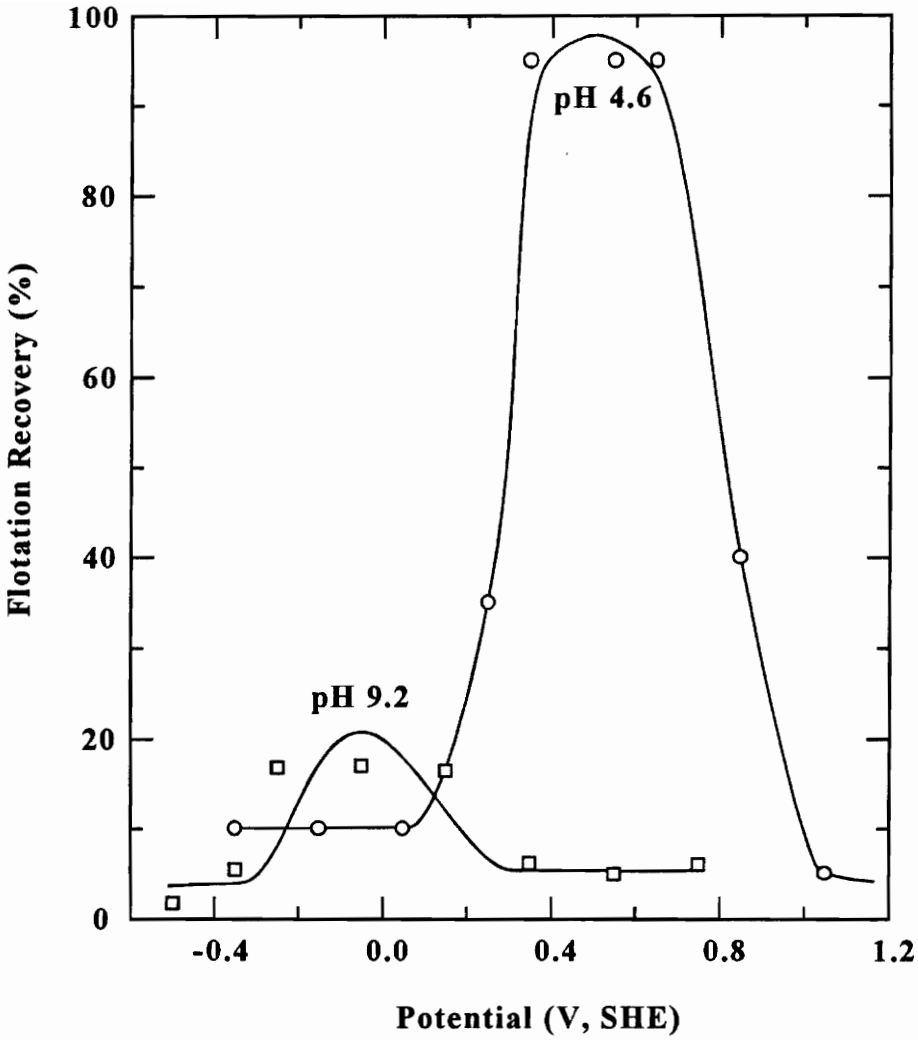

Figure 3.3 **Flotation recovery of freshly ground -100+65 mesh mineral pyrite as a function of potential at pH 4.6 and 9.2. Potential was controlled by a potentiostat.**

at pH 4.6, between -0.3 and 0.2 V at pH 9.2. These results appear to be in agreement with the known electrochemistry of pyrite oxidation. It is widely recognized that pyrite undergoes initial oxidation *via* reactions [10-12],

$$FeS_2 + 3OH^- = 2S^o + Fe(OH)_3 + 3e^- , \quad (3.3)$$

$$nFeS_2 + 3(n-2)OH^- = 2FeS_n + (n-2)Fe(OH)_3 + 3(n-2)e^-, \quad (3.4)$$

$$FeS_2 + 3xOH^- = Fe_{1-x}S_2 + xFe(OH)_3 + 3xe^-. \quad (3.5)$$

Electrochemical and XPS studies described in Chapter 2 have demonstrated that the most likely sulfur oxidation products of incipient oxidation of pyrite are polysulfides (reaction 3.4) or metal-deficient sulfides (reaction 3.5) while oxidation at moderate to high potentials can also produce elemental sulfur (reaction 3.3). Due to the pH-dependent nature of Reactions (3.3)-(3.5), oxidation takes place at lower potentials in alkaline solutions than in acidic solutions.

The above flotation tests establish explicitly that pyrite can be rendered floatable by electrochemical oxidation of pyrite at relatively low overpotentials. The flotation results appear to be in good agreement with electrochemical studies. The lower flotation edges observed at pH 4.6 and 9.2 are in coincidence with initial oxidation potentials revealed in Chapter 2. It can thus be concluded that superficial oxidation is responsible for collectorless flotation of pyrite.

The upper flotation edge was primarily determined by reaction (3.6), which

represents the aggressive oxidation of pyrite to ferric hydroxide and sulfate,

$$FeS_2 + 11H_2O = Fe(OH)_3 + 2SO_4^{2-} + 19H^+ + 15e^- , \qquad (3.6)$$

Reaction (3.6) is also pH-dependent and its equilibrium potential shifts to more negative values with increasing solution pH. The flotation of pyrite will be inhibited when the surface is predominately covered by iron hydroxide. Chander and his co-workers [13, 14] carried out a-c impedance spectroscopy of oxidized pyrite surface and proposed that iron hydroxide overlays a sulfur-rich layer which is adjacent to the bulk of unoxidized pyrite.

The loss of floatability at higher potentials is usually attributed to the oxidation of sulfur to sulfate [2], which reduces the amount of hydrophobic sulfur species on the surface. However, XPS results presented in Chapter 2 clearly showed that increased quantity of hydrophobic species including elemental sulfur and polysulfides were generated at higher potentials. Hamilton and Woods [12] determined by electrochemical methods that the amount of elemental sulfur increased steadily as the potential increased from 0.5 to 0.85 V at pH 4.6. It is the author's belief that although an increase in potential of pyrite facilitates the transformation of S^o-like species to sulfate, it also, probably more significantly, accelerates the formation of S^o-like products from oxidation of pyrite. Nevertheless, there is no doubt that increased amounts of iron hydroxides will be generated at higher potentials, as indicated by Equations (3.1)-(3.4). Therefore, the appropriate statement should be that the decreased floatability of pyrite at high positive

potentials is caused by the increased amount of ferric hydroxide formed on the surface that covers hydrophobic species underneath. Yoon et al. [10] observed a good correlation between the floatability of pyrite and the ratio of hydrophobic S^o-like species to hydrophilic iron hydroxide. Their work established that the surface hydrophobicity of pyrite is determined by the relative abundance of iron and sulfur oxidation products.

Illinois No. 6 coal-pyrite also exhibited significant collectorless flotation although the flotation recovery is lower than that of mineral-pyrite. Similar observation has been reported previously with other coal-pyrites. For example, Yoon et al. [10] showed that Pocahontas No. 3 coal-pyrite demonstrated significant self-induced flotation at certain potentials. It can be speculated based on the present study of surface reactions on pyrite (Chapter 2) and previous work on pyrite [15, 16] that the hydrophobicity of oxidized coal-pyrites is weaker than that of mineral-pyrite due to its faster oxidation kinetics, which results in the formation of less S^o-like species and higher amounts of insoluble iron hydroxides. The specific differences between coal- and mineral-pyrite were discussed in Chapter 2.

However, the relatively low hydrophobicity of coal-pyrites compared to mineral-pyrite does not indicate that pyrite will not float in coal flotation. It must be realized that the moderate hydrophobicity of coal-pyrite will induce a strong hydrophobic interaction [17] between pyrite and kerosene which will, in turn, considerably enhance the hydrophobicity of pyrite. This is shown in Figure 3.4. The addition of kerosene

increased the flotation recovery of pyrite by 30%-40%. Olson and Aplan [18] reported a similar result that an oil dosage of 0.35 kg/ton promoted the flotation of clean coal 3 times and that of pure pyrite 30 times, which made it much more difficult for pyrite to be rejected from coal. There may also be a hydrophobic interaction between pyrite and coal, resulting in a coal coating on the pyrite surface as observed by Jiang et al. [19], which makes coal-pyrite strongly floatable.

In industrial flotation processes, pyrite is expected to exhibit even stronger floatability than observed with microflotation cells. This is because negligible attrition between particles is created in microflotation cells. In contrast, vigorous turbulence in industrial flotation cells may generate particle-particle abrasion that is intense enough to strip the hydrophilic iron hydroxide overlayer from the surface of pyrite, exposing the sulfur-rich layer underneath and thus increasing the floatability of pyrite. This is simulated in the electrochemical-microflotation cell by the use of EDTA to remove iron hydroxide from the surface of pyrite. Results are also shown in Figure 3.4. A substantial increase in flotation recovery of pyrite is observed.

The most important conclusion that can be drawn from Figures 3.3 and 3.4 is that pyrite can be depressed under reducing or strongly oxidizing conditions. However, the latter route is not considered to be favorable to coal desulfurization. This is because:

(1) Under strongly oxidizing conditions, considerable quantities of hydrophobic sulfur oxidation species will be formed on the surface. Once ferric hydroxide is

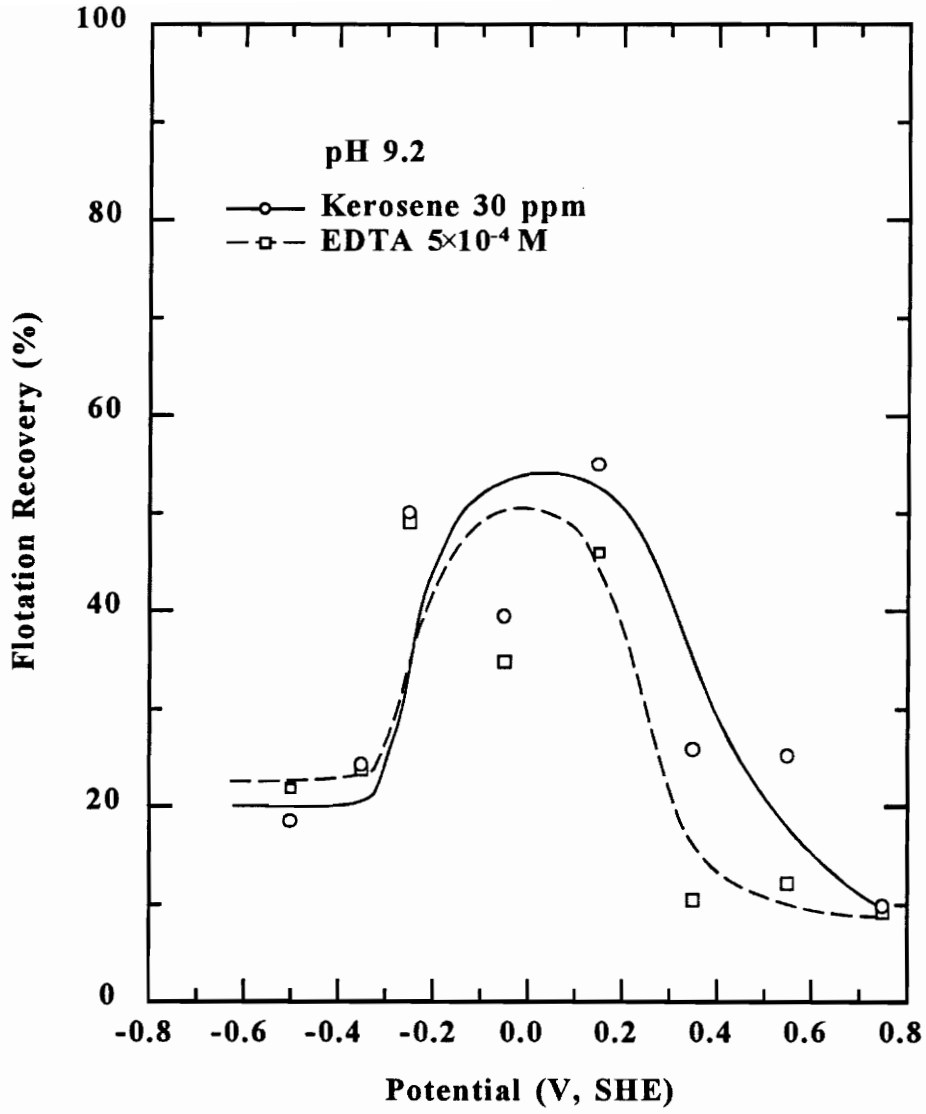

Figure 3.4 Flotation recovery of -100+65 mesh mineral pyrite as a function of potential at pH 9.2 with EDTA or kerosene.

removed from the surface, pyrite may exhibit a strong floatability. In fact, such a possibility has been demonstrated in the literature by the use of EDTA [2, 3].

(2) Massive precipitation of iron hydroxide formed at high potentials may also take place on the surface of coal particles, which will significantly increase coal hydrophilicity.

(3) Coal may also be oxidized under strongly oxidizing conditions, which will decrease its hydrophobicity and reduce the difference in hydrophobicity between coal and pyrite. As a consequence, selectivity of coal from pyrite by flotation may be lowered significantly.

Exploratory flotation experiments performed in the preliminary stage of this study showed that virtually no improvement can be achieved in pyrite rejection from coal by the use of oxidizing agents such as $KMnO_4$, $Fe_2(SO_4)_3$, H_2O_2, etc.

In contrast, reducing conditions may prevent the formation of hydrophobic products on the surface and therefore can eliminate the source of pyrite hydrophobicity. In addition, reducing condition will not adversely affect the floatability of coal. Therefore, reducing environments have advantages in enhancing pyrite rejection from coal.

3.4.2 Galvanic coupling between pyrite and sacrificial anodes

Galvanic coupling was explored as a practical method to lower the potential of pyrite. It is well known that some active metals are fairly strong reducing agents. For example, the standard redox potentials for the Al^{3+}/Al, Mn^{2+}/Mn, Zn^{2+}/Zn and Fe^{2+}/Fe couples are -1.662, -1.180, -0.763, and -0.440 V, respectively. Since pyrite possesses a much higher rest potential (0.6 V at pH 4.6 and 0.18 V at pH 9.2) [14, 20], galvanic interaction will take place upon its contact with these metals. Pyrite will act as a cathode and the metal as a sacrificial anode.

Galvanic interaction and its effect on the flotation of sulfide minerals have been reported in recent literature. Adam et al. [21] observed galvanic coupling between pyrrhotite and metal electrodes including mild steel, stainless steels, zinc and magnesium, which reduced the floatability of pyrrhotite. Pozzo et al. [22] reported that galvanic interaction between iron sulfides (pyrite and pyrrhotite) and steel balls used in grinding remarkably reduced the flotation recovery of sulfides using xanthates collectors when they were ground in nitrogen atmosphere. Berry et al. [23] showed leaching studies that pyrite corrodes more rapidly than chalcopyrite. However, when these two minerals were in contact with each other, chalcopyrite corrodes faster than pyrite. The change in corrosion rates was attributed to a galvanic interaction in which pyrite acted as the cathode and was passivated by copper- and iron-hydroxides. Nakazawa and Iwasaki [24]

suggested that galvanic coupling between nickel arsenide and pyrrhotite improved the floatability of nickel arsenide, which acted as the anode, and accelerated its dissolution, but adversely affected the floatability of pyrrhotite, which served as the cathode. These studies suggest that galvanic coupling of pyrite with active metals can be expected to have a profound influence on the floatability of pyrite.

The present galvanic coupling experiments were carried out in the apparatus illustrated in Figure 3.2. Galvanic coupling occurs only when both electrodes are in electronic and electrolytic contact. Electronic contact was achieved by a copper wire and electrolytic contact by the aqueous electrolyte solution in which both electrodes were immersed. Upon coupling, a current flows between the two electrodes with electrons moving toward the cathode in the external circuitry and ions carrying the current in the solution. The metal, which is more electronegative, becomes the anode while pyrite, which is more noble, becomes the cathode. The current flowing between the two electrodes accelerates the dissolution of the anode, which is thus sacrificed.

Figure 3.5 shows the potentials of Pittsburgh No. 8 coal-pyrite and metal (aluminum, zinc and manganese) electrodes as a function of time after galvanic coupling at pH 4.6. Prior to galvanic coupling, pyrite possessed a potential of about 0.3 V and aluminum, zinc, and manganese electrodes had potentials of -0.65, -0.84, and -1.10 V, respectively. Upon galvanic coupling, the potential of pyrite decreased rapidly within 100 seconds to -0.24, -0.35, and -0.42 V by contact with aluminum, zinc, and

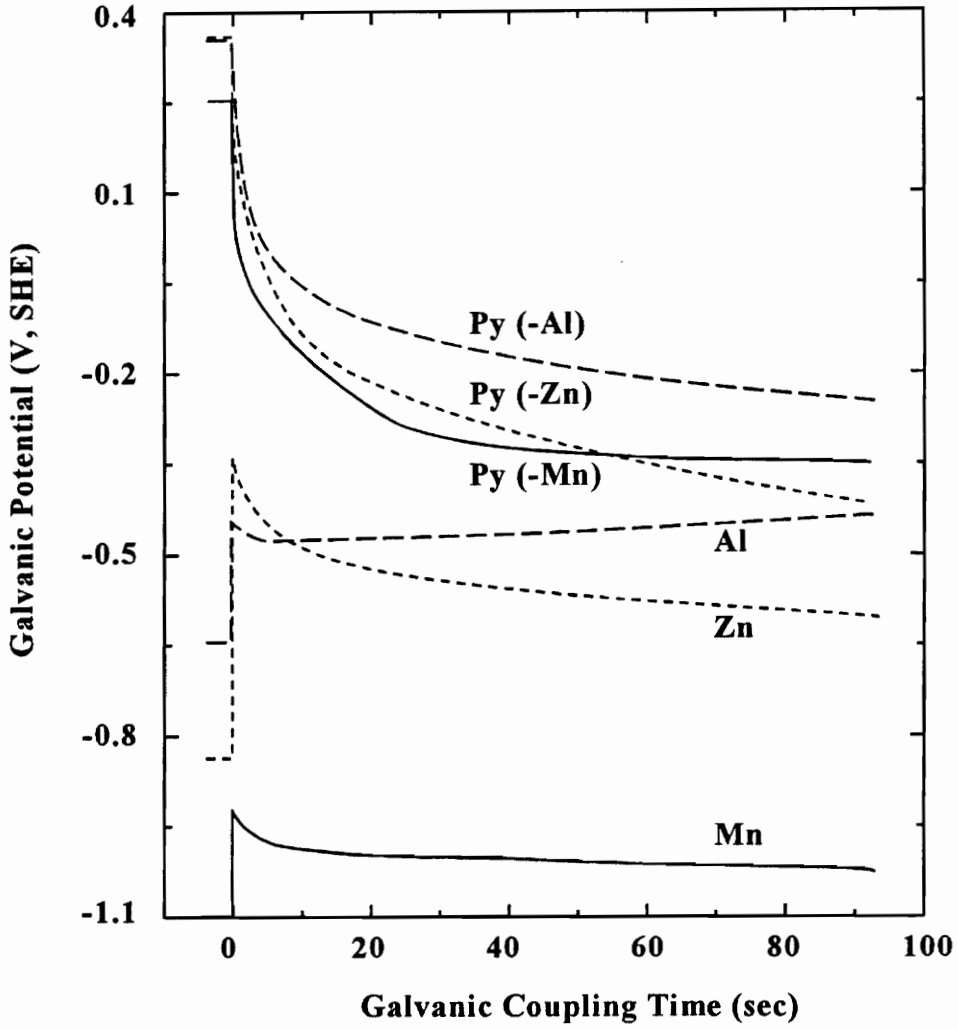

Figure 3.5 Potentials of Pittsburgh No. 8 coal-pyrite and metal electrodes as a function of galvanic coupling time at pH 4.6.

manganese, respectively. The corresponding galvanic current was found to depend on the different anode. Manganese gave rise to the highest current and aluminum the lowest. The chronoamperometry curves, i.e., galvanic current as a function of time after galvanic coupling, are shown in Figure 3.6.

Galvanic coupling experiments were also conducted at pH 9.2. Results similar to the above were obtained for manganese and aluminum. Figure 3.7 demonstrates the potentials when pyrite is coupled to aluminum and manganese electrodes. The rest potential of Pittsburgh No. 8 coal-pyrite was between -0.05 and -0.15 V at pH 9.2. Galvanic coupling with manganese, whose potential was originally -1.09 V, reduced the potential of pyrite to -0.43 V in about 1 minute. The increase of the potential of manganese electrode before equilibrium was achieved is believed to have been induced by the progressive build-up of manganese hydroxide on the surface. Similarly, the pyrite electrode assumed a potential of -0.38 V after galvanic interaction with aluminum having an initial rest potential of -0.97 V. The equilibrium potential of the aluminum electrode was achieved almost instantly, which may indicate that aluminum hydroxide was produced prior to galvanic coupling.

However, unlike at pH 4.6, zinc exhibited a unique behavior at pH 9.2. Figure 3.8 shows the potentials of both pyrite and zinc electrodes versus galvanic coupling time. Upon coupling, the potential of zinc increased drastically from -0.91 V to -0.31 V in 1.4 minutes while the pyrite potential decreased from -0.03 V to -0.17 V. After this normal

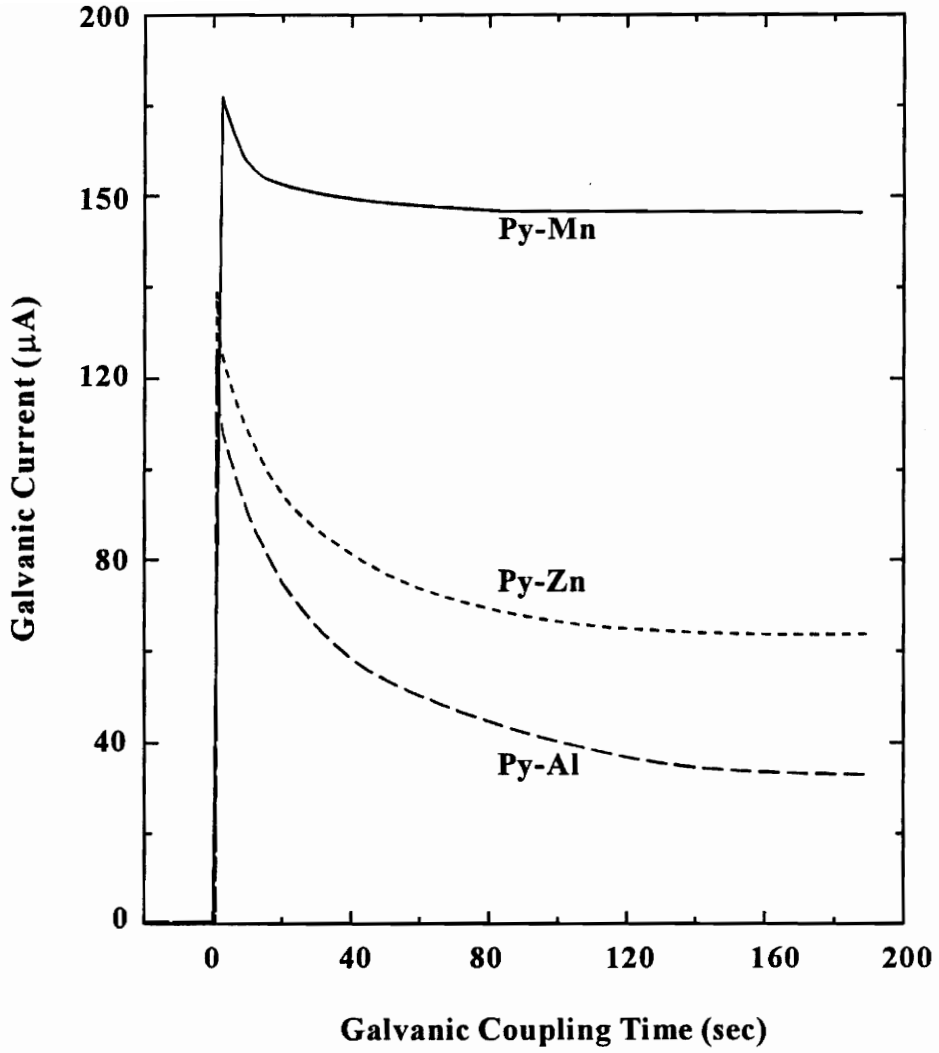

Figure 3.6 Galvanic coupling current between Pittsburgh No. 8 coal-pyrite and metals as a function of time at pH 4.6.

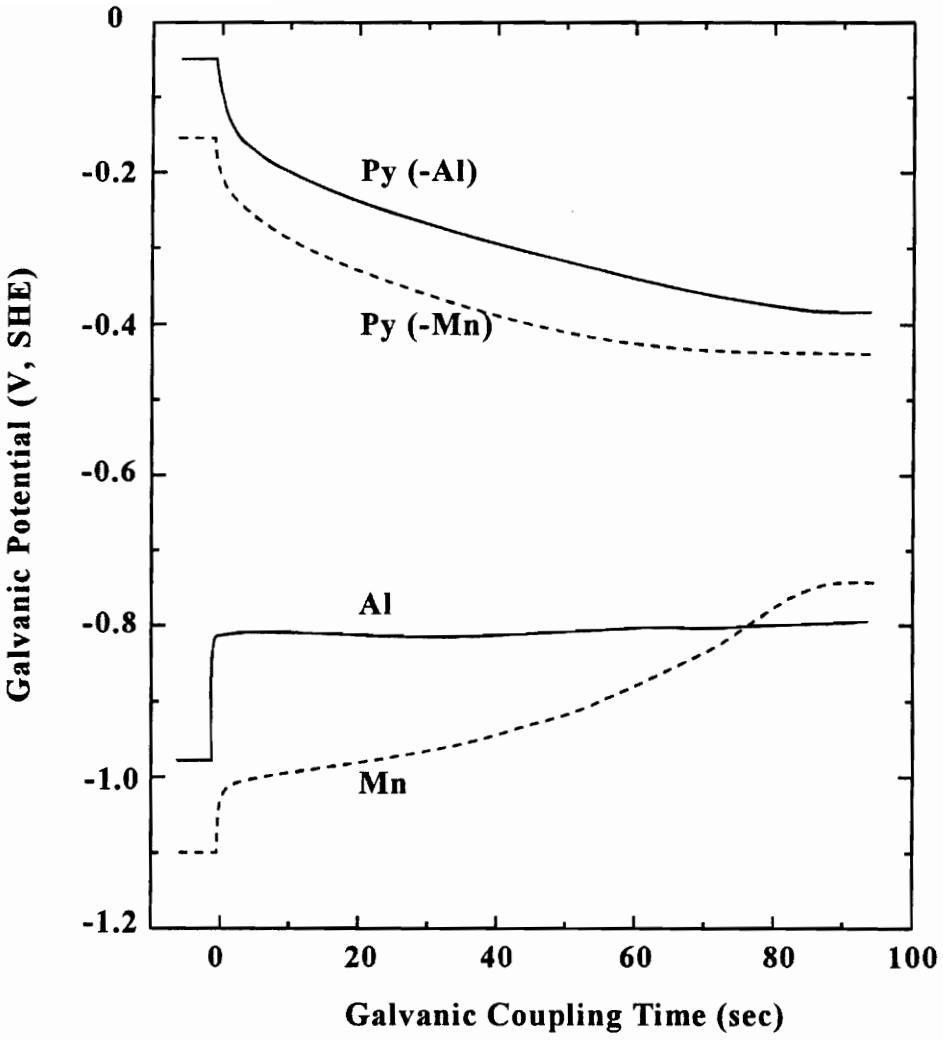

Figure 3.7 Potentials of Pittsburgh No. 8 coal-pyrite and metal (aluminum and zinc) electrodes as a function of galvanic coupling time at pH 9.2.

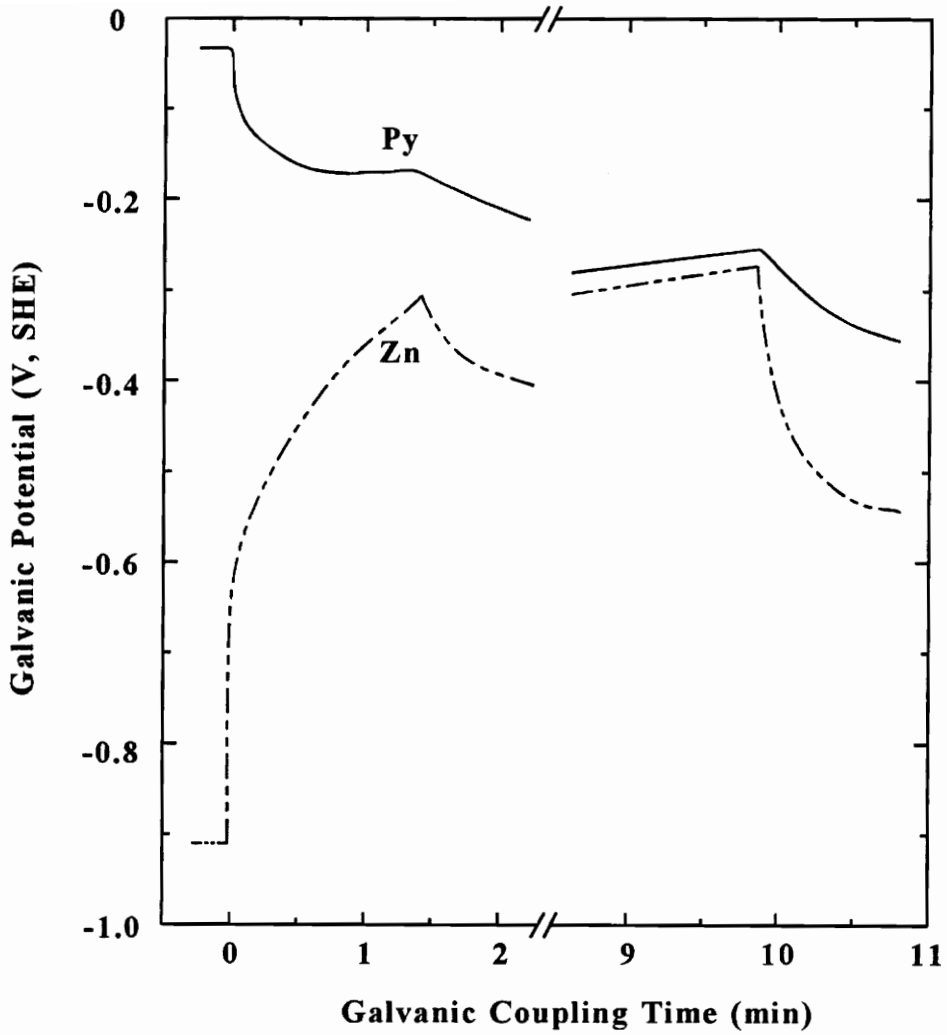

Figure 3.8 Potentials of Pittsburgh No. 8 coal-pyrite and zinc electrodes as a function of galvanic coupling time at pH 9.2.

process as observed with other sacrificial anodes, a decay in the potential of the zinc electrode took place for about 2.5 minutes, which was followed by a gradual increase to -0.27 V. The potential then decreased again and eventually reached the steady state value of -0.54 V. The potential of pyrite showed corresponding complex changes over the entire period of time. This experiment was repeated several times and reproducible results were obtained. The complex changes in potentials of zinc may be associated with the build-up and break-down of zinc hydroxide (K_{sp} 7.68×10^{-17}) on the surface. The process can be represented by the following reaction:

$$Zn + 2H_2O = Zn(OH)_2 + 2H^+ + 2e^- \qquad (3.7)$$

In fact, an appreciable amount of a white powder-like precipitate was observed on a number of sites on the zinc electrode surface after each experiment.

The above experiments demonstrate that galvanic coupling can substantially reduce the potential of pyrite. However, it should be noted that the data was acquired in oxygen-free aqueous solutions. In the presence of oxygen, the results are significantly different. Figure 3.9 shows the galvanic potential of Illinois No. 6 coal-pyrite as a function of coupling time with a zinc anode and an aluminum anode in oxygen saturated solutions. It is obvious that in both cases, pyrite potentials were reduced by only about 0.2 V, possibly because reactions involving oxygen occurs on both electrodes and consumes most of electrons produced by the anodic oxidation of the metal. In addition, metal hydroxides or oxides formed on the metal electrodes may passivate their surfaces.

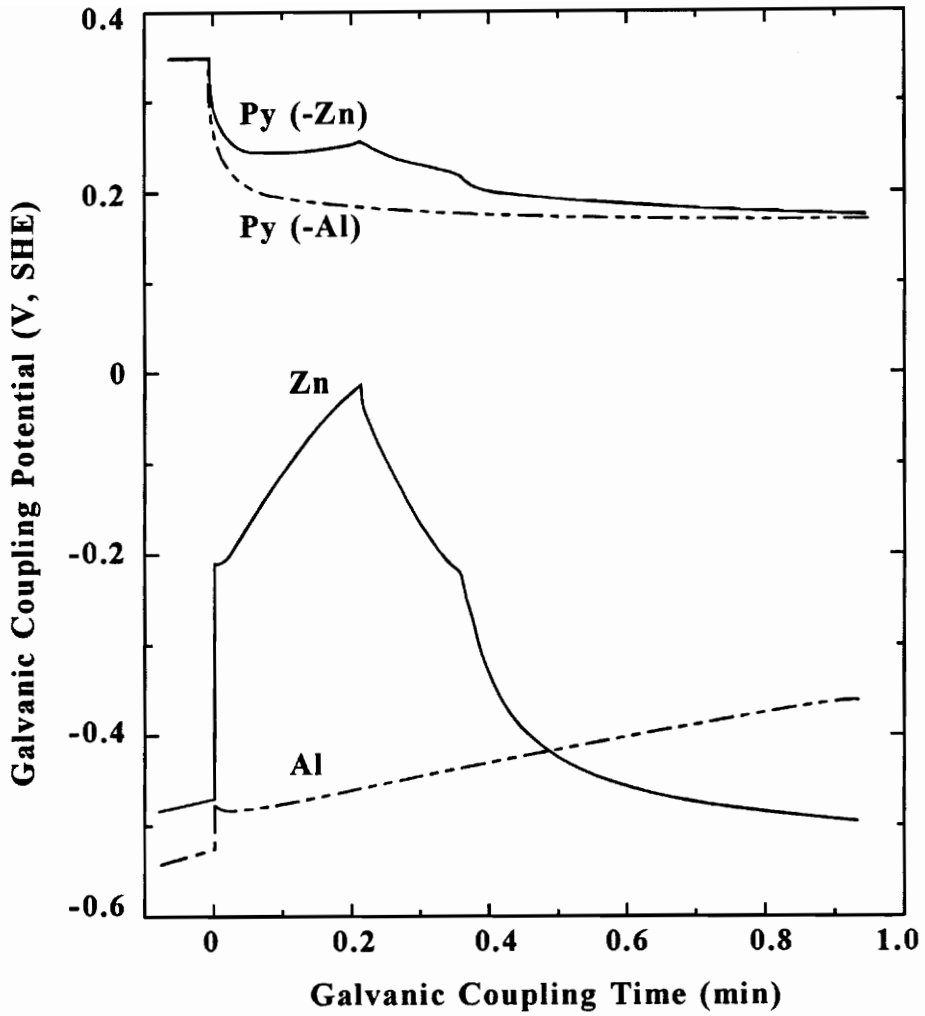

Figure 3.9 **Potential of Illinois No. 6 coal-pyrite as a function of galvanic coupling time with a zinc or aluminum anode in oxygen saturated solutions at pH 9.2.**

Adam et al. [21] observed a similar behavior by coupling the active metals zinc and magnesium to pyrrhotite in a solution exposed to air. Li and Iwasaki [25] also reported that the presence of oxygen in solutions substantially raised the combination potential (defined as the potential of a shorted-circuited pair of electrodes [21]) of chalcopyrite and a high carbon, low alloy steel. Fortunately, a level of 0.1 ~ 0.2 V cathodic polarization has been established to be adequate to effect considerable protection of the cathode from oxidation, as recognized by Morgan [26] and Shreir [27]. Therefore, a significant effect can be expected on the floatability of the mineral acting as the cathode. Nakazawa and Iwasaki [28] reported that the galvanic interaction between nickel arsenide and pyrrhotite reduced the combination potential by less than -0.1 V but decreased the flotation recovery of pyrrhotite acting as the cathode by 20%. Similarly, Adam et al. [21] observed a decrease of pyrrhotite flotation recovery from 90% to 50% after coupling with a magnesium anode which was accompanied with a reduction of potential of 0.12 V. Rao and Finch [29] reported a substantial decrease in pyrite flotation recovery when the mineral was mixed with galena or sphalerite, although the combination potential of pyrite-galena and pyrite-sphalerite electrodes were only about 0.1 V lower than the rest potential of pyrite alone.

It is believed that the following reactions occur on the anode (metal) and the cathode (pyrite) upon galvanic coupling,

$$M = M^{+} + e^{-} \quad (anodic), \tag{3.8}$$

$$Z^+ + e^- = Z \quad (cathodic) \tag{3.9}$$

where reaction (3.8) represents the oxidation of metal atoms, M, to cations, M^+, and reaction (3.9) is the reduction of some dissolved ion, Z^+ to Z. Both reactions occur simultaneously at the surface with the metal sacrificing by dissolution of surface atoms.

In the absence of oxygen in the electrolyte, the reduction reaction (3.9) may be the reduction of oxidation products of pyrite, such as reactions (3.10) and (3.11), and/or the reduction of hydrogen ions (reaction (3.12)), depending on solution pH,

$$Fe^{3+} + e^- = Fe^{2+} , \tag{3.10}$$

$$S^o + H^+ + 2e^- = HS^- , \tag{3.11}$$

$$2H^+ + 2e^- = H_2 . \tag{3.12}$$

If oxygen is present in the solution, the reaction (3.9) generally involves dissolved oxygen (reaction (3.13)) and/or hydrogen ions (reaction (3.12)),

$$O_2 + 2H_2O + 4e^- = 4OH^- . \tag{3.13}$$

The potential-lowering effect of a particular sacrificial anode on pyrite electrode also depends on the ratio of their surface areas. Figure 3.10 shows the effect of the surface area ratio of the aluminum anode and the pyrite cathode on the equilibrium potential of pyrite. The ratio exhibited a remarkable influence on the galvanic potential. The larger anode provides greater surface area on which the oxidation reaction occurs

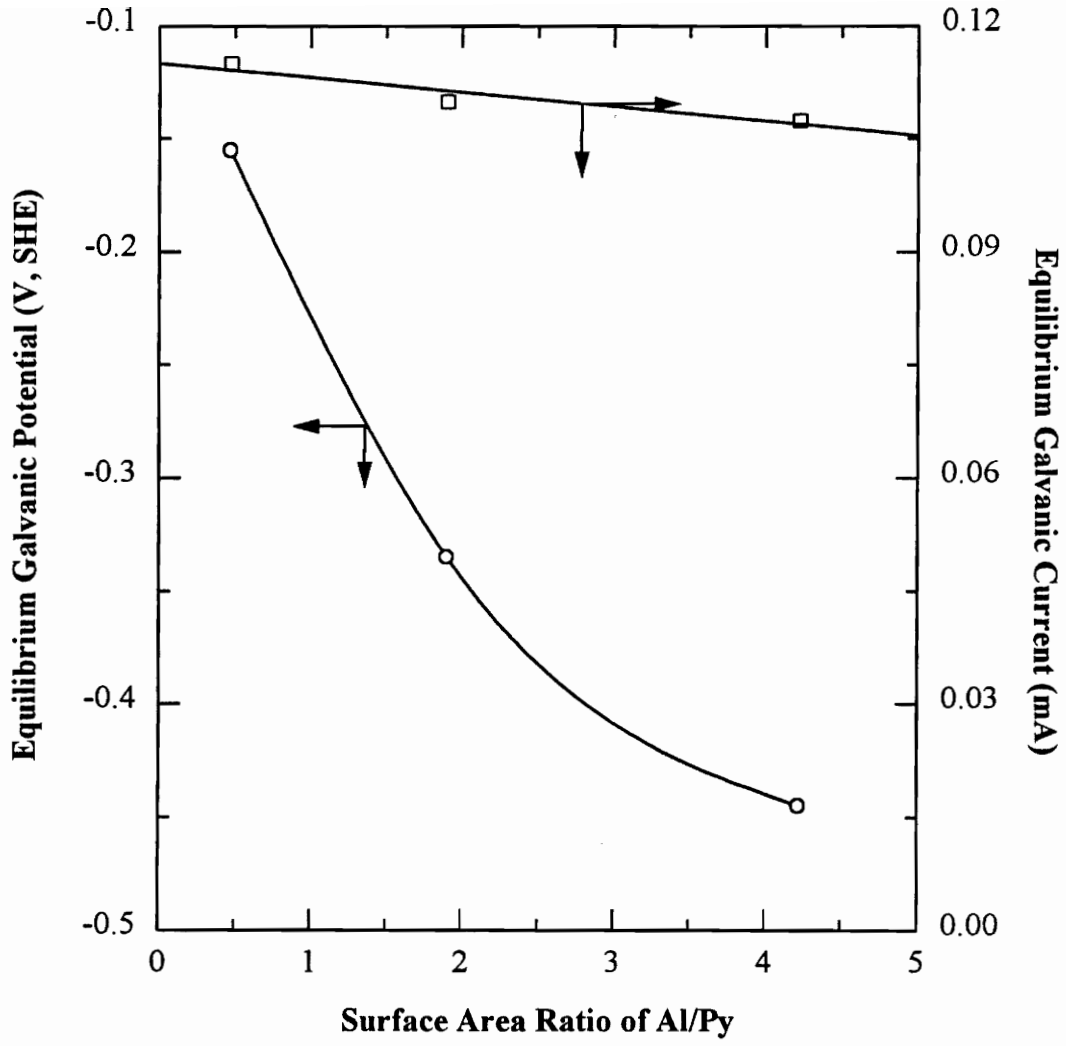

Figure 3.10 The effect of the surface area ratio of aluminum to pyrite on the equilibrium galvanic potential.

and, therefore, generates more electrons to migrate to the pyrite cathode. As a result, the potential of pyrite can be reduced more significantly. However, an excessively negative potential is not required since it leads to aggressive dissolution of the sacrificial anode without much additional benefit. It has been found that the surface area of the anode should be 2 ~ 3 times greater than that of pyrite.

3.4.3 The influence of galvanic coupling on pyrite surface products

The negative potentials of pyrite electrodes obtained by galvanic coupling with sacrificial anodes, as shown above, are certainly low enough to prevent the oxidation of pyrite which has been revealed to take place significantly at about -0.15 V at pH 9.2 and above 0 V at pH 4.6 (Chapter 2). Such negative potentials may also reduce hydrophobic sulfur species on pyrite that are produced by oxidation prior to the galvanic coupling. Therefore, surface products on oxidized pyrite are expected to be altered by galvanic interaction, which can be revealed by cyclic voltammetry.

Figure 3.11 illustrates the effect of galvanic coupling of Illinois No. 6 coal-pyrite with a manganese anode on the first voltammogram in quiescent and stirred solutions. Also shown in Figure 3.11 is the first voltammogram obtained prior to galvanic coupling. The potential sweep was initiated in the positive-going direction. Galvanic coupling greatly reduced, in quiescent solution, and essentially eliminated, in stirred solution, the

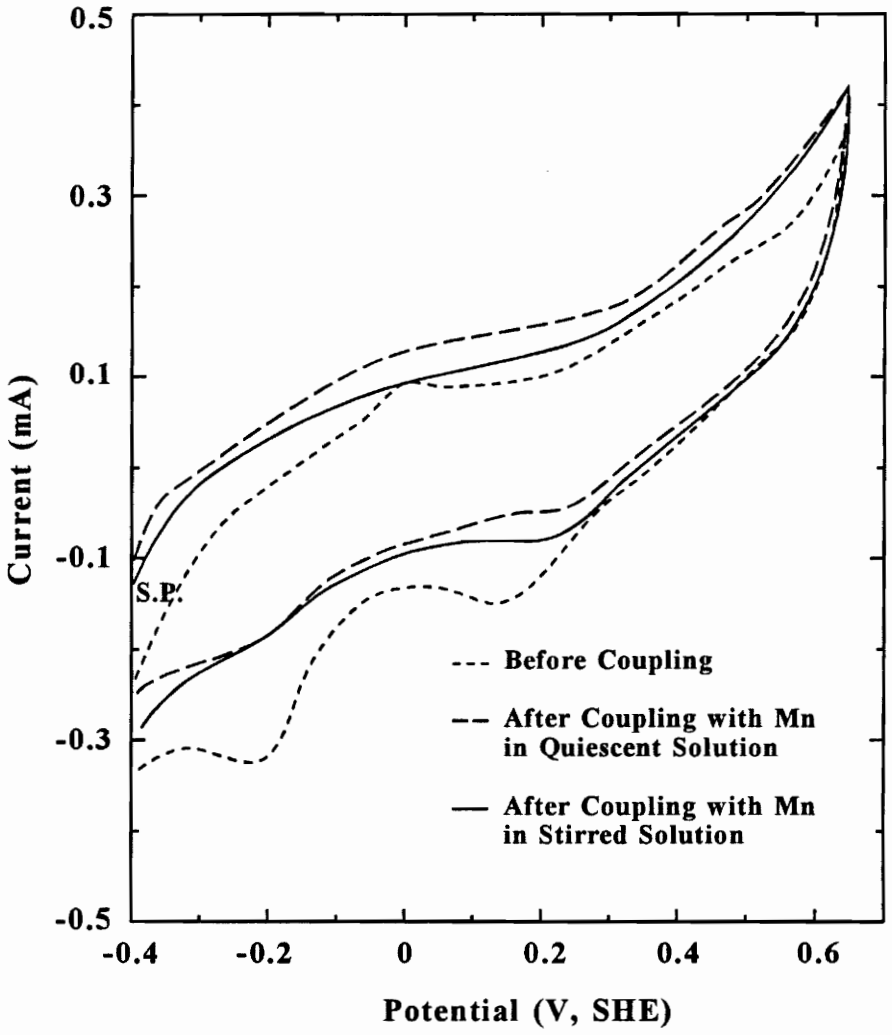

Figure 3.11 First-cycle voltammograms of Illinois No. 6 coal-pyrite at pH 4.6 before and after galvanic coupling with a manganese anode in quiescent and stirred solutions (S.P.: starting point).

anodic peak at 0 V and the cathodic peak at -0.2 V. These two peaks were shown in Chapter 2 to correspond to oxidation/reduction processes involving the S^o/HS^- couple. Apparently, galvanic coupling resulted in the reduction of S^o-like species to HS^- which diffused away from the surface. Solution stirring accelerated this diffusion process. The removal of S^o-like species from the surface reduces the source of the hydrophobicity of pyrite.

The same effect of galvanic coupling was observed with the pyrite electrode that was preoxidized at 0.65 V for 5 minutes at pH 4.6, as shown in Figure 3.12 in which the voltammetric sweep was initiated in the cathodic direction. An increased amount of S^o-like species was formed during preconditioning. Galvanic coupling with manganese was still able to remove essentially all the sulfur oxidation product, especially in stirred solutions. A similar study was done with Pittsburgh No. 8 coal-pyrite which was preoxidized at 0.55 V at pH 9.2 for 5 minutes. It was noticed that galvanic coupling with a zinc electrode altered the voltammetric behavior of the pyrite electrode and reduced the sulfur oxidation products on the surface to soluble HS^-.

3.4.4 The effect of galvanic coupling on the floatability of pyrites

Microflotation tests were conducted to examine the effect of galvanic coupling on the floatability of pyrites. Galvanic interaction between pyrite and sacrificial anodes was

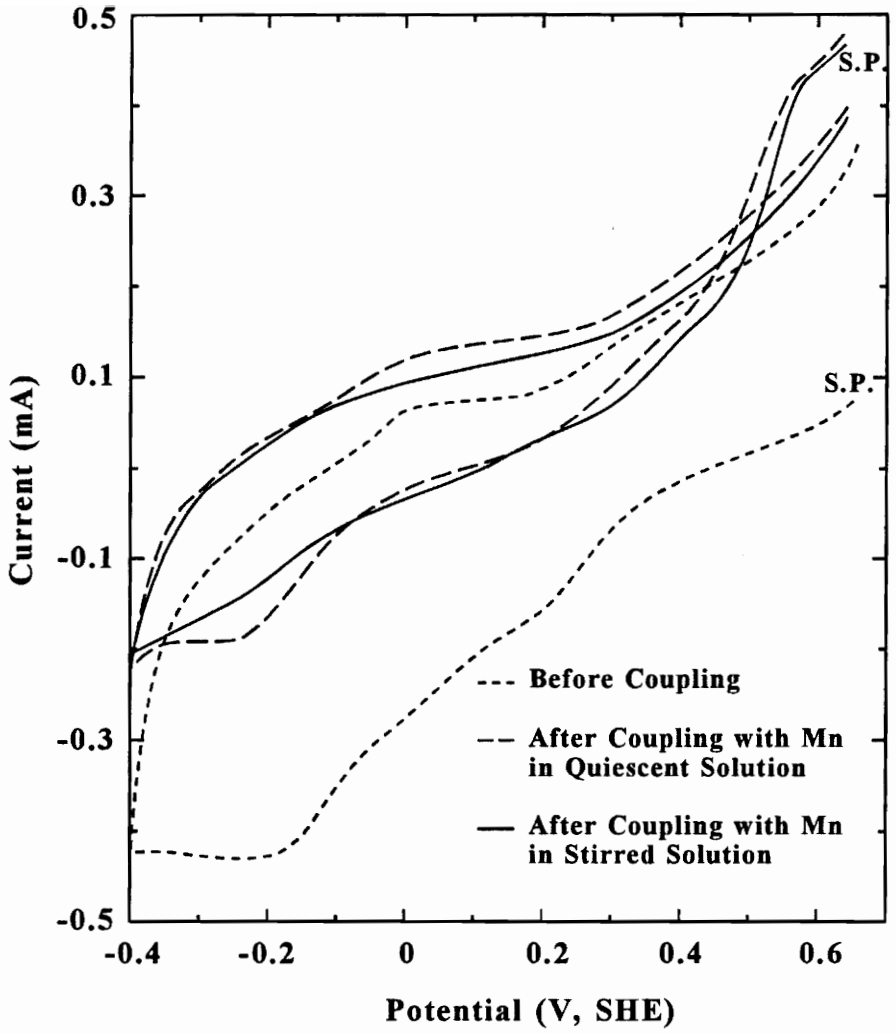

Figure 3.12 First-cycle voltammograms of Illinois No. 6 coal-pyrite oxidized at 0.65 V for 5 minutes at pH 4.6 before and after galvanic coupling with a manganese anode in quiescent and stirred solutions.

accomplished in these experiments by the addition into a conditioning cell of known amounts of metal powders of zinc, manganese, aluminum, and iron. To prevent excessive metal consumption and obtain low potentials, nitrogen was used as a purging and flotation carrier gas. Surface oxidation products on the metal powders were removed by the use of a small amount of dilute hydrochloric acid in the conditioning cell prior to the addition of specific buffer solution. A 0.75 g of 100-200 mesh coal pyrite sample, which was freshly ground in open air, was then transferred into the cell and conditioned for 20 seconds. Electrochemical potentials were measured on both pyrite and platinum electrodes. After conditioning, the solution was transferred to a microflotation cell and the sample was conditioned with 30 ppm emulsified kerosene for 2 minutes followed by a 2 minute conditioning with 50 ppm MIBC used as the frother. The recovery was determined after a three-minute flotation period at a nitrogen flow rate of 35 ml/min.

Figure 3.13 shows the flotation recovery of Illinois No. 6 coal-pyrite at pH 4.6, 6.8 and 9.2 in the presence and absence of metal powders of manganese, zinc and iron. It has been shown previously [30] that pyrite ground in open air will undergo superficial oxidation which produces S^{o}-like species on the surface. This is confirmed in Figure 3.13. In the absence of metal powders, the pyrite sample exhibited a collectorless flotation recovery of 65% at pH 4.6. At neutral or alkaline pH's, the floatability of pyrite is considerably lower than at pH 4.6 due to the formation of iron hydroxide on the surface. Metal powders caused a large reduction in pyrite recovery at pH 4.6. Galvanic

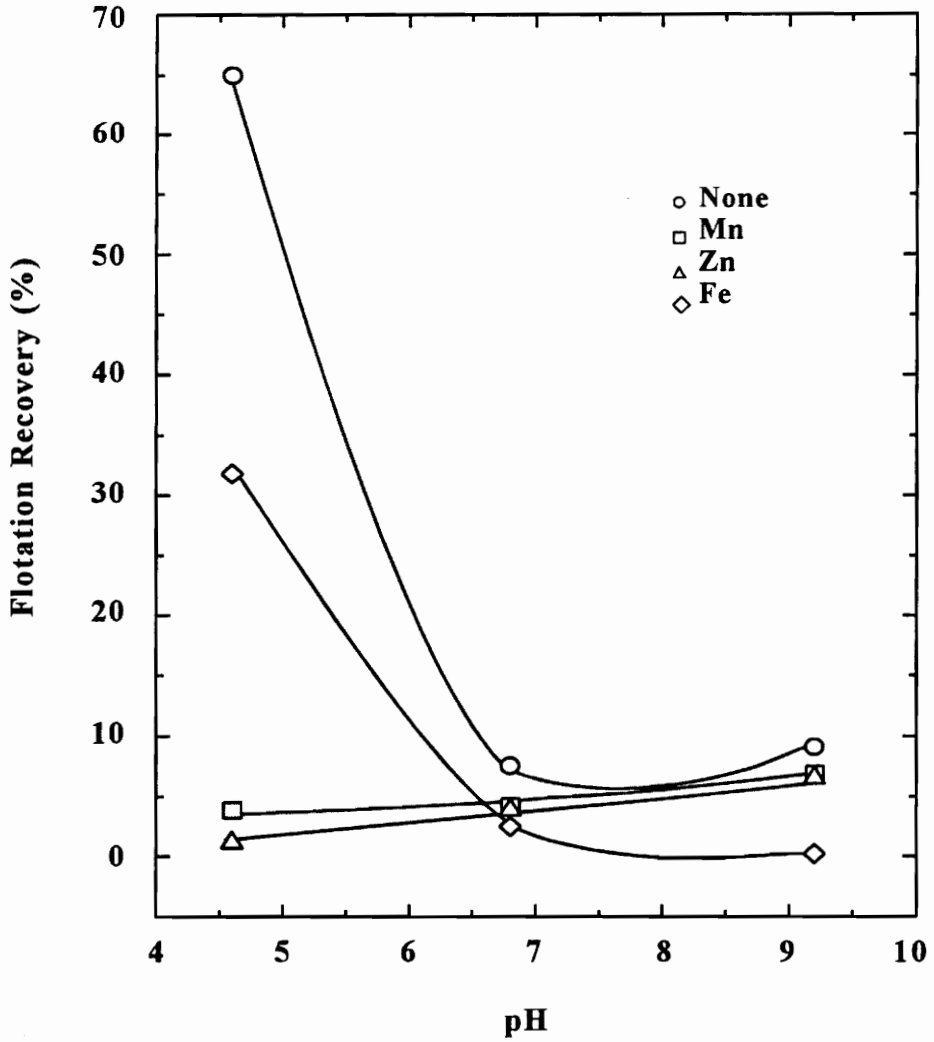

Figure 3.13 Flotation recovery of freshly-ground 100-200 mesh Illinois No. 6 coal-pyrite with Fe, Mn and Zn powder as reducing agents at different pH's.

coupling with zinc and manganese powders depressed pyrite almost completely whereas iron was less effective. The relatively inferior performance of iron powder may indicate that its reducing ability ($E(Fe^{2+}/Fe)$ = -0.440 V) is not sufficient to reduce all hydrophobic species on the surface of pyrite. At pH 6.8 and 9.2, the flotation recovery of pyrite was also reduced to some extent. A slightly higher flotation recovery at pH 9.2 than at pH 6.8 is possibly caused by the smaller bubble size generated at pH 9.2, which would increase flotation kinetics [31].

The quantity of metal powders has a pronounced influence on pyrite depression, as shown in Figure 3.14 with manganese and zinc. It should be pointed out that the dosage expressed in Figure 3.14 can not be considered as an actual consumption for the metal powder because it was not completely consumed during conditioning. Pyrite recovery decreased readily from 65% with the increase of the concentration of manganese and zinc powders in the solution. Higher powder content in the solution not only lowered the potential of pyrite to a more negative value, but also, and probably more importantly, provides longer contact time between pyrite particles and metal powders and provides a larger surface. Although manganese possesses a lower standard redox potential than zinc, it depressed pyrite less effectively. This may be because manganese has a higher specific density than zinc (Mn 7.43; Zn 7.13), which leads to a smaller surface area for the interaction with pyrite particles for manganese at the same dosage (grams of powders per liter of solution). Another reason, which is probably more

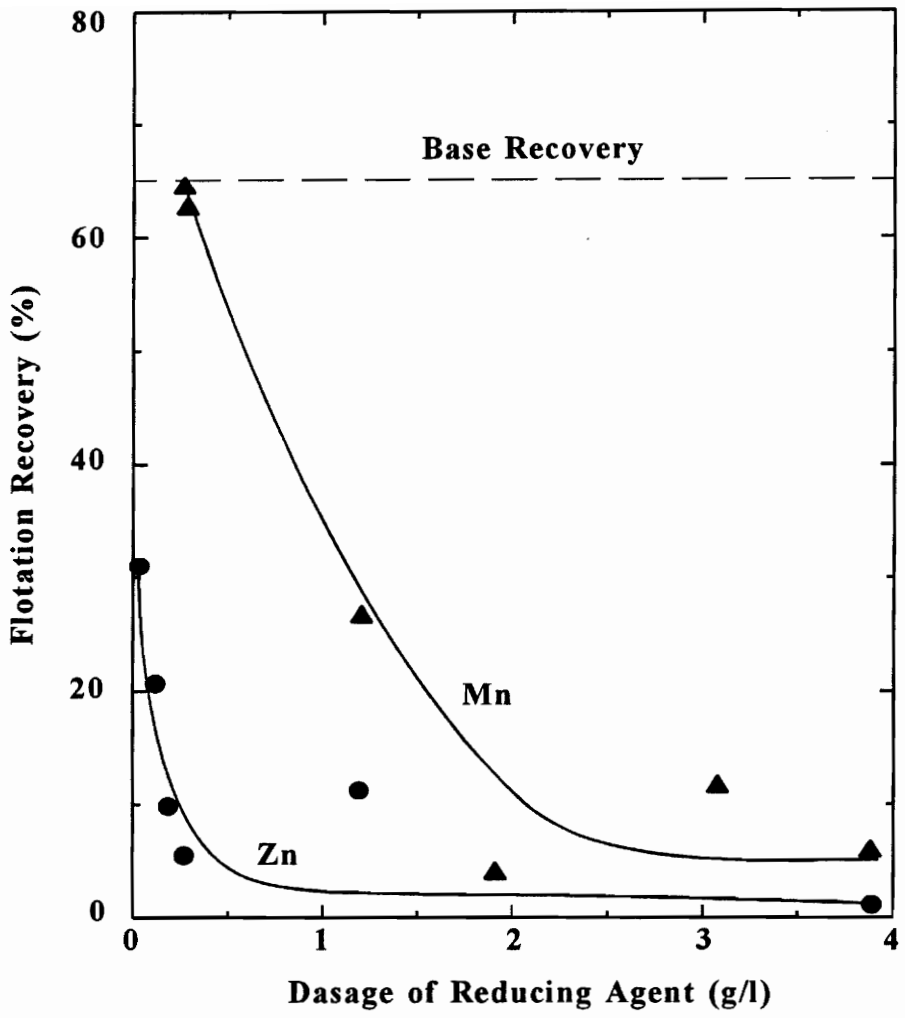

Figure 3.14 Flotation recovery of freshly ground 100-200 mesh Illinois No. 6 coal-pyrite as a function of dosage of manganese and zinc powder at pH 4.6.

important, is that manganese is believed to be oxidized to a higher degree than zinc and the use of dilute acid prior to the addition of pyrite may not sufficiently remove oxides on the surface. Oxide films may retard the galvanic interaction between manganese and pyrite.

Magnesium-aluminum-zinc alloy wire (Mg:Al:Zn = 93:6:1) with a diameter of 1.59 mm was also used as a sacrificial anode to effect galvanic coupling to cathodically polarize the pyrite. Wire of known length in the form of spirals was suspended in the microflotation cell for two minutes after kerosene was added. The wire spirals were removed immediately before flotation was initiated. The surface area ratio of the alloy to pyrite was controlled by adjusting the length of wire employed for the spiral.

Figure 3.15 shows the flotation recovery of -200+100 mesh Illinois No. 6 coal-pyrite as a function of the ratio of surface area of the alloy to pyrite at pH 4.6. Pyrite recovery decreased with increasing surface area ratio until a ratio of approximately unity, above which no further significant improvement in pyrite depression was observed. The results confirm that excessive quantities of reducing agents do not have additional benefits. The use of the alloy lowered the potential of pyrite from 0.5 V to -0.8 V in these experiments, which indicated that this alloy is a strong reducing agent. Figure 3.15 provides evidences that various shapes of active metals or alloys can be used to generate galvanic interaction and their effectiveness for depressing pyrite is dependent on the surface area of the sacrificial anode.

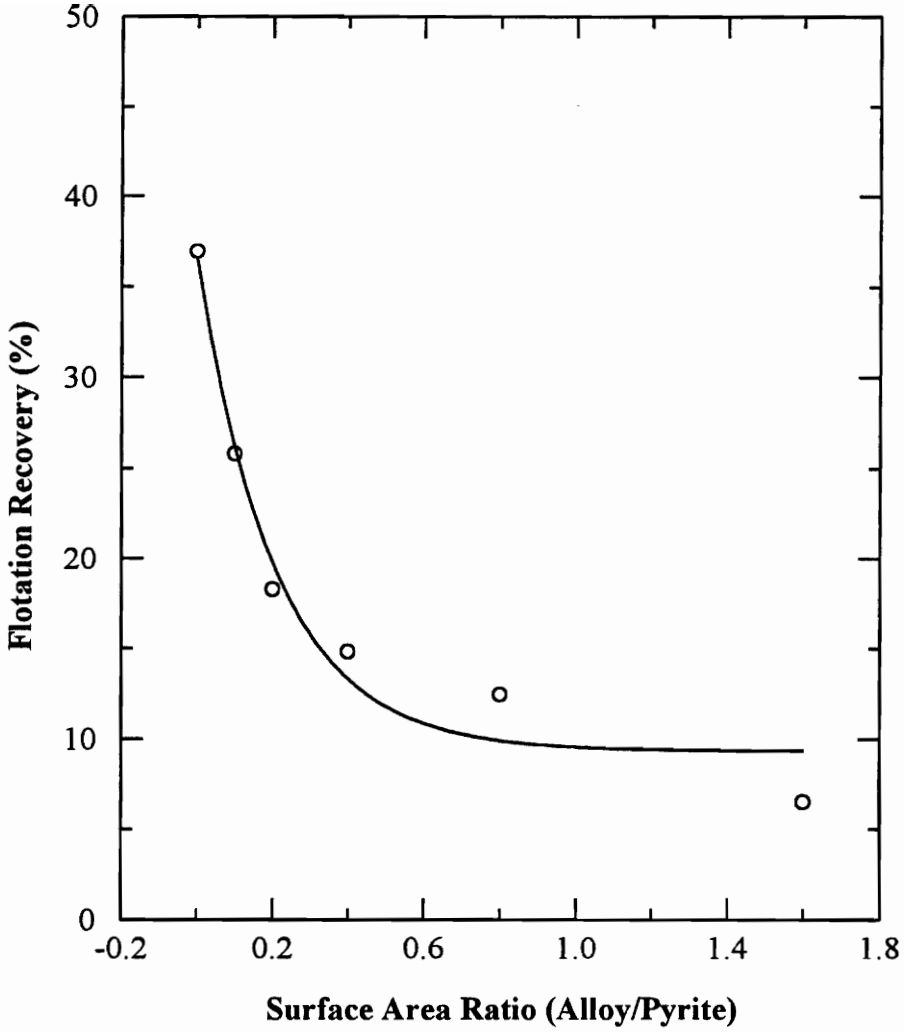

Figure 3.15 **The effect of the surface area ratio of Mg-Al-Zn alloy to pyrite on the flotation recovery of 100-200 mesh Illinois No. 6 coal-pyrite at pH 4.6.**

The above flotation tests with pure pyrite indicated that both metals and alloys can be used as sacrificial anodes to cathodically protect pyrite from oxidation. They also demonstrated that the shape or the form of sacrificial anode does not affect its ability to induce galvanic interaction with pyrite. The remarkable depression effects observed in these experiments suggest that galvanic coupling technique may be a viable method to enhance pyrite rejection, as will be discussed in detail in the following section.

3.4.5 Enhancing pyrite rejection in coal flotation by galvanic coupling

The ultimate objective of this study is to enhance pyrite rejection from coal by flotation. The above experiments showed that galvanic coupling of pyrite with active metals decreased the floatability of pyrite, which suggested that this technique may improve the separation efficiency of pyrite from coal by flotation. To verify the applicability of the technique to coal flotation, tests were carried out in both microbubble flotation columns and conventional mechanical flotation cells using a number of high sulfur coals. The operating conditions are described in Section 3.3.2.2.

For microbubble column flotation, galvanic interaction between the sacrificial anode and pyrite was obtained by adding -325 mesh manganese powders into a sealed conditioning sump. The water used for the slurry was bubbled with nitrogen for at least one hour before loading the coal sample. The solids concentration in the sump was

maintained at 20%, unless otherwise indicated, during the conditioning stage. The dosage of manganese powders was 5% of the coal weight, e.g., 20 g manganese powder was used for 400 g coal. In one series of flotation tests, the slurry was diluted to 5% solids content prior to flotation with nitrogenated water. In the other series of experiments, the solids concentration in the feed slurry to the column was 20%, i.e., no dilution of slurry was performed after conditioning. The conditioning lasted approximately 30 minutes. The measured slurry potential varied during the conditioning period from -0.35 V to -0.1 V. The feed rates were set at 500, 1000, and 1400 ml/min for the slurry containing 5% solids and 150, 300, and 450 ml/min for the feed of 20% solids.

For flotation tests carried out in a 5 L Denver flotation cell, conditioning was done in the cell prior to flotation. The conditioning time was fixed at 30 minutes. Flotation froth products were collected at 0.25, 0.5, 1.0, 2.0, and 4.0 minutes.

Figure 3.16 shows the microbubble column flotation results with Lower Kittanning coal samples. The addition of manganese powders shifted the curve of combustible recovery vs. sulfur rejection (Figure 3.16, top) to the upper right corner, which indicates a better rejection of pyrite from coal. For example, without the addition of manganese, the sulfur rejection is about 40% at a combustible recovery of 90%. The use of manganese enhanced the sulfur rejection by approximately 20% at the same combustible recovery. The depression of pyrite in the presence of manganese powders

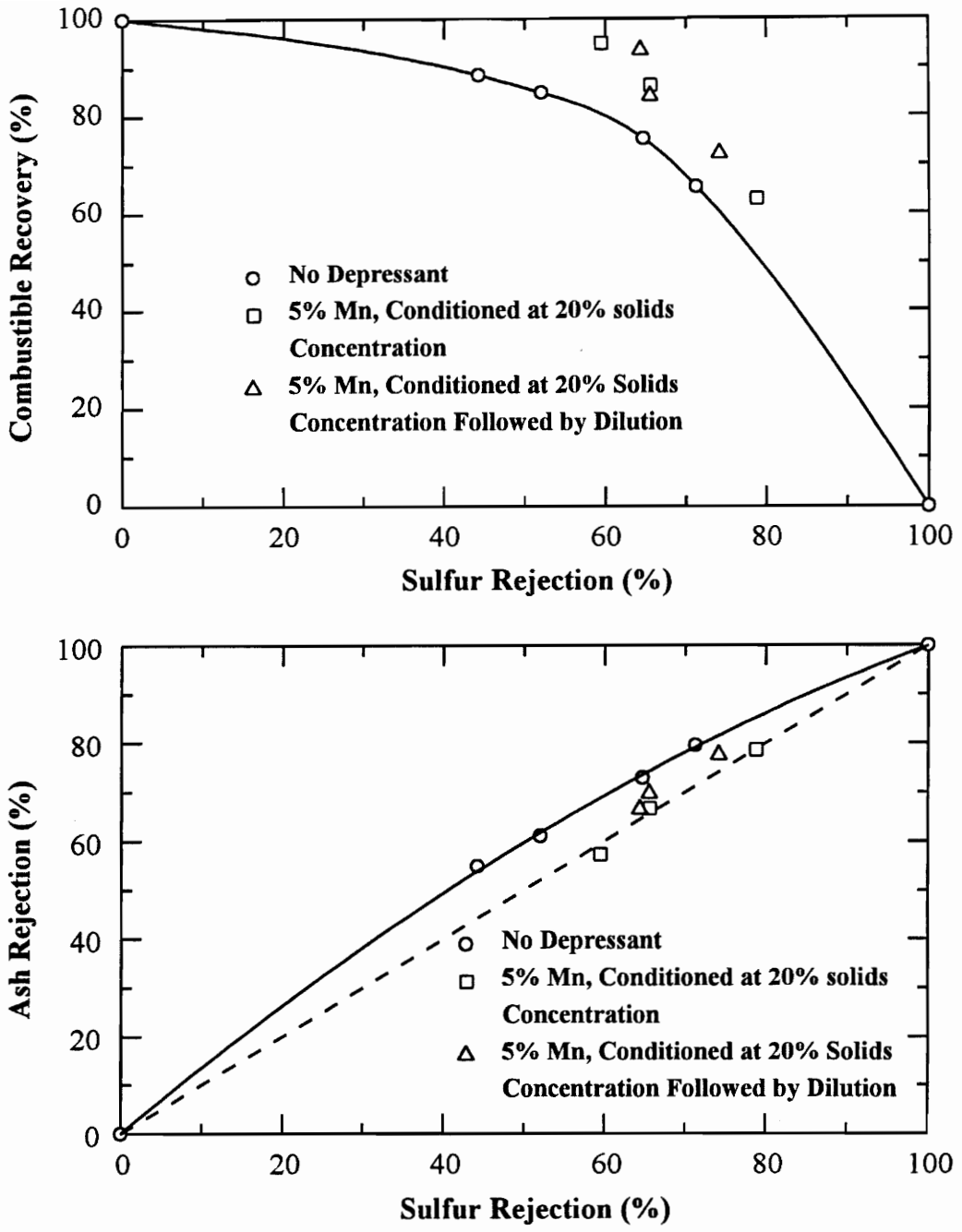

Figure 3.16 The effect of manganese powders on desulfurization of -100 mesh Lower Kittanning coal by microbubble column flotation at natural pH under conditions specified.

is demonstrated by the curve of ash rejection vs. sulfur rejection (Figure 3.16, bottom). If pyrite was completely nonfloatable like other ash-forming minerals such as clay, carbonates, etc., all data points would be on the dashed diagonal line, which represents ideal rejection. In reality, this situation is almost impossible to achieve due to the hydrophobicity of pyrite. As shown in Figure 3.16 (bottom), the data points are considerably above the dashed line in the absence of manganese, establishing that it is more difficult to reject pyrite than other ash-forming minerals. However, when manganese powders were used to control the potential of pyrite, the data points are on or close to the dashed line, establishing that pyrite is depressed.

Similar results were obtained when flotation was carried out in a conventional Denver flotation cell, as shown in Figure 3.17. In comparison with Figure 3.16, conventional flotation yielded relatively inferior performance due to the nonselective recovery of particles by hydraulic entrainment. However, the use of manganese powders also showed a substantial improvement of sulfur rejection. At the combustible recovery of 90%, sulfur rejection increased from 33% to 52% by the addition of manganese at a dosage of 5% of the coal weight. The curve of ash rejection vs. sulfur rejection reveals that pyrite could also be largely depressed when a sufficient amount of manganese was used.

Chinese Chongqing high-sulfur coal of -100 mesh size fraction was also employed to examine the effectiveness of galvanic coupling in the conventional cell. The dosage

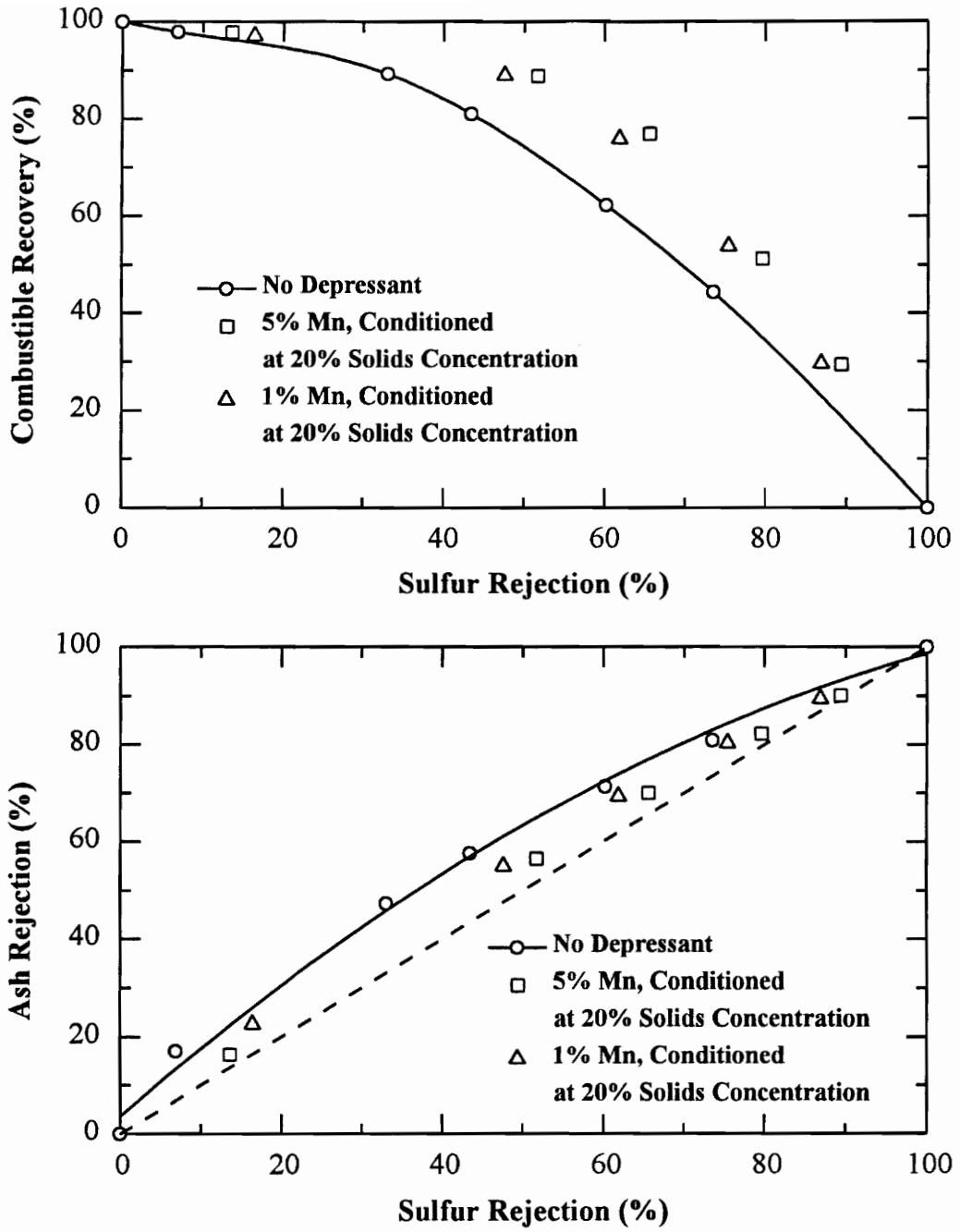

Figure 3.17 The effect of manganese powders on desulfurization of -100 mesh Lower Kittanning coal by conventional flotation at natural pH.

of manganese powders was 5% of the weight of feed. The results are shown in Figure 3.18. The sacrificial anode gave a significant improvement in sulfur rejection (Figure 3.18, top) by reducing the hydrophobicity of pyrite (Figure 3.18, bottom).

The conditioning time, conditioning solids content in slurry, powder dosage, and slurry pH were studied in order to achieve the optimum depression effect. It was found that the dosage of metal powders and the solids concentration of the slurry are the most important operating parameters in depressing pyrite. The effect of dosage of metal powders is indicated in Figures 3.14 and 3.15 with pure pyrite samples. Flotation tests with coal samples showed similar behavior. When the dosage of manganese powder was varied from 1%, 3% to 5% of the coal weight, a consistent increase in the pyrite rejection was observed. However, further increase in the dosage did not lead to a significant enhancement in pyrite removal.

Figure 3.19 shows the dependence of sulfur rejection on the conditioning solids content while the flotation solids concentration was maintained constant at 5%. When the coal slurry was conditioned by manganese powders at 5% solids concentration, sulfur rejection was not enhanced. When the conditioning solids concentration was raised to 20%, significant enhancement of sulfur rejection by galvanic coupling with manganese was observed. Since the collision probability between metal powder and pyrite particle is directly proportional to the product of their concentrations in well stirred solutions, the increase of solids concentration from 5% to 20% represents a 16-fold increase of the

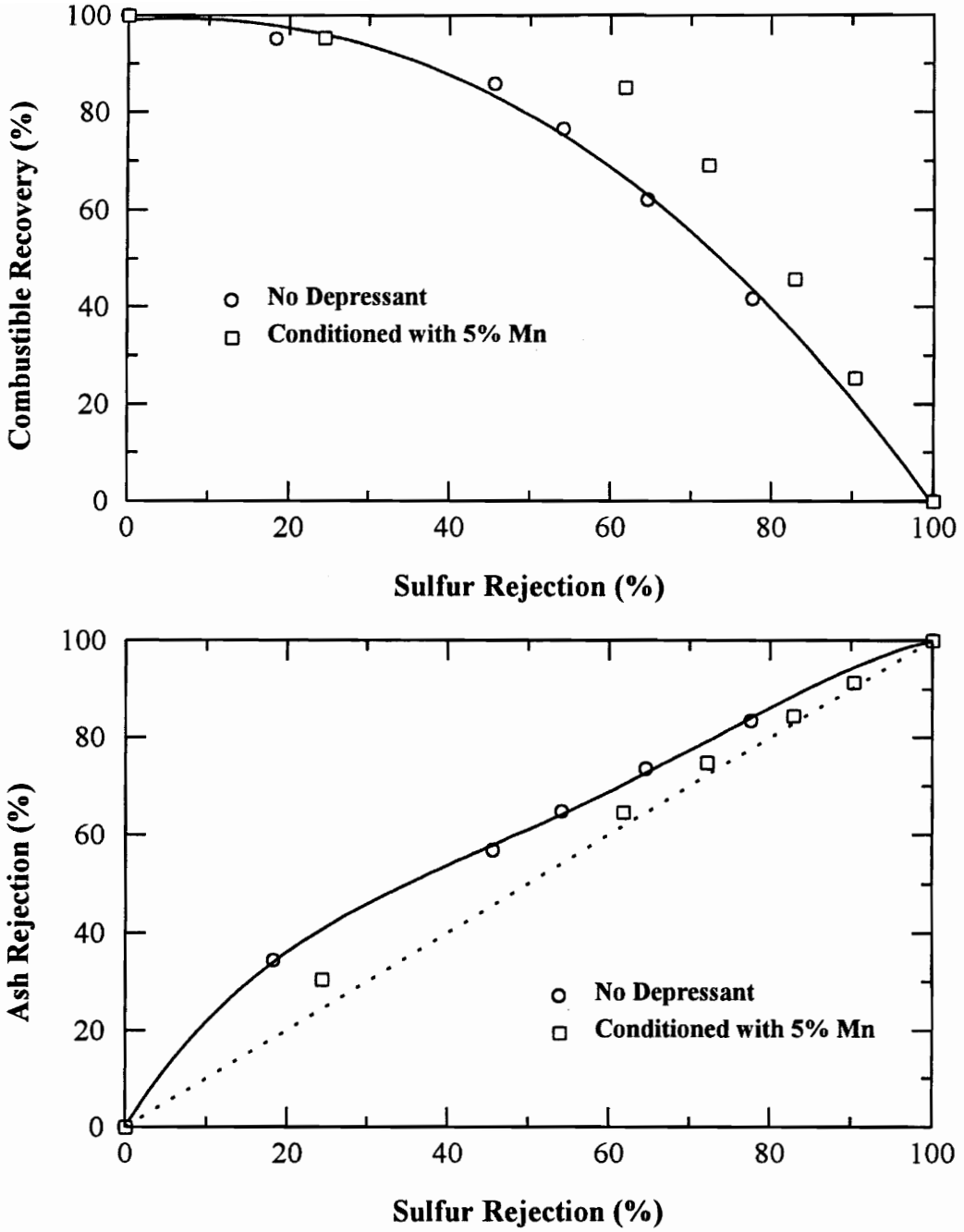

Figure 3.18 The effect of manganese powders on desulfurization of -100 mesh Chinese Chongqing coal by conventional flotation at natural pH.

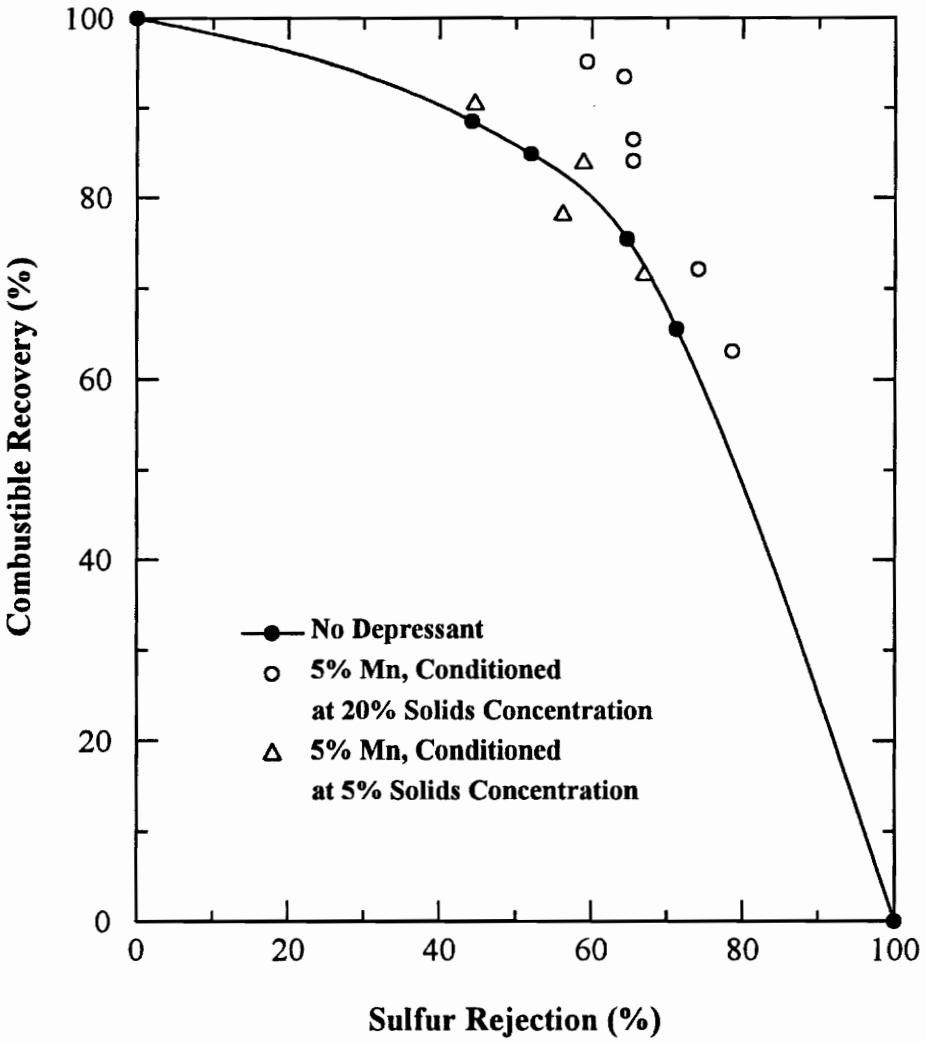

Figure 3.19 The effect on desulfurization of -100 mesh Lower Kittanning coal of manganese powder at different solids concentrations in conditioning stage by conventional flotation at natural pH.

collision probability. It is believed that the increased collision probability, and hence, the contact time between pyrite and metal powders was primarily responsible for the enhanced sulfur rejection observed at higher solids concentration in the conditioning stage.

Previous studies [21, 32, 33] have shown that the decreased floatability by xanthates of sulfide minerals in galvanic interaction with other sulfides or active metals results from the formation of metal hydroxides and the reduced potential that prevented the production of dixanthogen or metal xanthate. The metal cations result from the dissolution of the cathodic mineral and/or anodic oxidation. The hydroxyl ions are produced from reduction of oxygen at the cathode. The present study has shown that galvanic coupling of pyrite with active metals depressed pyrite possibly through two important mechanisms:

(1) Decreasing the potential of pyrite to a value that is negative enough to prevent the superficial oxidation of pyrite, thus minimizing the hydrophobic species on the mineral surface, or reducing the hydrophobic species already on the surface to hydrophilic or soluble products.

(2) Preferentially forming metal hydroxides on the surface of pyrite near the pyrite electrode either by the removal of hydrogen ions or by the generation of hydroxyl ions, which promotes the hydrophilicity of pyrite.

The floatability of coal is relatively unchanged since its component will not be altered

in reducing environment and there is no massive precipitation of metal hydroxide on its surface which is possible when the solution pH is adjusted to high values by the use of alkali. It was found in the present study that an increase of the pH of solution to 11 by the addition of NaOH or $Ca(OH)_2$ did not improve pyrite rejection in coal flotation.

3.5 Conclusions

1. Pyrite exhibits collectorless flotation as a result of surface oxidation. The flotation recovery is determined by the relative abundance of sulfur- and iron-oxidation products, which depends on the source of the sample and the oxidation conditions, i.e., E_h, pH and time.
2. Stronger collectorless flotation of pyrite was observed over a wider range of potential at acidic pH's than at alkaline pH's. This is because alkaline conditions favor the formation of iron hydroxides
3. Hydrophobic species, most likely polysulfides or metal-deficient sulfides, that are produced during the superficial oxidation of pyrite are responsible for the observed collectorless flotation of pyrite.
4. Galvanic coupling of pyrite with active metals such as zinc, manganese, aluminum and their alloys can effectively lower the potential of pyrite to a value that is negative enough to prevent the oxidation of pyrite and/or reduce

hydrophobic species already present on the surface of pyrite.

5. Galvanic coupling can effectively depress pyrite without adversely affecting the hydrophobicity of coal, resulting in enhanced pyrite rejection from coal by flotation.

6. The most important parameters that determine the effectiveness of galvanic coupling are the dosage of the sacrificial anodic powders and the solids concentration of the slurry in the conditioning stage.

3.6 References

1. Luttrell, G.H. and Yoon, R.-H., 1992. "Methods for improving sulfur rejection in fine coal flotation circuits," *Proceedings, The Coal Preparation '92 conference*, May 3-7, Cincinnati, Ohio.

2. Ahlberg, E., Forssberg, K.S.E., and Wang, X., 1990. "The surface oxidation of pyrite in alkaline solution," *Journal of Applied Electrochemistry*, **20**, pp. 1033-1039.

3. Pang, J. and Chander, S., 1992. "The effect of EDTA on collectorless flotation of pyrite," in: *Proceedings of the Third International Symposium on Electrochemistry in Mineral and Metal Processing*, Ed. by R. Woods, P.E. Richardson, The Electrochemical Society, Inc., Pennington, N.J., 221-234.

4. Chernosky, T.J. and Lyon, F.M., 1972. "Comparison of the flotation and adsorption characteristics of ore and coal-pyrite with ethyl xanthate," *Transactions of AIME*, March, pp. 11-14.

5. Rao, S.R. and Finch, J.A., 1987. "Electrochemical studies on the flotation of sulfide minerals with special reference to pyrite-sphalerite-II flotation studies," *Canadian Metallurgical Quarterly*, **26**(3), pp. 173-175.

6. Kawatra, S.K. and Eisele, T.C., 1991. "Recovery of pyrite in coal flotation, entrainment or hydrophobicity," *Proceedings, SME/AIME Annual Meeting*, Denver, Colorado, February 25-28, Preprint 91-89.

7. Finkelstein, N.P., Allison, S.A., Lovell, V.M., and Stewart, B.V., 1975. "Natural and induced hydrophobicity in sulfide mineral systems," In *Advances in Interfacial Phenomena of Particulate/Solution/Gas System, Applications to Flotation Research*, AIChE, Symp. Ser. No. 150, **71**, pp. 165-175.

8. Partridge, A.C. and Smith, G.W., 1971. "Small-sample Flotation Testing," *Trans. Inst. Min. Metall., Sec C*, **80**, pp. C199-205.

9. Yoon, R.-H., Luttrell, G.H., Adel, G.T., and Mankosa, M.J., 1989. "Recent advances in Fine coal flotation," in *Advances in Coal and Mineral Processing Using Flotation*, Ed. by S. Chander and R. Klimpel, Society of Mining Engineers, INC., Littleton, Colorado, pp. 211-218.

10. Yoon, R.-H., Lagno, M.L., Luttrell, G.H., and Mielczarski, J.A., 1991. "On

the hydrophobicity of coal pyrite," *Processing and Utilization of High Sulfur Coals IV*, Ed. by P.R. Dugan, D.R. Quigley, and Y.A. Attia, Elsevier Science Publishers, Amsterdam, pp. 241-253.

11. Buckley, A.N, and Woods, R., 1984. "An X-ray photoelectron spectroscopic investigation of the surface oxidation of sulfide minerals," *Proceedings of International Symposium on Electrochemistry in Mineral and Metal Processing*, Ed. by P.E. Richardson, S. Srinivasan, and R. Woods, The Electrochemical Society, Inc., Pennington, N.J., pp. 286-302.

12. Hamilton, I.C. and Woods, R., 1981. "An investigation of surface oxidation of pyrite and pyrrhotite by linear potential sweep voltammetry," *Journal of Electroanalytical Chemistry*, **118**, pp. 327-343.

13. Chander, S., 1991. "Electrochemistry of sulfide flotation: growth characteristics of surface coatings and their properties, with special reference to chalcopyrite and pyrite," *International Journal of Mineral Processing*, **33**, pp.121-134.

14. Chander, S. and Briceno, A., 1987. "Kinetics of pyrite oxidation," *Minerals and Metallurgical Processing*, **4,** pp. 171-176.

15. Tao, D.P., Richardson, P.E., Luttrell, G.H., and Yoon, R.-H., 1993. "An electrochemical investigation of surface reactions of coal- and mineral-pyrite in aqueous solutions," *Processing and Utilization of High Sulfur Coals V*, Ed. by B.K. Parekh and J.G. Groppo, Elsevier Science Publishers, Amsterdam, pp. 219-

235.

16. Zhu, X., Wadsworth, M.E., Bodily, D.M., and Riley, A.M., 1991. "Surface properties of mineral and coal pyrite after electrochemical alteration," *Processing and Utilization of High Sulfur Coals IV*, Ed. by P.R. Dugan, D.R. Quigley, and Y.A. Attia, Elsevier Science Publishers, Amsterdam, pp. 205-222.

17. Xu, Z. and Yoon, R.-H., 1989. "The role of hydrophobic interactions in coagulation," *Journal of Colloid and Interface Science*, **134**(2), pp. 532-541.

18. Olson, T.J. and Aplan, F.F., 1987. "The effect of frothing and collecting agents on the flotation of coal, pyrite and locked particles in a coal flotation system," Processing and Utilization of High Sulfur Coals II, Ed. by Y.P. Chugh and R.D. Caudle, pp. 71-82.

19. Jiang, C., Wang, X.H., Leonard, J.W., and Parekh, B.K., 1993. "On the natural and induced floatability of coal and pyrite," *Processing and Utilization of High Sulfur Coals V*, Ed. by B.K. Parekh and J.G. Groppo, Elsevier Science Publishers, Amsterdam, pp. 171-188.

20. Peters, E. and Majima, H., 1968. "Electrochemical reactions of pyrite in acid perchlorate solutions," *Canadian Metallurgical Quarterly*, **7**(3), pp. 111-117.

21. Adam, K., Natarajan, K.A., and Iwasaki, I., 1984. "Grinding media wear and its effect on the flotation of sulfide minerals," *International Journal of Mineral Processing*, **12**, pp. 39-54.

22. Pozzo, P.L., Malicsi, A.S., and Iwasaki, I., 1990. "Pyrite-pyrrhotite-grinding media contact and its effect on flotation," *Minerals and Metallurgical Processing*, February, pp. 16-21.

23. Berry, V.K., Murr, L.E., and Hiskey, J.B., 1978. "Galvanic interaction between chalcopyrite and pyrite during bacterial leaching of low-grade waste," *Hydrometallurgy*, **3**, pp. 309-326.

24. Nakazawa, H. and Iwasaki, I., 1985. "Effect of pyrite-pyrrhotite contact on their floatabilities," *Minerals and Metallurgical Processing*, November, pp. 206-211.

25. Li, X. and Iwasaki, I., 1992. "Effect of cathodic polarization on the floatability of chalcopyrite in the absence of oxygen," *Minerals and Metallurgical Processing*, Feb, pp. 1-6.

26. Morgan, M.H., 1959. "Cathodic Protection," Macmillan, New York, 325 pp.

27. Shreir, L.L., 1976. "Corrosion, vol 2, Corrosion Control," p. 11.9, Newnes-Butterworths, London.

28. Nakazawa, H. and Iwasaki, I., 1986. "Galvanic contact between nickel arsenide and pyrrhotite and its effect on flotation," *International Journal of Mineral Processing*, **18**, pp. 203-215.

29. Rao, S.R. and Finch, J.A., 1988. "Galvanic interaction studies on sulfide minerals," *Canadian Metallurgical Quarterly*, **2**(4), pp. 253-259.

30. Buckley, A.N. and Woods, R., 1987. "The surface oxidation of pyrite," *Applied*

Surface Science, **27**, pp. 437-452.

31. Yoon, R.-H. and Luttrell, G.H., 1986. "The effect of bubble size on fine coal flotation," Coal Preparation, **2**(3), pp. 179-192.

32. Kuhn, A.T. and Chan, C.Y., 1983. "pH changes at near-electrode surface," *Applied Electrochemistry*, **13**, pp. 187-207.

33. Learmont, M.E. and Iwasaki, I., 1984. "Effect of grinding media on galena flotation," *Minerals and Metallurgical Processing*, **1**, pp. 136-142.

CHAPTER 4 FROTH STABILITY AND ITS EFFECT ON COLUMN FLOTATION

4.1 Introduction

It has long been realized that froth stability and hydraulic entrainment of particles in flotation play important roles in determining flotation performance. For example, Tomlinson and Fleming [1] and Feteris et al. [2] showed that the flotation rate constant is directly proportional to the probability that a particle survives the cleaning action of the froth zone and reports to the froth product. Laplante et al. [3] emphasized the importance of froth kinetics in industrial flotation with mechanic cells. They showed that at low air flow rate and high froth depth ($>$ 5 cm), the transfer of material from the froth over the cell lip is the rate limiting step for the overall flotation process. If the froth phase is insufficiently stable, mineralized bubbles which enter the froth zone would rupture prematurely and valuable particles would drop back to the pulp, resulting in the loss of valuable recovery. On the other hand, too stable a froth is very difficult to handle and may cause excessive nonselective entrainment of large quantities of gangue particles which would reduce the product grade. Yianotos et al. [4] studied the selectivity in the froth zone of industrial flotation columns in a Mo-cleaning circuit and

demonstrated that froth depth is a significant factor. Bisshop and White [5] reported the strong dependence on the froth residence time of the amount of drainage of hydrophilic particles from the froth. It is generally accepted that a closely knit froth of small bubbles could enhance the recovery and a loosely knit froth of large bubbles could promote the grade. Therefore, a froth of appropriate stability is of great importance for the achievement of favorable metallurgical performance of flotation.

There are two major mechanisms for the recovery of particles during flotation, i.e., true flotation and entrainment. True flotation is induced by bubble-particle collision and adhesion which are primarily determined by the surface hydrophobicity of particles. Only hydrophobic minerals can be attached to the bubble surface. Hydraulic entrainment results from the mechanical carryover of particles suspended in liquid solution between bubbles. This process can occur to all particles regardless of their surface properties, and hence is nonselective. The particle size plays a critical role in determining the relative importance of these two mechanisms. It is known that true flotation is generally the main recovery mechanism for particles coarser than 10 μm while for particles smaller than 10 μm the collision efficiency is low and the recovery takes place predominately by entrainment.

Froth stability can be adjusted to control the contribution from entrainment. During the drainage of liquid through narrow channels between air bubbles, particles will be forced to contact with bubbles as liquid lamellae thins. Hydrophobic particles

originally entrained in suspended solutions can then adhere to the surface of bubbles. This is particularly important for fine particles < 10 μm whose probability of collision with bubbles in the pulp is negligible. Hemmings has shown [6, 7] that the aqueous lamella has to be thinned to a thickness of less than 10-20 μm for the concentration of these particles to occur by this mechanism. In the case that bubbles are fully loaded with coarse particles, only fine hydrophobic particles may still be enriched in the froth by adhering onto the bubble surface between coarser particles. By properly manipulating the stability and drainage of froth, better flotation recovery and concentrate grade can be achieved.

Few studies have been conducted which dealt with the impact of froth behaviour on the performance of column flotation cells. Work on froth with coal particles in flotation column has been extremely scarce. The froth phase is generally neglected in column flotation studies. This lack of information is surprising in light of the fact that the froth phase is primarily responsible for the improved metallurgical performance of columns over conventional flotation cells.

4.2 Research Objectives

The present study was conducted to provide a better understanding of the importance of the froth phase in flotation columns and develop approaches to improve

the separation efficiency of column flotation by minimizing unwanted entrainment. This was accomplished by conducting laboratory column flotation tests of finely pulverized coal to investigate the effects of various operating parameters on froth stability and entrainment. Variables examined included gas flow rate, wash water flow rate, bubble size, froth height, wash water addition point, solids concentration and particle size in the feed. Specific objectives also included the determination of the relative contributions of entrainment and true flotation to the recovery of coal and ash, respectively, and the establishment of the column froth profiles to show the upgrading action in the froth phase. Special efforts were directed to the study of influences of coal particles on froth behavior.

4.3 Experimental

4.3.1 Coal samples

Samples of run-of-mine coal from the Illinois No. 6 coal seam were used in the column flotation tests. The ash content of the raw coal samples was 10.8%. Once the sample was received, it was immediately downsized to -6 mm using a laboratory jaw crusher and split into representative parts of approximately 1.5 kg each. The samples were then stored in a freezer at -20° C to minimize oxidation. Prior to flotation, they

were dry pulverized in a laboratory hammermill to below 100 mesh. This step was followed by grinding in a ball mill, when necessary. The samples were then used to make up slurry containing 10% solids, unless otherwise specified, in a conditioning sump. A kerosene collector in a dosage of 1.0 kg/t of feed coal was added and conditioned for 5 minutes in all tests.

4.3.2 Column flotation

A microbubble flotation column having a diameter of 5 cm and height of 170 cm was used in most of flotation tests. A detailed description of this apparatus has been provided elsewhere [8]. In order to normalize the effect of column diameter, flow rates were usually expressed as superficial velocities. Unless otherwise noted, tests were carried out under the following conditions: conditioned slurry was fed to the column at a point 60 cm below the froth overflow lip at a rate of 0.17 cm/s. The froth height was approximately 30 cm. Bubbles were generated externally and introduced at the bottom of the column. Betz M-150 frother was added directly to the bubble generation circuit at a constant rate of 15 μl/min, which led to a frother concentration of approximately 18 ppm in the pulp zone. An aeration rate of 1.0 cm/s was employed for all tests. The wash water addition rate was held constant at 0.15 cm/s.

In experiments for the study of bubble size, froth height and froth profiles, a

column with a replaceable bubble generator, i.e, fritted gas sparger, was used. This column had a length of about 100 cm and a diameter of 9 cm. To determine the ash and solids profiles within the froth column, a sampling lance was inserted into the froth to take samples at various points along the column height. These tests were carried out as a function of wash water rate so that the impact of wash water rates could be examined.

4.4 Results and Discussion

4.4.1 Column operating parameters and their effects on froth stability

4.4.1.1 *Gas flow rate (V_g)*

The gas flow rate (V_g) is one of the dominant factors determining flotation rate constant (k). It has been theoretically established [9] that k is directly proportional to V_g. In industrial practice, flotation kinetics are commonly varied by adjusting gas flow rate. The gas flow rate also plays an important role in the establishment of froth. Too low a gas flow rate may be unable to generate a froth zone that is sufficiently stable to accomplish the task of transferring solids to the froth launder. On the other hand, very high gas flow rates may render the froth too wet, resulting in excessive entrainment.

The froth stability is often measured by the time of its persistence. Various methods have been suggested to perform froth stability tests [10, 11]. However, none

of them can be directly applied to continuous flotation experiments. It is known that the more stable the froth, the more water will be recovered in flotation. The water recovery can, therefore, be used as a convenient measure of froth stability for a given flow rate of wash water and feed water combined.

Figure 4.1 shows effects of gas flow rate on flotation performance and froth stability. It can be seen that water recovery increased considerably with the gas flow rate. There are two possible reasons for the observed increase in water recovery with increasing V_g. The first is associated with more bubbles generated at higher gas rates. Under the assumption that the size distribution of the bubbles is independent of gas flow rate and the thickness of water film of each bubble is constant, as proposed by Engelbrecht and Woodburn [12], the recovery of water is expected to be linearly dependent on gas flow rate. This is confirmed in Figure 4.1 showing that there is a linear correlation between water recovery and gas flow rate from 1.25 to 2.0 cm/s. The apparent nonlinear dependence observed in Figure 4.1 above V_g=2.0 cm/s indicated the contribution from the second reason, i.e., increased froth stability. This nonlinearity can not be explained by the increase in bubble size with gas flow rate [13, 14], which would make the curve deviate downward from the line. It may, instead, be caused by the decrease in residence time of bubbles in the froth, which diminished the coalescence of bubbles and drainage of liquid taking place in the froth phase. Bisshop and White [5] showed that the amount of drainage from the froth is strongly dependent on the froth

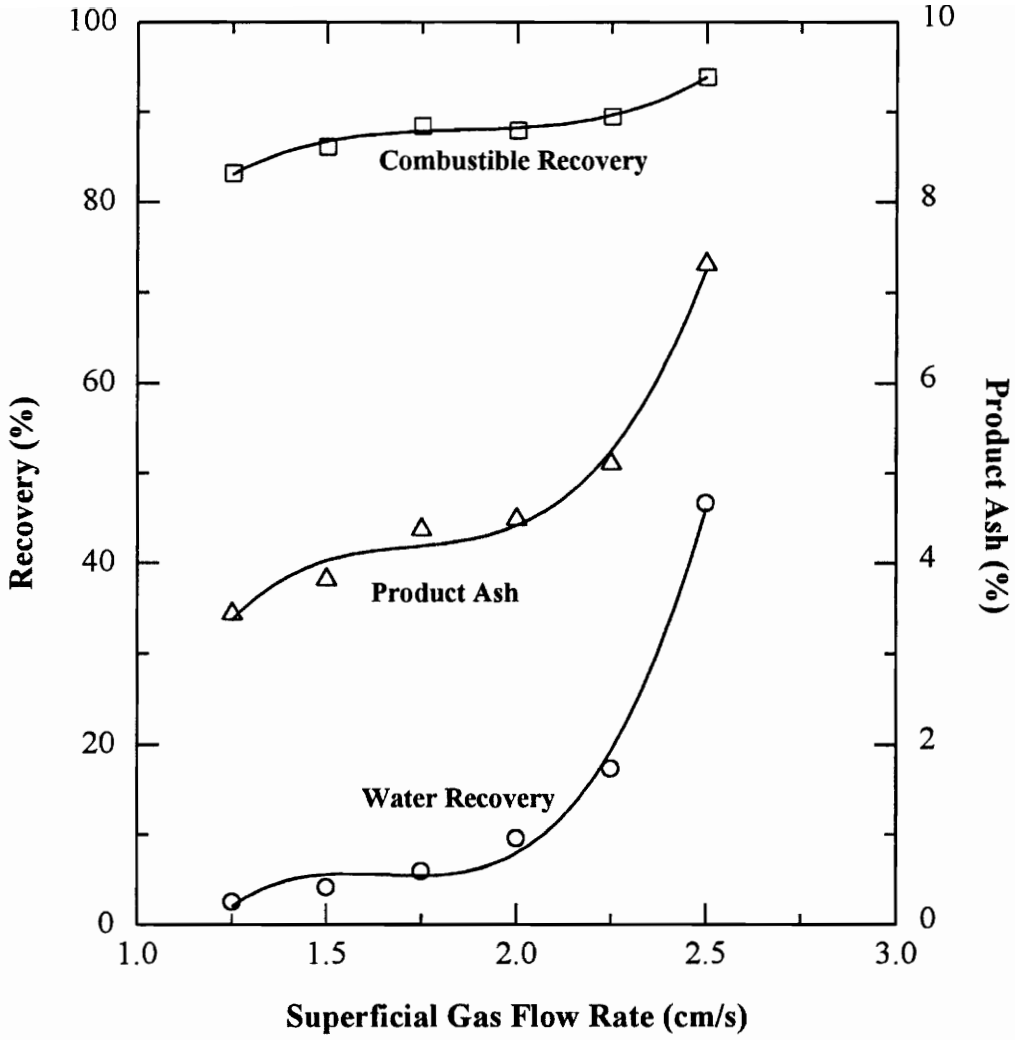

Figure 4.1 **The effect of gas flow rate on froth stability and flotation performance.**

residence time and the effect of residence time on drainage is more pronounced for larger particles.

Increasing gas flow rate resulted in a decrease in gas hold-up in the froth zone but an increase in the collection zone. This is because higher gas flow rate increased the number of bubbles in the pulp and carried more water into the froth. It was found in experiments that at a gas flow rate of 3.0 cm/s, the gas hold-ups in both zones were equal to each other and the interface between them disappeared, which is in good agreement with the previous observation of a two-phase column froth [15].

Ash recovery increased much more significantly than combustible recovery as gas flow rate increased, giving rise to a poorer product grade. This may be because the flotation of the fast-floating fraction of coal is independent of water recovery while the recovery of gangue is strongly dependent on entrainment [2, 16, 17]. The result suggested the importance of interactive adjustment of other operating parameters such as wash water flow rate to achieve the best separation in flotation.

It is interesting to notice that combustible recovery increased consistently with increasing gas flow rate in Figure 4.1. Laplante et al. [18] theoretically predicted and experimentally demonstrated that in a flotation system without a froth phase, the flotation rate constant increased to a maximum and then decreased as gas flow rate was increased. This is due to the fact that gas flow rate has two counteracting effects on the rate constant. Higher gas flow rate generates more bubble surface, which should increase the

flotation rate. On the other hand, an increase in the gas flow rate would also increase the average bubble size, which leads to a decrease in the flotation rate. At low gas flow rates, the first effect dominates; at higher gas flow rates, the second plays a more important role. The gas flow rate at which these two factors are of equal importance results in the maximum flotation rate constant. In contrast with Laplante's conclusion, Mehtrotra and Kapur [19] and Engelbrecht and Woodburn [12] reported that with the froth phase present, flotation rate increases with gas flow rate over its full range, which is in agreement with the present study. The difference observed in different studies appeared to arise from the influence of gas flow rate on the behavior of the froth. No explicit explanation is available in literature. Figure 4.1 revealed that at higher gas flow rates, the increase in flotation recovery was related to the increased froth stability which offset the effect of increased bubble size. Since flotation was carried out in the same period of time, higher flotation recovery is equivalent to higher flotation rate constant.

It is very important to notice that both water recovery and product ash increased tremendously with further increase in gas flow rate after it reached 2.0 cm/s. Coincidentally, Finch et al. [20] recommended from a study of two-phase column froths that gas flow rate should be less than 2 cm/s. They found from the impulse and response tracer technique that at low gas rates ($V_g < 1.5$ cm/s) feed water concentration approaches zero at a froth height of about 10 cm. At $V_g > 2$ cm/s feed water can penetrate 70-80 cm into the froth. As a result, relatively deep froths ($>$ 1 m) are necessary for a 10 m

high industrial column when high gas flow rates are used. Therefore, it appears reasonable to conclude that gas flow rate at about 2 cm/s is favorable for optimum performance of column flotation.

4.4.1.2 *Wash water flow rate (V_w)*

The most important characteristic that distinguishes flotation columns from conventional flotation cells is the addition of wash water to the froth. Klassen and Mokrousov [21] reported that sprinkling water on the top of the froth in mechanical cells improved both grade and recovery due to increased drainage of gangue particles and increased stability of the froth. However, this technique has never achieved much success in conventional flotation cells due to their huge surface, shallow froth, insufficient particle loading on bubbles, etc. On the other hand, studies performed with flotation columns have clearly shown the great effectiveness of wash water for upgrading the froth product [22-24]. Finch and Dobby [23] alleged that the wash water flow rate could be as low as possible, providing the bias water rate is greater than zero. Increase in wash water rate above zero has negligible effect on product grade. However, this conclusion does not appear to be consistent with results from other studies [22, 25] although the exact bias rate can not be readily determined due to incomplete description of operating parameters. Yianatos et al. also [26] suggested that bias rates should be 0.2-0.4 cm/s for industrial columns. To address this discrepancy, two series of tests were

carried out, with special attentions paid to the effect of wash water on the froth stability.

Figure 4.2 shows the results of flotation tests conducted under the condition that frother dosage was constant in lb/ton of feed solids. In this case, the amount of frother fed into the column was not altered as the wash water flow rate changed. The water recovery initially decreased rapidly with increasing wash water rate but was levelled out at about 0.2 cm/s. Although the total amount of water in the column increased with increasing wash water rate, the amount of water carried into the froth product was consistently reduced for $V_w < 0.2$ cm/s, i.e., from 0.132 cm/s at $V_w = 0.06$ cm/s to 0.038 cm/s at $V_w = 0.2$ cm/s, due to the sharp decrease in water recovery. For $V_w > 0.2$ cm/s, the amount of water reporting to the froth product was actually increased. The initial decrease in water recovery as well as water flow rate into the froth product could be attributed to the dilution of frother in the column and the subsequent levelling-off in water recovery, or increase in water flow rate, indicating that the effect of the wash water to prevent coalescence of rising bubbles and film thinning predominated, which enhanced the stability of froth. Combustible recovery and product ash decreased with more wash water added, which is in agreement with the previous results [22, 25].

The bias rate can be estimated from Equation (4.1),

$$V_b = V_w - V_{wp} = (1 - R_w)V_w - R_w V_{wf} \qquad (4.1)$$

where V_b is bias rate, V_w wash water rate, V_{wp} water flow rate to the froth product, V_{wf} water flow rate in the feed, and R_w is water recovery. It was determined that V_b was

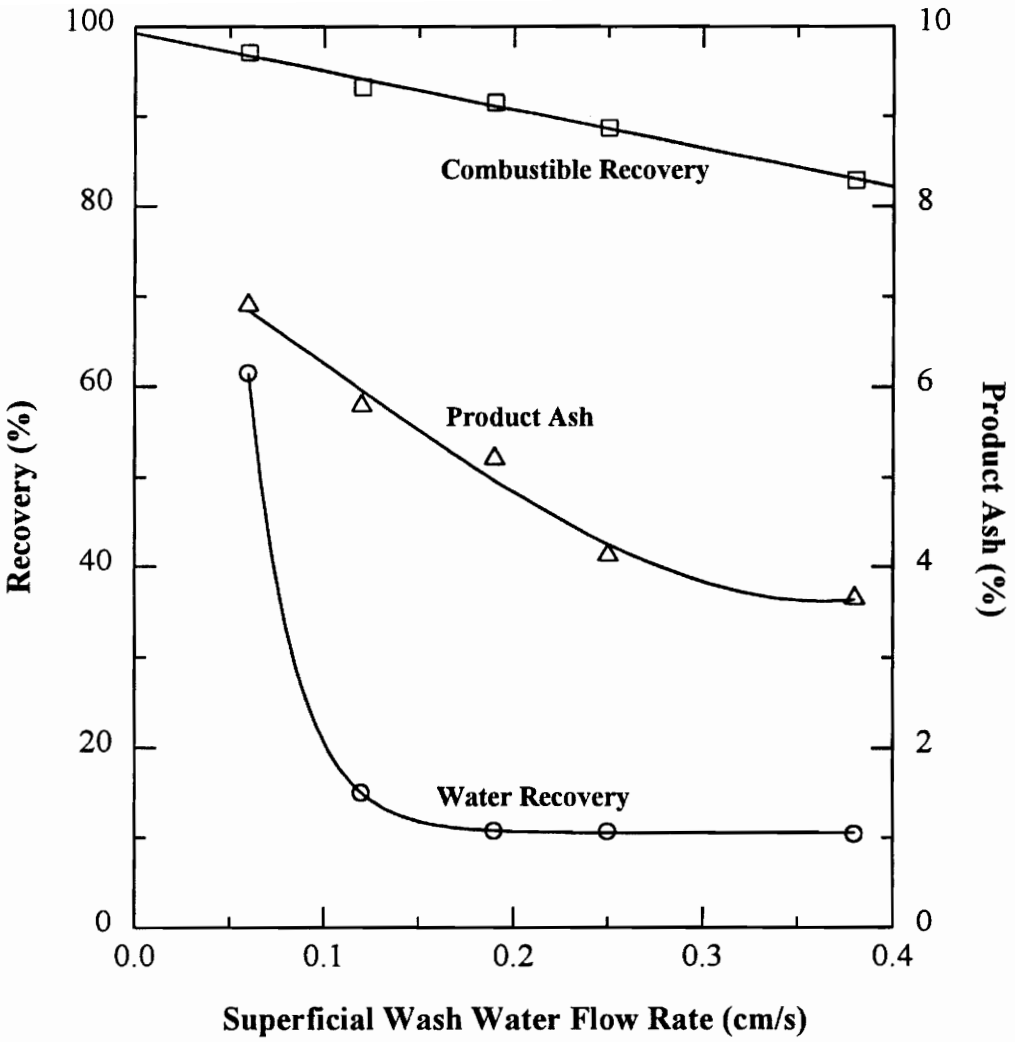

Figure 4.2 **The effect of wash water flow rate on froth stability and flotation. Froth dosage was kept constant in lb/ton of feed solids.**

-0.072 cm/s at V_w=0.06 cm/s and 0.079 cm/s at V_w=0.12 cm/s. The zero bias rate was achieved at V_w=0.09~0.10 cm/s. However, the product ash was minimized by V_b>0.2 cm/s or V_w>0.25 cm/s. Apparently, bias rate just above zero did not guarantee the achievement of the best product grade. In fact, Yianatos et al. [26] concluded from the study of industrial columns by the impulse and response tracer technique that bias rate of 0.3~0.4 cm/s is required to prevent feed entrainment into the froth.

Combustible recovery decreased over the entire range of wash water rate. This may result from increasingly larger bubbles observed in tests as the frother concentration in the collection zone of the column decreased with increasing the wash water flow rate. Since the objective of the addition of wash water is to achieve maximum ash rejection with minimum loss of combustible recovery, the most appropriate value of V_w should be around 0.30 cm/s or 18 cm/min, which is in excellent agreement with the previous study [22]. Further studies on the froth profile, which will be discussed later, confirmed this conclusion.

When the frother concentration in the column pulp was kept relatively constant by adjusting the frother addition to the column as wash water rate increased, the froth behavior and flotation performance were considerably different from Figure 4.2, as shown in Figure 4.3. The product ash was almost independent of wash water flow rate, which is the same conclusion as that arrived at from the study on sulphide minerals [20]. The combustible recovery changed with wash water flow rate in a way very similar to

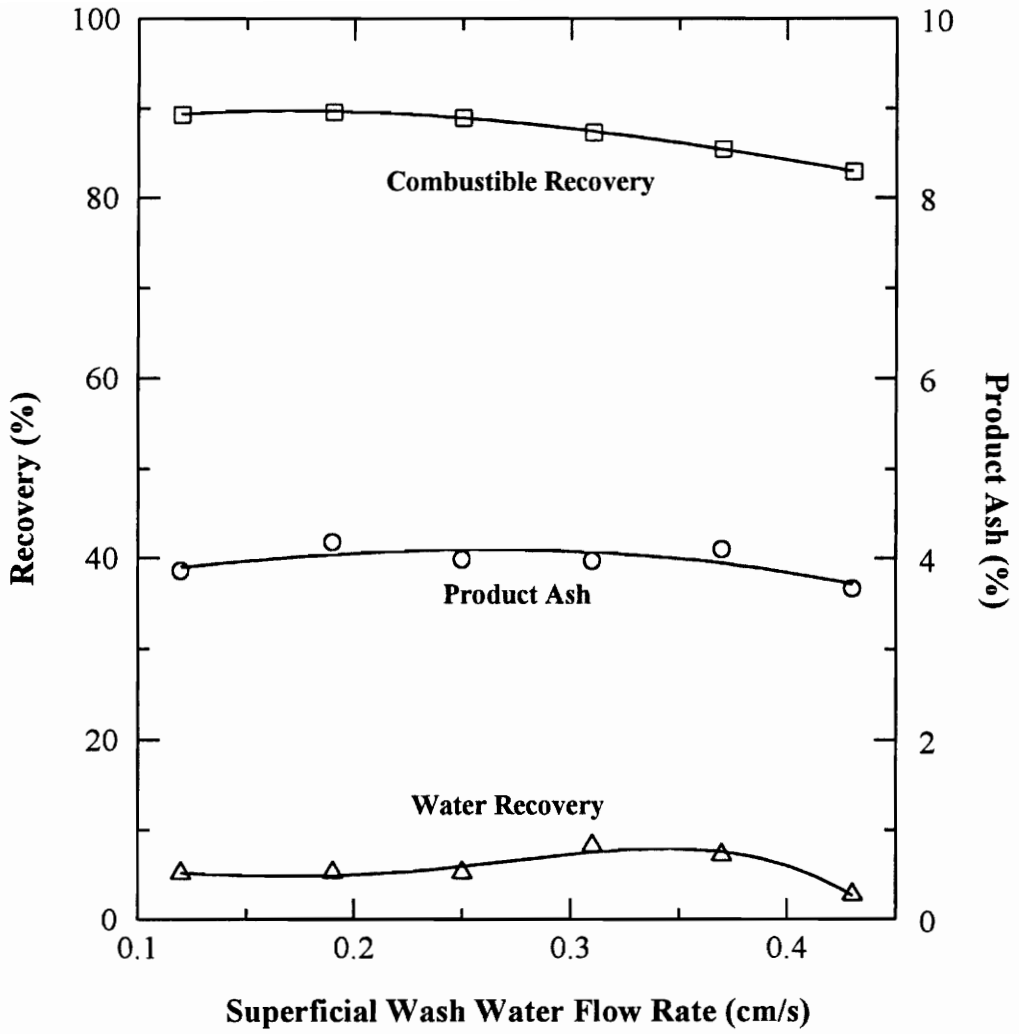

Figure 4.3 **The effect of wash water flow rate on froth stability and flotation performance. The frother concentration in column pulp was kept constant.**

that shown in Figure 4.2 except that the variation was less pronounced in this case. The change in water recovery in Figure 4.3 was relatively small compared to that exhibited in Figure 4.2. The amount of water entrained in the froth product was increased with increasing wash water flow rate, indicating increased froth stability. Bias rate was consistently positive at all wash water flow rates with its value ranging from 0.125 cm/s to 0.413 cm/s.

Based on the results in Figures 4.2 and 4.3, it can be reasonably concluded that the inconsistence in the literature on effects of wash water on separation performance may be associated with the way that frother dosage was regulated. It can be speculated that under conditions where bubbles are not heavily loaded and gangue particles are pure and completely hydrophilic, froth cleaning action may be insensitive to wash water flow rate. However, in cases where significant quantities of gangue particles are entrapped into the froth or gangue particles are moderately hydrophobic, wash water flow rate or bias rate may have to be maintained at a certain level in order to achieve optimum product grade.

4.4.1.3 *Bubble size (D_b)*

There is very little information available in literature on the effect of bubble size on froth stability although evidence has been shown that smaller bubbles can improve the recovery and selectivity in fine particle flotation [27-29]. Bubble size is generally

controlled by adjustment of frother dosage [23, 30] which, however, could introduce changes in flotation chemistry as well. A specially constructed column was therefore employed in which bubble size was varied simply by altering the bubble generator, i.e., fritted gas spargers of different pore sizes, while the frother dosage was kept constant. The average bubble size was calculated from the air hold-up which was directly measured using a differential manometer [31, 32]. It is believed that the bubble size thus determined may be slightly larger than that in the bubble generation circuit due to bubble coalescence in the pulp zone [22].

Figure 4.4 illustrates the importance of bubble size in determining froth stability and separation performance. The improvement in combustible recovery with decreasing bubble size is usually attributed to increased particle-bubble collision probability and bubble surface area which are directly proportional to flotation kinetics [33, 34]. It has also been shown [22, 35, 36] that flotation rate constant (k) is inversely proportional to D_b^3. The result in Figure 4.4 appears to be in general agreement with previous studies although the accurate degree of dependence of k on D_b can not be readily determined due to the limited range of D_b variation.

Figure 4.4 also shows that water recovery increased considerably with decreasing bubble size. This is because for a given gas flow rate, smaller bubbles led to more surface area entering the froth zone per unit time due to their higher specific surface area. Previous studies [5, 12, 37, 38] have explicitly demonstrated that the recovery of

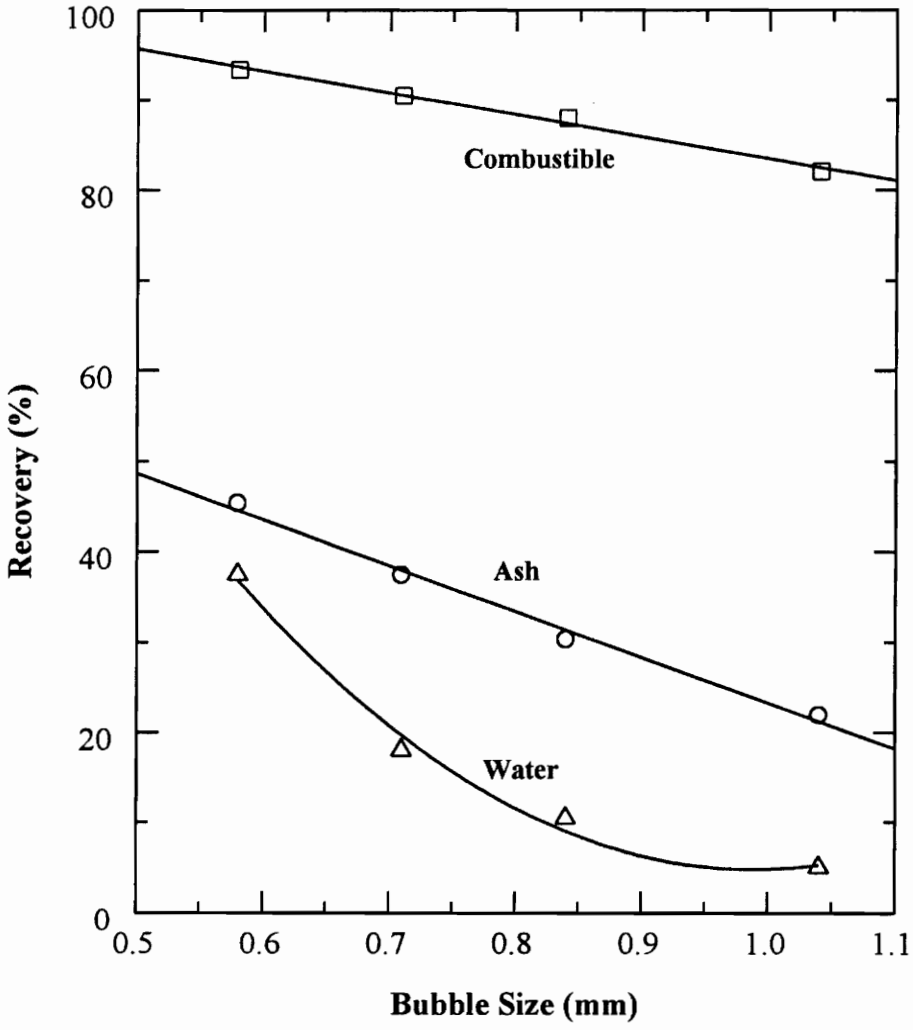

Figure 4.4 The effect of bubble size on froth stability and flotation performance.

hydrophilic particles was directly proportional to water recovery when water recovery was varied by manipulation of froth height, gas flow rate, froth removal rate, etc. This was confirmed in the present study and will be discussed in following sections. However, Figure 4.4 shows that when bubble size was a variable, the ash recovery did not exhibit a linear dependence on water recovery, as indicated by different degree of dependence of water recovery and ash recovery on bubble size. Decrease in bubble size increased water recovery more significantly than ash recovery, which suggests that decrease in bubble size may reduce the degree of entrainment of particles. In fact, Szatkowski [39] observed an increased degree of ash rejection with smaller bubbles as a result of increased bubble coalescence. This finding is of practical importance for design and optimization of a flotation process. Flotation kinetics can be increased by either increasing the gas flow rate or decreasing the bubble size, as described in Equation (4.2),

$$k = \frac{3P}{2D_b} V_g \tag{4.2}$$

where p is the probability of collection of particles and can be expressed by Equation (4.3) in most cases [22, 35, 36],

$$P = (\frac{3}{2} + \frac{4Re^{0.72}}{15})(\frac{D_p^{\,2}}{D_b^{\,2}})P_a(1 - P_d) \tag{4.3}$$

where Re is Reynolds Number, D_p particle size, P_a the probability of adhesion, and p_d is the probability of detachment. The present result suggests that decreasing bubble size

should be preferred to increasing gas flow rate for the achievement of higher recovery and better hydrometallurgical performance of flotation. There are several possible mechanisms for smaller bubbles to produce better separation.

Monsalve and Schechter [40] theoretically and experimentally revealed that the rate of froth destabilization depends on both the initial bubble surface area and the bubble size distribution. They obtained an empirical equation to describe the change in the dimensionless bubble surface area as a function of time (t):

$$a(t) = \frac{A(t)}{A_o(t)} = k_G \exp(-\frac{t}{\tau_G}) + k_D \exp(-\frac{t}{\tau_D}) \qquad (4.4)$$

where a is the relative bubble surface area, A(t) bubble surface area at time t, $A_o(t)$ bubble surface area at time zero, k_G fractional area decrease due to gravity drainage, k_d fractional area decrease due to diffusion and collapse, τ_D time constant for the diffusional process, and τ_G is time constant for the gravitational process. This bi-linear exponential function suggests that although smaller bubbles may entrain more slurry into the froth at the pulp-froth interface, substantially faster kinetics of film drainage and bubble coalescence associated with them may create a more favorable environment for froth cleaning action to occur.

Szatkowski [39] recognized that fine bubbles will be more heavily covered with coal particles than coarse bubbles since smaller bubbles tend to collect coal particles more rapidly than do larger bubbles, as indicated in Equation (4.2). The ratio of coal to ash in the liquid film that surrounds each fine bubble, therefore, would be higher than

that for the larger bubbles that are less completely covered. As a result, the ash content of the froth relative to coal can be expected to be lower.

The benefit of the use of smaller bubbles can also be understood from the bubble wake theory proposed by Smith and Warren [41]. The amount of slurry transferred into a froth in the wake behind an ascending bubble will decrease with decreasing bubble size due to reduced Reynolds Number (Re). Clift et al. [42] concluded that the wake will disappear when $Re < 20$. Luttrell et al. [29] demonstrated in frothless flotation using a column-type flotation cell that bubbles less than approximately 300 μm in diameter carried no wake. Their results also showed that bubbles larger than 300 μm exhibited a substantial wake which increased remarkably with increasing bubble size.

4.4.1.4 *Froth height (H_f)*

Froth height has been realized to be an important factor in flotation processes since the earliest days of its application. Taggart [43] observed the effects of froth depth in different types of flotation machines. Lawver and Barbarowicz [44] applied the scheme of regulating pulp depth to automatic control of flotation circuits. Paakkinen and Cooper [45] reported in a survey that half of the 34 concentrators examined employed pulp level and froth depth in the control strategy. Nevertheless, the importance of this parameter is often overlooked in practice, especially in column flotation [24], mainly due to the lack of relevant knowledge.

It is known that for effective operation of a flotation column, the pulp-froth interface must be maintained at a certain level. If the level is too high, there will be an insufficiently long froth zone, resulting in poor concentrate grade; if the level is too low, pulp phase is shortened, consequently giving rise to a reduced recovery due to decreased residence time of particles in the pulp. Finch et al. [20] suggested that for a typical 10 m collection zone height of industrial columns, a 50 cm change in level means only about 5% change in collection zone volume and, therefore, little impact on recovery should be expected. Espinosa-Gomez et al. [46] concluded that the change in level had a marginal effect on flotation recovery, especially when the column was operating near its maximum carrying capacity. Ynchausti et al. [47] experimentally demonstrated that deeper froth significantly enhanced fluorite grades without hindering recovery. Finch et al. [20] postulated that superior selectivity between particles differing in hydrophobicity exhibited by columns compared to mechanical cells may be related to froth depth.

The present study was carried out to reveal the influence of froth height on the stability of froth which was correlated with separation performance. Experiments were performed with four different bubble generators which produced bubbles of differing sizes. Results were similar in all cases and only those obtained with the finest generator were plotted in Figure 4.5 for the purpose of clarity.

Figure 4.5 indicates that there is apparently a linear dependence of combustible recovery, ash recovery, and water recovery on the froth height and the degree of

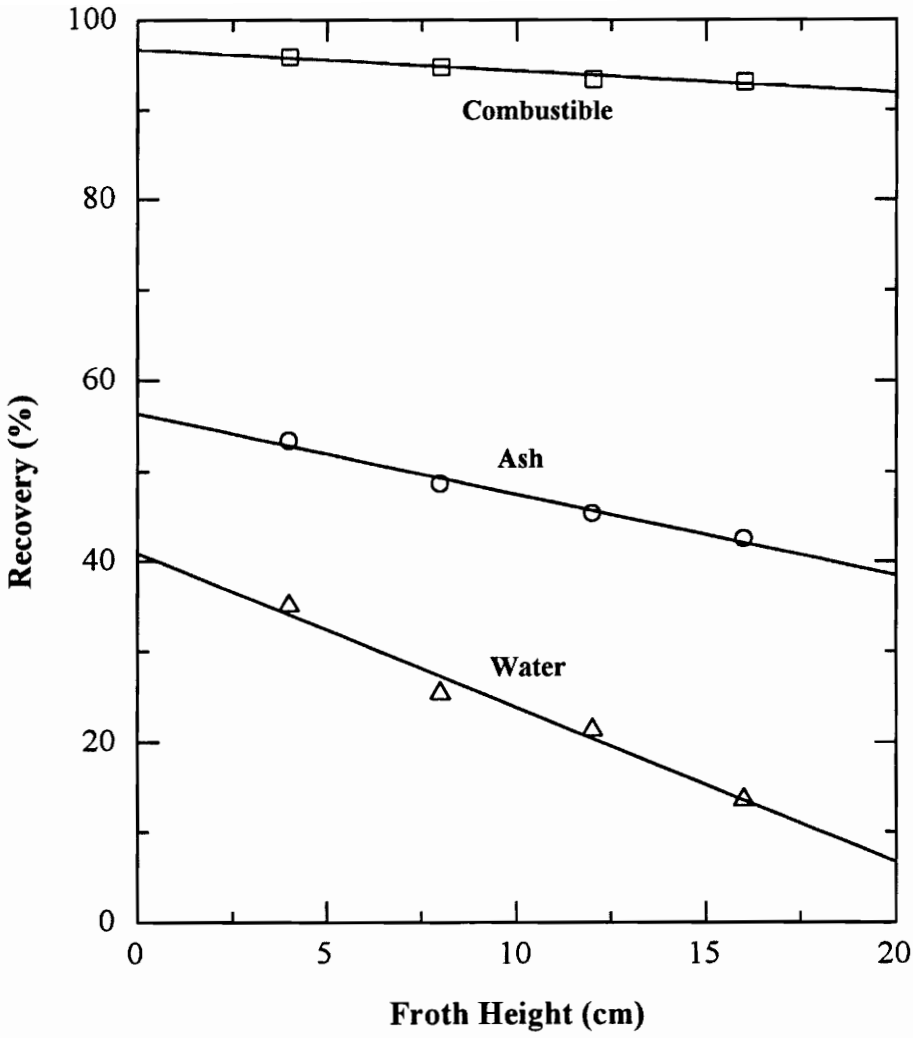

Figure 4.5 The effect of froth height on froth stability and flotation performance.

dependence is different from each other. The linear correlations and negative slopes are in good agreement with the results obtained in previous studies with pyrite [12] and with galena [2, 3] in mechanic batch flotation cells. Feteris et al. [2] derived a mathematical equation which explicitly showed that the overall flotation rate constant (k) is directly proportional to the probability (P_f) that a particle-bubble aggregate survives the cleaning action of the froth. They also found a linear relationship between P_f and the depth of froth phase.

Bisshop and White [5] have shown that the drainage of hydrophilic particles from the froth back to the pulp is dependent on the froth residence time. The residence time of bubbles and particles attached in froth is found by Moys [48] to be directly proportional to the froth height. Deeper froth enables liquid and particles to maintain longer times and, therefore, more chances to drain from the bubble surface and drop back to the collection zone. In each coalescence, more hydrophobic particles will be preferentially reattached to new bubbles. The fact that water recovery and ash recovery decreased more significantly than combustible recovery with increasing froth height is intimately associated with their different recovery mechanisms. While water and ash material reported to the concentrate mainly due to entrainment, hydrophobic coal particles were recovered essentially by attachment to bubble surface. Therefore, the decrease in water recovery and ash recovery with increasing froth height is directly caused by froth destabilization which reduces the entrainment of feed pulp, whereas, the

major mechanism for the reduced combustible recovery is the decrease in bubble surface area in the froth due to bubble coalescence in addition to the slight decrease in residence time of particles in the pulp zone.

The decrease in froth stability with increasing froth height is the consequence of two processes occurring in the froth phase:

1. The slow diffusion of gas from small bubbles into larger ones. The driving force for this diffusion is the high Laplace capillary pressure ($2\gamma/r$) within the smaller bubbles [49].
2. The thinning by drainage and, ultimately, the rupture of the liquid lamellae separating the bubbles [50].

In initial stages of film drainage where relatively thick lamellar films exist between gas bubbles, the drainage of films occurs under gravitational forces. Once the films have thinned to a thickness of a few hundred nanometers, gravity effects become negligible and thinning is predominately caused by capillary suction into the Plateau borders. When two sides of a film are in sufficiently close proximity, interfacial interactions involving the dispersion, electrostatic, and hydrophobic forces begin to play an important role. Film drainage and thinning constantly reduces hydraulic entrainment of hydrophilic particles but will not affect the recovery of hydrophobic particles attached on bubble surface until the film ruptures and bubbles coalesce.

The difference in slopes for three lines in Figure 4.5 is of particular significance

since it demonstrates the cleaning action in the froth. The behavior of floating species in the froth can be characterized by the froth transfer coefficient, a first-order constant. Laplante et al. [3] found that this coefficient decreased with increasing froth depth. Ross [51] developed a plug-flow model that describes the behavior of an equilibrium flotation froth, i.e., a froth from which no concentrate is removed. The model indicates that the concentration of weakly hydrophobic particles decreases with increasing froth height, presumably due to displacement by more hydrophobic particles on the bubble surface during coalescence in addition to the drainage of the slurry. It was assumed that the probability of displacement of a particle is inversely proportional to its hydrophobicity, which can be substantiated by the results of sulfide flotation performed by Moys [52]. Figure 4.5 shows that recovery of ash-bearing particles decreased more significantly with increasing froth height than that of combustible material. This provides further evidence that more hydrophobic particles will be preferentially attached to bubbles if particles are subjected to repeated detachment/reattachment events occurring in the froth due to coalescence that makes less bubble surface available.

It should be pointed out that experiments with bubbles larger than 1 mm in diameter showed only marginal improvement in selectivity with increasing froth depth, which may be responsible for the fact that thin froth is usually used in conventional flotation cells as well as some columns [53, 54] in which bubbles are believed to be 1-2 mm in diameter.

4.4.2 Effects of coal particles on froth stability

4.4.2.1 *Solids concentration*

Effects of solid particles on froth stability can be investigated as a function of feed flow rate. However, the adjustment in feed flow rate will inevitably cause variation in reagent concentration in the column. This disadvantage could be essentially avoided if solid concentration in the feed is changed during tests while feed flow rate is maintained at a constant value.

Figure 4.6 shows the effects of 10 μm coal particles on froth stability and flotation results as a function of percent solids in the feed of up to 5%, above which froth was almost destroyed. As can be seen, water recovery consistently decreased with increasing solids concentration, indicating that the coal particles destabilized the froth. When solids concentration in the feed increased from 0.025% to 5% (solids concentration in the cell varied correspondingly from 0.1 g/l to 20.0 g/l), the water recovery drastically decreased from 65% to 3.5%. It is thus believed that hydrophobic fine particles can destabilize froth by accelerating the coalescence of bubbles. The froth-destabilizing effect of fine hydrophobic particles may also be related to the consumption of frother in the column due to its adsorption on solids, as suggested by the increase in bubble size.

The larger bubble size at higher solids concentration could increase the retention time of solid particles due to decreased gas hold-up in the pulp, which should have

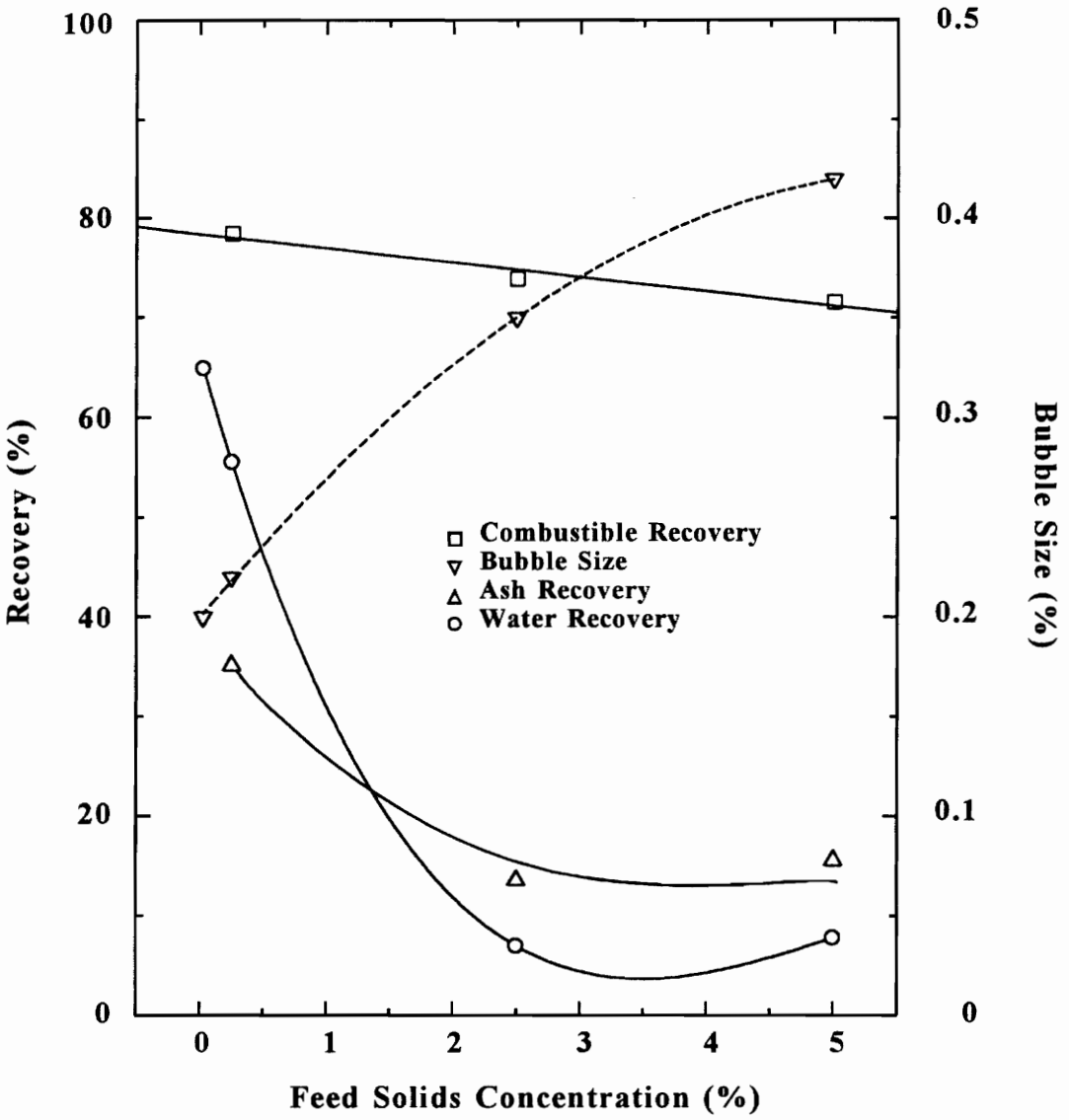

Figure 4.6 The impact of 10 μm coal particles on froth stability, bubble size and flotation as a function of feed solids concentration

increased combustible recovery. However, decreases in the flotation rate constant caused by the larger bubble size and poor froth stability apparently offset the effect of increased retention time and lead to a slight decrease in combustible recovery as observed in Figure 4.6. The considerable decrease in ash recovery with increasing feed solids concentration is associated with more substantial froth cleaning action at higher feed solids concentration. Szatkowski [39] reported that higher coal concentrations in the pulp resulted in higher ash content entering the froth. He postulated that this can be ascribed to more vigorous coalescence at the bottom of a froth of less heavily loaded bubbles obtained at lower coal concentrations in the pulp. However, bubble coalescence and film drainage facilitated by an increased amount of hydrophobic coal at higher solids concentration along the froth height could apparently offset this effect and produce higher ash rejection eventually.

In order to investigate the role of particle size in determining froth stability, -100 mesh coal samples were also used in flotation tests and the results are shown in Figures 4.7 and 4.8 for different solids concentration ranges. A linear relationship exists in the semi-log scale between water recovery and solids concentration up to 5% and can be expressed as:

$$R_w = -4.74 \log P_s + 12.76 \qquad (P_s \leq 5\%) \tag{4.5}$$

Where R_w is water recovery and P_s is the solids percentage in feed.

Apparently, -100 mesh coal particles still destabilized the froth at relatively low

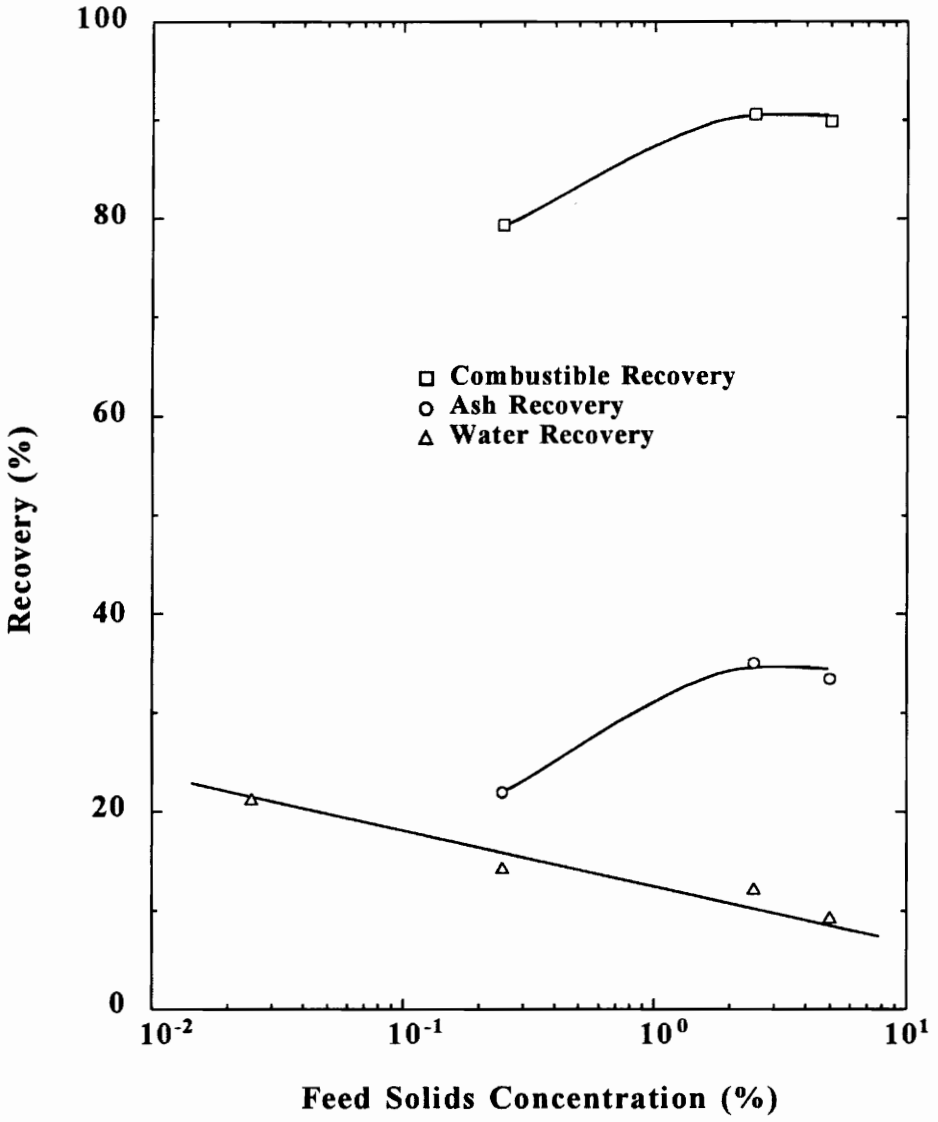

Figure 4.7 **The impact of -100 mesh coal particles on froth stability and flotation as a function of feed solids concentration from 0.025 to 5%.**

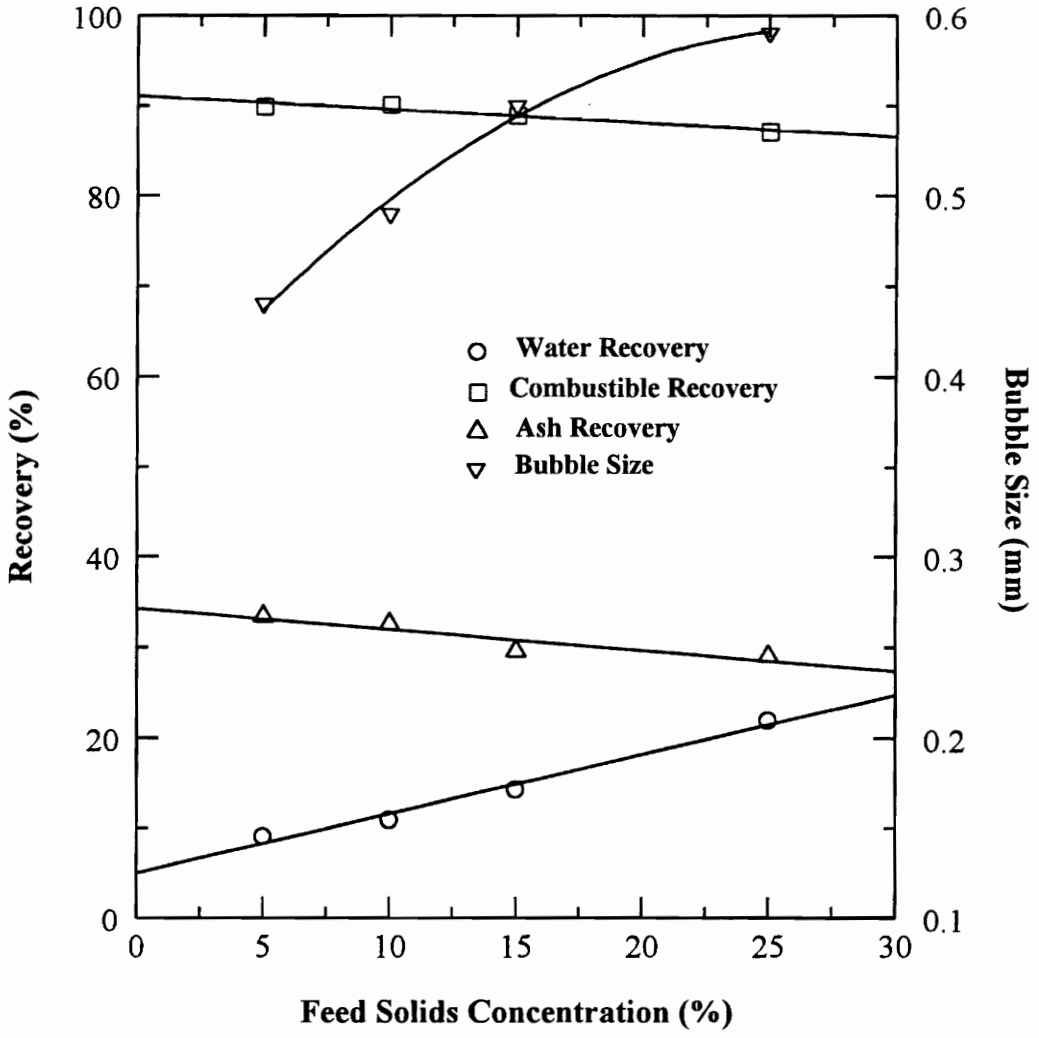

Figure 4.8 **The impact of -100 mesh coal particles on froth stability and flotation as a function of feed solids concentration from 5 to 25%.**

solids concentrations. Data on combustible and ash recoveries were not available at very low solids concentrations due to insufficient quantity of particles present in slurry. When solid percentage in the feed increased from 5 to 25 (corresponding solids concentration in the cell was increased from 20 g/l to 100 g/l), water recovery consistently increased. It is interesting to point out that over this range of solids concentration, bubbles became increasingly larger due to the adsorption of frother on particles, which would reduce water recovery if no other factors affected the froth stability. The result explicitly suggests that froth can be stabilized by coarse hydrophobic particles at relatively high solids concentration. The decrease in combustible and ash recoveries is believed to arise from a lower collection probability of particles associated with larger bubbles in the pulp. The best fit line for the R_w vs. P_s curve in Figure 4.8 is,

$$R_w = 0.66P_s + 5.03 \qquad (P_s \geq 5\%) \tag{4.6}$$

4.4.4.2 *Particle size*

Figure 4.9 demonstrates the effect of particle size on froth stability at a constant particle concentration of 15 g/l in the column. Four feed samples of 100-200, 200-270, 270-400 and -400 mesh were obtained by wet-screening hammer-milled products, and two other samples were prepared by 2.5 and 5 minute ball-mill grinding which generated particles of a mean size of 15 and 10 μm, respectively.

All three recoveries shown in Figure 4.9 maintained relatively constant for

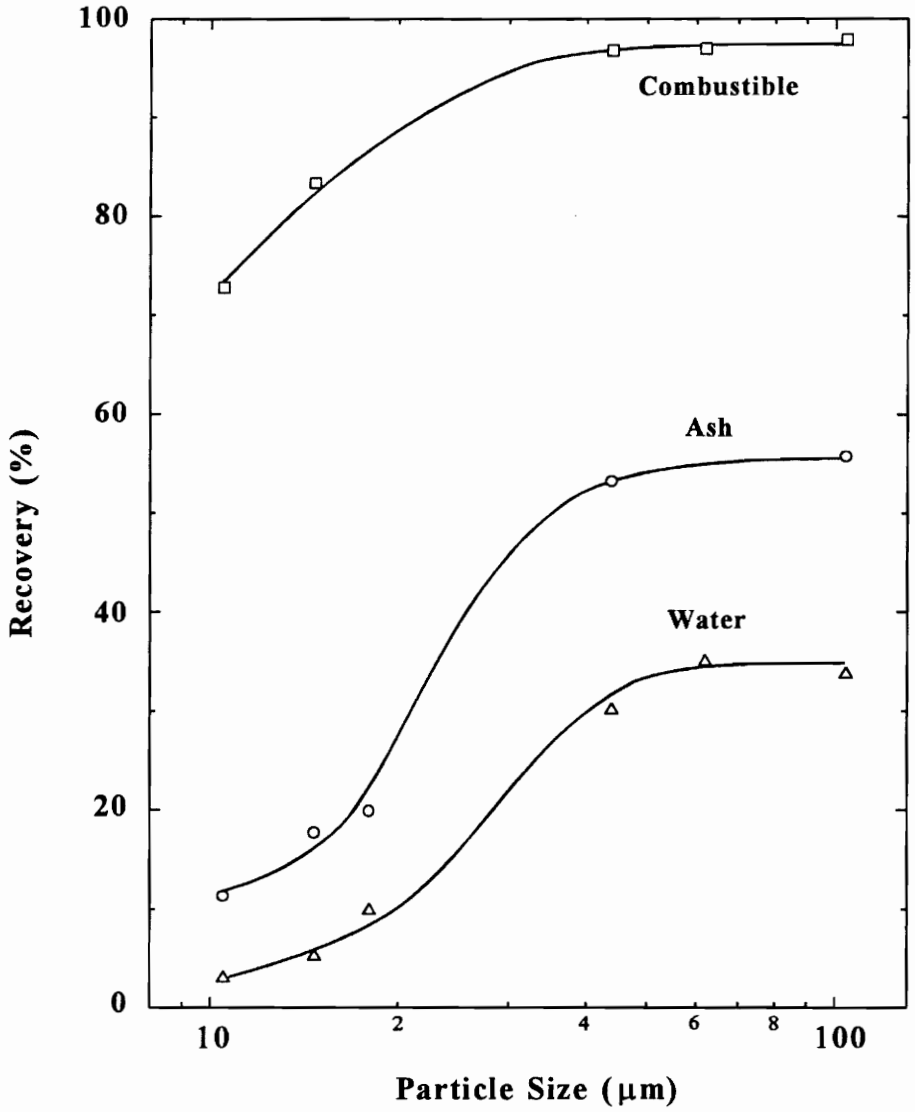

Figure 4.9 The influence of particle size on froth stability and flotation at constant solids concentration.

particles in 270-400 mesh fraction and larger. Coal particles in -400 mesh and finer decreased recoveries substantially. Finer coal particles exhibited a more substantial froth destabilizing influence, which is consistent with previous results obtained with methylated quartz and galena [55] and rutile [7]. Since water recovery was around 22% in the absence of solids, Figure 4.9 indicates that coal particles smaller than 30 μm or so could considerably destabilize the froth. In addition, very fine particles can adsorb a greater proportion of frother in the column because of the enormous surface area and therefore, considerably reduce the frother concentration at the air-water interface.

The above results are in good agreement with Lovell's conclusion [30] derived from the work on phosphate flotation that froth can be destabilized by hydrophobic minerals at lower concentrations and stabilized at higher concentrations. Increased froth stability at higher solids concentration is generally attributed to increased surface viscosity of liquid films which hinders film drainage. However, this theory obviously fails to explain the observation that fine particles in higher concentrations showed a more significant froth destabilizing effect.

According to the protruding particle theory proposed by Hemmings [7], the condition that is required to produce a destructive compressive stress reaction in the liquid lamella is,

$$\cos\theta < \frac{\delta}{D_p} < \cos\frac{\theta}{2} \tag{4.7}$$

Where θ is the contact angle, δ lamellae thickness, and D_p is the diameter of particle or

floccule. The condition that is needed to produce a supportive tensile stress reaction is,

$$0 < \frac{\delta}{D_p} < \cos\theta \tag{4.8}$$

However, if $\theta > 90°$, particles always tend to destabilize the froth. From the above criteria, it is obvious that small particles are more likely to destabilize the froth and big particles tend to satisfy the requirement for a stabilizing tensile stress. Solids concentration is not directly considered in this theory but its effect on froth stability can be understood by taking into account its impact on the floccule size. In fact, Lovell [30] explained froth stabilization at high solids concentration as a result of increased particle size by agglomeration. The protruding theory also indicates that more hydrophobic particles are more likely to destabilize froth.

Using high speed cinematography, Dippenaar [55] established that a particle causes a film to rupture only when the two, three-phase boundary lines are forced to migrate to the same point on the particle and the liquid film is thinned to half the diameter of the particle or less. This conclusion also indicates that smaller particles destabilize liquid films more readily than bigger ones. Dippenaar's flotation tests [56] showed that 0.16 mg of 5 μm hydrophobic particles had the same froth breaking power as 18.8 mg of 54.5 μm particles.

Johansson and Pugh [57] studied effects of methylated quartz particles on the stability of froth. They reported that particles in 74-106 μm fraction generally increased froth stability. This effect reached a maximum at a relatively low hydrophobicity and

further increases in hydrophobicity exhibited negligible influence. For particles in the 26-44 μm fraction, those of moderate hydrophobicity (contact angle $\theta \approx$ 50-65°) showed substantial froth-stabilizing effect. Less hydrophobic particles did not have an influence on froth stability and more hydrophobic ones destabilized the froth. Mougdil and Gupta [58] observed similar behavior with phosphate fines. It is believed that the presence of smaller particles with moderate hydrophobicity at the interface of the Plateau border increased the rigidity and surface viscosity. More hydrophobic particles penetrated the gas/liquid interface and the capillary pressure accelerated liquid drainage. Particles with low hydrophobicity remained in bulk liquid and could not affect froth stability.

It is apparent from the above results and discussion that there are many factors determining the effects of solid particles on froth stability. They include particle size, hydrophobicity, concentration, shape, roughness, etc. More importantly, these factors affect froth stability interactively. Inconsistent observations and conclusions reported in literature may stem from different conditions various investigators employed in their studies.

4.4.3 Hydraulic Entrainment

One of the main mechanisms for the recovery of fine particles in flotation is hydraulic entrainment which is closely related to the froth stability. The establishment

of relationship between froth stability and particle recovery is of great importance for better understanding the contribution of entrainment in the recovery of both hydrophobic and hydrophilic particles. It is also necessary in the operation and design of columns to minimize the entrainment by optimizing operating parameters.

Flotation tests were conducted in which gas flow rate and froth height were changed to acquire different degrees of froth stability and particle separation. The combustible and ash recoveries are shown in Figure 4.10 as a function of water recovery. Apparently, there is a linear dependence of ash recovery and product ash content on water recovery. The fact that product ash decreases with decreasing water recovery clearly demonstrates the secondary cleaning action in the froth. As hydrophilic ash particles constantly drain with water and slightly hydrophobic middling particles preferentially detach from the bubble surface, hydrophobic coal particles are progressively concentrated in the froth, resulting in a better product grade.

The results shown in Figure 4.10 are not in complete agreement with those of Englebrecht and Woodburn [12] who demonstrated that not only was the recovery of hydrophilic species (silica) directly proportional to the water recovery but also the line crossed the origin based on continuous laboratory flotation tests with pyrite and silica. This may be due to the fact that they used an artificial mixture of finely ground silica and pyrite as feed in which hydrophilic silica particles were perfectly free of hydrophobic pyrite, while in the present study coal was pulverized to -100 mesh and minerals were

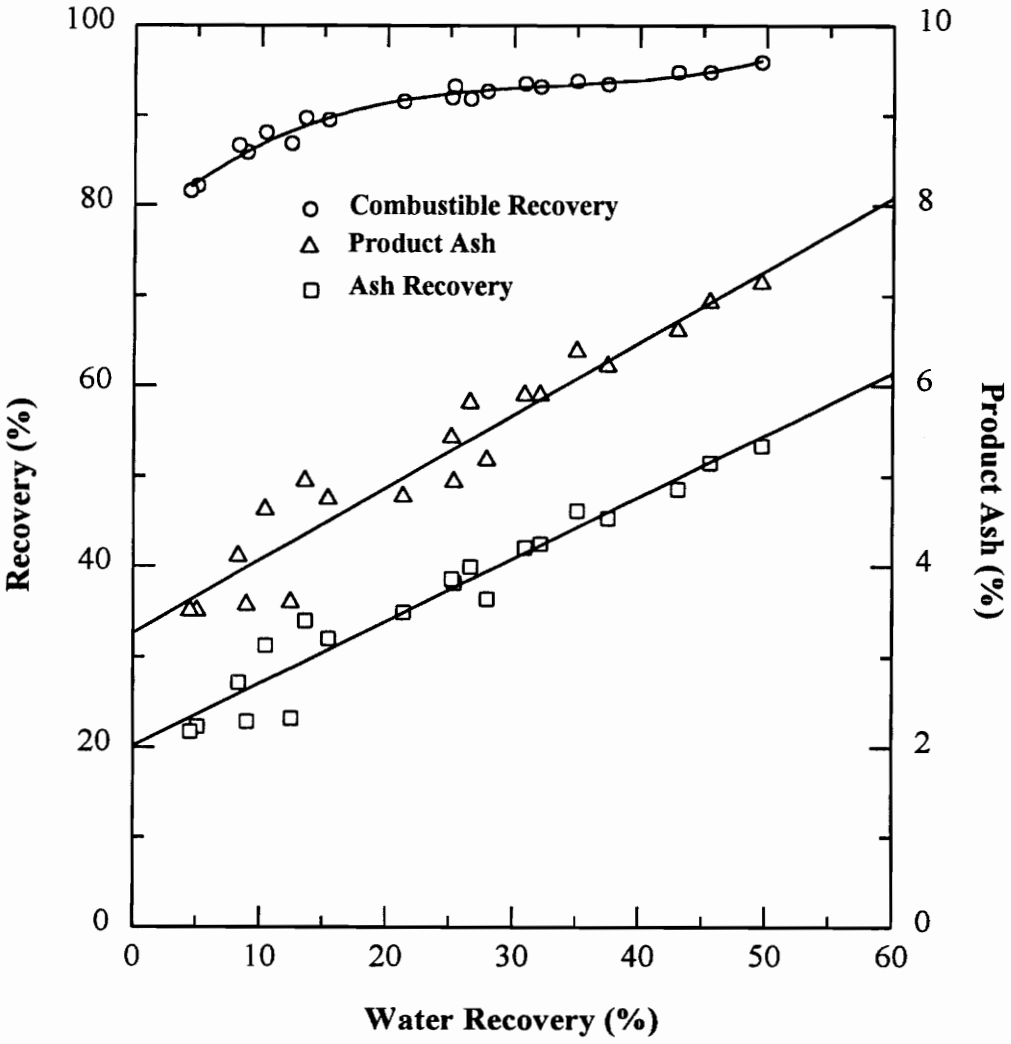

Figure 4.10 The dependence of combustible recovery, ash recovery and product ash on water recovery.

only incompletely liberated from coal matrices. The straight line in Figure 4.10 can be described by an equation of the form:

$$R_a = F_a + e_a R_w \tag{4.9}$$

Where R_a is ash recovery, R_w water recovery, e_a slope of the line or entrainment factor, and F_a is the intercept of the extrapolated line on the ash recovery axis.

The values of e_a and F_a should depend on the properties of feed (for example, size) and the chemical environment in the flotation column. For well-liberated or ultrafine hydrophilic particles, $F_a=0$ [12]. The e_a and F_a in Figure 4.10 were determined to be 0.68 and 20, suggesting that a 20% recovery of ash was accomplished by true flotation of composite particles. The establishment of this correlation is very helpful for automatic control of the flotation process since water recovery can be instantly determined by means of the on-line measurement of conductivity of the froth in a flotation column, while on-line determination of ash content is relatively difficult and inaccurate.

Combustible recovery exhibited a somewhat different and complex dependence on water recovery. Mathematical models describing their relationship that are available in literature can not be used to fit all the data satisfactorily. Vanangamudi and Rao [59] conducted coal flotation tests with a mechanical cell and reported similar results with the difference being that their data appeared to pass through the origin. Warren [38] carried out flotation tests of several minerals and coal in which water recovery was changed by

adjusting pulp level, rate of froth removal, height of cell lip, depth of froth removed, and surface area for froth formation. He proposed a model for the correlation between the recovery of hydrophobic particles and the weight of water recovered (or recovery of water R_w):

$$R_m = F_m + e_m W_{water} \tag{4.10}$$

Where R_m is recovery of hydrophobic particles, F_m intercept of the extrapolated line on the hydrophobic mineral recovery axis, e_m entrainment factor for hydrophobic mineral and W_{water} is the weight of water recovered. F_m was considered to be the relative contribution of true flotation and could also be determined by measuring the flotation recovery in the presence and absence of a collector. This linear model does not appear to fit the combustible recovery curve in Figure 4.10.

Kirjavainen [60] and Vanangamudi and Rao [59] suggested models of the following forms to characterize the entrainment mechanism:

$$R = 1 - \exp(-PR_w) \qquad (Kirjavainen) \tag{4.11}$$

$$R = R_\infty(1 - \exp(-aW_{water}^b)) \qquad (Vanangamudi\ and\ Rao) \tag{4.12}$$

Where R_w is recovery of water, R recovery of particles, R_∞ maximum recovery of particles that can be obtained practically, P specific entrainment factor, W_{water} weight of water recovered, and a and b are constants. These two models can not be used to describe the combustible recovery curve because when R_w or W_{water} is zero, R calculated from them is also zero, which apparently is different from the observation.

There is an obvious need for the establishment of a new model for the relationship between combustible recovery and water recovery. Figure 4.10 was replotted in a full log scale, as shown in Figure 4.11. It is quite obvious that two separate models are required to represent the change of combustible recovery versus water recovery. In the region of R_w between 0 and 0.18, the relationship can be best fitted by the equation:

$$\log(1 - R_c) = \log a + b \log(1 - R_w) \tag{4.13}$$

or:

$$R_c = 1 - a(1 - R_w)^b \tag{4.14}$$

where R_c is the combustible recovery and other variables are the same as designated above. When R_w=0, R_c=1-a, which can be considered as the contribution from true flotation. In the linear region for R_w between 0 and 0.18, the best fitting values for a and b are 0.218 and 4.683, respectively. This indicates that true flotation resulted in a combustible recovery of 78.2%. For the region with R_w ranging from 0.18 to 0.50, the respective values of a and b were determined to be 0.1183 and 1.446. The correlation coefficients are 0.938 and 0.934 in these two cases. When Equation (4.10) was used to correlate combustible recovery and water recovery in the second case, the best-fitting values for F_m and e_m were determined to be 0.887 and 0.139, respectively. Table 4.1 summarizes the values of R_c that were measured and predicted using different models for a given R_w. Apparently, true flotation is the predominant recovery mechanism in the present flotation tests. It should be noted, however, that the relative contribution of true

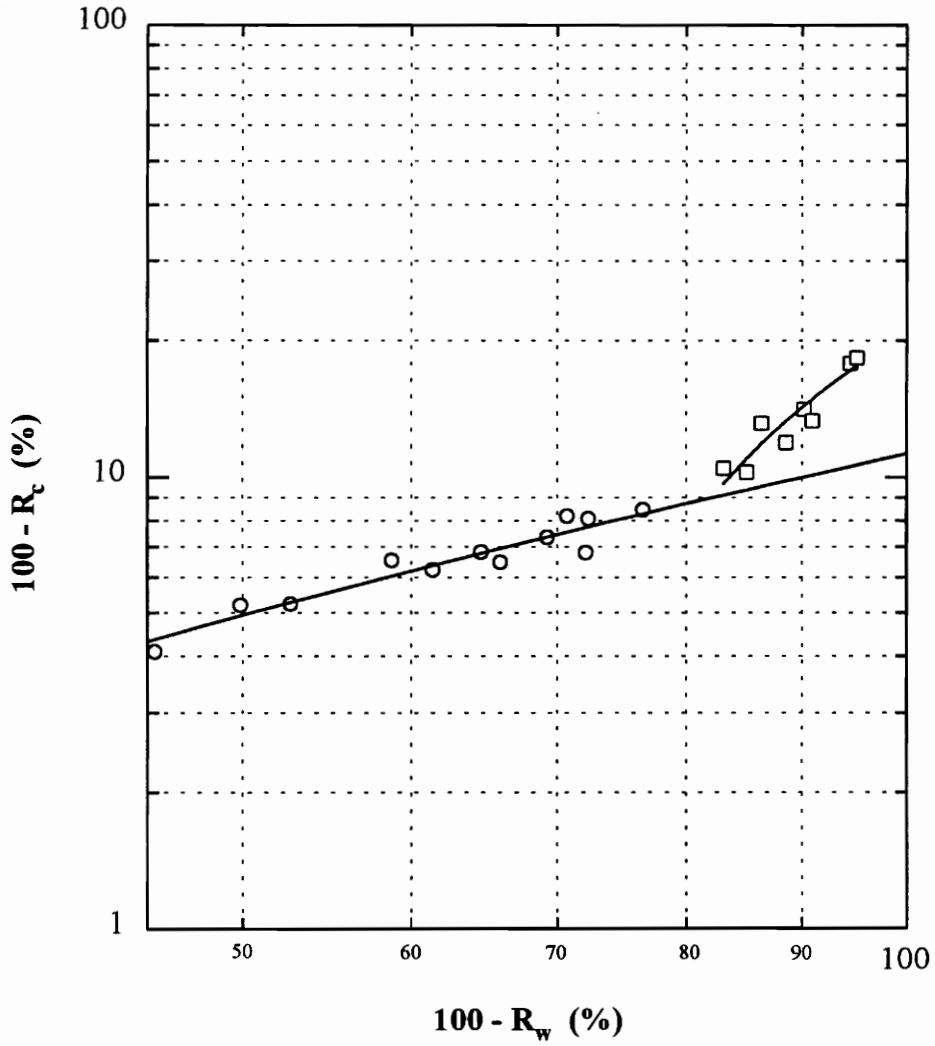

Figure 4.11 The relationship between combustible recovery and water recovery on the full log scale.

Table 4.1 Summarization of measured and predicted values for R_c at a given R_w.

R_w	R_c (measured)	R_c (predicted)*	R_c (predicted)**	R_c (Predicted)***
49.66	95.90	95.62	95.60	
45.56	94.81	95.09	95.03	
43.01	94.77	94.75	94.68	
37.47	93.46	94.00	93.91	
35.08	93.77	93.67	93.58	
32.15	93.18	93.24	93.17	
30.96	93.53	93.08	93.40	
27.93	92.64	92.63	92.58	
26.61	91.80	92.43	92.40	
25.35	93.20	92.25	92.22	
25.15	91.92	92.22	92.20	
21.34	91.54	91.64	91.66	
15.38	89.51			90.02
13.58	89.82			88.99
12.43	86.84			88.29
10.44	88.05			86.99
8.96	85.87			85.95
8.28	86.68			85.46
5.01	82.16			82.86
4.45	81.61			82.38

* $R_c = 1 - 0.1183\ (1 - R_w)^{1.446}$

** $R_c = 0.887 + 0.139R_w$

*** $R_c = 1 - 0.218(1 - R_w)^{4.683}$

flotation and entrainment to the overall recovery of hydrophobic particles is strongly dependent on the particle size. For example, Warren [38] has shown that for iron sulfide particles of intermediate size, entrainment played a small role in overall recovery and true flotation was predominant, which is in agreement with the present study. For ultrafine cassiterite particles the overall recovery was largely caused by entrainment and contribution from true flotation is small. Englebrecht and Woodburn [38] made similar observations with pyrite.

The fact that data in Figure 4.11 requires two distinct equations to describe can be understood by considering that coal contained a fast-floating hydrophobic component and a slow-floating component. Englebrecht and Woodburn [12] interpreted the behavior of pyrite flotation in a similar way. The dependence of recovery of the fast-floating coal component may be caused by the demand for sufficient surface area to load all fast-floating particles, which can be achieved with a relatively wet and stable froth. Figure 4.11 also shows that the entrainment factor for the fast-floating coal component is much larger than that for the slow-floating component. This is because strongly hydrophobic particles are floated more readily than weakly hydrophobic ones.

4.4.4 Froth Profile

4.4.4.1 *Effects of wash water flow rate.*

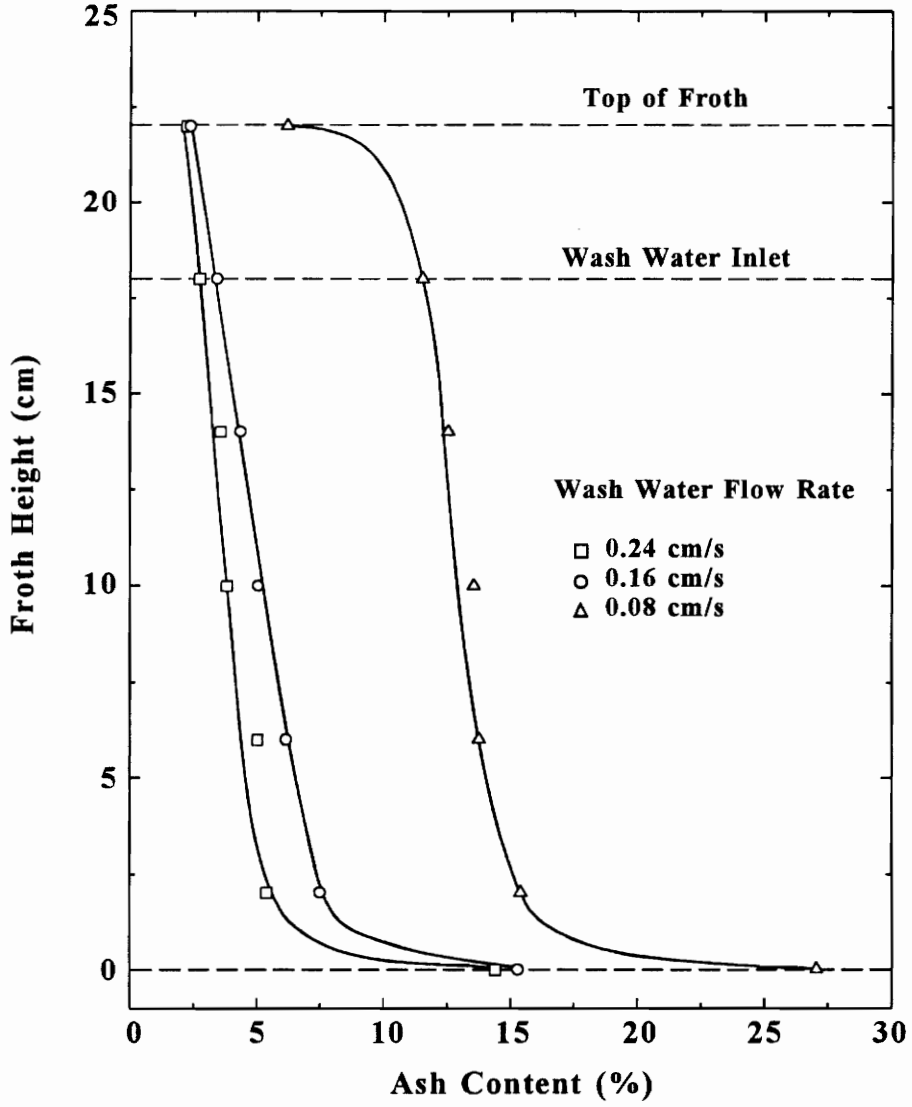

Figure 4.12 The froth profile at different superficial wash water flow rates.

Figure 4.12 shows the ash profiles in the froth established at different superficial wash water rates. As shown, an abrupt decrease in the particle ash content occurred just above the pulp-froth interface. This region may correspond to what is called the expanded bubble bed [20]. The upgrading in this region can be largely attributed to the efficient cleaning action of the wash water which prevents ash-bearing minerals from entering the base of the froth. Szatkowski [39] made observations of the pulp-froth interface with the aid of television equipment. He noticed a vigorous coalescence of air bubbles in the lowest layer of the froth and this process was accompanied with the drop of many particles. Finch et al. [20] suggested that the main reason for bubble coalescence in this region is the shock pressure waves generated by collisions against the interface of bubbles moving upward from the pulp. It is believed that under conditions of vigorous rearrangement of the froth structure less hydrophobic particles that are weakly attached to bubbles would be rejected first.

Above the expanded bubble bed, ash content decreased slowly with froth height up to the wash water inlet (which was located 18 cm above the pulp). This section of the froth column is referred to as the stabilized froth zone since the flow of wash water through this zone retards bubble coalescence and stabilizes the froth. Bubbles in this zone are relatively uniform in size and coalesce very slowly. Bubble coalescence in this region is mainly caused by collisions of larger bubbles which ascend faster in the froth.

The froth section above the wash water inlet is called the draining froth and is

similar to the froth typically found in conventional flotation cells. The cleaning action in this zone is a result of bubble coalescence resulting from film thinning and rupture. Hydrophilic particles that survived cleaning actions in the first two regions may have one last opportunity to drop from bubbles in this region. This effect was well exhibited at low wash water flow rates where cleaning action in this section was substantial.

The ash profiles obtained at higher wash water rates remained relatively constant from the pulp-froth interface to the top of the froth. At these higher addition rates, hydraulic entrainment is largely eliminated at the pulp-froth interface and, as a result, no significant additional upgrading would occur in the draining froth. These results indicate that superficial wash water rates greater than approximately 0.25 cm/s are sufficient to prevent entrainment of feed water into the froth product under the given experimental conditions. This result agrees very well with the previous conclusion drawn directly from the study of wash water rate.

Yianatos et al. [4] established the froth profile of two industrial molybdenite (MoS_2) cleaning flotation columns and also reported that rejection of entrained particles occurred very close to the pulp/froth interface. Further upgrading through the froth occurred when it was deeper than 1 m, which increased molybdenite grade by 10-15% absolute. Simultaneously, other less hydrophobic sulfides such as pyrite or chalcopyrite behaved like hydrophilic silica and were progressively rejected in the froth.

Szatkowski [39] measured froth ash profile in coal flotation performed in a

column-like mechanic cell and demonstrated that ash rejection was essentially done in the first 1-3 cm of the froth phase. Moys [52] conducted experiments with a complex sulfide mineral in a flotation cell using a deep froth phase. He found that the rejection of entrained gangue mainly occurred at the base of the froth. Cutting et al. [61] showed that gangue rejection in froth in continuous flotation of sulfides extended to 10 cm up from the interface. It is possible that for sulfide froths, rates of gangue drainage are lower than those for coal froths due to smaller particle size, higher viscosity, etc., and, therefore, higher froth is needed. The lack of wash water in mechanical flotation cells may also be responsible for the longer froth height required to reject entrained particles.

Froth selectivity is believed to be a result of competition of particles of differing hydrophobicity for decreased attachment sites on bubbles along the froth. Less hydrophobic minerals have higher detachment rate constants, and consequently can be preferentially rejected from the froth. Too shallow a froth may not exhibit selectivity because of increased mixing.

The effects of wash water addition rate on the solids content of the froth is shown in Figure 4.13. The data indicate that the solids content of the froth remained relatively constant in the stabilized froth zone, but then increased rapidly above the wash water inlet as a result of bubble coalescence and film drainage in the draining froth. The highest solids content obtained at each of the wash water rates was obtained at the top of the froth where maximum froth drainage and bubble coalescence had occurred. These

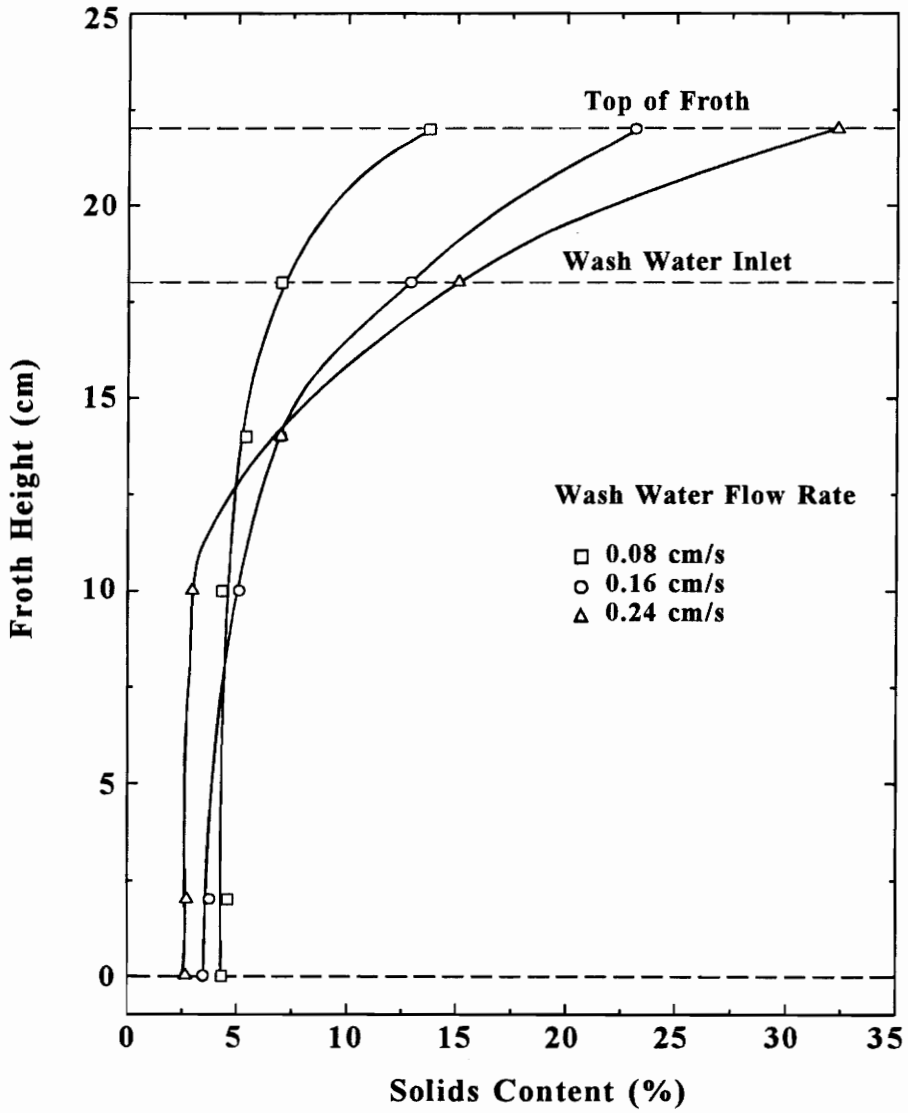

Figure 4.13 The froth solids profile at different superficial wash water flow rates.

results are in agreement with observation of Yianatos et al. [4]. It should also be noted that the solids content at the top of the froth increased with the wash water addition rate, i.e., the least stable froth was obtained at the highest wash water addition rates. These results suggest that the wash water may rinse away frother as well as unwanted mineral matter from the stabilized froth zone, generating very unstable froths above the wash water addition point.

4.4.4.2 *Effects of wash water addition point*

The results shown above suggest that the wash water addition point may be a key variable in column flotation. In order to examine this possibility, additional tests were conducted with the microbubble flotation column in which the wash water addition point was varied within the froth height. The aeration rate, feed rate, and wash water rate were held constant throughout these tests.

Figure 4.14 shows the effects of the wash water addition point on the bias factor and product solids content. The bias factor is defined as the fraction of wash water introduced to the column which flows through the stabilized froth into the flotation pulp. Since it is bias flow that prevents the entrainment of fine particles into the froth, a higher bias factor is generally associated with more efficient froth washing. As shown, the bias factor increased sharply as the wash water addition point was lowered deeper into the froth. This was a result of the increase in froth drainage rate (decrease in froth stability)

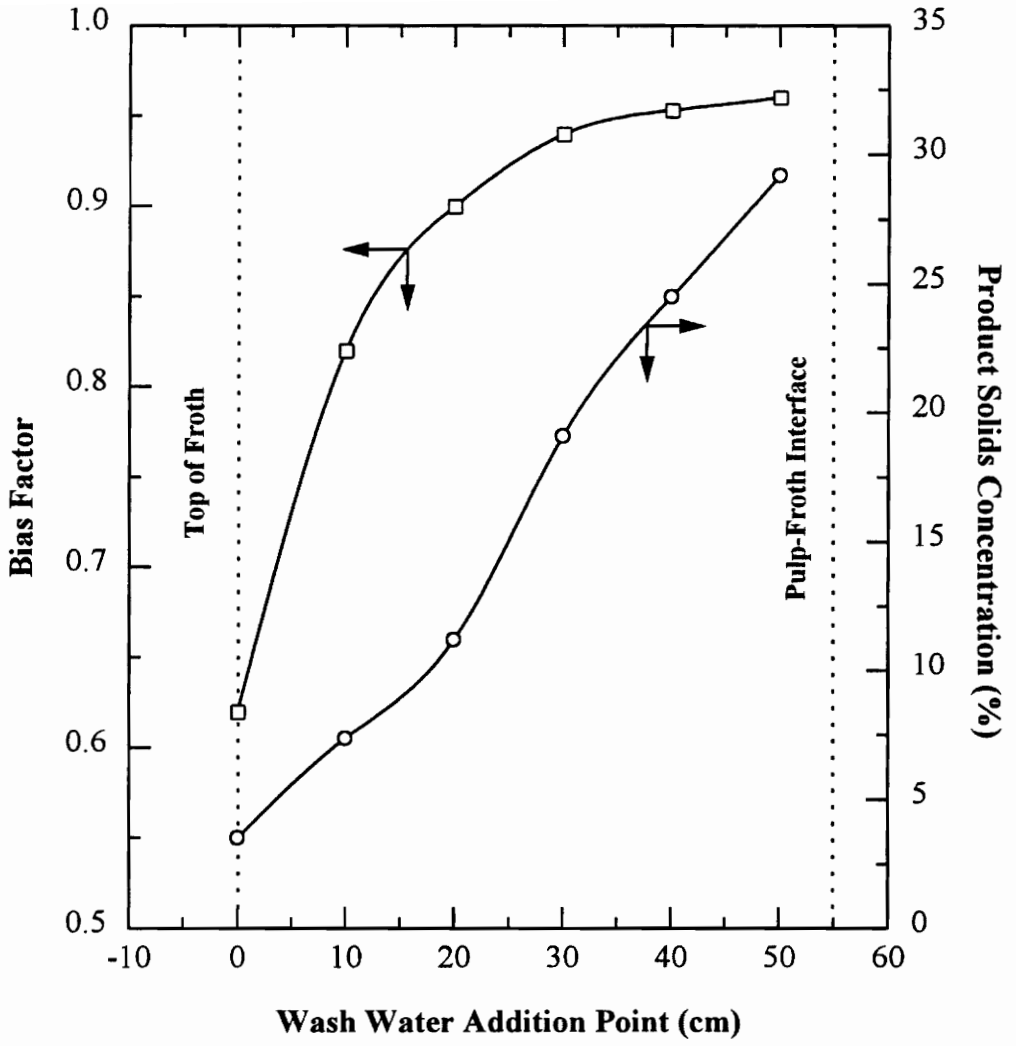

Figure 4.14 The influence of wash water addition point on the bias factor and product solids content.

above the wash water inlet as the addition point was lowered into the cell. In response to the increase in froth drainage rates, the solids content of the froth product increased sharply as the wash water addition point was lowered. As shown, the solids content of the froth product increased from approximately 5% to over 30% by moving the wash water addition point from the top of the froth to 50 cm lower.

The effects of wash water addition point on the product ash content is shown in Figure 4.15. The ash content decreased as the wash water addition point was lowered from the top of the froth into the cell. The decrease in ash content can be largely attributed to the improvement in froth washing associated with the increased bias factor. However, as the addition point was moved closer to the pulp-froth interface, the stabilized froth zone became too short to effectively flush away entrained fine particles. As a result, a slight increase in product ash content was observed when the wash water addition point was moved too close to the pulp-froth interface.

Up to this point, the test data indicates that column performance can be improved by lowering the wash water addition point, i.e., lower product ash and higher solids content. Unfortunately, the data shown in Figure 4.15 indicates that this improvement came at the expense of column capacity. As shown, a lower wash water addition point produced a sharp decrease in the mass rate of product reporting to the froth launder. The lower capacity was due to the decrease in the froth stability in the froth drainage zone which occurred as the wash water addition point approached the pulp-froth

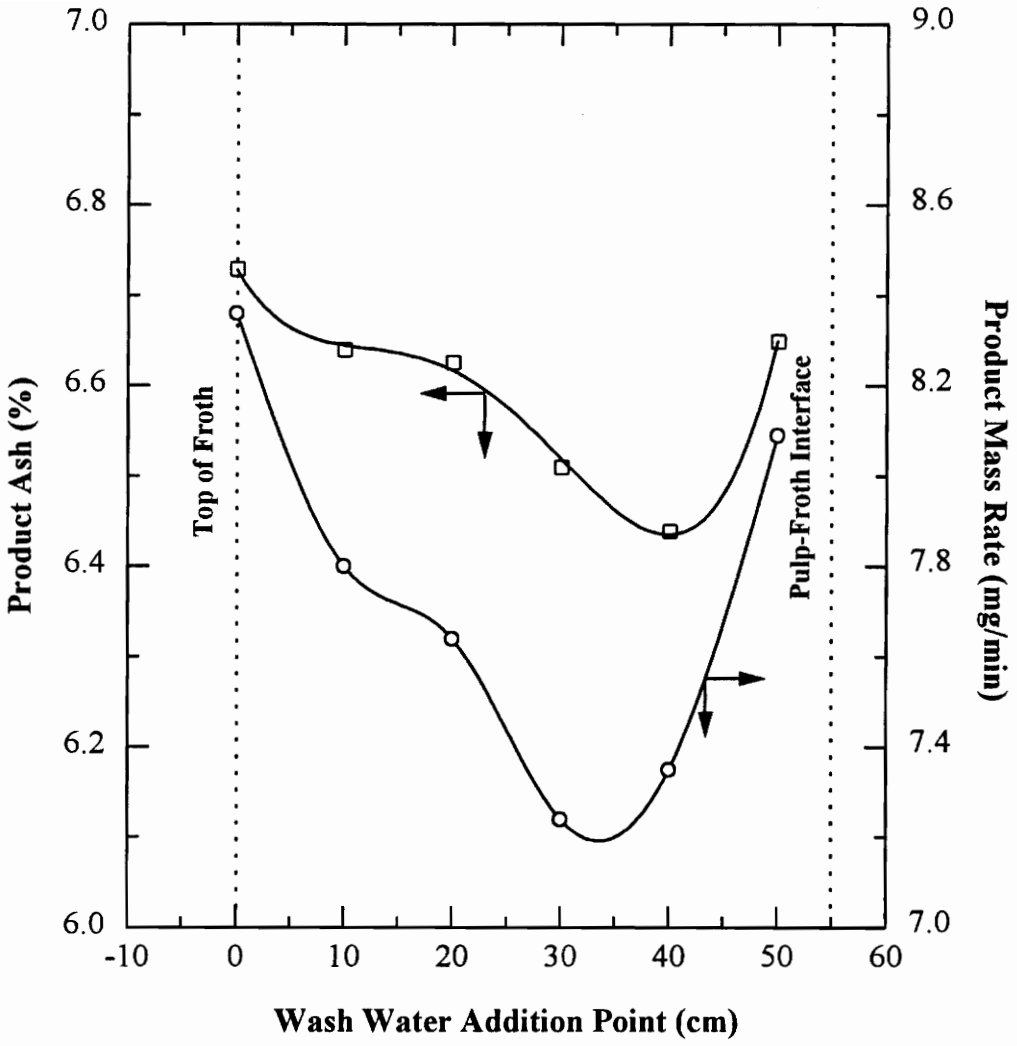

Figure 4.15 The impact of the wash water addition point on the product ash content and the product mass rate.

interface. Since wash water was not effective in generating flushing action when it was added at positions very close to the interface, less of the frother was washed from the froth phase back to the pulp. The increased frother concentration provided an increase in the froth stability which, in turn, allowed a higher mass rate.

4.5 Conclusions

1. Column flotation froth exhibits substantial cleaning action which is intimately related to froth stability. While attachment of hydrophobic particles to bubbles occurs in the pulp zone as the fundamental process in flotation, the separation of particle-bubble aggregates from the pulp is critical and is accomplished *via* the froth zone. Preferential reattachment of more hydrophobic particles to bubble surface in the froth as a result of froth drainage and bubble coalescence leads to the selective rejection of less hydrophobic and completely hydrophilic particles which enter the froth mainly by hydraulic entrainment. This process improves ash and pyrite rejection, thus producing higher product grade.
2. The use of smaller bubbles is strongly recommended for column flotation. Not only does it increase flotation kinetics as $k \propto 1/D_b^3$, but also improves flotation selectivity due to more vigorous coalescence, less significant wake, heavier particle loading on the surface associated with smaller bubbles.

3. Increase in gas flow rate promotes froth stability. However, it may reduce ash rejection more significantly than increase combustible recovery due to increased nonselective hydraulic entrainment. Therefore, the gas flow rate should be selected carefully to optimize the flotation process.

4. Froth should be made as deep as possible at the expense of a slight decrease in collection kinetics in the pulp to reduce entrainment and achieve better grade.

5. Froth stability varies significantly with increasing wash water flow rate if frother dosage is maintained constant in terms of lb/ton feed solids. However, if more frother is added into the pulp to keep its concentration in the column constant as wash water increases, froth stability will be relatively constant. Corresponding flotation performance shows a much greater dependence on wash water rate in the former case than in the latter.

6. The effect of coal particles on the froth stability depends on its size and concentration in the pulp. Micronized coal particles destabilize froth irrespective of their concentrations. The -100 mesh coal particles have a froth destabilizing effect at lower solids concentrations ($<$ 20 g/l in pulp phase of column) and a froth stabilizing effect at higher concentrations ($>$ 20 g/l in pulp phase of column).

7. For -100 mesh coal particles, water recovery decreases as a logarithmic function of solids concentration when it is lower than 20 g/l in the pulp phase (5% solids

in feed). For higher solids concentrations, water recovery increases linearly but combustible recovery and ash recovery decrease linearly with increasing solids concentration due to larger bubble size generated at higher solids content in the pulp that reduces flotation kinetics.

8. Product ash content or ash rejection is linearly dependent on water recovery while combustible recovery shows a nonlinear dependence due to different behavior of fast-floating and slow-floating fractions of coal in flotation. A new model has been proposed to describe the correlation between combustible recovery and water recovery.

9. The cleaning action of the froth zone in the column has been characterized by establishing froth profiles under different conditions. At sufficiently high wash water addition rates, most of the upgrading in a flotation column occurs near the pulp-froth interface; at lower wash water rates, additional upgrading occurs along the entire froth column in response to increased froth drainage (decreased froth stability). A wash water flow rate of approximately 0.25 cm/s is required to effectively clean the froth without causing a significant loss of combustible recovery.

10. For a fixed set of experimental conditions, lowering of the wash water addition point into the froth increases bias rate or bias factor. In some cases, this course of action can be used to improve the effectiveness of the wash water and to

increase the product grade. However, excessive drainage will cause the formation of an unstable froth which adversely affects column performance, particularly in terms of capacity.

4.6 References

1. Tomlinson, H.S. and Fleming, M.G., 1965. "Flotation rate studies," *Proceedings, 6th International Mineral Processing Congress*, Cannes, Pergamon, Oxford, pp. 563-579.
2. Feteris, S.M., Frew, J.A., and Jowett, A., 1987. "Modelling the effect of Froth depth in flotation," *International Journal of Mineral Processing*, **20**, pp. 121-135.
3. Laplante, A.R., Toguri, J.M., and Smith, H.W., 1983. "The effect of air flow rate on the kinetics of flotation. Part 2: The transfer of material from the froth over the cell lip," *International Journal of Mineral Processing*, **11**, pp. 221-234.
4. Yianatos, J.B., Finch, J.A., and Laplante, A.R., 1988. "Selectivity in column flotation froths," *International Journal of Mineral Processing*, **23**, pp. 279-292.
5. Bisshop, J.P. and White, M.E., 1976. "Study of particle entrainment in flotation froths," *Trans. Instn. Min. Metall., (Sec. C, Mineral Process. Extr. Metall.)*, C191-194.
6. Hemmings, C.E., 1980. "An alternative view point on flotation behavior of

ultrafine particles," *Trans. Instn. Min. Metall. (Sect. C, Mineral Process. Extr. Metall.)*, **89**, C113-120.

7. Hemmings, C.E., 1981. "On the significance of flotation froth liquid lamellae thickness," *Trans. Instn. Min. Metall.(Sec. C, Mineral Process. Extr. Metall.)*, **90**, C96-102.

8. Yoon, R.-H., Luttrell, G.H., Adel, G.T., and Mankosa, M.J., 1989. "Recent advances in fine coal flotation," in *Advances in Coal and Mineral Processing Using Flotation*, Ed. by S. Chander and R. Klimpel, SME, Inc., Littleton, Colorado, pp. 211-218.

9. Luttrell, G.H., Adel, G.T., and Yoon, R.-H., 1988. "Hydrodynamics and mathematical modelling of fine coal flotation," *Proceedings, XVI International Mineral Processing Congress*, Ed. by E. Forssberg, Elsevier, Amsterdam, pp. 1791-1802.

10. Harris, P.J., 1982. "Frothing phenomena and frothers," in *Principles of Flotation*, Ed. by R.P. King, Instn. Min. Metall., Monograph Ser., No. 3, pp. 237-250.

11. Livshits, A.K. and Dudenkov, S.V., 1965. "Some factors in flotation froth stability," in *Proceedings, VIIth Int. Proc. Longr Gordon and Breach*, New York, N. Y., pp. 597-621.

12. Engelbrecht, J.A. and Woodburn, E.T., 1975. "The effect of froth height,

aeration rate and gas precipitation on flotation," *Journal of S. African Institute of Mining and Metallurgy*, **76**, pp. 125-132.

13. Yianatos, J.B., Finch, J.A., Dobby, G.S., and Xu, Manqiu, 1988. "Bubble size estimation in a bubble swarm," *Journal of Colloid and Interface Science*, **126**(1), pp. 37-44.

14. Manqiu Xu and Finch, J.A., 1988. "Bubble diameter estimation in a mechanically agitated flotation cell," *Minerals and Metallurgical Processing*, **5**(1), pp. 43-44.

15. Yianotos, J.B., Laplante, A.R., and Finch, J.A., 1985. "Estimation of local hold-up in the bubbling and froth zones of a gas liquid column," *Chem. Eng. Sci.*, **40**(10), pp. 1965-1968.

16. Kelsall, D.F., 1961. "Application of probability in the assessment of flotation systems," *Trans. Instn. Min. Metall.*, **70**, pp. 191-204.

17. Dowling, E.C., Klimpel, P.R., and Aplan, F.F., 1985. "Model discrimination in the flotation of a porphyry copper ore," *Miner. Metall. Process.*, **3**, pp. 87-101.

18. Laplante, A.R., Toguri, J.M., and Smith, H.W., 1983. "The effect of air flow rate on the kinetics of flotation. Part 1: The transfer of material from the slurry to the froth," *International Journal of Mineral Processing*, **11**, pp. 203-219.

19. Mehtrotra, S.P. and Kapur, P.C., 1974. "The effects of aeration rate , particle

size and pulp density on the flotation rate distributions," *Powder Technology*, **9**, pp. 213-219.

20. Finch, J.A., Yianatos, J., and Dobby, G., 1989. "Column froths," *Mineral processing and Extractive Metallurgy Review*, **5**, pp. 281-305.

21. Klassen, V.I. and Mokrousov, V.A., 1963. "An introduction to the theory of flotation," London, Butterworth.

22. Luttrell, G.H., Weber, A.T., Adel, G.T., and Yoon, R.-H., 1988. "Microbubble flotation of fine coal," in *Column Flotation '88*, Ed. by K.V.S. Sastry, SME, Inc., Littleton, Colorado, pp. 205-211.

23. Finch, J.A. and Dobby, G.S., 1990. "Column flotation," Pergamon Press.

24. Clingan, B.V. and McGregor, D.R., 1987. "Column flotation experience at Magma Copper Co.," *Minerals and Metallurgical Processing*, **3**(3), pp. 121-125.

25. Parekh, B.K., Groppo, J.G., and Bland, A.E., 1986. "Optimization studies of column flotation for fine coal cleaning," *Proceedings. The Third Pittsburgh Coal Conference*, Pittsburgh, Pennsylvania, Sep 8-12.

26. Yianatos, J.B., Finch, J.A., and Laplante, A.R., 1987. "Cleaning action in column flotation froths," *Trans. Instn Min. Metall. (Sect C: Mineral Process. Extr. Metall.)*, **96**, December, pp. C199-205.

27. Yoon, R.-H., 1982. "Flotation of coal using microbubbles and inorganic salts," *Mining Congress Journal*, **68**(12), pp. 76-80.

28. Yoon, R.-H., 1986. "Microbubble flotation of fine coal," Final Report prepared for the U. S. Department of Energy, Report No. DOE/PC/30234-T3, 182 pp.

29. Luttrell, G.H., Keyser, P.M., Adel, G.T., and Yoon, R.-H., 1985. "Improvements in recovery and selectivity with the microbubble flotation process," *Proceedings, Second Annual Pittsburgh Coal Conference*, Pittsburgh, Pennsylvania.

30. Lovell, V.M., 1976. "Froth characteristics in phosphate flotation," in *Flotation A. M. Gaudin Memorial Volume, I*, Ed. by M. C. Fuersteau, AIME, New York, N. Y., pp. 597-621.

31. Mankosa, M.J., 1990. "Scale-up of microbubble column flotation," Ph.D. Dissertation, Department of Mining and Minerals Engineering, Virginia Polytechnic Institute and State University, Blacksburg, Virginia.

32. Xu, M. and Finch, J.A., 1989. "Effect of sparger surface area on bubble diameter in flotation columns," *Canadian Metallurgical Quarterly*, **28**(1), pp. 1-6.

33. Yoon, R.-H. and Luttrell, G.H., 1986. "The effect of bubble size on fine coal flotation," *Coal Preparation*, **2**, pp. 179-192.

34. Yoon, R.-H., Boron, D.J., Adel, G.T., Luttrell, G.H., and Weber, A., 1987. "The Virginian Tech microbubble column flotation technology," *Proceedings. Electric Power Research Institute Microbubble Flotation Workshop*, Homer City, Pennsyvania, Dec 3.

35. Yoon, R.-H., Luttrell, G.H., and Adel, G.T., 1989. "Advances in fine particle flotation," in *Challenges in Mineral Processing*, Ed. by K.V.S. Sastry and M.C. Fuerstenau, Proceedings of a symposium honoring D.W. Fuerstenau on his 60th birthday, Berkeley, California, December 7-9, pp. 487-505.

36. Yoon, R.-H., 1993. "Microbubble flotation," *Minerals Engineering*, **6**(6), pp. 619-630.

37. Jowett, A., 1966. "Gangue mineral contamination of froth," *British Chemical Engineering*, **2**, pp. 330-333.

38. Warren, L.J., 1985. "Determination of the contribution of true flotation and entrainment in batch flotation tests," *International Journal of Mineral Processing*, **14**, pp. 33-44.

39. Szatkowski, M., 1987. "Factors influencing behaviour of flotation froth," *Trans. Instn. Min. Metall., Sec. C, Mineral Process. Extr. Metall.*, **96**, C115-122.

40. Monsalve, A., and Schechter, R.S., 1984. "The stability of foams: dependence of observation on the bubble size distribution," *Journal of Colloid and Interface Science*, **97**(2), pp. 327-335.

41. Smith, P.G., Warren, L.J., 1989. "Entrainment of particles into flotation froths," *Mineral Processing and Extractive Metallurgy Review*, **5**, pp. 123-145.

42. Clift, R., Grace, J.R., and Weber, G.W., 1978. "Bubbles, Drops and Particles," Academic Press, New York.

43. Taggart, A.F., 1945. "Handbook of mineral dressing," Wiley, New York, N. Y., pp. 12-53.

44. Lawver, J.E. and Barbarowicz, W., 1962. "Mill control: Part 1, automatic controls for flotation plants," in: *Froth Flotation: 50th Anniversary Volume*, Ed. by D. W. Fuersteau, AIME, New York, N. Y.

45. Paakkinen, U.E. and Cooper, H.R., 1979. "Flotation process control," In, *Computer Methods for the 80's in the Mineral Industry*, A.I.M.E., Ed. by A. Weiss, New York, N.Y., pp. 787-798.

46. Espinosa-Gomez, R., Yianatos, J.B., Finch, J.A., and Johnson, N.W., 1988. "Carrying capacity limitations in flotation columns," in *Column Flotation '88*, Ed. by K.V.S. Sastry, SME Annual Meeting, Phoenix, Arizona, pp. 143-148.

47. Ynchausti, R.A., McKay, J.D., and Foot, D.G., 1988. "Column flotation parameters-their effects," in *Column Flotation '88*, Ed. by K.V.S. Sastry, SME Annual Meeting, Phoenix, Arizona, pp. 157-172.

48. Moys, M. H., 1984. "Residence time distribution and mass transport in the froth phase of the flotation process," *International Journal of Mineral Processing*, **13**, pp. 117-142.

49. Kitchener, J.A., 1964. "Foams and free liquid films," in *Recent Progress in surface Science*, Vol. 1, Ed. by J.F. Danielli, K.G.A. Pankhurst and A.C. Riddiford, Academic Press, New York, pp. 51-93.

50. Mysels, K.J., Shinoda, K., and Frankel, S., 1959. "Soap films - studies of their thinning," Pergamon Press, New York.

51. Ross, V.E., 1991. "An investigation of sub-processes in equilibrium froths (I): the mechanisms of detachment and drainage," *International Journal of Mineral Processing*, **31**, pp. 37-50.

52. Moys, M.H., 1978. "A study of a plug-flow model for flotation froth behaviour," *International Journal of Mineral Processing*, **5**, pp. 21-38.

53. Amelunxen, R., Lierena, R., Dunstan, P., and Huls, B., 1988. "Mechanics of column flotation operation," in *Column Flotation '88*, Ed. by K. V. S. Sastry, SME Annual Meeting, Phoenix, Arizona, pp. 149-156.

54. Kosick, G.A., Freberg, M., and Kuehn, L.A., 1988. "Column flotation of galena at the polaris concentrator," CIM Bulletin, **81**(920), pp. 54-60.

55. Dippenaar, A., 1982. "The destabilization of froth by solids, I. The mechanism of film rupture," *International Journal of Mineral Processing*, **9**, pp. 1-14.

56. Dippenaar, A., 1982. "The destabilization of froth by solids, II. The rate determining step," *International Journal of Mineral Processing*, **9**, pp. 15-27.

57. Johansson, G. and Pugh, R.J., 1992. "The influence of particle size and hydrophobicity on the stability of mineralized froths," *International Journal of Mineral Processing*, **34**, pp. 1-21.

58. Moudgil, B.M. and Gupta, D., 1989. "Flotation of coarse phosphate particles,"

In: *Advances in Coal and Mineral Processing Using Flotation*, Ed. by S. Chander and R. R. Klimpel, pp. 164-168.

59. Vanangamudi, M. and Rao, T.C., 1989. "A Model for the prediction of fines recovery in batch coal flotation," *Mineral Engineering*, **2**, pp. 185-192.

60. Kirjavainen, V.M., 1989. "Application of a probability model for the entrainment of hydrophilic particles in froth flotation," *International Journal of Mineral Processing*, **27**, pp. 63-74.

61. Cutting, G.W., Watson, D., Whitehead, A., and Barber, S.P., 1981. "Froth structure in continuous flotation cells: relation to the prediction of plant performance from laboratory data using process models," *International Journal of Mineral Processing*, **7**, pp 347-369.

CHAPTER 5 COLUMN CIRCUITS FOR COAL FLOTATION

5.1 Introduction

It has been shown in Chapter 1 that the presence of coal-pyrite middlings is one of the major causes for poor pyrite rejection in coal flotation processes, simply due to the fact that the middlings can float readily by attachment onto bubble surfaces through coal inclusions. In an endeavor to improve the rejection of middlings, various column flotation circuits were studied.

Flotation circuits are composed of a number of similar units that are connected with each other in some way [1]. Flotation columns can be incorporated into existing flotation circuits of conventional mechanical cells. In fact, this is becoming increasingly common industrial practice [2]. Nevertheless, studies of various column circuit configurations are scarce and problems relating to the selection of an appropriate circuit have not been addressed. Circuit selection is largely done on case-by-case basis from individual pilot-plant test results and personal experiences. No general guidelines for the selection of a proper circuit are available.

The configuration of a flotation circuit has important effects on the overall performance for a given feed material. Circuit optimization deals with the determination of the best interconnection of cell units. This can be done by means of modeling,

simulation, synthesis, mathematical analysis, graphics, etc [3-16]. However, Sutherland [6] has concluded that simulation of flotation systems may not be able to distinguish between different circuit arrangements unless effects of changes in circuit arrangements on the flotation rate constants of mineral components are known and are accounted for. Since such a prerequisite can not be met at the present time, experimental examination of various flotation circuit arrangements was considered necessary to reveal the importance of circuit configurations in column flotation.

5.2 Research Objectives

The present study was aimed at revealing the influence of column flotation circuit configurations on the overall separation performance. Research objectives were accomplished by carrying out experiments on a three-column system for coal flotation at various feed flow rates with different coal samples. The focus of the study was placed on the general characterization of the most commonly used coal flotation circuits. Separation efficiency was used as criterion function along with separation curves to evaluate the metallurgical performance of the circuit configuration.

Coal flotation is usually conducted in a single stage, i.e., rougher. However, complex coal flotation circuits have been industrially practiced, especially in the treatment of coking coals [17,18] and poorly floatable coals [7]. They have also been used to generate ultra-clean coal products and improve sulfur rejection [1, 19, 20].

Column flotation circuits examined in this study included:

a) single-stage (SS)

b) rougher-scavenger (RS)

c) rougher-cleaner (RC)

d) rougher-scavenger-scavenger cleaner (RSSC)

e) rougher-scavenger-cleaner (RSC)

f) rougher-cleaner-recleaner (RCRC)

Schematic representations of these circuit arrangements are provided in Figure 5.1. Some of them have been employed in industry [21].

5.3 Experimental

5.3.1 Sample Preparation

The circuit tests were carried out using samples obtained from the Pittsburgh No. 8, Illinois No. 6 and Upper Freeport coal seams. These coal samples were precleaned by Babcock & Wilcox using conventional, sub-aeration cells and shipped in slurry form to the laboratory in several 55 gallon drums. Grab samples indicated that components of each drum were highly variable and that blending would be required to obtain representative samples for testing. The homogenization of the sample was performed in several steps. First, the content of each drum was thoroughly agitated using a low-speed

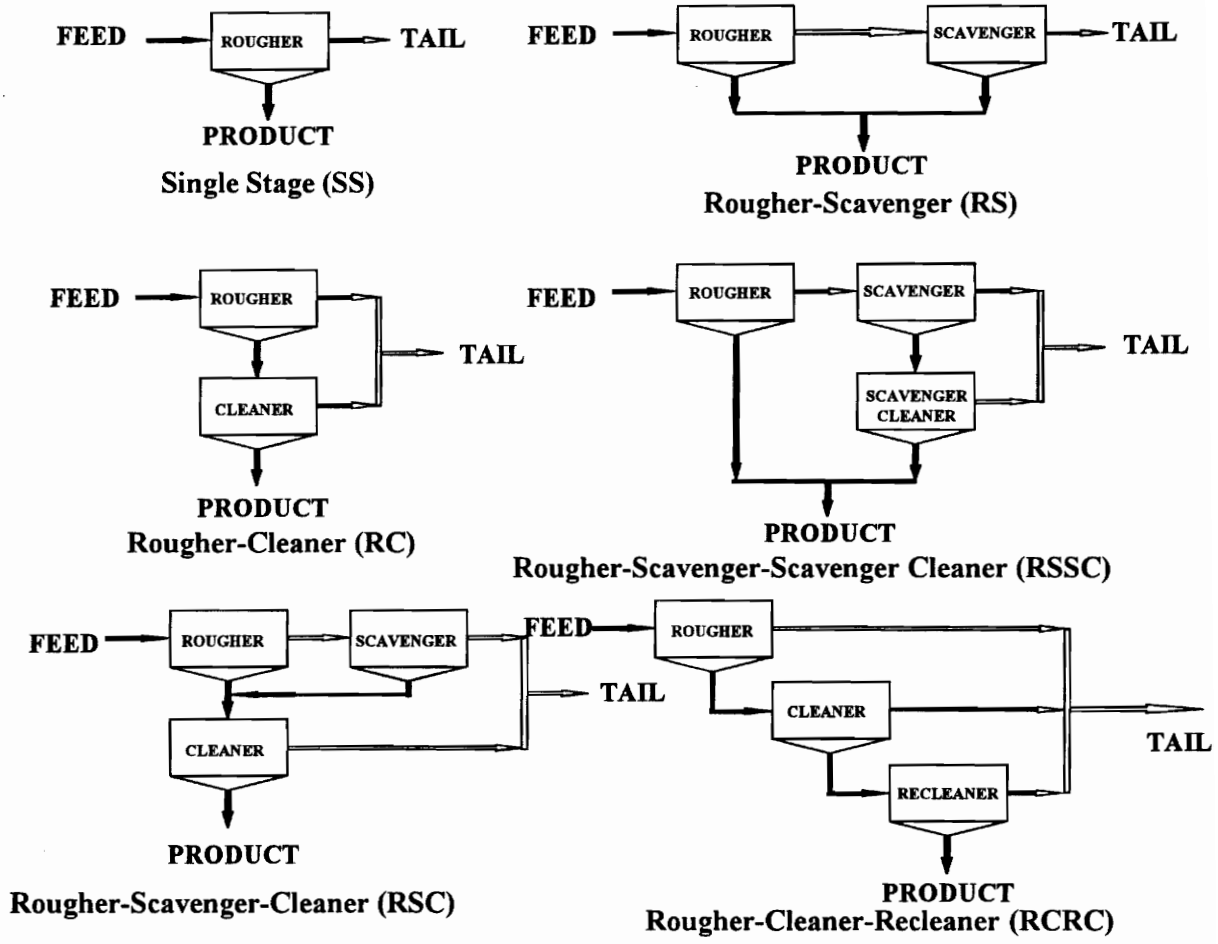

Figure 5.1 Schematic representations of the various circuit configurations examined in the present work

drum mixer to redisperse coarse particles which had settled to the bottom of the drum during shipment. The slurry in each drum was then transferred to a 500-gallon sump equipped with a propeller-type mixer and pumping circuit which continuously recirculated the slurry. After emptying all drums for a given coal, representative samples of the well-mixed slurry were pumped from the sump into individual 5-gallon containers. Each container was flooded with nitrogen and sealed prior to storage.

Flotation samples were prepared by grinding each coal sample using a Union Process stirred ball mill. Samples were ground at 30% solids using 3.2 mm diameter stainless steel grinding media. The Pittsburgh No. 8 sample was ground to a nominal size of -325 mesh using a grinding time of approximately 4 minutes. The Illinois No. 6 and Upper Freeport samples were each ground to a nominal -200 mesh product size in a period of 1.5 minutes. Representative particle size distributions for the various coals thus prepared were determined using an Elzone 80-XY particle size analyzer to be approximately the same as required.

5.3.2 Apparatus

Three identical flotation column cells were constructed for use in the evaluation of various circuit configurations. Each 152-cm (60-inch) high column was made from clear, cylindrical Plexiglass tubing having an inside diameter of 5 centimeters. Feed slurry was injected into the flotation column at a distance of approximately 35

centimeters below the product overflow lip using a variable-speed pump. Wash water was added into column through a spider-type distributor mounted in the middle of the froth zone. Pulp level was maintained approximately 30 centimeters below the product overflow lip through the use of a simple overflow weir connected to the reject line. Air sparging was accomplished by pumping a portion of the flotation slurry through an in-line static mixer into which compressed air was injected.

Three different experimental circuit configurations were assembled and tested using each of the three column cells. The first set-up was the traditional flotation circuit used in most mineral processing operations. In this set-up, feed was pumped to a rougher column which produced a primary clean coal concentrate and primary tailings. The rougher tailings were pumped to a scavenger column which produced the final reject stream and intermediate clean coal product. The clean coal products from the rougher and scavenger columns were combined and fed to a cleaner column which produced the final clean coal concentrate. This configuration allowed SS, RS and RSC circuits to be evaluated with a minimum number of experimental runs.

The second experimental set-up was the grab-and-run circuit configuration. This configuration was similar to the traditional configuration described above except that the rougher concentrate was taken as the final product without recleaning. This type of circuit, which was originally promoted by Aplan [22], was designed to cut down on the tonnage of material that must be treated in subsequent operations by immediately removing the cleanest coal as final product. The slower floating middling particles were

passed to a scavenger cell which produced the final reject stream and an intermediate clean coal product. The intermediate product was recleaned and combined with the rougher product to produce a final clean coal product. This configuration enabled the SS, RS and RSSC circuits to be examined.

The final configuration was the basic cleaner circuit. This configuration was designed to produce the cleanest possible product by repetitive cleaning of the flotation concentrate. Miller [20] specifically advocated this type of configuration for the rejection of pyrite during coal flotation. In this configuration, the concentrate from the final cleaning stage was taken as the final clean coal product, while the tailings from each column were combined to form the final reject stream. The evaluation of SS, RC and RCRC circuits was made possible by this configuration.

5.3.3 Procedure

A standard test procedure was employed throughout the flotation circuit test program. In each series of tests, the ground coal was placed into a well-agitated 8 gallon sump and diluted to 5% solids using tap water. Kerosene was added directly as collector to the coal in the feed sump at a constant dosage of 0.225 kg/ton of feed solids for all tests. The collector was allowed to condition for at least 10 minutes before being fed into the column. Dowfroth M-1012 frother was injected directly into the bubble generator of the column at a concentration of 0.05% by volume. Frother dosages varied

from 0.45-1.3 kg/ton of feed solids, depending on the given feed slurry flow rate and circuit arrangement. Proper frother addition rates were determined by observing the size of bubbles in the cell, along with a measurement of the air hold-up in the column as determined by pressure transducers. The superficial aeration rate was held constant during testing at 76 cm/min (corresponding flow rate 1500 ml/min) and a superficial wash water rate of at least 20 cm/min was maintained in all tests. After initial start-up of the column, feed slurry was injected into the column using a variable speed peristaltic pump. The column operation was allowed to come to steady-state, which required a period of time roughly equivalent to 2-3 times the mean slurry retention time. Throughout the period of operation, a small amount of spray water was added to the froth overflow launder to ensure that the froth product would overflow uniformly.

After the column reached the steady-state, froth product and tailings were collected in separate sumps to be used as feed to next stages of flotation. Timed sampling of the froth product and flotation tailings were done simultaneously to obtain representative specimens for analysis. After collecting the desired quantity of samples from each column, the column operating conditions were changed and the same procedure was repeated until the desired number of data points were obtained. The volumetric flow rate of feed slurry was the primary operating parameter varied in most tests. Feed rates of 100, 200 and 300 ml/min were tested for each base coal. In addition, the Pittsburgh No. 8 seam coal was also tested at a feed flow rate of 50 ml/min. Overall feed samples were collected from the feed stream for comparison with

the recombined product analyses from each test. This procedure provided a check on the laboratory analyses and an indication of the reliability of the test results. All collected samples were filtered, dried, weighed and analyzed according to ASTM standards.

In order to obtain consistent sets of results, the experimental data obtained in each test on column flotation circuit were adjusted using the BILMAT material balance program developed by Canada Center for Mineral and Energy Technology. This program uses the weighted least-square method to correct all measured data to produce best estimates of all variables (measured and unmeasured) for a mineral processing circuit. Material balance calculations were performed for each coal as a function of circuit configuration and feed flow rate. In most cases, only minor adjustments were required to obtain a suitable balance.

In addition to the column circuit tests, a timed release analysis study was conducted for each of the coal seam. A standard Model D-12 Denver flotation machine equipped with a 5-liter cell was used for these tests. The release analysis results provided a baseline for comparing the effectiveness of the various circuit configurations. The frother and collector dosages for all of the release analysis tests were maintained at approximately 1.75 and 0.45 kg/ton, respectively.

5.4 Results and Discussions

5.4.1 Results

5.4.1.1 *Release analysis of three coal samples*

Release analysis [23, 24] can be considered as a counterpart in froth flotation to the float-sink analysis in gravity separation. It provides the best possible flotation separation for a given coal and a given set of reagent conditions and can be used to characterize the floatability of the coal. Release analysis was performed in two major stages. The principal purpose of the first stage was to remove all non-floatable material from floatable material by repeated cleaning and recleaning of the froth products to eliminate entrained mineral matter. In the second stage, the floatable material was separated into several fractions characteristic of different degrees of floatability in order to establish the combustible recovery against ash rejection or combustible recovery against sulfur rejection correlation for a given coal. This was done by beginning the flotation at a very low aeration rate and impeller speed and gradually increasing both parameters to recover progressively less floatable material. Detailed conditions are specified in Table 5.1. A 5-liter Denver laboratory flotation cell was used in the present study to conduct release analysis.

The results of the release analysis tests for all of the three base coal samples are shown in Figure 5.2, which indicated that the Pittsburgh No. 8 coal sample possessed the highest potential for ash rejection, while the Upper Freeport possessed the lowest. This conclusion was supported by SEM pictures which demonstrated that both mineral matter and pyrite were more coarsely distributed in the Pittsburgh No. 8 sample than in the Upper Freeport sample. The ash rejection values for the Illinois No. 6 sample fall

Table 5.1 Specific flotation conditions for the second stage of release analysis

Product	Impeller Speed (rpm)	Air Valve Openness
1	1100	< 1/4
2	1300	1/2
3	1500	3/4
4	1700	1

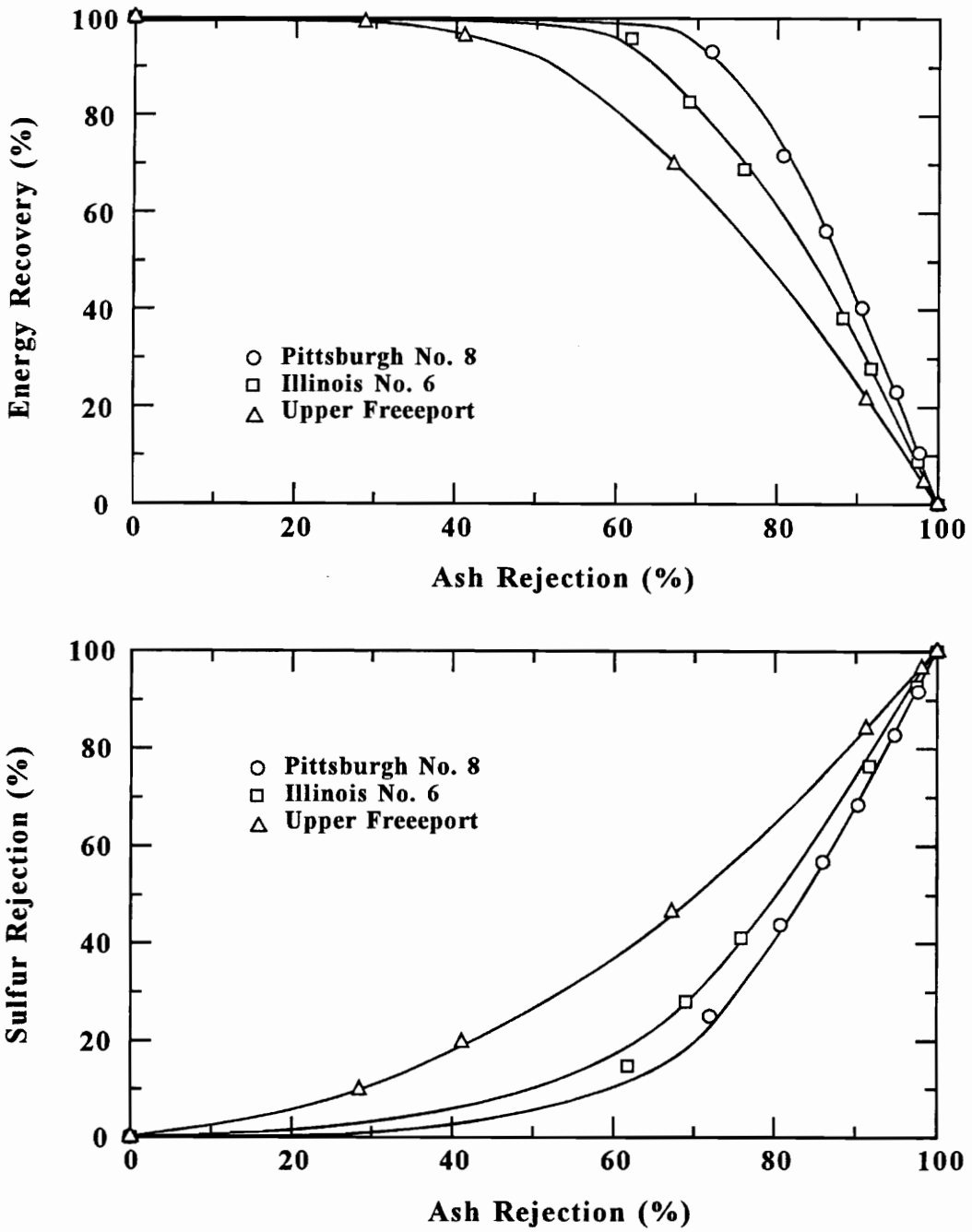

Figure 5.2 Results of release analysis tests conducted on the Pittsburgh No. 8, Illinois No. 6 and Upper Freeport coal seams.

almost exactly between those of the Pittsburgh No. 8 and Upper Freeport samples. At a combustible recovery of 90%, the release analysis results suggest that the maximum ash rejections that can be expected for the Pittsburgh No. 8, Illinois No. 6 and Upper Freeport samples may not exceed 72%, 64% and 52%, respectively, for the given grind size and reagent package. The corresponding sulfur rejections may not be larger than 27%, 24% and 30%.

5.4.1.2 *Circuit performance with Pittsburgh No. 8 seam coal*

This coal sample was shown to have 9.8% ash, 3.63% sulfur and 1.25% pyritic sulfur. The results of the circuit tests on this coal are summarized in Figures 5.3 and 5.4. These figures show the energy recovery versus ash and sulfur rejections for each circuit over a wide range of feed flow rates. Although some degree of data scatter is noted, essentially the same recovery-grade relationship was obtained for each of the six circuit configurations examined in the present work. The single-stage test results appear to be slightly inferior to those obtained with the other circuits, possibly owing to a small degree of particle entrapment or entrainment in these experiments. However, it is doubtful that the slight improvement in metallurgical performance would justify the costs associated with the multi-column circuit configurations.

According to the results shown in Figures 5.3 and 5.4, an energy recovery of 90% will produce corresponding ash and sulfur rejections of approximately 70% and 26%, respectively. These rejections can be further increased to 77% and 35%,

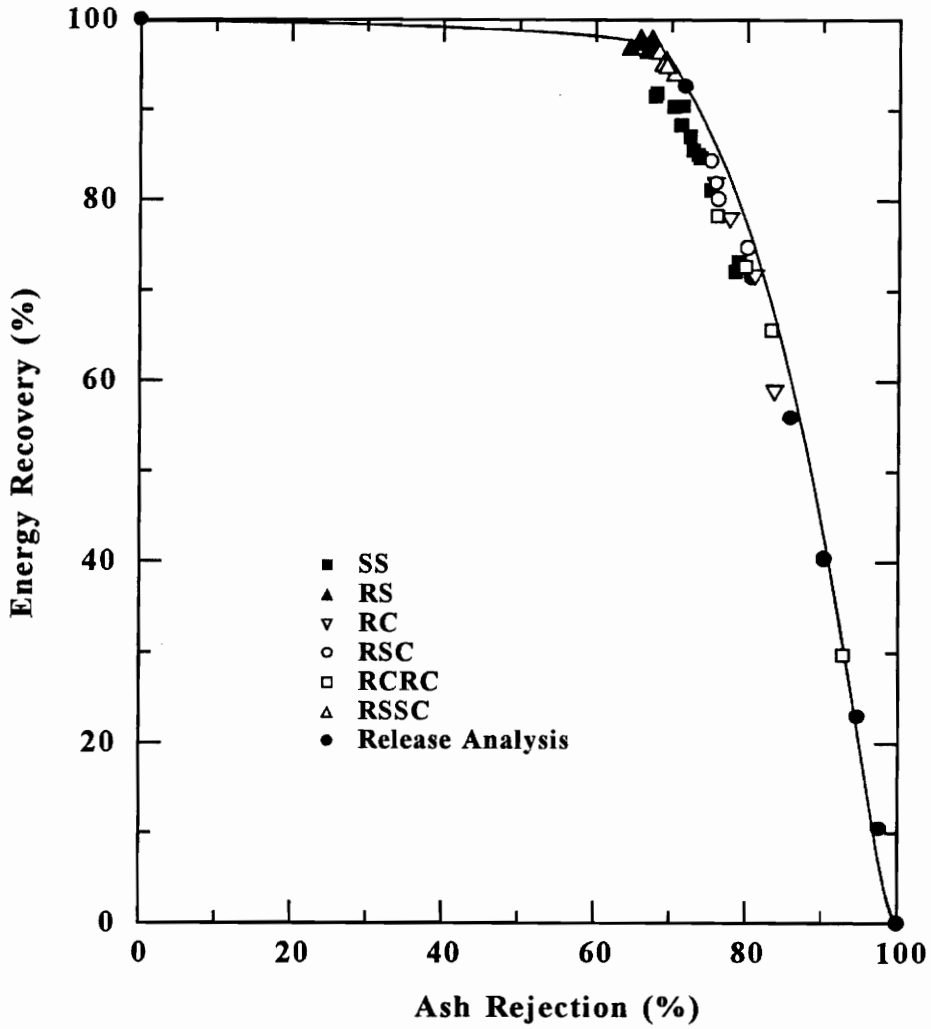

Figure 5.3 Effect of circuit configuration on energy recovery versus ash rejection for the Pittsburgh No. 8 seam coal.

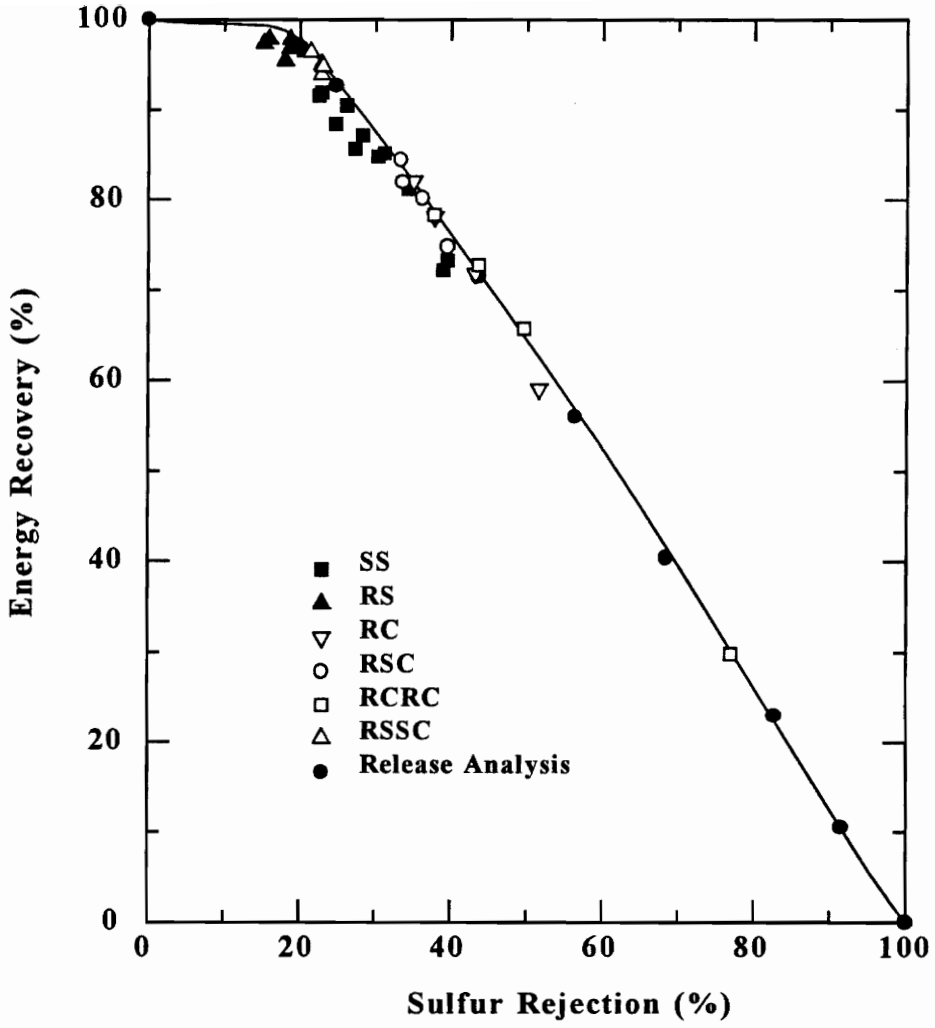

Figure 5.4 Effect of circuit configuration on energy recovery versus sulfur rejection for the Pittsburgh No. 8 seam coal.

respectively, by allowing the energy recovery to fall to 80%. It is also interesting to note that the test results obtained for the various circuits fall on or just below the performance curve predicted by the release analysis technique. The good agreement between the release analysis data and column flotation results suggests that the column was operating near its optimum level of performance.

Figure 5.5 provides a summary of the separation efficiencies (defined as energy recovery minus ash recovery) obtained as a function of ash rejection for each circuit. As shown, the maximum separation efficiencies occurred at ash rejection values near 70%, which is in the neighborhood of the "elbow" in the recovery-ash rejection curve shown previously in Figure 5.3. This result is in agreement with the conclusion from theoretical analysis that the maximum efficiency takes place at the point on the energy recovery versus sulfur rejection curve where the slope is equal to -1. Another interesting result can be obtained by plotting sulfur rejection versus ash rejection for each circuit. These results, which are plotted in Figure 5.6, demonstrate that a single curve can be used to correlate the ash and sulfur rejections. This figure also indicates that pyritic sulfur is more difficult to reject than ash since the curve tends to bend toward the lower right-hand corner of the plot.

5.4.1.3 *Circuit performance with Illinois No. 6 seam coal*

The ash content, sulfur content, and pyritic sulfur were found to be 9.5%, 2.91% and 0.61%, respectively, in the Illinois No. 6 seam coal. Figures 5.7 and 5.8 summarize

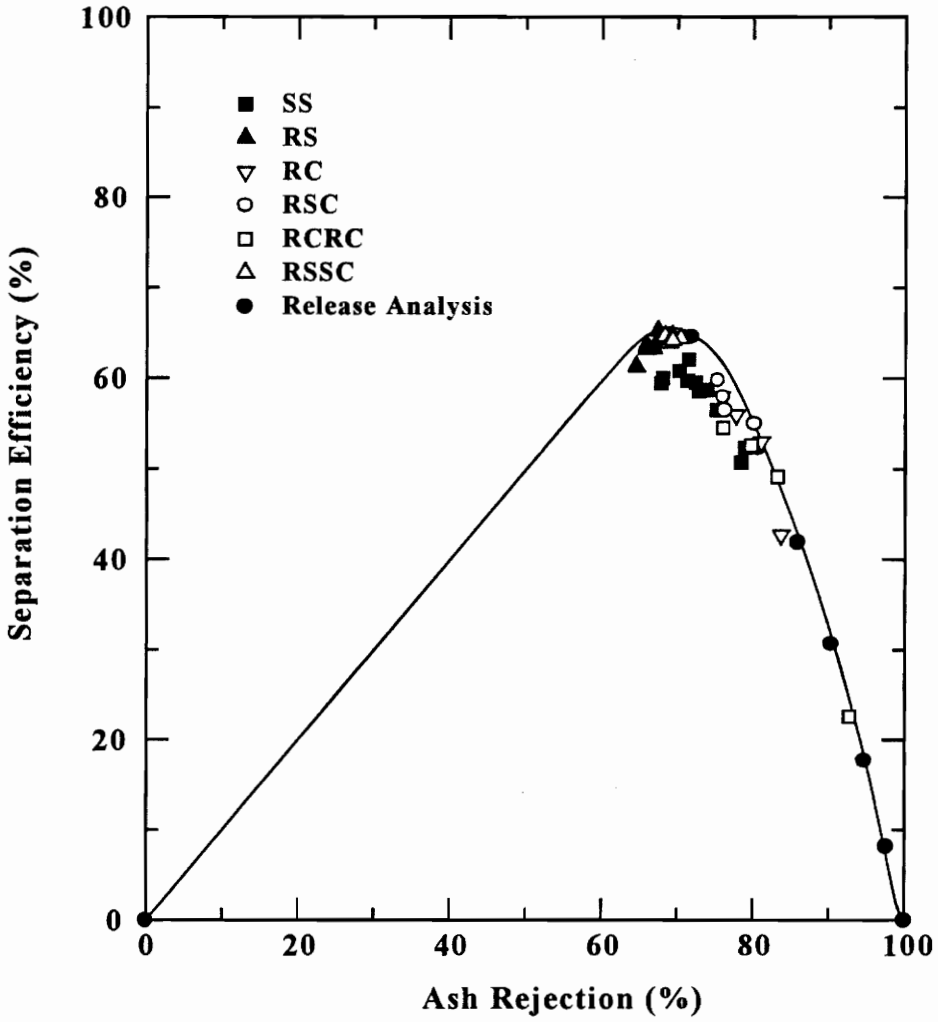

Figure 5.5 Effect of circuit configuration on separation efficiency versus ash rejection for the Pittsburgh No. 8 seam coal.

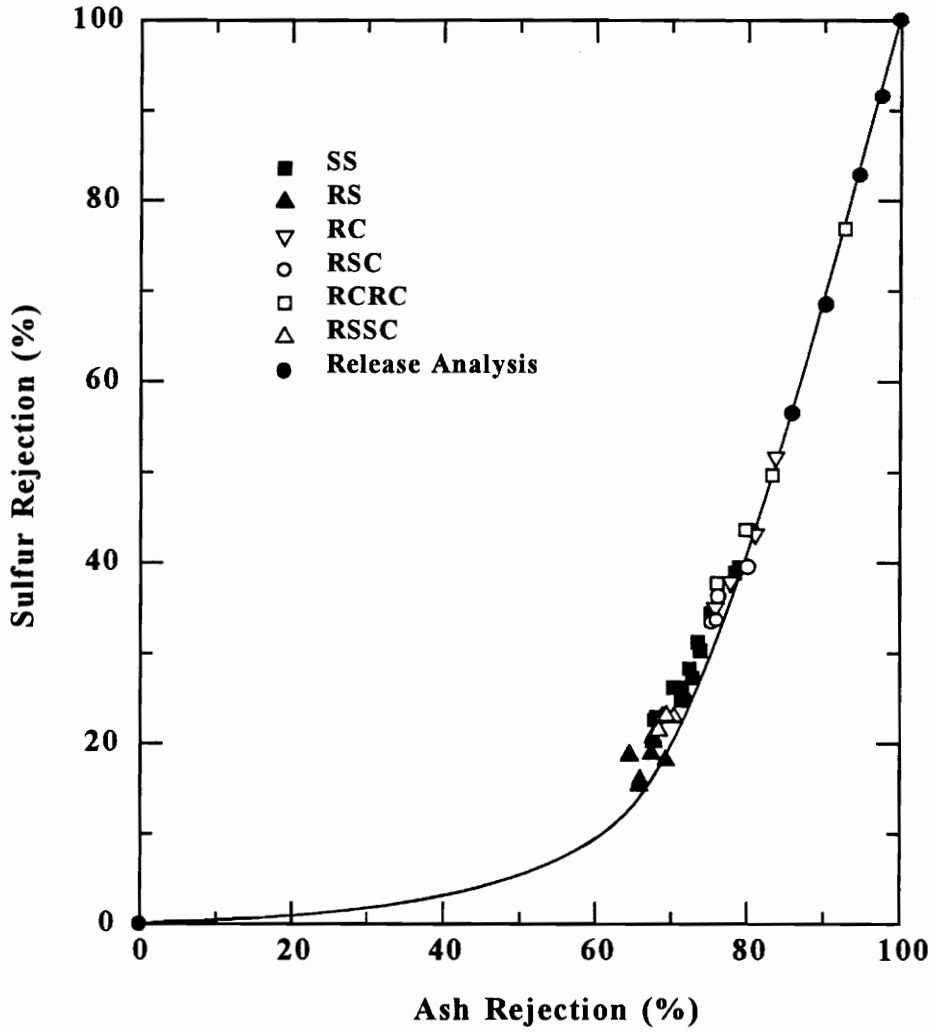

Figure 5.6 Effect of circuit configuration on sulfur rejection versus ash rejection relationship for the Pittsburgh No. 8 seam coal.

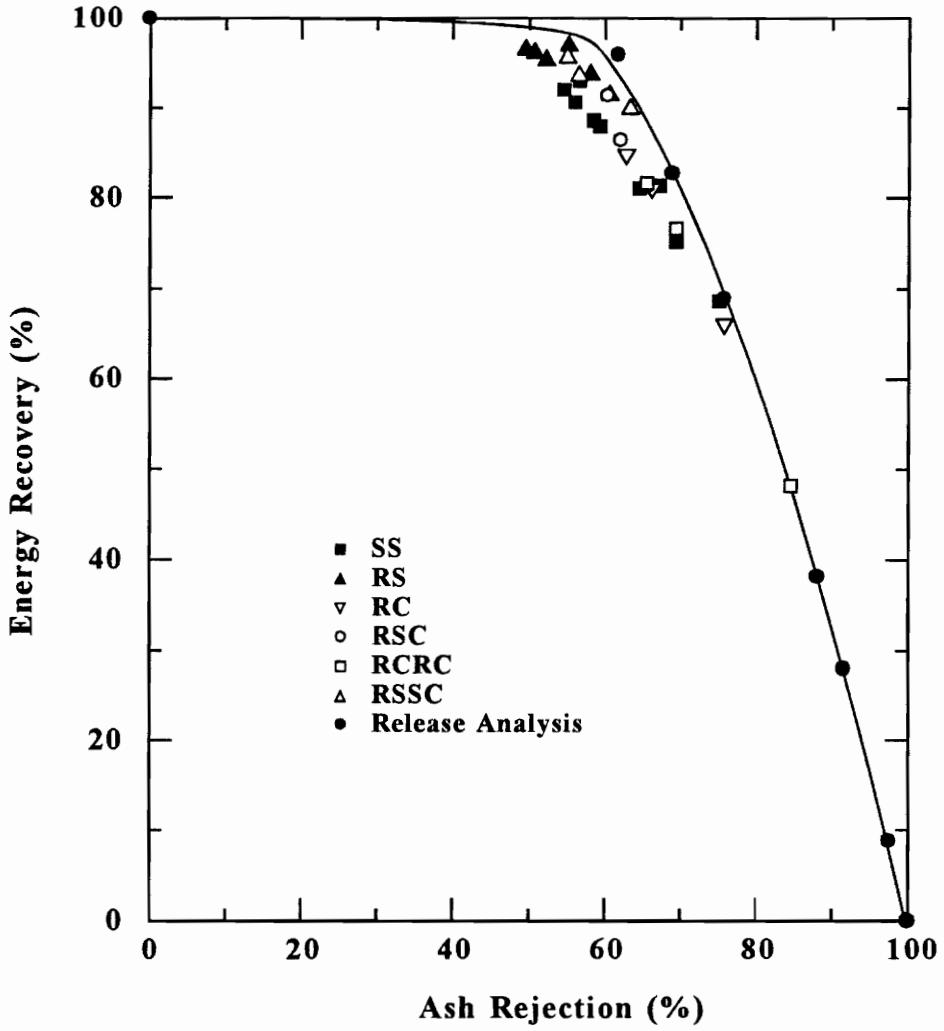

Figure 5.7 Effect of circuit configuration on energy recovery versus ash rejection for the Illinois No. 6 seam coal.

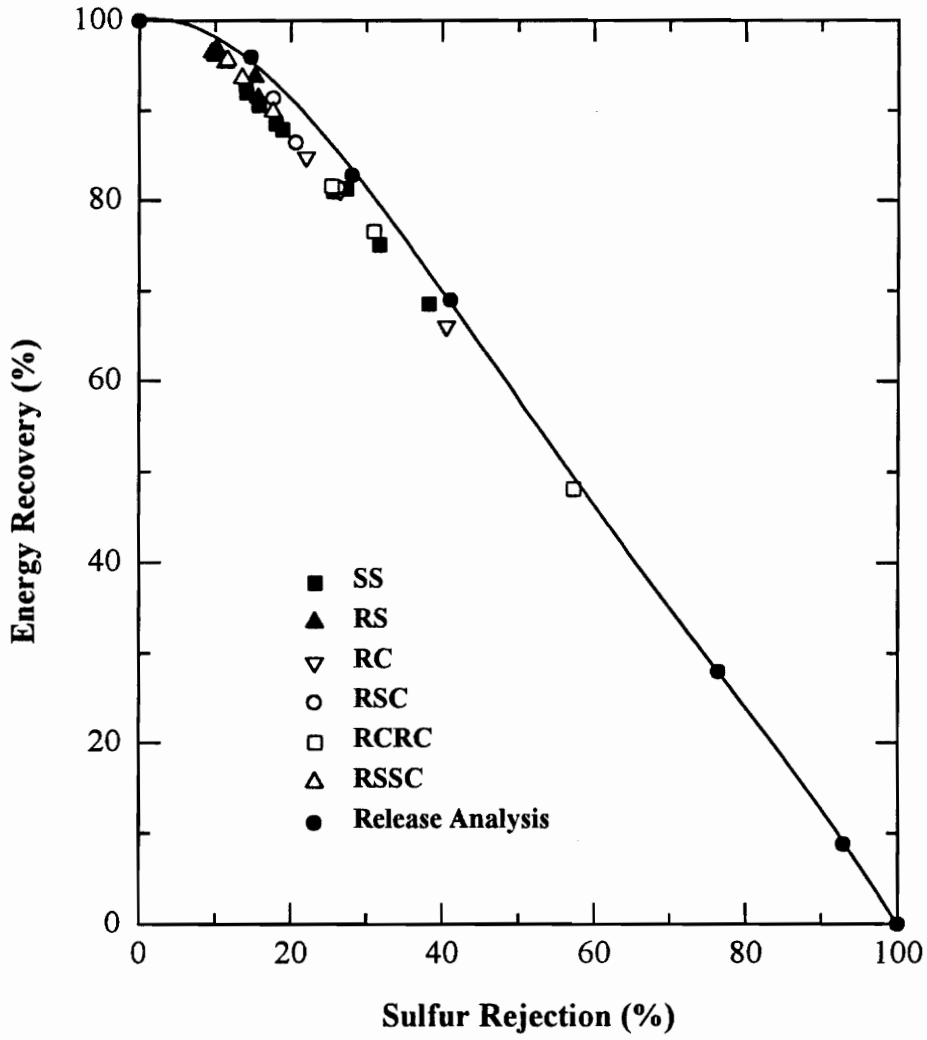

Figure 5.8 Effect of circuit configuration on energy recovery versus sulfur rejection for the Illinois No. 6 seam coal.

the circuit test data obtained using this coal. As with the Pittsburgh No. 8 seam coal, the data obtained for this coal indicates that a single recovery-grade curve can be used to represent the results obtained from the various circuit configurations. In general, the test data shows that an ash rejection of 63% and sulfur rejection of 19% can be achieved with this coal at a 90% energy recovery. At an 80% energy recovery, the ash and sulfur rejections can be improved to 68% and 27%, respectively. These values are considerably lower than those obtained for the Pittsburgh No. 8 seam coal. The poorer cleanability of the Illinois No. 6 seam coal is also supported by the separation efficiency values plotted in Figure 5.9. The maximum separation efficiencies for this particular coal sample fall approximately 10-15 percentage points below those obtained with the Pittsburgh No. 8 coal. These conclusions are not surprising in light of the release analysis results shown in Figure 5.2.

The relationship between sulfur rejection and ash rejection for the circuit tests conducted with the Illinois No. 6 seam coal are shown in Figure 5.10. Although some degree of data scatter is observed, a distinct relationship clearly exists between the rejections of ash and sulfur. It is also interesting to note that the plot shown in Figure 5.10 is characterized by a lesser degree of curvature, indicating that the ash-bearing minerals and pyritic sulfur are more closely associated in the Illinois No. 6 coal sample. This association may offer a partial explanation for the poorer response of this particular coal sample to flotation.

A comparison between the release analysis data shown in Figure 5.2 and the

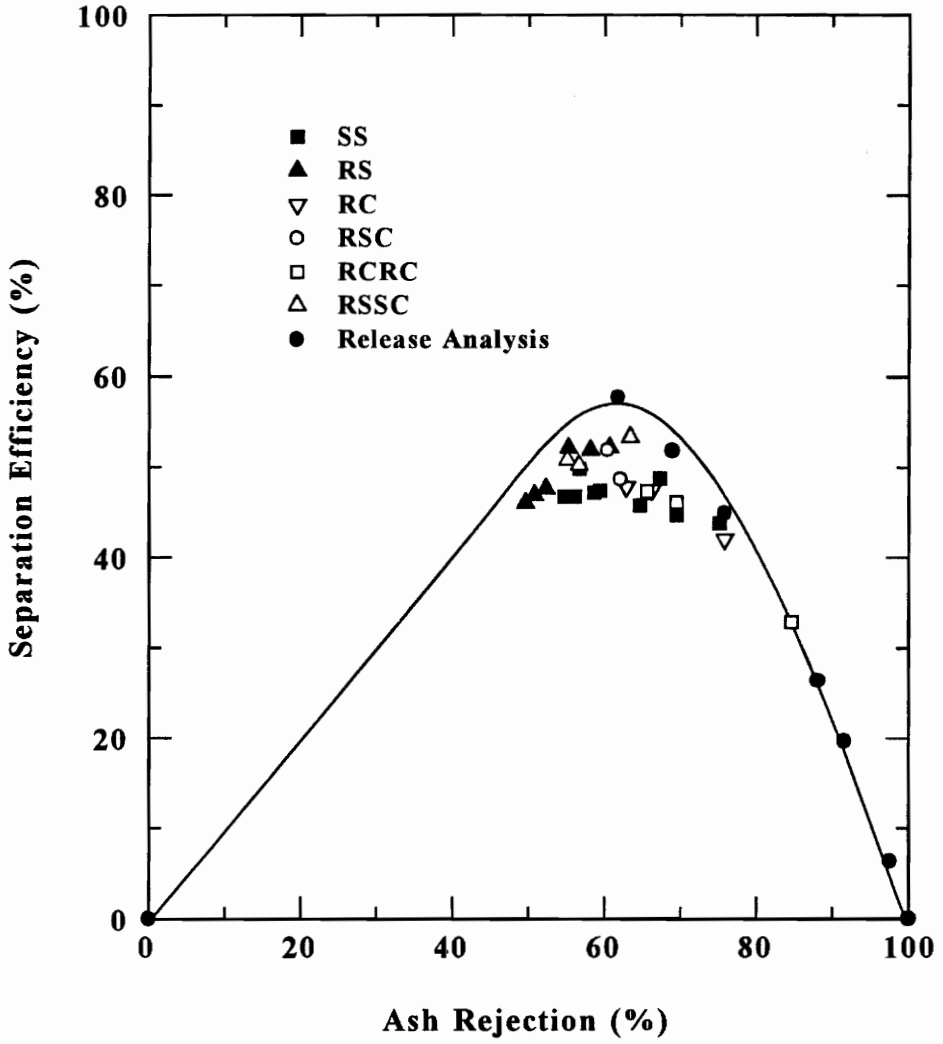

Figure 5.9 Effect of circuit configuration on separation efficiency versus ash rejection for the Illinois No. 6 seam coal.

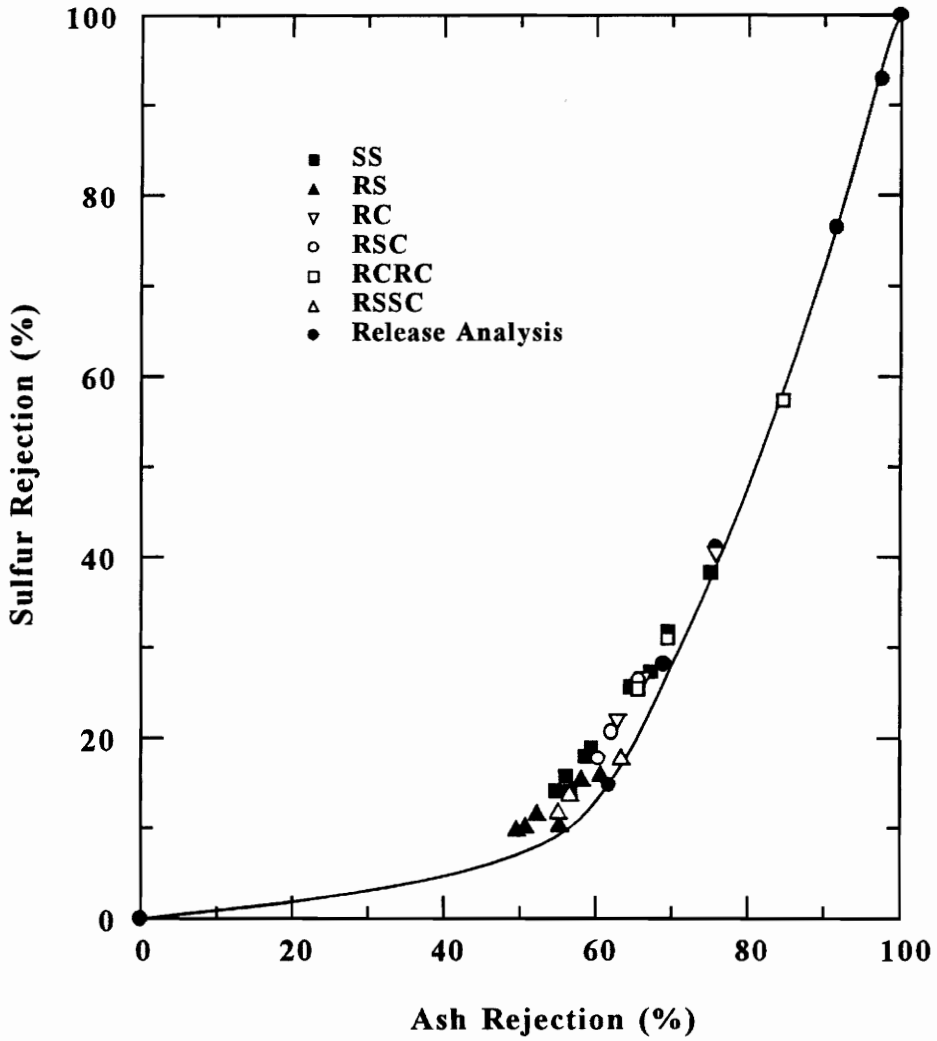

Figure 5.10 Effect of circuit configuration on sulfur rejection versus ash rejection relationship for the Illinois No. 6 seam coal.

circuit test results given in Figure 5.7 again demonstrates that the release analysis technique provides a good estimate of coal cleanability. In general, the test data achieved for the various circuits fall on or just below the performance curve predicted by release analysis.

5.4.1.4 *Circuit performance with Upper Freeport seam coal*

This coal sample contains 9.9% ash content, 1.45% sulfur content and 0.74% pyritic sulfur. The results of the circuit tests are summarized in Figures 5.11 and 5.12. Despite a certain degree of data scatter, essentially the same recovery-grade relationship was obtained for each of the six circuit configurations. With this particular coal, an energy recovery of 90% will produce corresponding ash and sulfur rejections of only about 45% and 25%, respectively. These values once again fall very close to those predicted by the release analysis technique. Considering that almost one-half of total sulfur in this coal is due to pyrite, the cleanability of the Upper Freeport coal with respect to ash and pyrite appears to fall considerably below that attained with either the Pittsburgh No. 8 or Illinois No. 6 seam coal.

Figure 5.13 provides a summary of the separation efficiencies obtained as a function of ash rejection for the Upper Freeport seam coal. As shown, the separation efficiencies do not vary substantially over a rather wide range, suggesting that they are not very sensitive to separation conditions. A distinct maximum in the separation efficiency for this coal is difficult to define. This difficulty can be largely attributed to

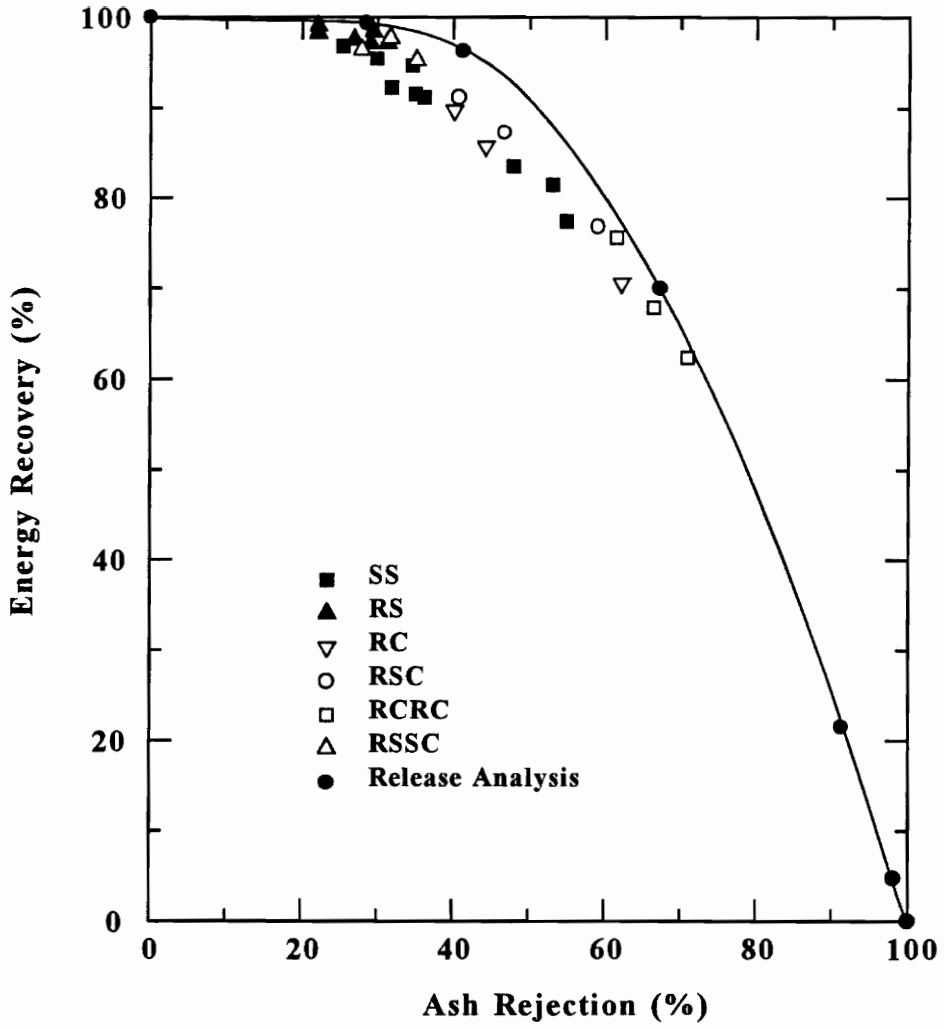

Figure 5.11 Effect of circuit configuration on energy recovery versus ash rejection for the Upper Freeport seam coal.

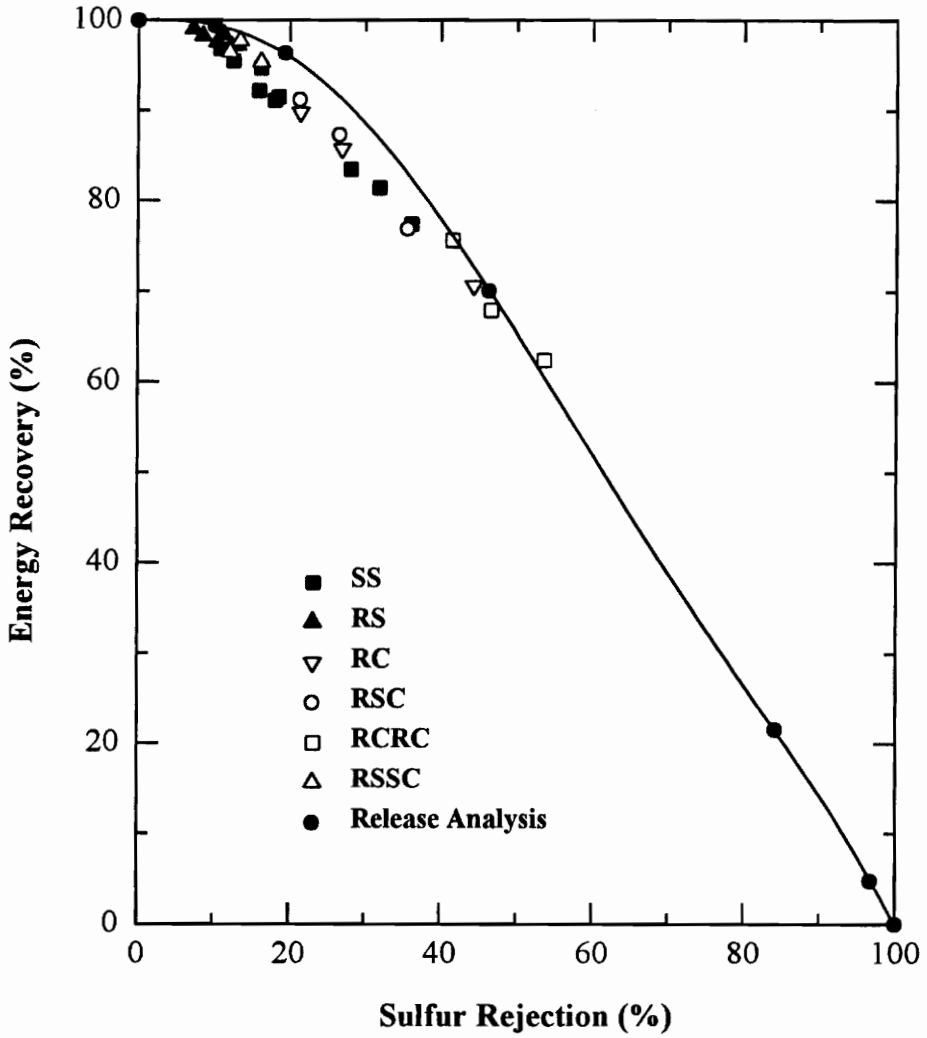

Figure 5.12 Effect of circuit configuration on energy recovery versus sulfur rejection for the Upper Freeport seam coal.

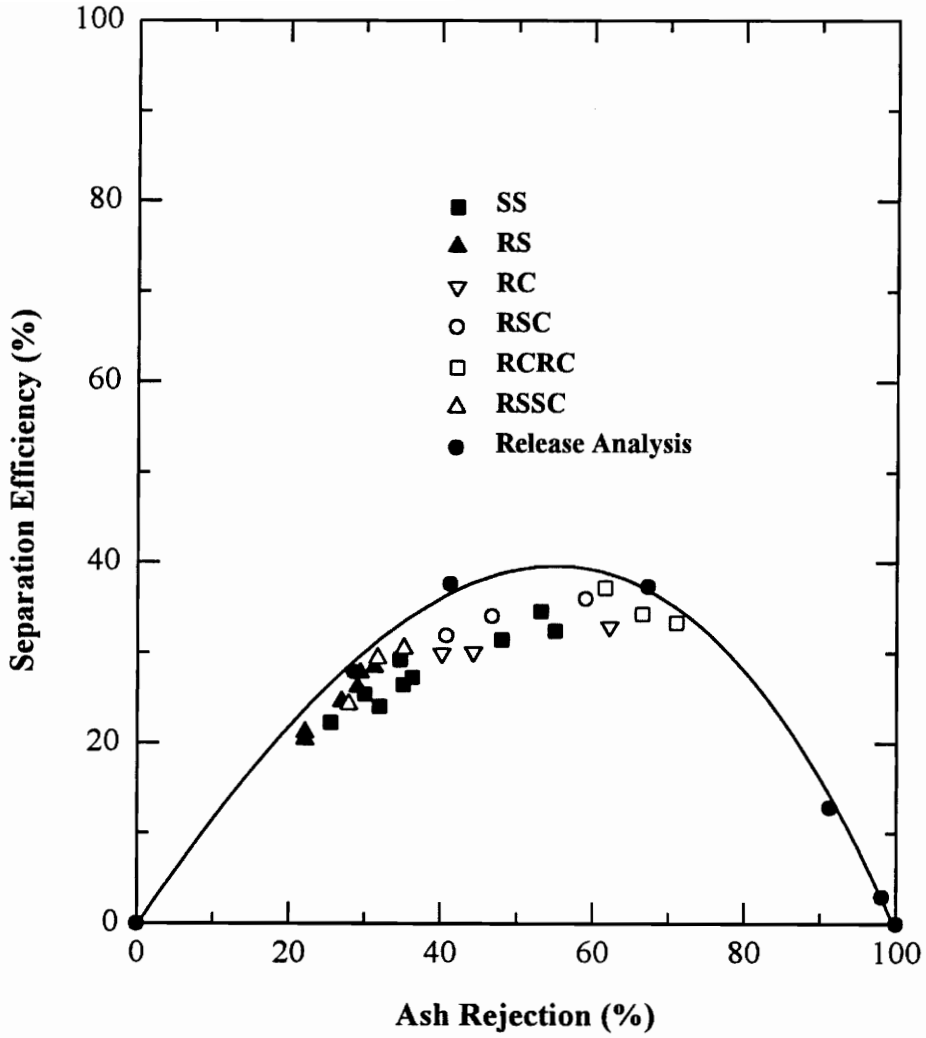

Figure 5.13 Effect of circuit configuration on separation efficiency versus ash rejection for the Upper Freeport seam coal.

the absence of a distinct "elbow" in either of the recovery-rejection curves shown in Figures 5.11 and 5.12. However, it appears that the maximum separation efficiency for this particular coal can be achieved at an ash rejection of approximately 50%. The data suggests that the separation efficiencies for the Upper Freeport coal fall approximately 30 percentage points lower than those obtained for the Pittsburgh No. 8 seam coal. The ash versus sulfur rejection plot is shown in Figure 5.14. In this particular case, the sulfur rejection versus ash rejection curve is relatively flat, indicating a very close association between the ash-bearing minerals and pyrite remaining in the coal matrix. It is possible that both pyrite and other ash-forming minerals are more finely disseminated in this coal and, therefore, more difficult to remove.

5.4.1.5 *Column circuit capacity*

The effect of circuit feed rate on the product rate for each of the circuits is shown in Figures 5.15-5.17. For a given feed rate, the single stage circuit produced the highest overall product mass rate, while the rougher-cleaner-recleaner circuit generated the lowest. With the exception of the last data point from the rougher-scavenger-cleaner circuit for Pittsburgh No. 8 coal, all column circuits led to an increase in product capacity with increasing feed flow rate. The unit capacities (lb/hr/column) for each circuit can be ranked from highest to lowest in the following order:

$$SS > RS > RC > RSSC > RSC > RCRC$$

In terms of recovery and grade, the circuit configurations which produced the lowest

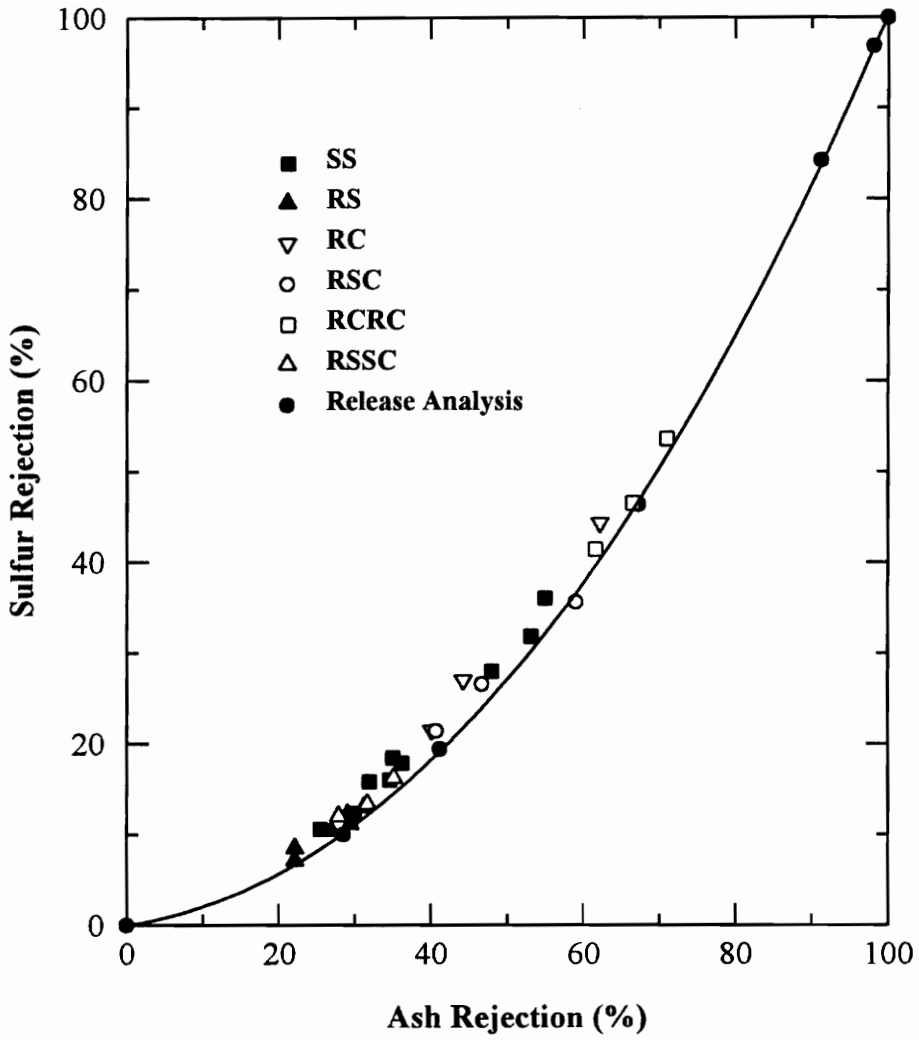

Figure 5.14 Effect of circuit configuration on sulfur rejection versus ash rejection relationship for the upper Freeport seam coal.

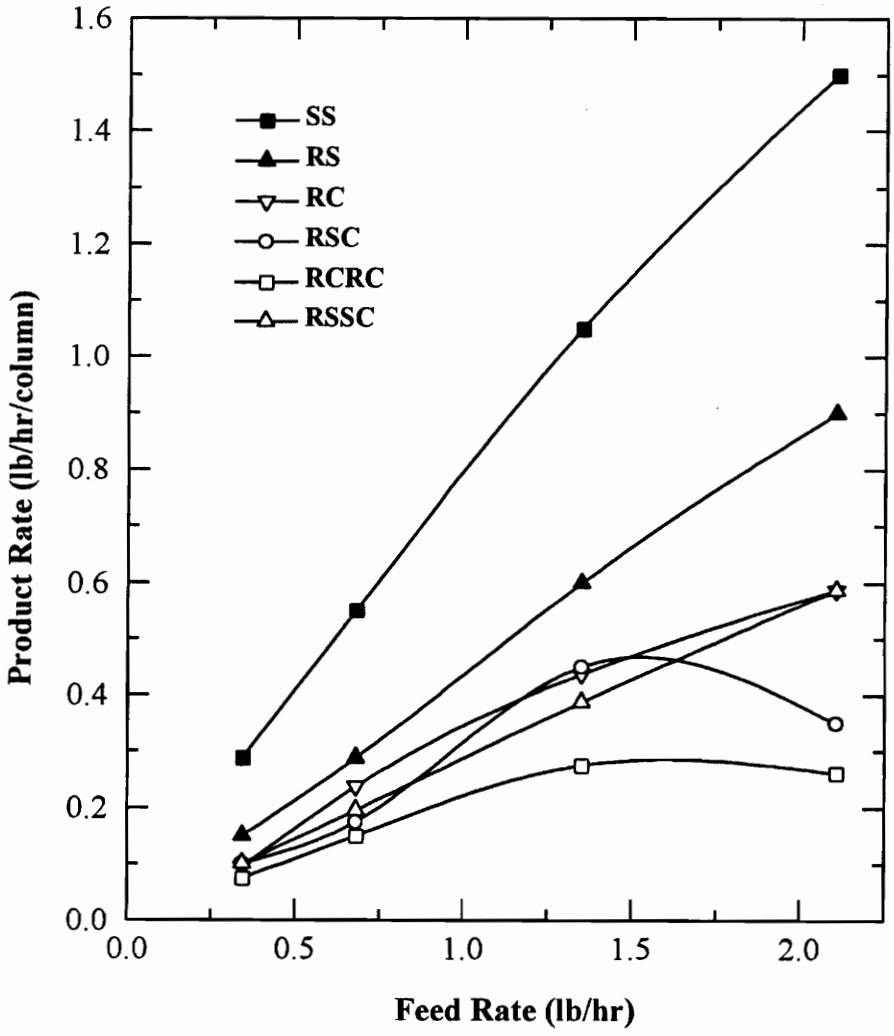

Figure 5.15 Effect of circuit configuration on column capacity for the Pittsburgh No. 8 seam coal.

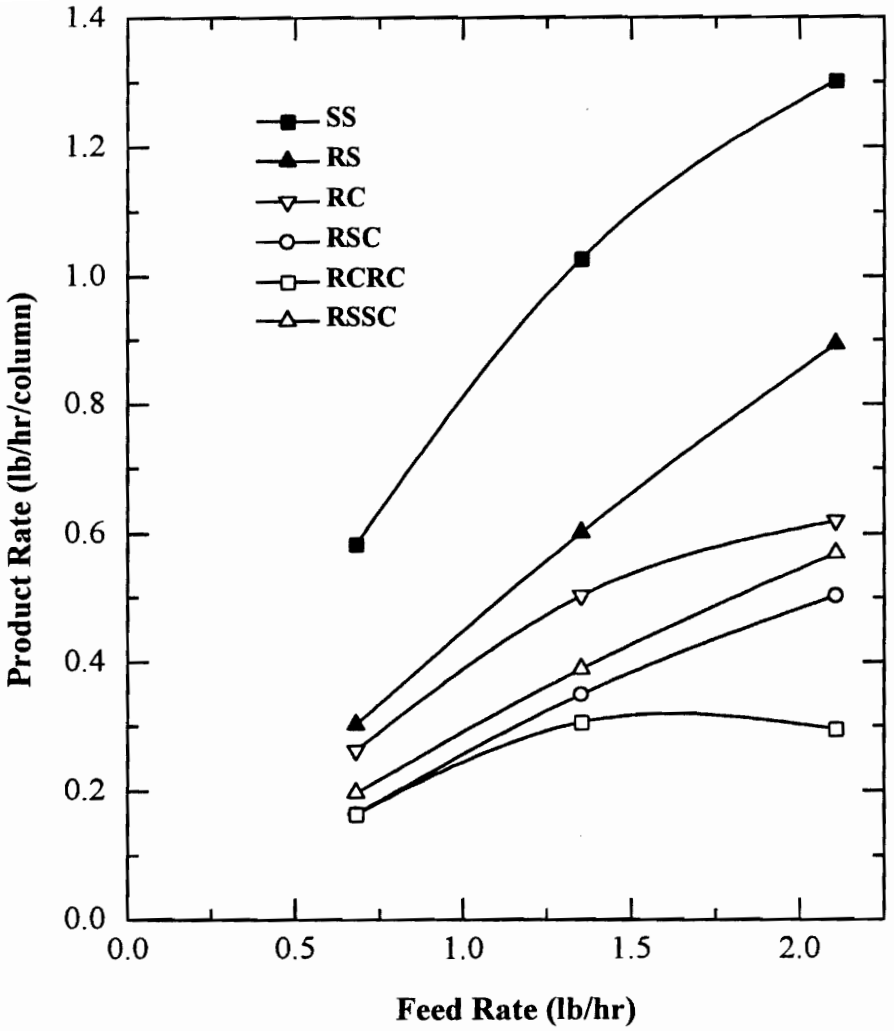

Figure 5.16 Effect of circuit configuration on column capacity for the Illinois No. 6 seam coal.

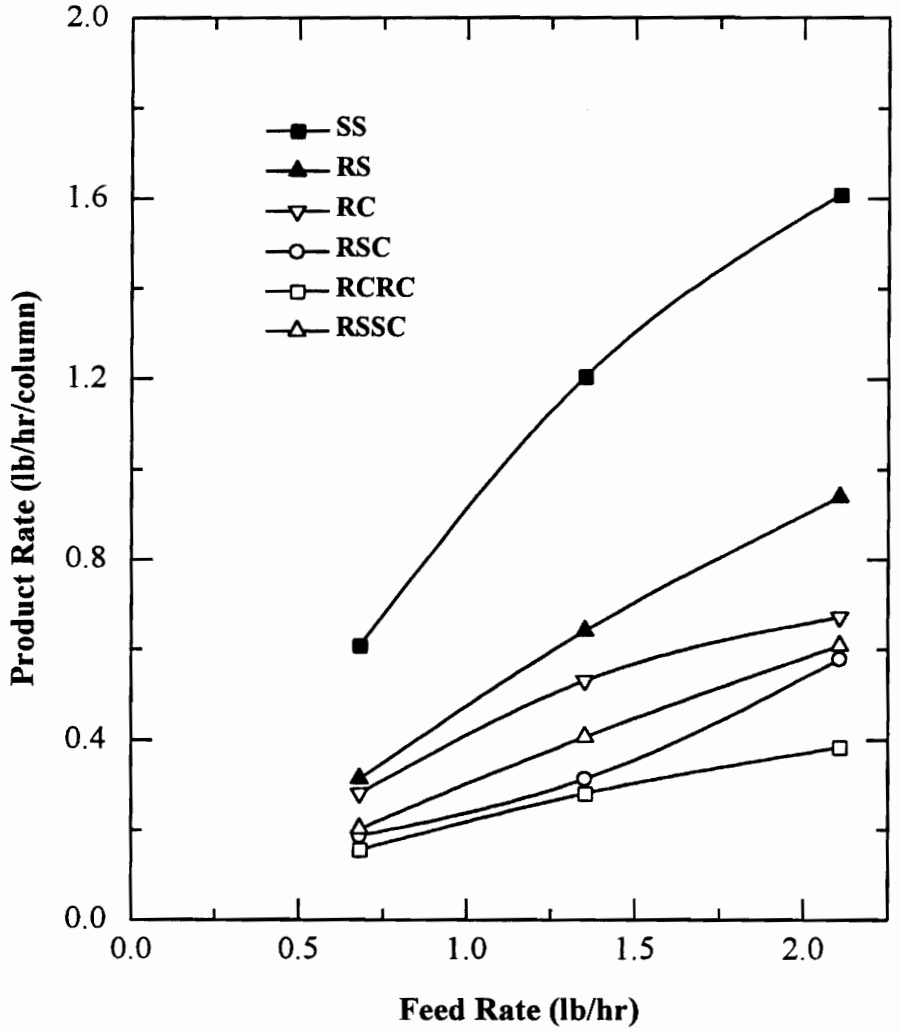

Figure 5.17 Effect of circuit configuration on column capacity for the Upper Freeport seam coal.

overall recoveries generated the highest ash and sulfur rejections (as dictated by the respective recovery-grade curves).

5.4.2 Discussion

Circuit analysis, as introduced by Meloy [25] and later used by Williams and Meloy [12] and Williams et al. [13], is a very useful technique for analyzing and designing flotation circuits. Under the assumption that individual unit operations are linear, i.e., the probability of a particle to report to the product or waste stream is independent of the feed, circuit analysis generates valuable information regarding the general behavior of separating circuits. For example, Meloy [25] confirmed by circuit analysis that the best piece of separation equipment should be invariably placed in the rougher position in a rough-cleaner-scavenger circuit to obtain optimum overall separation efficiency. He also concluded that the most efficient circuit is one which has unit operations only in the legs, i.e., no side loops or components. One major advantage of the circuit analysis technique is that resulting equations for the description of processing units thus obtained using the linearity assumption are linear, algebraic ones that can be solved without the use of numerical methods.

There are two parameters employed in circuit analysis to describe separation process: selectivity function, R, and separation efficiency, K. Selectivity function, R, represents the probability of particles of given properties that appear in the product,

which can be expressed by the following equation:

$$R = e^{-KZ} / (e^{-KZ} + e^{KZ}) \qquad (5.1)$$

where Z is the characteristic variable, e.g., the difference in specific gravity between the particle and the liquid medium in dense medium separation. K is the process constant. It is a measure of the efficiency of the separation and is defined as K=dR/dZ when Z =0 or R=0.5. The higher the K value, the more accurate the process.

Table 5.2 summarizes the results derived from circuit analysis technique for the flotation circuits examined in tests described above. Comparison of the overall selection functions and separation efficiency expressions in all cases gave rise to the following rank of magnitude from the highest to the lowest:

Recovery: RS > RSSC > SS > RSC > RC > RCRC

Separation efficiency: RSC = RSSC > SS = RS = RC > RCRC

From figures showing the relationship between energy recovery and ash rejection for three coal samples (Figures 5.3, 5.7 and 5.11) and figures correlating energy recovery and sulfur rejection (Figures 5.4, 5.8 and 5.12), the order of recovery appears to be in agreement with this theoretical consideration.

The order of unit capacity is as follows,

Unit capacity: SS > RS > RC > RSSC > RSC > RCRC

which is different from the recovery order simply because increase in the number of flotation stage did not increase the recovery to the same extent. Rather, for circuits such

Table 5.2. Circuit analysis results for six flotation circuits

Configuration	Overall Selectivity Function	Separation Efficiency
SS	R	dR/dZ
RC	R^2	dR/dZ
RS	$2R - R^2$	dR/dZ
RCRC	R^3	0.75 dR/dZ
RSC	$2R^2 - R^3$	1.25 dR/dZ
RSSC	$R + R^2 - R^3$	1.25 dR/dZ

as RC and RCRC the overall product rate was lower than that obtained from the single stage. Although higher overall recovery or product rate could be achieved with RS and RSSC circuits than with the single stage, the unit capacity was lower because the addition of another stage could not increase the recovery by 50% for the single stage circuit or by 33% for the two-stage circuits.

There are numerous versions of definition of separation efficiency that is used to describe the effectiveness of a separation process [26]. Maximum separation efficiency represents the minimum amount of material misplaced. The separation efficiency used in the present study was derived from general definition,

Separation efficiency = energy recovery - ash recovery.

It should be mentioned that it was found that energy recovery was almost identical to combustible recovery in all cases encountered in this study. Based on the plots of separation efficiency versus ash rejection, as shown in Figures 5.5, 5.9 and 5.13, two observations can be made:

1. RSC and RSSC circuits showed slightly better separation efficiency than other circuits in most cases, especially for Pittsburgh No. 8 and Illinois No. 6 coal samples. However, there are some exceptions, particularly in Figure 5.13, for the Upper Freeport coal sample. This is possibly due to the well-known fact that flotation column performance is determined by numerous physical and chemical parameters [27-29], and it is extremely difficult to achieve the same recovery and separation efficiency in all three

columns, which is the assumption under which the expressions for separation efficiency of each circuit was derived.

2. Improvement in metallurgical performance of column flotation by varying circuit configuration, however, can only be considered to be marginal. Castillo et al. [30] reached a similar conclusion from the study of sulfide flotation using columns. There appears to be little advantage in using multiple column circuits for flotation of the coals tested in the present work. This can be explained by considering the fine particle recovery mechanisms in flotation. For conventional flotation circuits, differences in performance can usually be attributed to wide variations in the nonselective entrainment of fine particles of mineral matter into the froth product. Multiple cleaning stages are generally capable of reducing entrainment, thereby improving the final separation. However, since a countercurrent flow of wash water is added into the froth phase in flotation columns, hydraulic entrainment can be essentially eliminated in the first column. In addition, flotation columns possess a froth zone considerably deeper than that used in mechanical cells. Substantial secondary cleaning action occurring in the froth, as demonstrated by results shown in Chapter 4, promotes the preferential flotation of more hydrophobic particles and selectively rejects less hydrophobic ones back into the pulp. Therefore, potential of improving metallurgical performance by using the second and the third stages is minimized. Subramanian et al. [2] have demonstrated that if one combines columns with mechanical cells, satisfactory separation performance could be achieved when flotation columns were used as either rougher, scavenger or cleaner. This is

apparently in agreement with the present study.

In order to obtain truly optimum circuit performance, operating parameters should be considered simultaneously with the circuit configuration. Feed rates, aeration rates, reagent type and dosage, and residence time are some of important operating parameters in the flotation process [12]. Williams and Meloy [31] suggested that feed rate is the most critical operating parameter for many types of process units. Increasing feed rate usually has an adverse effect on flotation cell performance. Various feed rates were thus adopted in the present study to explore possible influences on separation performance. Nevertheless, no significant difference was observed with all three coal samples. This indicates that flotation columns can be operated at best performance in a relatively wide range of feed rates. It can be speculated that when the carrying capacity limit of the rougher column is reached, multiple stages of column flotation may provide substantial benefits in improvement of separation performance.

Flotation columns are not only capable of achieving the highest possible separation efficiency in a single stage, but also exhibit better performance in terms of recovery. Yoon et al. [32] and Mankosa et al. [33] have shown that at the same retention time column flotation produces higher recovery than conventional flotation. Another interesting feature associated with column flotation, which could also affect flotation circuit, will be discussed as follows.

It is well established [28, 34] that the pulp is well mixed in a conventional flotation cell, whereas, in a flotation column it is in a nearly plug-flow pattern. As a

result, flotation recovery for a column and for a conventional cell can be approximately determined from the following expressions [32],

$$R = 1 - e^{-k\tau} \qquad \textit{(flotation columns)} \tag{5.2}$$

$$R = \frac{k\tau}{1 + k\tau} \qquad \textit{(conventional flotation cells)} \tag{5.3}$$

where R is flotation recovery, k flotation rate constant, and τ is the retention time. When τ is increased n times by increasing the cell volume by use of a larger cell, the flotation recovery (R_n) can be increased to,

$$R_n = 1 - e^{-nk\tau} \qquad \textit{(flotation columns)} \tag{5.4}$$

$$R_n = \frac{nk\tau}{1 + nk\tau} = 1 - \frac{1}{1 + nk\tau} \qquad \textit{(conventional flotation cells)} \tag{5.5}$$

Alternatively, the cell volume can be increased by using n identical flotation units in series with floats from all units as final products and tailings as feed to the next unit. The overall flotation recovery (R_n) for this circuit can be described in Equations (5.6) and (5.7) under the assumption that R in each unit is equal,

$$R_n = 1 - (1 - R)^n = 1 - (e^{-k\tau})^n = 1 - e^{-nk\tau} \qquad \textit{(flotation columns)} \tag{5.6}$$

$$\begin{aligned} R_n &= 1 - (1 - R)^n = 1 - \left(\frac{1}{1 + k\tau}\right)^n = 1 - \frac{1}{(1 + k\tau)^n} \\ &= 1 - \frac{1}{1 + nk\tau + \dfrac{n(n-1)}{2}(k\tau)^2 + \cdots} \qquad \textit{(conventional flotation cells)} \end{aligned} \tag{5.7}$$

Comparison of Equation (5.5) with Equation (5.7) reveals that for conventional flotation, recovery obtained from n flotation cells of volume V in series is significantly larger than that from a single flotation cell with a volume of nV. Meloy [25] reached the same conclusion from release analysis. However, for column flotation the recovery is identical to each other, as shown in Equations (5.4) and (5.6). This characteristic of flotation columns is of practical significance. Under conditions that recovery is of greater importance than grade, such as in molybdenite flotation, it is common to use more than twenty flotation cells in series such that the tailings from the previous cell is the feed to the next cell in order to achieve the highest possible recovery of molybdenite. This arrangement requires huge space and causes inconvenience in operation and maintenance. Thus, a large cell is always preferred to many small ones. With conventional cells, a single large cell with a volume much greater than the total volume of all small units is required to achieve the same recovery. With flotation columns, however, only equal volume is needed, which implies great economic advantages.

The release analysis consists of several consecutive flotation tests in which the froth product of a preceding test is used as the feed of subsequent flotation test followed by the final test in which froth products representing coal of different hydrophobicity are obtained under gradually intensified flotation conditions [23, 35, 36]. It is widely recognized that release analysis results represent ultimate beneficiation potentialities of coal fines by flotation based on differences in surface characteristics. It has been observed in the present study that a single stage of column flotation is capable of

achieving results similar to these attainable using release analysis, which is consistent with previous work [37]. Therefore, for a properly operated flotation column, the effectiveness of the separation is primarily controlled by the characteristics of the coal and is relatively independent of the number of flotation stages and the arrangement of circuits used to perform the separation. The present work supported Sutherland's conclusion that flotation circuit performance is insensitive to circuit arrangement unless the circuit becomes seriously unbalanced, resulting in deteriorated operating conditions for some of the cells [6].

The lower sulfur rejection than ash rejection, as shown in Figures 5.6, 5.10, and 5.14, may be due to at least two factors: poorer liberation of sulfur and self-induced hydrophobicity of pyrite. The self-induced hydrophobicity of pyrite arises from superficial oxidation which generates a sulfur-rich surface. The flotation recovery of pyrite is determined by the difference in amounts of hydrophobic sulfur-rich sulfides and hydrophilic iron oxides/hydroxides [38]. Unoxidized pyrite may not be hydrophobic enough to be floatable in a mineral/vapor/water system but hydrophobic enough to be floated in a mineral/oil (isooctane)/water system [39]. It has been revealed that mildly oxidized pyrites could show widely varying flotation recoveries depending on oxidation circumstances. More details on this aspect have been provided in Chapters 2 and 3. Poorer liberation of sulfur than ash is the other factor contributing to its lower rejection. While organic sulfur is intimately contained in coal matrices and nonseparable by physical means, it is necessary to pulverize coal to very fine sizes, often to micron sizes

and sometimes submicron sizes, to liberate pyrite, especially that existing in the form of framboids [33]. Other ash-forming minerals in coal, e.g. clay, quartz, calcite, and gypsum, may be liberated at larger sizes. It has also been demonstrated that small amounts of coal associated with the pyrite surface would significantly enhance the pyrite floatability and make composite particles behave more like coal than pyrite [33, 40].

The results obtained in the present work suggest that factors, other than simple metallurgical performance, should be considered in the selection of an appropriate column flotation circuit for coal cleaning. For example, the use of multiple column circuits may be desirable from an operational point of view since additional columns provide safeguards in the event that one of the columns is not operating properly. In cases where high recovery is required (as in the treatment of gold ores), RSC or RSSC circuits will be more favorable than the single stage since the scavenger provides other opportunities for particles to be recovered if they are unexpectedly lost in the rougher tailings. In other cases where high grade is more important, circuits such as RC and RCRC would be better than the single stage because of their ability to reject unwanted material in cleaner(s). However, multiple-stage flotation circuits will inevitably cause higher capital cost and operating expenses. As a result, the selection of column circuit arrangements which are most capable of meeting individual requirements needs to be made on a case-by-case basis. A similar approach should be adopted when columns are to be included in conjunction with existing mechanical flotation circuits. What columns are to be used as, rougher, cleaner or scavenger, not only depends on technical

requirements for product grade and recovery, but also on economical and operational factors. For example, Subramanian et al. [2] applied column flotation to processing of gold sulfide ore. They compared several possible flotation circuits composed of columns and mechanical cells and selected the circuit that required the lowest operating and capital cost and had minimum technical risk.

5.5 Conclusions

Various flotation circuit configurations commonly encountered in mineral processing and coal preparation plants were experimentally examined using microbubble flotation columns developed at Virginia Tech. These circuits included single-stage (SS), rougher-scavenger (RS), rougher-cleaner (RC), rougher-scavenger-scavenger cleaner (RSSC), rougher-scavenger-cleaner (RSC), and rougher-cleaner-recleaner (RCRC). The circuit configuration showed only marginal effects on circuit performance evaluated by separation efficiency and separation curves. Data produced from various circuits appeared to be on the same energy recovery-ash rejection (or sulfur rejection) curve, implying that a single stage column flotation was able to achieve the same metallurgical performance as a three-stage flotation process. The insensitivity of the circuit performance to circuit configuration was attributed to the addition of wash water which essentially eliminated the nonselective entrainment and selectively rejected less hydrophobic particles. It has been shown that a single column could accomplish the best

possible separation of particles by flotation usually achieved by release analysis. From an operational point of view, it is suggested that cleaner(s) be used to guarantee the product quality and scavenger(s) to safeguard the recovery.

Three different coal samples from the Pittsburgh No. 8, Illinois No. 6, and Upper Freeport coal seams precleaned by Babcock & Wilcox using conventional sub-aeration flotation showed different coal floatability and pyrite removability. The Pittsburgh No. 8 coal sample possessed the highest potential for ash rejection, while the Upper Freeport showed the lowest. The pyritic sulfur in all three coal samples was shown to be more difficult to reject than ash, which could be attributed to the oxidation-induced hydrophobicity and finer dissemination size of pyrite. Multi-stage column flotation showed marginal improvement in pyrite rejection.

The separation efficiency of column flotation was demonstrated to be a function of ash rejection. The Pittsburgh No. 8 and Illinois No. 6 coal samples showed a stronger dependence of separation efficiency on ash rejection than the Upper Freeport coal sample. The maximum separation efficiency occurred at ash rejection values near 70% for the Pittsburgh No. 8 coal, 60% for the Illinois No. 6 coal, and 50% for the Upper Freeport coal. An energy recovery of 90% produced corresponding ash and sulfur rejections of 70% and 26% for the Pittsburgh No. 8 coal, of 63% and 19% for the Illinois No. 6 coal, and of 45% and 25% for the Upper Freeport coal. The sulfur rejection was approximately 15% lower than ash rejection at the same energy recovery.

5.6 References

1. Lynch, A.J., Johnson, N.W., Manlapig, E.V. and Thorne, C.G., 1981. "Mineral and Coal Flotation Circuits: Their Simulation and Control," Elsevier, Amsterdam.
2. Subramanian, K.N., Lonnelly, D.E.G., and Wong, K.Y., 1988. "Commercialization of a Column Flotation Circuit for Gold Sulphide Ore," *Column Flotation'88*, Ed. by K. V. S. Sastry, Society of Mining Engineers, Inc., Littleton, Colorado, pp. 13-18.
3. Green, J.C.A., 1984. "The Optimization of Flotation networks," *International Journal of Mineral Processing*, **13**, pp. 83-103.
4. Reuter, M.A. and Van Deventer, J.S.J., 1990. "The use of Linear Programming in the Optimal Design of Flotation Circuits Incorporating Regrind Mills," *International Journal of Mineral Processing*, **28**, pp. 15-43.
5. Agar, G.E., Startton-Crawley, R., and Bruce, T.J., 1980. "Optimizing the design of Flotation Circuits," *CIM Bulletin*, December, 173-181.
6. Sutherland, D.N., 1981. "A Study on the Optimization of the Arrangement of Flotation Circuits," *International Journal of Mineral Processing"*, **7**, pp. 319-346.
7. Firth, B.A., Swanson, A.R., and Nicol, S.K., 1979. "Flotation circuits for Poorly Floating Coals," *International Journal of Mineral Processing*, **11**, pp. 321-334.

8. Davis, W.J.N., 1964. "The Development of a Mathematical Model of the Lead Flotation Circuit at the Zinc Corp. Ltd," *Proceedings*, Australasian Institute of Mining and Metallurgy, **212**, pp. 61-89.

9. Agar, G.E. and Stratton-Crawley, R., 1982. "Bench Scale Simulation of Flotation Plant Performance," *Bulletin*, Canadian Institute of Mining and Metallurgy, **75**, pp. 93-98.

10. King, R.P., 1975. "Simulation of Flotation Plants," *Trans. SME-AIME*, **258**, pp. 286-293.

11. King, R.P., 1976. "The use of Simulation in the Design and Modification of Flotation Plants," *Flotation, Vol. 2*, Ed. by M.C. Fuerstenau, AIME, New York,pp. 937-961.

12. William, M.C. and Meloy, T.P., 1983. "Dynamic Model of Flotation Cell Banks-Circuit Analysis," *International Journal of Mineral processing*, **10**, pp. 141-160.

13. William, M.C., Fuersteau, D.W., and Meloy, T.P., 1986. "Circuit Analysis-General Product Equations for Multifeed, Multistage Circuits containing Variable Selectivity function," *International Journal of Mineral Processing*, **17**, pp. 99-111.

14. Mehrotra, S.P. and Kapur, P.C., 1974. "Optimal-Suboptimal Synthesis and Design of Flotation Circuits," *Separation Science*, **9**, pp. 167-184.

15. Umeda, T., Hirai, A., and Ichikawa, A., 1972. "Synthesis of Optimal

Processing System by an Integrated Approach," *Chemical Engineering Science*, **27**(IV), pp. 795-804.

16. Williams, M.C. and Meloy, T.P., 1991. "Feasible Designs for Separation Networks: A Selection Technique," *International Journal of Mineral Processing*, **32**, pp. 161-174.

17. Osborne, D.G., 1988. "Coal Preparation Technology," Graham & Trotman Limited.

18. Leonard, J.W., 1979. "Coal Preparation," The American Institute of Mining, Metallurgical and Petroleum Engineers, Inc., pp. 10-75.

19. Miller, F.G., 1964. "Reduction of Sulfur in Minus 28 Mesh Bituminous Coal," *Trans. SME-AIME*, **229**, pp. 7-15.

20. Miller, K.J., 1975. "Coal-Pyrite Flotation," *Trans. SME-AIME*, **258**, pp. 30-33.

21. Espinosa-Gomez, R., Johnson, N.W., Pease, J.D., and Munro, P.D., 1989. "The commissioning of the first flotation columns at Mount Isa Mines Limited," in *Processing of Complex Ores*, Ed. by G.S. Dobby and S.R. Rao, CIM Conference of Metallurgists, Halifax, Pergamon, pp. 293-302.

22. Aplan, F.F., 1977. "Use of the Flotation Process for Desulfurization of Coal," in *Coal Desulfurization - ACS Symposium Series*, No. 64, Ed. by T.D. Wheelock, American Chemical Society, Washington, D.C., pp. 70-82.

23. Dell, C.C.,1964. "An Improved Release Analysis Procedure for Determining Coal Washability," *J. Inst. Fuel*, **37**, pp. 149-150.

24. Dell, C.C., Bunyard, M.J., Rickelton, W.A., and Young, P.A., 1972. "Release analysis: a comparison of techniques," *Trans. IMM (Sect. C, Min. Proc. Extr. Metall.)*, **81**, pp. C89-C96.

25. Meloy, T.P., 1983. "Analysis and Optimization of Mineral Processing and Coal cleaning Circuits-Circuit Analysis," *International Journal of Mineral Processing*, **10**, pp. 61-80.

26. Schulz, N.F., 1970. "Separation efficiency," *Trans. Am. Inst. Min. Engrs.*, **247**, pp. 81-87.

27. Luttrell, G.H., Adel, G.T., and Yoon, R.-H., 1987. "Modeling of Column Flotation," *Preprint No. 87-130*, AIME Annual Meeting, Denver, Colorado.

28. Luttrell, G.H., Adel, G.T., and Yoon, R.-H., 1988. "Hydrodynamics and Mathematical Modeling of Fine Coal Flotation," *Proceedings, XVI Int. Mineral Processing Congress*, Ed. by E. Forssberg, Elsevier, Amsterdam, pp. 1791-1802.

29. Finch, J.A., and Dobby, G.S., 1989. "Column Flotation," Pergamon Press.

30. Castillo, D. Dobby, G.S., and Kosick, G.A., 1990. "Column Flotation Circuit Design," *Preprint No. 90-101*, SME Annual Meeting, Salt Lake City, Utah.

31. Williams, M.C. and Meloy, T.P., 1989. "On the definition and separation of fundamental process functions," *International Journal of Mineral Processing*, **26**, pp. 65-72.

32. Yoon, R.-H., Luttrell, G.H., and Adel, G.T., 1989. "Advances in Fine Particle Flotation," *Challenges in Mineral processing*, ED. by K. V. S. Sastry and M. C.

Fuerstenau, Society of Mining Engineers, Inc., Littleton, Colorado, pp. 487-505.

33. Wang, D.M., 1994. "Image analysis characterization of fine coal," *Ph.D. Dissertation*, Department of Mining and Minerals Engineering, Virginia Polytechnic Institute and State University, Blacksburgh, Virginia.

34. Luttrell, G.H., 1986. "Hydrodynamic Studies and Mathematical Modeling of Fine Coal Flotation," *Ph.D. Dissertation*, Department of Mining and Minerals Engineering, Virginia Polytechnic Institute and State University, Blacksburgh, Virginia.

35. Dell, C.C., 1953. "Release Analysis, a New Tool for Ore Dressing research," *Recent developments on Mineral Dressing*, Inst. Mining and Metallurgy, London, pp. 75-84.

36. Dell, C.C., 1957. "Determination of Froth-Flotation Washability data," *J. Inst. Fuel*, **30** (200), pp. 523-526.

37. Forrest, P.R., 1990. "Processing of High-Sulfur Coals Using Microbubble Column Flotation," *Thesis*, Department of Mining and Minerals Engineering, Virginia Polytechnic Institute and State University, Blacksburgh, Virginia.

38. Yoon, R.-H., Lagno, M.L., and Luttrell, G.H., 1991. "On the Hydrophobicity of Coal Pyrite," *Processing and Utilization of High-Sulfur Coals IV*, Ed. by P.R. Dugan, D.R. Quigley and Y.A. Attia, Elsevier Science Publishers B.V., Amesterdam, pp. 241-253.

39. Kocabag, D., Shergold, H.L., and Kelsall, G.H., 1990. "Natural Oleophilicity/

Hydrophobicity of Sulphide Minerals, II: Pyrite," *International Journal of Mineral Processing*, **29**, pp. 211-219.

40. Kawatra, S.K. and Eisele, T.C., 1991. "Recovery of Pyrite in Coal flotation, Entrainment or Hydrophobicity," *Preprint* No. 91-89, SME Annual Meeting, Denver, Colorado.

CHAPTER 6 SUMMARY AND CONCLUSIONS

The most important conclusions on electrochemistry and floatability of pyrite in coal flotation obtained from the present study are summarized as follows:

1. Pyrite recovery in flotation takes place *via* three major mechanisms: hydrophobicity, entrainment, and middlings. Problems associated with them have been addressed by conducting studies on superficial oxidation and collectorless flotation of pyrite, stability of flotation froths, and column circuit configuration, respectively. Significant enhancement of pyrite rejection can be achieved by controlling the surface electrochemistry of pyrite and minimizing hydraulic entrainment. However, column circuit configuration showed only marginal effects on the separation of pyrite from coal.

2. Incipient oxidation of pyrite occurs above -0.28 V at pH 9.2 and 0 V at pH 4.6, which is usually masked on the voltammetry curve by the oxidation of ferrous to ferric hydroxide when polished electrodes are used. This process produces sulfur-rich hydrophobic species that are responsible for the floatability of the mineral. These species are most likely polysulfides (FeS_n, $n>2$) or metal-deficient sulfides ($Fe_{1-x}S_2$, $x<1$). It has also been found that soluble ferrous hydroxide species are produced by oxidation and reduction processes on pyrite.

Pittsburgh No. 8 coal-pyrite exhibited electrochemical behaviors considerably different from mineral-pyrite or Chinese coal-pyrite.

3. Pyrite exhibits collectorless flotation as a result of superficial oxidation. The flotation onset correlates well with the commencement of oxidation to form sulfur-rich species. Flotation recovery of pyrite is determined by the relative abundance of sulfur-rich species and iron hydroxides and, therefore, is dependent on E_h, pH, etc. Stronger flotation of pyrite was observed over a wider range of E_h at pH 4.6 than at pH 9.2. Pyrite can be depressed by galvanic coupling with active metals by preferentially generating metal hydroxides on the mineral and lowering its potential to a value that is negative enough to prevent superficial oxidation and reduce hydrophobic species already present on the surface. This technique has been shown to be able to significantly enhance the rejection of pyrite in coal flotation.

4. The stability of flotation froths can be manipulated to minimize hydraulic entrainment of weakly hydrophobic and hydrophilic particles into the froth product. The secondary cleaning action of froth is accomplished through the preferential reattachment of strongly hydrophobic particles to bubble surface during froth drainage and bubble coalescence. High product grade can usually be achieved by use of low gas flow rate, high wash water rate, and deep froth

height, but probably at the expense of recovery and column capacity. The optimum gas flow rate and wash water flow rate have been determined to be approximately 2 cm/s and 0.25 cm/s, respectively. Small bubble size is beneficial for both product grade and recovery. A new model has been developed to describe the correlation between combustible recovery and water recovery in coal flotation.

5. Six flotation circuits that are commonly encountered in mineral processing and coal preparation have been examined experimentally using microbubble flotation columns. The circuit configuration showed only marginal effects on circuit performance. A single column can accomplish the best possible separation by flotation as determined by release analysis. From an operational point of view, it is suggested that cleaner(s) be used to guarantee the product grade and scavenger(s) to safeguard the recovery. Of three coals tested in the present work, Pittsburgh No. 8 coal possessed the highest potential for pyrite rejection, Upper Freeport coal the lowest, and Illinois No. 6 coal the intermediate.

CHAPTER 7 RECOMMENDATIONS FOR FUTURE WORK

The electrochemistry of surface reactions on pyrite has been extensively studied in the present work. Emphasis was placed on the identification of conditions under which pyrite oxidation produces a hydrophobic surface and, therefore, collectorless flotation. A novel electrochemical technique has been developed to minimize the ratio of hydrophobic to hydrophilic species on the mineral and enhance pyrite rejection during coal flotation. Froth stability and circuit configuration in microbubble column flotation was investigated to eliminate the hydraulic entrainment of hydrophilic particles for the improvement of separation efficiency. However, more work is needed before problems associated with pyrite rejection in coal flotation can be fully addressed. The following work is recommended for the future study:

1. The floatability of pyrite is determined by the relative abundance of hydrophobic and hydrophilic species on the surface. The removal of either species will considerably affect the hydrophobicity of the mineral. A study that deduces the structure of surface oxidation products on pyrite will be important in understanding and predicting flotation behavior in flotation processes. It is also of great importance that development of techniques which retain the hydrophilic species on, or remove the hydrophobic products from pyrite, be undertaken. Applications of surface analysis techniques, such as scanning tunneling microscopy, may be pertinent to such a study.

2. The electrochemical and flotation behavior of coal-pyrites is significantly

different from that of mineral-pyrite. One of possible reasons is the presence of enormous amounts of coal around the pyrite in the course of the oxidation. The oxidation of coal may generate some unique species on pyrite. Simultaneously, some products formed during pyrite oxidation may deposit on the surface of coal rather than pyrite. Surface analysis of pyrite after oxidation in the environment rich in coal could provide valuable information on surface properties of coal-pyrites. This work would also improve the understanding of mechanisms from which differences between coal- and mineral-pyrites are developed.

3. More XPS work is required to identify hydrophobic species formed in the initial oxidation of pyrite. Fresh surfaces fractured under controlled potentials are preferred for this study. Moderate oxidation conditions should be employed under both alkaline and acidic solution pH's. The use of other surface analysis techniques, e.g., Raman spectroscopy, may be necessary to provide unambiguous information on oxidation species in certain cases.

4. More collectorless flotation tests in the electrochemical-microflotation cell is needed for various coal-pyrites, especially in alkaline solutions. The results are important to delineate differences in electrochemical studies and flotation results reported in the literature.

5. A convenient and effective procedure needs to be developed to induce galvanic interaction between pyrite and sacrificial anodes. This can possibly be achieved by designing an appropriate conditioning sump as the reactor. Analysis of pyrite surface

after galvanic coupling should be conducted to better understand the mechanism of pyrite depression by this technique.

6. Hydrophobic solid particles such as coal have a strong effect on froth stability. This effect depends on particle size, hydrophobicity, concentration, shape, roughness, etc. The particle hydrophobicity is one of the most important factors and more work on this topic is required to better understand froth behavior in flotation. Coal coatings on pyrite surfaces may substantially increase pyrite recovery. The extended DLVO (Derjaguin-Landau-Vervey-Overbeek) theory should be applied to the investigation of this phenomenon.

VITA

Dongping Tao was born on November 20th, 1962, in Wuxi County, Jiangsu Province, People's Republic of China, where he lived until graduation from the Gangxia High School in 1979. He enrolled in Beijing University of Science and Technology in the same year and received his B.S. degree in July, 1983. Subsequently, he attended the Beijing Graduate School of China University of Mining and Technology and obtained his M.S. in July, 1986.

After working in China University of Mining and Technology as a teaching and research faculty for three years, he was selected by the government in March, 1989, to do advanced research as a visiting scholar in the Department of Mining and Minerals Engineering, Virginia Polytechnic Institute and State University, Blacksburg, Virginia. He entered the Ph.D. program in August, 1990.

He has 12 publications/presentations and completed manuscripts for four additional papers that are to be published shortly. He has accepted a research associate position in the Department of Mining and Minerals Engineering at Virginia Polytechnic Institute and State University.